

https://dspace.org/

Optimization of the synthesis and performance of Polyaspartamide (PAA) material for carbon dioxide capture in South African coal-fired power plants

Chitsiga, Tafara Leonard

2016

http://hdl.handle.net/10539/21104

Chitsiga,Tafara Leonard (2016) Optimization of the synthesis and performance of Polyaspartamide (PAA) material for Carbon Dioxide capture in South African coal-fired power plants, University of Witwatersrand, Johannesburg, <http://wiredspace.wits.ac.za/handle/10539/21104>

Downloaded from a DSpace repository. https://dspace.org/

Optimization of the Synthesis and Performance of Polyaspartamide (PAA) Material for Carbon Dioxide Capture in South African Coal-fired Power Plants.

Tafara Leonard Chitsiga

A dissertation submitted to the Faculty of Engineering and the Built Environment, University of the Witwatersrand, Johannesburg, in fulfillment of the requirements for the degree of Master of Science in Engineering

Supervisor: Dr M.O. Daramola

Co-supervisor: Prof. N. Wagner

24 May 2016

Declaration

I declare that this dissertation is my own unaided work. It is being submitted for the degree of Master of Science in Engineering to the University of the Witwatersrand, Johannesburg, South Africa. It has not been submitted before for any degree or examination to any other University.

……...

(Signature of Candidate)

……day of……2016

(Day) (Month) (Year)

Abstract

Global climate change is among the major challenges the world is facing today, and can be attributed to enhanced concentrations of Greenhouse Gases (GHG), such as carbon dioxide (CO_2), in the atmosphere. Therefore, there is an urgent need to mitigate CO_2 emissions, and carbon capture and storage (CCS) is amongst the possible options to reduce CO_2 emissions. Against this background, this work investigated the synthesis and performance evaluation of Polyaspartamide (PAA) adsorbent for CO_2 capture. In particular, the effect of the presence of water-soluble amines in the amine-grafted poly-succinimide (PSI) (referred to as Polyaspartamide (PAA) adsorbent), was investigated.

Methyl Amine (MA) and Mono-Ethanol Amine (MEA) were employed as water-soluble amines and the effect of changes in their concentration on CO_2 adsorption capacity was investigated as well. Water-soluble amines were incorporated to allow water solubility of the adsorbent paving the way for freeze-drying to improve the geometric structure (surface area, pore volume and pore size) of the adsorbent. Initially, the PSI was loaded with Ethylenediamine (EDA), forming PSI-EDA. The water-soluble amines were grafted to PSI-EDA, with the EDA added to improve the chemical surface of the adsorbent for CO_2 capture.

NMR and FTIR analyses were performed and confirmed the presence of MA and MEA amine groups in the PAA, thereby indicating the presence of the grafted amines on the backbone polymer. BET analysis was performed and reported the pore volume, pore size and surface area of the freeze-dried material. It was observed that the physical properties did not change significantly after the freeze-drying compared to literature where freeze-drying was not employed. An increase in adsorption capacity with an increase in MA and MEA concentrations in MA-PAA and MEA-PAA samples was observed. At low amine concentrations (20% amine and 80% EDA grafted), MEA-PAA was observed to exhibit higher adsorption capacity compared to the MA-PAA samples. At high amine (100% amine grafted) concentrations, MA-PAA samples displayed higher adsorption capacity. Three runs were performed on each sample and the results obtained were reproducible. The best adsorption capacity obtained was 44.5 g CO_2/kg Ads.

Further work was then performed to understand the effects of operating variables on CO_2 adsorption as well as the interactive effect using the Response Surface Methodology approach.

The experiments were done by use of CO_2 adsorption equipment attached to an ABB gas analyzer. A central composite design of experiment method with a total of 20 experiments was employed to investigate three factors, namely, temperature, pressure and gas flow rate. Six regression models were drawn up and mean error values computed by use of Matlab, followed by response surfaces as well as contours, showing the influence of the operating variables on the adsorption capacity as well as interaction of the factors were then drawn up.

The results obtained displayed that each of the factors investigated, temperature, pressure and gas flowrate had an incremental effect on the adsorption capacity of PAA, that is, as each factor was increased, the adsorption capacity increased up to a point where no more increase occurred. Adsorption was seen to increase for both an increase in gas flowrate and adsorption pressure to a maximum, thereafter it starts to decrease. A similar trend was observed for the interaction between temperature and pressure. However, the interaction between gas flowrate and temperature was such that, initially as the temperature and the gas flowrate increase, the adsorption capacity increases to a maximum, thereafter, the temperature seizes to have an effect on the adsorption capacity with a combined effect of decreasing temperature and increasing gas flowrate resulting in a further increase in adsorption capacity.

It was confirmed that the operating variables as well as the flow regime have an effect on the CO_2 adsorption capacity of the novel material. The highest adsorption capacity was obtained in the pressure range 0.5 bar to 1.7 bar coinciding with the temperature range of 10 ^oC to 45 ^oC. The interaction of gas flowrate and adsorption pressure was such that the highest adsorption capacity is in the range 0.8 bar to 1.5 bar which coincides with the gas flowrate range from 35 ml / min to 60 ml / min. In conclusion, the best adsorption capacity of 44.5 g / kg via the TGA and 70.4 g / kg via the CO_2 adsorption equipment was obtained from 100 % MA grafted PSI.

Acknowledgements

I would to acknowledge the efforts of my supervisors, Dr. Michael Daramola, Prof Nicola Wagner and Mr. Jacob Masiala Ngoy. Thank you all for your tremendous support during the course of this project, academic and otherwise. It is greatly appreciated and will always be treasured. I would also like to acknowledge Mr. Willie from Chemvak for his continuous availability to assist with the training and servicing of the CO_2 adsorption equipment used in this project. Also, many thanks go to Mr. Osler and the ABB crew for making an ABB gas analyzer available for the project and their training on the use of it. Thank You!! A big thank you to the Norwegian Petroleum Energy (EnPe) for the grant to undertake this project.

I would also like to warmly appreciate and thank my Mum and Dad. These two amazing human beings started with me on this long academic journey, from pre-school through to post-graduate studies at Wits! Your love for me and my success in academics is overwhelming. Thank you for drilling in me those soft skills that have seen me through. Thank You!!! A big thank you to my siblings for their awesome support, love and for allowing me to be away from home for very long periods of time. Love you guys!

Lastly, I would like to acknowledge all those (The School of Chemical and Metallurgical Engineering staff at Wits University, The Coal Group, fellow postgraduate students and not least many others who I cannot name individually) who contributed to this project materially or otherwise. Without you all, this project would not have been a success.

Presentations and Publications

Several conference papers and research publications have emanated from this research project and are as listed below:

Publications

1. T. Chitsiga, M.O. Daramola, N. Wagner, J. Ngoy (2016) Effect of the presence of water-soluble amines on the carbon dioxide (CO_2) adsorption capacity of amine-grafted poly-succinimide (PSI) adsorbent during CO_2 capture, Energy Procedia, 86: 90–105.

2. **T. Chitsiga**, M. O. Daramola, N. Wagner, J. Ngoy. Effect of operating variables on the CO_2 adsorption capacity of amine-Polyaspartamide composite adsorbent: a statistical approach. *Manuscript in preparation, 2016.*
3. J.M. Ngoy, **T. L. Chitsiga**, M.O. Daramola, N. Wagner, H. Potgieter, O. Bolland. CO_2 adsorption using water soluble and water insoluble nanocomposites combined with multi-walled carbon nanotubes. *Manuscript in preparation, 2016.*

Conference papers

1. **Tafara Chitsiga**, Michael O. Daramola, Nicola Wagner, Jacob Ngoy. Optimization of the synthesis and performance of Polyaspartamide (PAA)/Carbon nanotubes (CNT) material for Carbon Dioxide Capture. **Oral Presentation**. Carbon Capture Workshop, University of the Western Cape, Cape Town, South Africa. 24 – 26 March 2014.
2. **Tafara Chitsiga**, Michael O. Daramola, Nicola Wagner, Jacob Ngoy. Optimisation of the Synthesis and Performance of Polyaspartamide (PAA) Material for CO_2 Capture in Coal-fired Power Plants. **Oral Presentation**. Fossil Fuel Foundation Coal, Energy and Sustainability Conference, University of Cape Town, South Africa. 27 – 28 November 2014.
3. **Tafara Chitsiga**, Michael O. Daramola, Nicola Wagner, Jacob Ngoy. Optimisation of the Synthesis and Performance of Polyaspartamide (PAA) Material for CO_2 Capture in Coal-fired Power Plants. **Oral Presentation**. Coal Colloquium, North-West University, Northwest Province, South Africa. 8 July 2014.
4. **Tafara Chitsiga**, Michael O. Daramola, Nicola Wagner, Jacob Ngoy. Effect of the presence of water-soluble amines on the Carbon Dioxide (CO_2) adsorption capacity of amine-grafted

poly-succinimide (PSI) adsorbent during CO_2 Capture. **Oral Presentation**. Trondheim Carbon Capture and Storage Conference – 8 (TCCS-8), Norwegian University of Science and Technology, Trondheim, Norway. 16-18 June 2015.

Contents

Declaration i
Abstract ii
Acknowledgements iv
Presentations and Publications v
Publications v
Conference papers v
List of Figures x
List of Tables xiv
Nomenclature xvi
Chapter 1: Introduction 1
1.1 Motivation and Background 1
1.2 Possible effects of Global Warming 2
1.3 Existing CO_2-reduction technologies 3
1.4 Applications of CCS 4
1.5 Problem Identification 5
1.6 Research Hypotheses and Questions 7
1.7 Research Aim and Objectives 7
1.8 Expected outcomes 8
Chapter 2: Literature Review 9
2.1 Introduction 9
2.2 History of Carbon dioxide capture and storage 9
2.3 Mitigating CO_2 emissions 10
2.4 Carbon dioxide Capture and Storage (CCS) 12
2.4.1 Meaning of CCS and its benefits 12
2.4.2 CO_2 emissions and CCS in South African coal-fired power plants 23
2.4.3 Techniques for CO_2 capture in coal-fired power plants 24
2.4.4 CO_2 capture via adsorption 36
2.4.5 Types of adsorbents for CO_2 capture 41
2.4.6 Amine grafted Polysuccinimide (PSI) for CO_2 capture via adsorption 50
2.4.7 Adsorption mechanism during CO_2 capture 52

2.4.8 Factors influencing post-combustion CO_2 capture via adsorption 54
2.4.9 Optimization studies in CO_2 capture 56
2.5 Chapter Summary 57
Chapter 3: Materials and Experimental Procedures 59
3.1 Introduction 59
3.2 Material and equipment used for the study 59
3.3 Experimental procedure 59
3.3.1 Synthesis of PSI and the water-soluble amine-grafted PSI 60
3.3.2 Characterization of the synthesized PSI and amine-grafted PSI (PAA) 63
3.3.3 Evaluation of CO_2 adsorption performance of amine-grafted PSI (PAA) 65
Chapter 4: Synthesis and Characterization of amine-grafted PSI for CO_2 adsorption 70
4.1 Introduction 70
4.2 Synthesis 71
4.3 Characterization 72
4.3.1 NMR Analysis 72
4.3.2 BET Analysis 74
4.3.3 SEM Analysis 76
4.3.4 FTIR Analysis 77
4.3.5 TGA Analysis 80
4.3.6 Solubility determination 82
4.4 Chapter Summary 84
Chapter 5: Effect of the presence of water-soluble amines on the CO_2 adsorption capacity of amine-grafted PSI (PAA) 86
5.1 Introduction 86
5.2 Evaluation of CO_2 adsorption capacity of amine-grafted PSI 87
5.3 Evaluation of the rate of adsorption with time 91
5.4 Chapter Summary 94
Chapter 6: Influence of operating variables on the CO_2 adsorption capacity of amine-grafted PSI (PAA) 95
6.1 Introduction 95
6.2 Model formulation and parameter estimation 97

6.3 Analysis of Variance (ANOVA) test 98
6.4 Effects of process variables on the adsorption capacity of MA grafted PSI 100
6.5 Model cross validation 105
6.6 Chapter Summary 106
Chapter 7: General conclusions and recommendations 108
7.1 Summary 108
7.2 Results 109
7.3 Recommendations 111
References 112
Appendices 125
Appendix A: Synthesis and characterization information 125
A1 Percentage Yield Calculation: 125
A2 Reaction scheme showing PSI monomer being grafted with amines: 125
Appendix B: TGA adsorption results 126
Appendix C: Matlab code used in optimization studies 169
Appendix D: Experimental equipment 170
Appendix E: Further information on model formulation and parameter estimation 171
Appendix F: Plagiarism report 179
Appendix G: Publications 180

List of Figures

Figure 1.1: World energy supply proportions (International Energy Agency, 2013)..... 1
Figure 2.1: World energy supply proportions (International Energy Agency, 2013)..... 9
Figure 2.2: Possible solutions to reducing CO_2 emissions (International Energy Agency, 2012). 11
Figure 2.3: Schematic showing the stages in Carbon Capture and Storage (CCS) 12
Figure 2.4: CO_2 storage projects all around the world (Understanding the Long-Term fate of geologically, 2015). 13
Figure 2.5: Schematic showing the four different types of sedimentary formations suitable for CO_2 storage (Liebscher and Munch, 2015)..... 15
Figure 2.6: Post-combustion capture system in a power plant (Chao *et al.*, 2015). 20
Figure 2.7: Schematic showing the main steps in pre-combustion capture..... 22
Figure 2.8: South Africa's highest CO_2 emitters (adapted from Urban Earth (2015))……23
Figure 2.9: Typical structure of a coal fired power plant (The USGS Water Science School, n.d.) 24
Figure 2.10: Simplified adsorption process diagram (Worch, 2012). 27
Figure 2.11: Possible adsorption isotherms according to the BET theory (Crittenden and Thomas, 1998). 30
Figure 2.12: Possible adsorption isotherms (Wilcox, 2012; Shi and Morreale, 2015). 31
Figure 2.13: Adsorption potential energy diagram (Crittenden and Thomas, 1998)..... 32
Figure 2.14: Typical costs associated with CO_2 adsorption (Wilcox, 2012). 37
Figure 2.15: Examples of amines used in grafting or impregnation to enhance CO_2 capture (Yu *et al.*, 2012). 50
Figure 2.16: CO_2 adsorption mechanisms onto a solid adsorbent (Song et al., 2015)..... 53
Figure 3.1: Flow diagram showing a summary of the procedure……..60
Figure 3.2: Schematic showing the experimental procedure for the synthesis of PSI. 61
Figure 3.3: Process flow diagram of equipment used for optimization studies. 66
Figure 4.1: NMR analysis of PSI confirming the expected structure qualitatively. 73
Figure 4.2: NMR analysis showing relevant peaks in the chemical structure of PSI-MA-EDA.. 74

Figure 4.3: SEM imaging of PSI-MA, PSI-MEA, PSI-MA-EDA (20 % and 100 % respectively), and PSI-MEA-EDA (20 % and 100 % respectively) to a magnification of 2000 X. 76
Figure 4.4: FTIR analysis showing relevant peaks in the chemical structure of PSI. 78
Figure 4.5: FTIR analysis showing relevant peaks in the chemical structure of PSI-MA-EDA.. 78
Figure 4.6: FTIR analysis showing relevant peaks in the chemical structure of PSI-MEA-EDA.79
Figure 4.7: Thermal stability analysis of the synthesized PSI showing variation of weight with temperature, comparing PSI 1 adapted from the study by (Ngoy *et al.*, 2014), and PSI 2 – the sample from this study. 80
Figure 4.8: Thermal stability analysis of PSI-MA-EDA samples showing variation of weight loss with temperature. 81
Figure 4.9: Thermal stability analysis of PSI-MEA-EDA samples showing variation of weight loss with temperature. 81
Figure 4.10: Comparison of solubilities of varying amine-grafted PSI samples. 83
Figure 5.1: Average adsorption capacities of MA-EDA grafted PSI of varying concentrations of MA and EDA. 89
Figure 5.2: Average adsorption capacities of MEA-EDA grafted PSI of varying concentrations of MEA and EDA. 90
Figure 5.3: Rate of adsorption of PSI and amine-grafted PSI, samples 1 – 5 as a function of time. 92
Figure 5.4: Rate of adsorption of PSI and amine-grafted PSI, samples 6 – 10 as a function of time. 93
Figure 6.1: 3D surface plot of adsorption capacity with respect to flow rate and adsorption pressure at 25^{o}C. 100
Figure 6.2: Contour diagram showing the interaction between the gas flowrate and the adsorption pressure. 101
Figure 6.3: 3D surface plot of adsorption capacity with respect to flow rate and adsorption temperature at 1.6 bar. 102
Figure 6.4: Contour diagram showing the interaction between the flowrate and the adsorption temperature. 103
Figure 6.5: 3D surface plot of adsorption capacity with respect to adsorption pressure and adsorption temperature at 45 ml/min of gas. 104

Figure 6.6: Contour diagram showing the interaction between the adsorption pressure and the adsorption temperature..... 105
Figure B1: TGA results for the first adsorption run on 100 % MA grafted polysuccinimide.... 126
Figure B2: TGA results for the second adsorption run on 100 % MA grafted polysuccinimide. 127
Figure B3: TGA results for the third adsorption run on 100 % MA grafted polysuccinimide... 128
Figure B4: Average adsorption capacity of 20 % MA- 80 % EDA in 100 % CO_2 using the Q600 TA TGA. 162
Figure B5: Average adsorption capacity of 40 % MA- 60 % EDA in 100 % CO_2 using the Q600 TA TGA. 163
Figure B6: Average adsorption capacity of 60 % MA- 40 % EDA in 100 % CO_2 using the Q600 TA TGA. 163
Figure B7: Average adsorption capacity of 80 % MA- 20 % EDA in 100 % CO_2 using the Q600 TA TGA. 164
Figure B8: Average adsorption capacity of 100 % MA in 100 % CO_2 using the Q600 TA TGA. 164
Figure B9: Average adsorption capacity of 20 % MEA- 80 % EDA in 100 % CO_2 using the Q600 TA TGA. 165
Figure B10: Average adsorption capacity of 40 % MEA- 60 % EDA in 100 % CO_2 using the Q600 TA TGA. 166
Figure B11: Average adsorption capacity of 60 % MA- 40 % EDA in 100 % CO_2 using the Q600 TA TGA. 167
Figure B12: Average adsorption capacity of 80 % MEA- 20 % EDA in 100 % CO_2 using the Q600 TA TGA. 168
Figure B13: Average adsorption capacity of 100 % MEA- 0 % EDA in 100 % CO_2 using the Q600 TA TGA. 168
Figure D1: CO_2 adsorption equipment used for optimization studies.
Figure E1: Correlation between observed and estimated adsorption capacity by use of model 1. 173
Figure E2: Correlation between observed and estimated adsorption capacity by use of model 2. 174

Figure E3: Correlation between observed and estimated adsorption capacity by use of model 3. 175
Figure E4: Correlation between observed and estimated adsorption capacity by use of model 4. 176
Figure E5: Correlation between observed and estimated adsorption capacity by use of model 5. 177
Figure E6: Correlation between observed and estimated adsorption capacity by use of model 6. 178

List of Tables

Table 2.1: Formation CO_2 storage capacities (Benson, 2005; Intergovernmental Panel on Climate Change, 2005). 17

Table 2.2: Differences between physisorption and chemisorption (Wilcox, 2012). 29

Table 2.3: Different types of pores and their properties (Crittenden and Thomas, 1998). 42

Table 2.4: Some of the possible DoE designs applied in optimization studies (Lazic, 2004). 57

Table 3.1: Materials used in the synthesis of the PAA. 62

Table 3.2: Experimental range and levels 67

Table 3.3: Central composite design experimental plan 69

Table 4.1: Adsorbent synthesis yields 72

Table 4.2: BET analysis of the synthesized samples, Samples 1-10. 75

Table 4.3: Solubilities of PSI and amine-grafted PSI samples. 82

Table 5.1: Adsorption capacities of synthesized samples. 88

Table 6.1: Variance and mean error values for the best model 97

Table 6.2: ANOVA of the regression model for CO_2 adsorption by Methyl-amine (MA) grafted PSI.

Table 6.3: Cross validation results 106

Table 6.4: ANOVA analysis for the results obtained in Table 6.3 106

Table B1: TGA results for the first adsorption run on 100 % MA grafted polysuccinimide. 129

Table B2: TGA results for the second adsorption run on 100 % MA grafted polysuccinimide. 130

Table B3: TGA results for the third adsorption run on 100 % MA grafted polysuccinimide. ... 131

Table B4: TGA results for the first adsorption run on 80 % MA grafted polysuccinimide. 132

Table B5: TGA results for the second adsorption run on 80 % MA grafted polysuccinimide... 133

Table B6: TGA results for the third adsorption run on 80 % MA grafted polysuccinimide. 134

Table B7: TGA results for the first adsorption run on 60 % MA grafted polysuccinimide. 135

Table B8: TGA results for the second adsorption run on 60 % MA grafted polysuccinimide... 136

Table B9: TGA results for the third adsorption run on 60 % MA grafted polysuccinimide. 137

Table B10: TGA results for the first adsorption run on 40 % MA grafted polysuccinimide. 139

Table B11: TGA results for the second adsorption run on 40 % MA grafted polysuccinimide. 140

Table B12: TGA results for the third adsorption run on 40 % MA grafted polysuccinimide. ... 141

Table B13: TGA results for the first adsorption run on 20 % MA grafted polysuccinimide. 142

Table B14: TGA results for the second adsorption run on 20 % MA grafted polysuccinimide. 143
Table B15: TGA results for the third adsorption run on 20 % MA grafted polysuccinimide. ... 144
Table B16: TGA results for the first adsorption run on 100 % MEA grafted polysuccinimide. 145
Table B17: TGA results for the second adsorption run on 100 % MEA grafted polysuccinimide. 146
Table B18: TGA results for the third adsorption run on 100 % MEA grafted polysuccinimide.148
Table B19: TGA results for the first adsorption run on 80 % MEA grafted polysuccinimide... 149
Table B20: TGA results for the second adsorption run on 80 % MEA grafted polysuccinimide. 150
Table B21: TGA results for the third adsorption run on 80 % MEA grafted polysuccinimide.. 151
Table B22: TGA results for the first adsorption run on 60 % MEA grafted polysuccinimide... 152
Table B23: TGA results for the second adsorption run on 60 % MEA grafted polysuccinimide. 153
Table B24: TGA results for the third adsorption run on 60 % MEA grafted polysuccinimide.. 154
Table B25: TGA results for the first adsorption run on 40 % MEA grafted polysuccinimide... 155
Table B26: TGA results for the second adsorption run on 40 % MEA grafted polysuccinimide. 157
Table B27: TGA results for the third adsorption run on 40 % MEA grafted polysuccinimide.. 158
Table B28: TGA results for the first adsorption run on 20 % MEA grafted polysuccinimide... 159
Table B29: TGA results for the second adsorption run on 20 % MEA grafted polysuccinimide. 160
Table B30: TGA results for the first adsorption run on 20 % MEA grafted polysuccinimide... 161
Table E1: Variance and mean error values for the proposed models.
Table E2: Coefficient values for models 1 to 6 shown in Equations 5 to 10.

Nomenclature

Ads: Adsorbent

BET: Brunauer, Emmett, and Teller

CCS: Carbon Capture and Storage

DCC: Di-cyclo-hexyl-carbodiimide

DMF: Dimethylformamide

EDA: Ethylenediamine

EOR: Enhanced Oil recovery

FTIR: Fourier transform infrared

GHG: Greenhouse gas

IEA: International Energy Agency

MA: Methyl Amine

MEA: Mono-ethanol Amine

NMR: Nuclear Magnetic Resonance

PSA: Pressure Swing Adsorption

PSI: Poly-DL-Succinimide

RSM: Response Surface Methodology

SACCCS: South African Centre for Carbon Capture and Storage

SEM: Scanning Electron Microscope

Syngas: Synthetic Gas

TGA: Thermo-gravimetric Analyzer

TSA: Temperature Swing Adsorption

VSA: Vacuum Swing Adsorption

Chapter 1: Introduction

1.1 Motivation and Background

The world today is facing an ever-increasing demand for cheap, reliable energy, most of which is met by use of fossil fuels (Kohli *et al.*, 2004). The increasing demand can be attributed to the fact that global population has been increasing since the industrialization age, with a world population in the year 2009 of approximately 6.8 billion (Administration, 2013). The world population is expected to rise to about 7.3 billion by the year 2015 and about 8.3 billion by the year 2030 (Administration, 2013). The increase in the world population implies an increase in the demand for energy as producing industries and economies will have to grow to accommodate the population growth (Koskimäki, 2012; Mohammed *et al.*, 2013). This implies that the exploitation of fossil fuel reserves will continue for the greater part of the century (Höök & Tang, 2013). The fossil fuels mainly used for the supply of energy are oil, natural gas and coal (Pires *et al.*, 2011). Figure 1.1 shows that the world is largely dependent on fossil fuels (International Energy Agency, 2012; International Energy Agency, 2013).

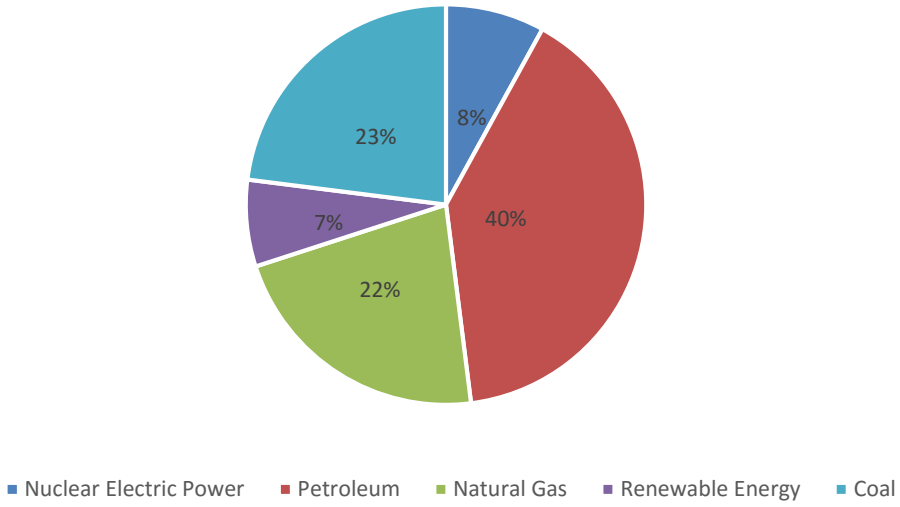


Figure 1.1: World energy supply proportions adapted from (International Energy Agency, 2013).

Thus, fossil fuels are projected to remain a major source of energy for future decades. This is because of the abundant supply of fossil fuels on the planet and their ease of accessibility for

processing to produce cheap, reliable energy (Jian-Rong *et al.*, 2011). However, fossil fuels produce combustion products that are harmful to the environment (Garret, 1992). In the production of energy, fossil fuels combust to create heat energy and carbon dioxide (CO_2) as the main products (Casper, 2010; Garret, 1992). Carbon dioxide (CO_2) is a greenhouse gas (GHG) which contributes significantly to the greenhouse effect (Garret, 1992). The greenhouse effect is the containment of heat radiated by the earth's surface by the GHG's. An increase in CO_2 atmospheric concentration results in gradual increase in the earth's temperatures (Garret, 1992).

Energy production counts for approximately 80% of the world's CO_2 emissions (Höök & Tang, 2013; Susarla *et al.*, 2015). Since the beginning of the industrial age, CO_2 atmospheric concentrations have risen from approximately 280 to 390 ppm in 2011 (Jian-Rong *et al.*, 2011). In as much as CO_2 is a GHG, it is still uncertain that the recent climate changes can be completely attributed directly to CO_2, but there are strong correlations between global warming and the increase in the concentration of CO_2 in the atmosphere (Jian-Rong *et al.*, 2011).

1.2 Possible effects of Global Warming

According to Bouzalakos and Mercedes Maroto-Valer (2010), there is no doubt that anthropogenic GHG's will result in global warming, as their presence in the atmosphere intensifies the greenhouse effect. The expanse of global warming and its impacts are, however, uncertain (Bouzalakos & Mercedes Maroto-Valer, 2010). Bouzalakos and Mercedes Maroto-Valer (2010) and the Intergovernmental Panel on Climate Change (IPCC) have called for the stabilization of GHG concentrations as a precaution as the effects of climate change can be devastating in different regions of the world (Intergovernmental Panel on Climate Change, 2005). According to Tao *et al.* (2014) it is estimated that warming of the atmosphere might result in pest management challenges and ultimately food security issues; outbreaks in pests are expected particularly during periods of long drought with heavy rainfall following the drought. In China, there have been studies on wheat growth from 1981-2009, and the results from the study show that lengths of growth periods had significantly become shorter. This was correlated to significant changes in the climate during the wheat growing period (Tao *et al.*, 2014). From the aforementioned, mitigation of climate change causes is necessary as it will impact positively on food security in different regions.

Furthermore, climate change may result in a rise in global surface temperatures, changes to hydrological cycles, ocean acidification and rise in mean sea levels. Higher occurrences of harsh weather events such as storm surges, heavy precipitation and heat waves, amongst others (Bouzalakos & Mercedes Maroto-Valer, 2010; Chandramowli & Felder, 2014). These harsh weather occurrences will most likely have impacts on supply and generation of power with detrimental effects on world economies and the growing global population (Chandramowli & Felder, 2014). For the power plant production side of the power industry, warming temperatures may result in higher surface temperatures and higher cooling water temperatures which will lead to lower equipment efficiencies and lower equipment life spans (Chandramowli & Felder, 2014). This will impact the consumers, with more power cuts being experienced as there will be production cuts due to insufficient production.

Water bodies on the planet such as oceans act as sinks for CO_2 and participate in the world carbon cycle (Czaun *et al.*, 2013). As the CO_2 concentrations in the atmosphere increase, more CO_2 dissolves into the water bodies lowering water pH making the water acidic (Czaun *et al.*, 2013). In oceans, coral reefs and shell making organisms are destroyed by the acidic water, leading to crumbling of food chains and possible extinction of some aquatic living organisms (Czaun *et al.*, 2013). Mitigation of CO_2 emissions will therefore alleviate the destruction of such eco-systems. Furthermore, the projected effects of increasing CO_2 concentrations in the atmosphere have severe consequences on the environment and well-being of human beings and thus require solutions to reduce CO_2 emissions (Intergovernmental Panel on Climate Change, 2005).

1.3 Existing CO_2-reduction technologies

Several solutions to reduce CO_2 emissions are currently in application. These technologies include renewable energy technologies such as wind and solar energy, the use of less carbon intensive fuels such as natural gas and hydrogen, the improvement of energy efficiency of electrical appliances in industry and in homes, enhancing biological sinks such as forests, and the use of CO_2 capture and storage (CCS) technology (Intergovernmental Panel on Climate Change, 2005; Letcher, 2014).

CCS is a technology in which CO_2 is separated from other gases at a point source, compressed, transported and stored in various geological formations (Hammond & Spargo, 2014; Pires *et al.*, 2011). Three CO_2 capture methods exist and these are pre-combustion capture, post-combustion capture, and oxy-fuel combustion capture (Bouzalakos & Mercedes Maroto-Valer, 2010). The capture techniques that are available for application in these three methods are membrane separation, cryogenic distillation, absorption and adsorption (Pires *et al.*, 2011). Carbon Capture and Storage (CCS) technology is advantageous compared to most other technologies used to mitigate the global warming challenge, because it enables the continued use of fossil fuels for the supply of energy with a limited impact on the environment (Bouzalakos & Mercedes Maroto-Valer, 2010; Intergovernmental Panel on Climate Change, 2005; Pires *et al.*, 2011)

It is estimated that 47% of total CO_2 emissions in Europe can be reduced by the use of CCS technology (Bouzalakos & Mercedes Maroto-Valer, 2010). Globally, it is estimated that application of CCS technology could potentially reduce CO_2 emissions by between 14 % and 40 % per annum (Bouzalakos & Mercedes Maroto-Valer, 2010). Carbon Capture and Storage (CCS) is thus a promising technology, and if applied could result in significant CO_2 abatement. In sub-Saharan Africa, South Africa is the largest emitter of CO_2 with an economy predominantly dependent on coal for energy production, and is the thirteenth highest emitter of CO_2 globally (Seymore *et al.*, 2014). South Africa's position in the world CO_2 emission rankings and sub-Saharan rankings due to high reliance on coal for energy show the need for mitigating CO_2 emissions (Pollet *et al.*, 2015). It is therefore necessary that drastic measures be taken to reduce CO_2 emissions in South Africa. In this regard, CCS technology is ideal in the South African context as South Africa is and will be depending heavily on coal for energy for a significant part of the century (Pegels, 2010; Surridge & Cloete, 2009).

1.4 Applications of CCS

Data obtained from the International Energy Agency (2012, 2013) shows that electricity generation, transport and industrial sectors are the most dominant sources of CO_2 emissions, accounting for a total of 80 % of the world's CO_2 emissions. Therefore, application of CCS technologies to these three major sources could reduce CO_2 emissions significantly.

In the world at large, power plants are the leading contributors of anthropogenic CO_2 emissions and similarly this is the case in South Africa. Cutting down CO_2 emissions from power plants will invariably decrease CO_2 emissions significantly (Hammond & Spargo, 2014). Applying CCS to large point sources such as power plants will also bring about favorable economies of scale (Nordic Council of Ministers, 2007). As the point source increases in size, the cost of CCS of that source will decrease as the fixed costs will be distributed over a larger source (Nordic Council of Ministers, 2007). This will make the technology cheaper to apply, while at the same time cutting down on CO_2 emissions. In CCS technology, the capture component is the most costly component, costing approximately two thirds of the total CCS process cost (Bouzalakos & Mercedes Maroto-Valer, 2010; Pires *et al.*, 2011). In this regard, there is need to investigate economical ways of capturing CO_2. CCS is being applied at several large scale projects around the world. For example, CCS is being applied at the Boundary Dam project in Canada where a power plant was retrofitted with a CO_2 capturing capacity of 1 Million tonnes per annum and at In Salah in Algeria (Global CCS Institue, 2015). This project was commissioned in October 2014 and has so far been a success. The Sleipner CO_2 storage project has been capturing CO_2 and storing it in the North Sea since 1996 (Global CCS Institue, 2015). According to the Global CCS Institute (2015), there are fifteen large scale CCS projects in operation and a further seven are under construction.

1.5 Problem Identification

South Africa's energy demands are largely met by the use of coal in coal-fired power plants (Snyman & Botha, 1993). Coal, being a fossil fuel, produces CO_2 when combusted to produce energy. South Africa ranks highly in global CO_2 emissions, contributing approximately 1.5 % of the world's CO_2 emissions while coming third in the global CO_2 emissions per capita (Urban Earth, 2012). South Africa's grid system is supported by a mix of coal-fired power stations, a nuclear power station, hydroelectricity and pump storage as well as gas turbines (Eskom, 2015). Coal-fired power stations supply approximately 77 % of South Africa's energy needs consequently making them the highest emitters of CO_2 in the country (Eskom, 2015). Given that these coal-fired power stations are already in existence with two major ones coming online at their full capacity soon, post-combustion capture CO_2 capture is a probable solution to reducing CO_2 emissions. Currently in South Africa, CCS has not been commercialized. The government

of South Africa has mandated the South African Centre for Carbon Capture and Storage (SACCCS) to tackle the CO_2 emissions mitigation challenge by research and use of CCS.

As stated, CCS is a technology with potential to reduce CO_2 emissions. CCS offers the incentive of continued fossil fuel use with reduced CO_2 emissions. However, CCS technology in South Africa is still at the research stage, with particular emphasis on the storage component. Research in this area is largely managed by the South African Centre for Carbon Capture and Storage (SACCCS), along with the Council for Geosciences and academic institutions. There is need to focus on the capture component because CO_2 has to be captured first before it can be stored. The most mature technologies in CO_2 capture are absorption and adsorption with absorption being the more mature of the two (Pires *et al.*, 2011). Absorption, however, presents several challenges when applied to CO_2 capture. To mention a few, the solvents (predominantly alkanolamines) used in absorption are corrosive to equipment as well as toxic to the environment, and this implies high capital costs and environmental degradation (Bouzalakos & Mercedes Maroto-Valer, 2010; Dasgupta *et al.*, 2015; Susarla *et al.*, 2015). High energy is also required for the regeneration of the solvents after the CO_2 capture resulting in high operating costs (Bouzalakos & Mercedes Maroto-Valer, 2010). Absorbents are also generally required in large quantities and they degenerate easily when exposed to oxygen (Svendsen *et al.*, 2011).These challenges with absorption have paved the way for the application of adsorption technology in CO_2 capture. However, the adsorption technology is faced with challenges such as low adsorption capacity, poor adsorption selectivity and adsorbent regeneration (Spigarelli & Kawatra, 2013).

Against this background, effort has been aimed at synthesizing and optimizing the performance of Polyaspartamide (PAA) material, an adsorbent for the post-combustion CO_2 capture from South African coal-fired power plants. The scope of the study was limited to synthesis, characterization, performance evaluation of the synthesized PAA using laboratory scale equipment and optimization of the adsorption capacity using the response surface methodology (RSM) approach. At this stage, the developed material has not been tested for CO_2 capture at any of the South African coal-fired power plants but it is aimed that the performance evaluation of the material will be conducted on-site in the near future.

1.6 Research Hypotheses and Questions

In this research, it was expected that CO_2 adsorption capacity might be higher in amine-grafted Poly-DL-Succinimide (PSI) (Polyaspartamide (PAA)) than PSI without amine grafting, due to the presence of the amine group available on PAA. In addition, it was expected that the adsorption performance of this material might be influenced by the conditions at which the adsorption is carried out. To evaluate these hypotheses, the following questions were examined in the course of this research.

i. Can amine-grafted PSI (PAA) display higher adsorption capacity for CO_2 than PSI with no amines?
ii. Could variation of the amines grafted onto PSI affect the adsorption capacity for CO_2?
iii. What will the effect of adsorption operating variables (temperature, pressure and gas flowrate) be on CO_2 adsorption capacity of the best amine-grafted PSI sample?

1.7 Research Aim and Objectives

The aim of this research is to synthesize, characterize, determine the adsorption capacity and investigate the effects of operating variables on the adsorption capacity of the material via RSM approach. The specific objectives of the research were:

i. To synthesize Poly-DL-Succinimide (PSI) and amine-grafted PSI (PAA) with varying amounts of amine as well as different amines, and to characterize the synthesized material with Nuclear Magnetic Resonance (NMR) analysis, Fourier Transform Infrared Spectroscopy (FTIR), Scanning Electron Microscopy (SEM), N_2 physisorption (by BET analysis) and thermo-gravimetric analyses (TGA).
ii. To conduct CO_2 adsorption tests on the materials to evaluate and compare their performance for CO_2 adsorption.
iii. To synthesize amine-grafted PSI with varied water-soluble component, characterize and conduct CO_2 adsorption test to compare their performance and hence deduce the effect of the water-soluble component on their adsorption performance.

iv. Conduct statistically designed experiments to investigate the effects of operating variables (adsorption temperature, adsorption pressure, gas flowrate) on the CO_2 adsorption capacity of the materials.

1.8 Expected outcomes

The following outcomes were anticipated from the research:

i. A synthesized water soluble PAA (amine-grafted PSI) adsorbent with higher CO_2 adsorption capacity relative to the base material.
ii. Information on the effect of operating variables in the CO_2 adsorption performance of PAA (amine-grafted PSI) and the optimum operating conditions possible for the material.
iii. Peer reviewed paper publications.
iv. Conference presentations
v. A well-documented report in the form of a dissertation and an award.

Chapter 2: Literature Review

2.1 Introduction

The literature review delves into the details of CCS, starting with the history of CCS followed by technologies for mitigating the effects of CO_2 emissions on the environment. The stages in CCS will then be discussed, with emphasis on CO_2 capture. Different approaches to capture CO_2, and techniques for CO_2 capture with emphasis on adsorption are discussed. The literature review goes on to look at different types of adsorbents, adsorption mechanisms during CO_2 capture, factors influencing adsorption and lastly optimization studies in CO_2 capture via adsorption.

2.2 History of Carbon dioxide capture and storage

Fossil fuels such as crude oil, natural gas and coal are the major sources of energy today (Pires *et al.*, 2011). Figure 2.1 shows that approximately 40 years ago the world was dependent on fossil fuels and in the modern day, the world is still dependent on fossil fuels (International Energy Agency, 2012; International Energy Agency, 2013). However, as mentioned in Chapter 1, fossil fuels result in CO_2 emissions which have detrimental effects on the environment. This led to the need and development of solutions to reduce CO_2 emissions, with the continued supply of energy from fossil fuels, resulting in the initiation of CCS.

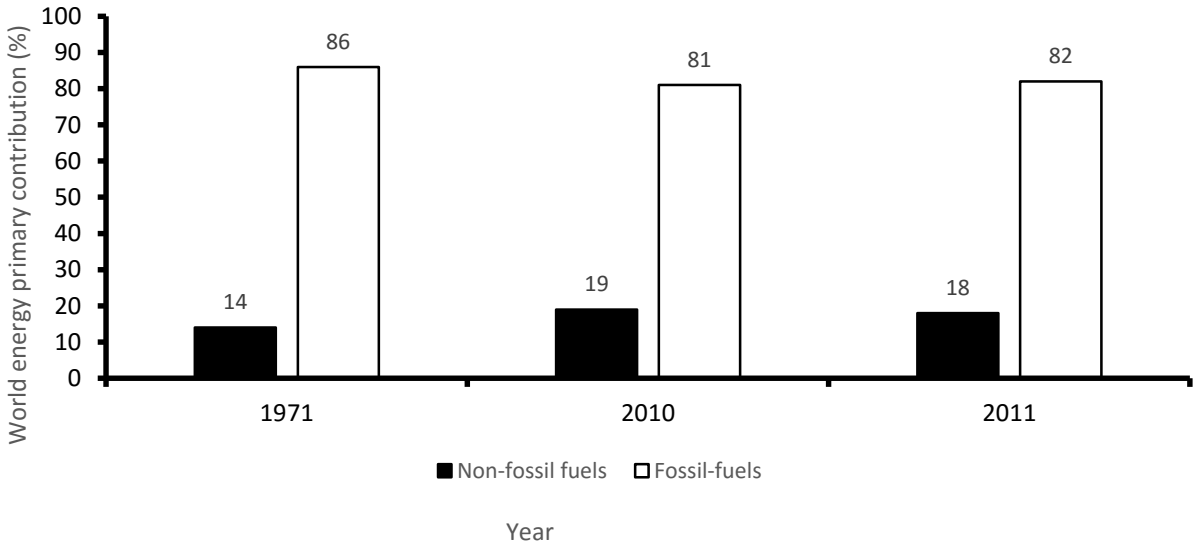


Figure 2.1: World energy supply proportions (Adapted from International Energy Agency (2013)).

CCS originated from the use of Enhanced Oil Recovery (EOR) which began in the United States of America (USA) in the early 1970s (Capture Ready, n.d.). Studies on CCS commenced in 1989 under the Carbon Capture and Sequestration Technologies (CCSTP) at MIT (Capture Ready, n.d.). Elsewhere in the world, the Norwegian government implemented a tax on CO_2 emissions in 1991, which was to be the major driver for the establishment of the world's first commercial CCS project (Black *et al.*, 2013; Capture Ready, n.d.). Five years later, the world's first major CCS project commenced in Norway in the North Sea at Sleipner where 1 million tonnes per annum of CO_2 are being captured up to today and stored in the Utsira formation (Capture Ready, n.d.; Global CCS Institute, 2015). From this point in time, CCS has been proven to be a possible solution to the reduction of CO_2 emissions. Further research, as well as other large scale CCS projects were initiated and today there are 15 large scale CCS projects in operation with a further 7 under construction (Global CCS Institute, 2015). Further information on this is further discussed in section 2.2.

2.3 Mitigating CO_2 emissions

Carbon dioxide emissions can be related to the size of a population, level of global wealth, energy intensity of the global economy and emissions arising from production and use of energy by the Kaya relation in Equation 2.1 (Intergovernmental Panel on Climate Change, 2005; Olajire, 2010; Pires *et al.*, 2011):

$$CO_2 emissions = P \times \frac{GDP}{P} \times \frac{E}{GDP} \times \frac{E_m}{E} - S \qquad (2.1)$$

Kaya's relationship shows that the terms that can be manipulated to successfully reduce anthropogenic CO_2 emissions are $\frac{E_m}{E}$ and S. To reduce anthropogenic CO_2 emissions the ratio $\frac{E_m}{E}$ has to decrease. This can be achieved by the use of renewable energy rather than fossil fuels, improving energy end-use efficiency, improving power plant efficiency and using less carbon intensive fuels such as natural gas (Intergovernmental Panel on Climate Change, 2005). Anthropogenic CO_2 emissions can also be reduced by increasing CO_2 sinks, S. This can be achieved by increasing the natural CO_2 sinks such as forests, using CO_2 in the manufacture of products or by capturing CO_2 at the point of production and storing it (Carbon Capture and Storage-CCS). Figure 2.2 shows the various technologies that can be adopted to reduce CO_2

emissions. There is need to incorporate several technologies to effectively reduce CO_2 emissions as there is no single technology that can solve the challenge alone (Intergovernmental Panel on Climate Change, 2005).

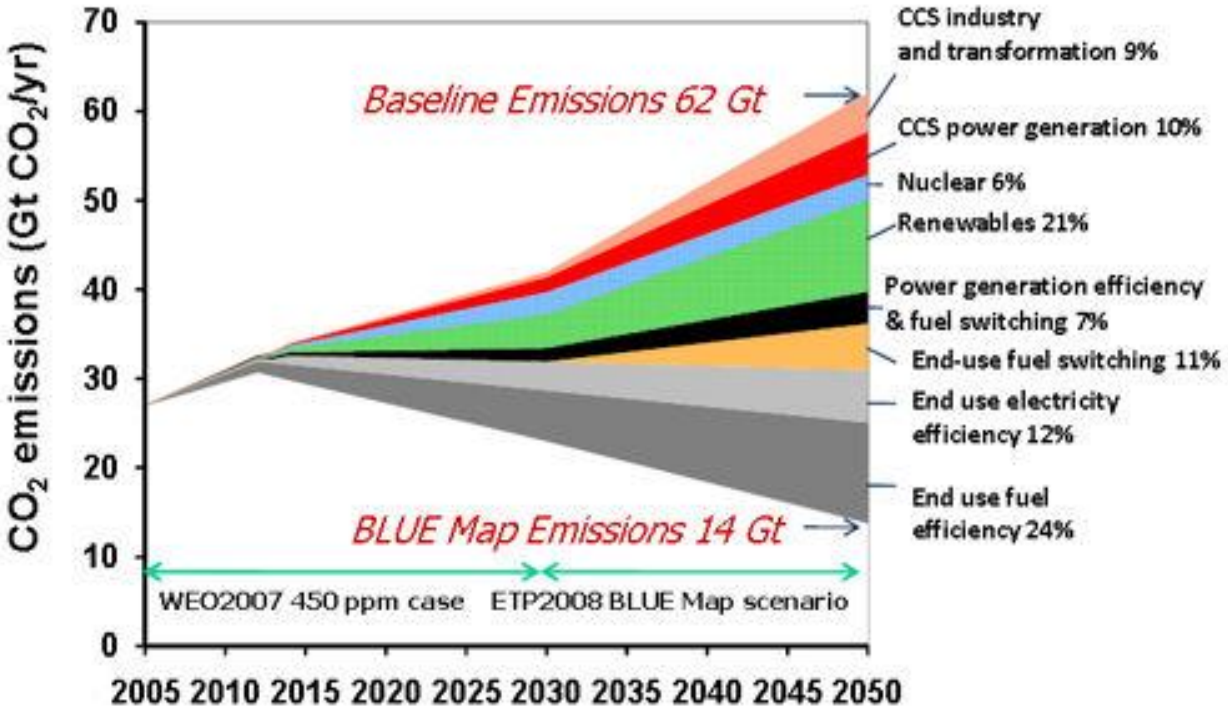


Figure 2.2: Possible solutions to reducing CO_2 emissions (International Energy Agency, 2012).

The dependence of the world on fossil fuels implies that CO_2 emissions are likely to continue for the greater part of the century (Höök & Tang, 2013). This implies that there is need to continue using fossil fuels, but with minimum impact on the environment. It is therefore of paramount importance that research into ways of continued fossil fuel use with minimum possible environmental impact be done. Of the possible solutions in Figure 2.2, CCS allows for the continued use of fossil fuels with minimum impact on the environment as the CO_2 will be captured at the point of production and stored (Pires *et al.*, 2011). Figure 2.2, known as a wedge diagram, shows the possible ways of reducing CO_2 emissions, with each wedge representing how much CO_2 emissions as a percentage may be avoided. Here, CCS coupled to power generation as well as to industry has the potential to reduce CO_2 emissions by 20 %. The need to continue using fossil fuels is what fueled the birth of CCS. Thus, this research focuses on CCS as a method of reducing CO_2 emissions with continued use of fossil fuels, and in particular carbon capture.

2.4 Carbon dioxide Capture and Storage (CCS)

2.4.1 Meaning of CCS and its benefits

CCS is a common abbreviation for CO_2 Capture and Storage (Intergovernmental Panel on Climate Change, 2005). CCS has three major processes in which CO_2 is handled. The first is CO_2 capture, which is a process in which CO_2 gas is concentrated and separated from other gases (Intergovernmental Panel on Climate Change, 2005; Pires *et al.*, 2011). The second process is CO_2 compression and transport which entails the compression of gaseous CO_2 to a super critical fluid and the ferrying of the super critical CO_2 fluid to the storage site (Intergovernmental Panel on Climate Change, 2005; Wang *et al.*, 2011; Yang, 2003). The final process is the storage of the super critical CO_2 fluid into a storage site (Intergovernmental Panel on Climate Change, 2005). Figure 2.3 shows the stages involved within CCS.



Figure 2.3: Schematic showing the stages in Carbon Capture and Storage (CCS).

The aforementioned stages in CCS are discussed as follows:

(i) CO_2 storage

CO_2 storage is defined as the long-term quarantine of CO_2 from the atmosphere (Bouzalakos & Mercedes Maroto-Valer, 2010). The quarantine of CO_2 is done by injection into the sub-surface of the earth (Intergovernmental Panel on Climate Change, 2005; Mabon *et al.*, 2014). This long-term time period has been defined to be approximately 1000 years. The long-term quarantine of CO_2 is most promising in underground geological formations with a few large scale projects currently running (Intergovernmental Panel on Climate Change, 2005).

Injection of CO_2 underground was first explored in West Texas in the early 1990's, particularly for EOR (Intergovernmental Panel on Climate Change, 2005). CO_2 injection has continued since

then and is still on-going in West Texas, Weyburn Saskatchewan and many other parts of the world. The storage of CO_2 in geological formations gained momentum in the 1990's when research in CO_2 storage as a CO_2 emission mitigation option became popular. Geological storage of CO_2 is considered a significant solution for CO_2 emission reduction (Mabon *et al.*, 2014). The world's first large scale storage project started in 1996, being the Sleipner Gas field in the North Sea, where approximately 1Million tonnes of CO_2 is stored annually in saline aquifers; the CO_2 is extracted from the natural gas (Intergovernmental Panel on Climate Change, 2005). Several other projects are currently running or are in the planning phase. Figure 2.4 is a snip from the Understanding the Long-Term fate of geologically stored CO_2 (ULTimate CO_2) (2015) interactive map which shows commercially significant CO_2 storage projects all around the world.



Figure 2.4: CO_2 storage projects all around the world (Understanding the Long-Term fate of geologically, 2015).

For CO_2 to be stored underground, it must be compressed to a dense supercritical fluid (Intergovernmental Panel on Climate Change, 2005). In this state, the available geological storage space will be maximized allowing for maximum possible storage. This is because the density of CO_2 increases with depth. At a depth of about 800 m, the density rapidly increases with an associated rapid decrease in volume (Intergovernmental Panel on Climate Change, 2005). Geological formations are first characterized to determine if they are suitable for long-

term quarantine of CO_2 (Intergovernmental Panel on Climate Change, 2005; Manancourt & Gale, 2005). The characterization process entails studies on permeability, thickness, capacity, geological structure and lithology of the storage site (Câmara *et al.* 2013). The characterization process aims to determine whether the storage site has adequate capacity for storage of CO_2, whether the storage site is CO_2 injectable, whether the storage site has a capable seal and whether the environment of the storage is geologically stable (Intergovernmental Panel on Climate Change, 2005).

Carbon dioxide storage starts with the drilling of wells to inject the CO_2 into the geological storage media (Liebscher & Munch, 2015). The CO_2 is then pumped down the injection well which has perforations in the section that is inside the geological formation being used for storage (Intergovernmental Panel on Climate Change, 2005; Liebscher & Munch, 2015). As the CO_2 is injected into the well, it flows through several different mechanisms from the well into the storage site. These several different mechanisms include fluid flow due to pressure gradients, buoyancy, pore space trapping, dissolution and diffusion (Gluyas & Mathias, 2013). For CO_2 to remain in the geological formation, it has to be trapped by some mechanism. There are several mechanisms by which CO_2 can remain underground: trapping in permeable rock overlain by an impermeable rock, confining layer, retention as an immobile phase trapped in the pore spaces of the storage formation, dissolution in the in-situ formation fluids and/or adsorption onto organic matter in coal and shale, reaction with minerals in the storage formation and cap-rock to produce carbonate minerals (Intergovernmental Panel on Climate Change, 2005). Due to the occurrence of multiple trapping mechanisms, CO_2 becomes less mobile with time implying lower chances of leakage. During the storage project up to the end of the CO_2 injection and for a considerable time after the injection is stopped, it is essential that the formation be monitored for leaks and for knowledge as to how the CO_2 is migrating through the formation (Benson, 2005).

According to Bouzalakos and Mercedes Maroto-Valer (2010), there are three main types of sedimentary formations proposed for underground storage: deep saline aquifers, depleted oil and gas reservoirs (with EOR included here as well), and deep unmineable coal seams. Manancourt and Gale (2005), however, define depleted gas reservoirs and depleted oil reservoirs as two different types of geological sedimentary formations suitable for CO_2 storage, increasing the different types of formations from three to four. Sedimentary basins are most suitable for CO_2

storage with caverns, basalt and organic rich shales in consideration (Intergovernmental Panel on Climate Change, 2005; Manancourt & Gale, 2005). Figure 2.5 shows the different types of formations in a sedimentary basin, suitable for CCS, each of which is briefly discussed below. Injection of CO_2 for storage in geological formations can be done on-shore and/or offshore (Intergovernmental Panel on Climate Change, 2005). In addition Figure 2.5 also shows EOR, Enhanced Coal Bed Methane (ECBM) recovery as well as Enhanced Gas Recovery (EGR).

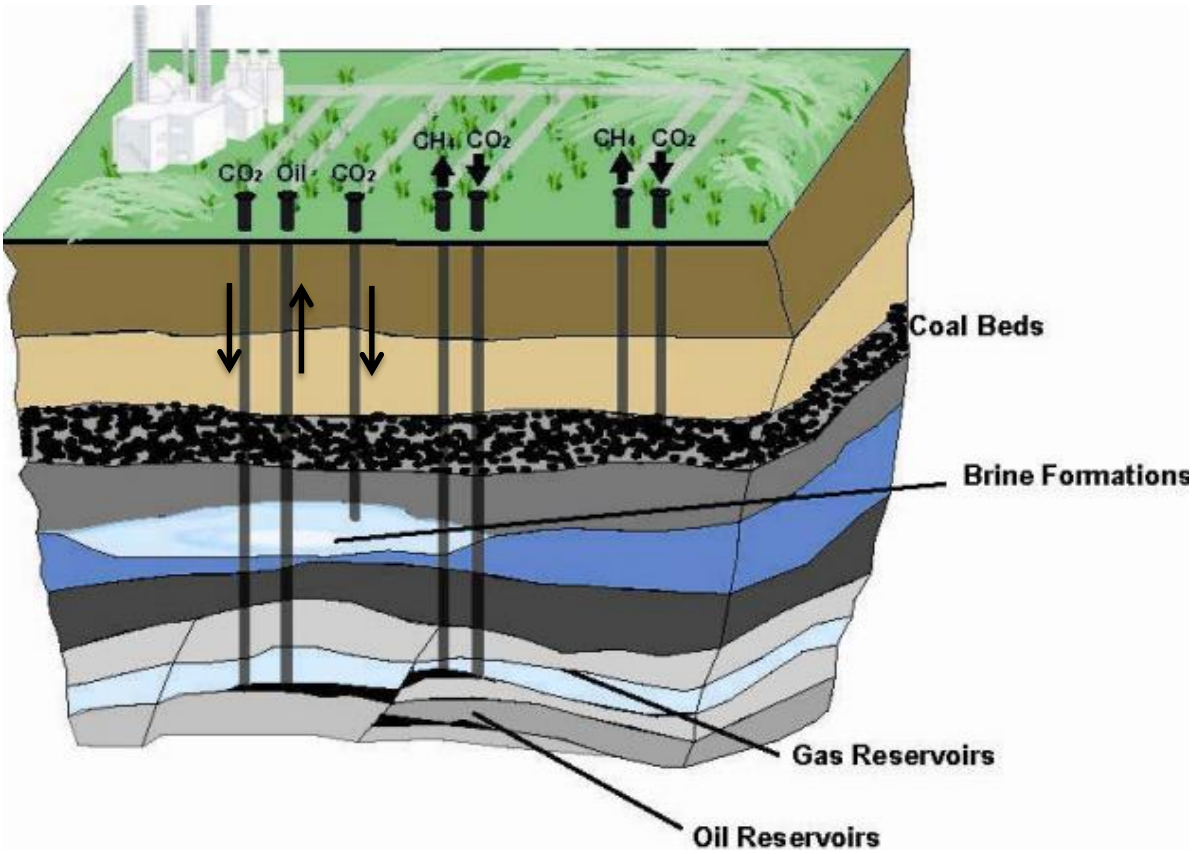


Figure 2.5: Schematic showing the four different types of sedimentary formations suitable for CO_2 storage (Liebscher & Munch, 2015).

Benson (2005) and the Intergovernmental Panel on Climate Change (2005) state that depleted oil and gas reservoirs are primary targets for CO_2 capture. The reason for this being that these reservoirs held oil and gas for several million years with no structural failure, resembling storage security. Information on these reservoirs is already quite extensively known, as they have been studied and well characterized, hence allowing for further study for CO_2 storage (Benson, 2005). Oil and gas have already been or are still being extracted from these reservoirs, implying that infrastructure is still in place at these sites (Intergovernmental Panel on Climate Change, 2005).

This infrastructure may also be used for exploration of CO_2 storage within these reservoirs. In addition, CO_2 injection may aid oil and gas recovery, thus extending the life of the oil / gas field. An example of a successful EOR project is at Weyburn in Canada where over 20 million tonnes of CO_2 have been injected since October 2000 (Intergovernmental Panel on Climate Change, 2005). The source of the CO_2 is the coal gasification from the Great Plains Synfuels Plant near Beulah, North Dakota.

Saline formations also make good storage sites for CO_2. Saline formations are defined in the Intergovernmental Panel on Climate Change (2005) report as deep sedimentary rocks with formation water containing high concentration of dissolved salts (brine). The CO_2 is injected into the saline formation and dissolves in the brine solution (Intergovernmental Panel on Climate Change, 2005). The Sleipner project in the North Sea is an example of CO_2 storage in a saline formation. Studies and simulations at this particular storage site have shown that the CO_2 dissolved in the brine will eventually sink to the bottom of the reservoir, ensuring that no CO_2 will leak from the formation (Intergovernmental Panel on Climate Change, 2005; Liebscher & Munch, 2015).

Coal seams are also a possible formation that can be used for CO_2 storage. Coal contains cleats which have significantly large number of micro-pores which enable movement of gas molecules and adsorption onto the coal (Maroto-Valer, 2010). Coal also has a higher affinity for CO_2 than methane (CH_4) and hence CO_2 can be applied in Enhanced Coal Bed Methane Recovery (ECBM). This offers some advantage as there is financial gain from CH_4 production and CO_2 is also stored. Other possible CO_2 storage geological media still under research include basalts, oil and gas rich shale, salt caverns and abandoned mines.

Thus, there is a wide range of possible storage capacity of CO_2 reported. Column 1 (Table 2.1) has been adopted from Benson (2005) and shows the capacities of different geological formations. Similarly, Column 2 has been adopted from the Intergovernmental Panel on Climate Change (2005) and shows capacities of different geological formations as well.

Table 2.1: Formation CO_2 storage capacities (Benson, 2005; Intergovernmental Panel on Climate Change, 2005).

Formation type	**Capacity ($GtCO_2$)** (Benson, 2005)	**Capacity ($GtCO_2$)** (Intergovernmental Panel on Climate Change, 2005)
Oil and Gas fields	~ 450	~ 675
Coal seams	60 - 150	3 – 200
Saline formations	300-10 000	1 000 – 10 000

The data in the two columns shows some degree of variation. These figures also include the storage sites that cannot be exploited economically.

With regards to legal, regulatory framework and safety, Benson (2005) and Intergovernmental Panel on Climate Change (2005) mention that it is important for regulations to be put in place for effective CCS. Currently in South Africa, research is underway, facilitated by SACCCS, to determine CO_2 storage potential (Chabangu *et al.*, 2014; Chabangu *et al.*, 2014). In 2010, a storage atlas showing the potential CO_2 storage sites in South Africa was published. However, the general overview is that South Africa does has limited storage capacity with no significant oil / gas industry to apply EOR and no saline aquifers (Chabangu *et al.*, 2014; Chabangu *et al.*, 2014). Whilst this aspect is very important, it is beyond the scope of the current project and is not discussed further.

(ii) CO_2 transport

CO_2 transport entails the movement of CO_2 from the source to the storage site (Intergovernmental Panel on Climate Change, 2005), thus acting as a link between where the CO_2 is produced and where the CO_2 is stored (Forbes *et al.*, 2008). Transportation of CO_2 can be done in its three different phases, which are solid, liquid and gas (Forbes *et al.*, 2008; Intergovernmental Panel on Climate Change, 2005). However, CO_2 is predominantly transported as a liquid due to the high energy costs associated with solidifying and transporting it as a solid, and also the large volume that would be required to transport it as a gas (Intergovernmental Panel on Climate Change, 2005). According to Forbes *et al.* (2008), to achieve efficient CO_2 transport,

the CO_2 being transported should be in the supercritical state. CO_2 exists in a supercritical state from a pressure of 73 atm and a temperature of 31 ^oC (Brown *et al.*, 2012). Forbes *et al.* (2008) states that CO_2 is usually transported in the temperature range from 12.8 ^oC to 43.3 ^oC and a pressure range from 85 atm to 149.6 atm. Pipelines, ship, rail and road tankers are the means used to transport CO_2 (Forbes *et al.*, 2008; Intergovernmental Panel on Climate Change, 2005).The ship, rail and road tanker system requires storage at the site of CO_2 production in the event that the carrier is not available and the actual tanker to ferry the CO_2 to the storage site (Forbes *et al.*, 2008; Intergovernmental Panel on Climate Change, 2005). The pipeline system consists of compressors, valves, booster pumps, pig launchers and receivers, batching stations and instrumentation, metering stations and Supervisory Control and Data Acquisition (SCADA) systems (Forbes *et al.*, 2008; Holloway et al., 2006). To mitigate CO_2 emissions, large amounts of CO_2 will have to be transported from capture points, to storage points hence pipelines are the most favorable means of transport (Intergovernmental Panel on Climate Change, 2005). According to Forbes *et al.* (2008), the ship, rail and road tankers cost twice that which pipelines cost to transport CO_2 hence making pipeline transport the preferred means of transport for bulk CO_2 for CCS.

Currently, bulk CO_2 transport is done in the food and beverage industry, as well as the oil and petroleum industry (Intergovernmental Panel on Climate Change, 2005). In the food and beverage industry, CO_2 transport is done by means of road and ship tankers, because of the small quantities transported, whereas the oil and petroleum industry makes use of pipeline transport (Holloway *et al.*, 2006). In the world today, most CO_2 transport is done for EOR, mainly in the United States of America (USA) (Intergovernmental Panel on Climate Change, 2005). Examples of existing pipelines used for CO_2 transport include the Canyon Reef, which was the first CO_2 pipeline in the USA. Its stretches for 352km and has moved 12000 tonnes of man-made CO_2. The Bravo Dome Pipeline with a possible capacity of 7.3 Mt of CO_2 per year is also an example. Further examples include the Cortez pipeline and the Sheep Mountain pipeline (Intergovernmental Panel on Climate Change, 2005). These examples display the possibility and feasibility of pipeline networks that can transport CO_2 over long distances from source points to storage points.

Pipelines used for CO_2 transport extend to more than 2500 km in western USA where over 50 Mt of CO_2 are transported for EOR (Intergovernmental Panel on Climate Change, 2005). Pipelines have already been and are used extensively in the oil and petroleum industry hence knowledge in design and operation is readily available. This also adds to them being the preferred means of CO_2 transport for CCS. Pipelines also have the added advantage that they are able to maintain a continuous supply of CO_2 whereas ship, road and rail tankers are batch transporters of CO_2 which means there is no need for intermediary storage of CO_2 in pipeline transport (Forbes *et al.*, 2008). There is, however, a need for intermediary pumping stations to counteract the effect of pressure drop along the length of pipe (Forbes *et al.*, 2008). The CO_2 transportation industry makes use of centrifugal, single-stage and radial split pumps for re-compression. Further discussion on CO_2 transport is beyond the scope of the project, but further information can be found in the Intergovernmental Panel on Climate Change (2005).

(iii) CO_2 capture

CO_2 capture is the separation of CO_2 from a mixture of gases at the point of CO_2 production (Intergovernmental Panel on Climate Change, 2005). Sreenivasulu *et al.* (2015) defines CO_2 capture as the removal of CO_2 from product gases of combustion or removal of CO_2 from the fuel. In CO_2 capture, the CO_2 must be separated from other gases in the gas stream concerned, which in conventional power plants is the flue gas stream produced from combusting fossil fuel (Yang *et al.*, 2008). Alternatively, the fuel (for solid fuels only) can be gasified before combustion; a process which produces CO_2 and hydrogen (H_2), after which the CO_2 can be taken for storage and the H_2 can be utilized as a fuel (Intergovernmental Panel on Climate Change, 2005). Hence, there are three main approaches that can be implemented for CO_2 capture: 1. pre-combustion capture; 2. post-combustion capture; 3. oxy-fuel combustion capture (Intergovernmental Panel on Climate Change, 2005; Sreenivasulu *et al.*, 2015; Wall *et al.*, 2009; Wu *et al.*, 2014). There is, however, an emerging approach to capturing CO_2 using chemical looping combustion (Wall *et al.*, 2009). Post-combustion capture is commonly used and is the most developed of the three approaches (Jiang *et al.*, 2015). The major factors affecting the choice of approach for CO_2 capture are the fuel phase that is whether the fuel is gaseous, liquid or solid, the concentration of CO_2 in the gas stream and the pressure of the gas (Intergovernmental Panel on Climate Change, 2005; Olajire, 2010).

Post-combustion capture

Post combustion capture refers to when the capture technology is applied after the combustion process has occurred (Intergovernmental Panel on Climate Change, 2005; Sreenivasulu *et al.*, 2015). CO_2 is separated from flue gases produced from the combustion process (Chao *et al.*, 2015; Olajire, 2010; Pires *et al.*, 2011). Figure 2.6 shows a typical post-combustion CO_2 capture process with typical process conditions in an electricity generating plant showing the point at which the CO_2 is captured. Figure 2.6 also shows the typical process conditions for such a process.

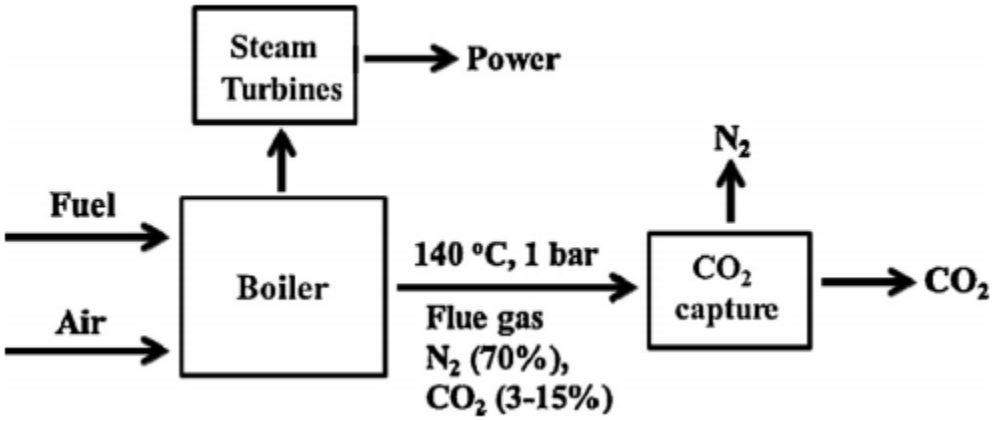


Figure 2.6: Post-combustion capture system in a power plant (Chao *et al.*, 2015).

In a similar manner to desulphurization, post-combustion capture is a downstream process (Olajire, 2010). According to Olajire, (2010), flue gas has low CO_2 concentrations; approximately 3-15% by volume and as such for the capture to be effective, large gas volumes are required. The large gas volumes handled subsequently impact negatively on the equipment cost and capital cost (Olajire, 2010; Pires *et al.*, 2011). There are some challenges posed by post-combustion design systems, and these include the low CO_2 partial pressure and the high flue gas temperatures (Olajire, 2010). Sreenivasulu *et al.* (2015) and Wu *et al.* (2015) state that post-combustion capture offers an advantage in that it can be retrofitted to existing power plants as an end-pipe technology. Additionally, the CO_2 in flue gas is dilute and for storage there is need for high CO_2 concentrations thus, high recoveries will be required (Sreenivasulu *et al.*, 2015). Post-combustion capture thus requires high capital costs and approximately 25-30% supplementary energy for plant operation (Sreenivasulu *et al.*, 2015). Post-combustion capture is most suitable

for current coal-fired power plants as they are the major sources of electricity generation and ultimately CO_2 emissions (Goto *et al.*, 2013). Wu *et al.* (2014) further explains that post-combustion capture can be divided into three aspects: 1. biological; 2. chemical; 3. physical methods. The biological method makes use of living organisms such as algae, plants and photosynthetic bacteria to fix the CO_2 (Wu *et al.*, 2014). The biological method occurs without energy consumption, but it has low absorption capacities and efficiencies (Wu *et al.*, 2014). The physical method makes use of organic solutions where no chemical reaction occurs (Wu *et al.*, 2014), based on physical adsorption, cryogenic condensation and membrane separation technology for separation (Wu *et al.*, 2014). According to Wu *et al.* (2014), the chemical method makes use of techniques such as chemical adsorption, absorption and chemical looping combustion, amongst others. Of the three methods performed in post-combustion capture, the chemical method offers several advantages, which include high efficiencies, low cost and maturity of the techniques used in the technology (Wu *et al.*, 2014). Sorption for CO_2 is discussed further in Section 2.3.3.

Pre-combustion capture

The goal of this technology is to produce carbon free fuel from carbon fuel (Olajire, 2010). The capture technique is applied before the combustion of the fuel. The fuel is reacted with oxygen (O_2), air or steam to form carbon monoxide (CO) and H_2 in a process known as reforming (Intergovernmental Panel on Climate Change, 2005; Pires *et al.*, 2011; Sreenivasulu *et al.*, 2015). Sreenivasulu *et al.* (2015) mentions that approximately 90% of the fuel is converted to synthesis gas. The gas product from the reforming reaction is then reacted with steam in a catalytic reactor to form more H_2 and CO_2 (Olajire, 2010). Synthesis gas has an approximate composition of 40 mol% CO_2 and 60 mol% H_2 (Gholinezad *et al.*, 2011). CO_2 separation is then performed and the H_2 is used as a fuel where it is then combusted after CO_2 removal (Olajire, 2010). Pre-combustion capture is mainly used in Integrated Coal Gasification Cycle (IGCC) plants (Garcia *et al.*, 2011; Gholinezad *et al.*, 2011; Olajire, 2010). Pre-combustion capture technology has not yet reached commercial maturity due to high capital costs, as significant changes to the existing design of the power plants is required (Sreenivasulu *et al.*, 2015). The major advantage of pre-combustion capture is that there is a CO_2 stream with high pressure, approximately 5-15 bar and low temperature approximately in the range 25 - 65 ^oC (Garcia *et al.*, 2011; Pires *et al.*, 2011),

which aids with the compression and transportation process. Figure 2.7 shows the major steps in pre-combustion capture. In South Africa, Sasol is already performing the production of syngas, releasing a highly concentrated CO_2 capture stream which is ready for storage from fixed bed gasification with the aim of producing liquid fuels and chemical products (Global CCS Institute, 2014).

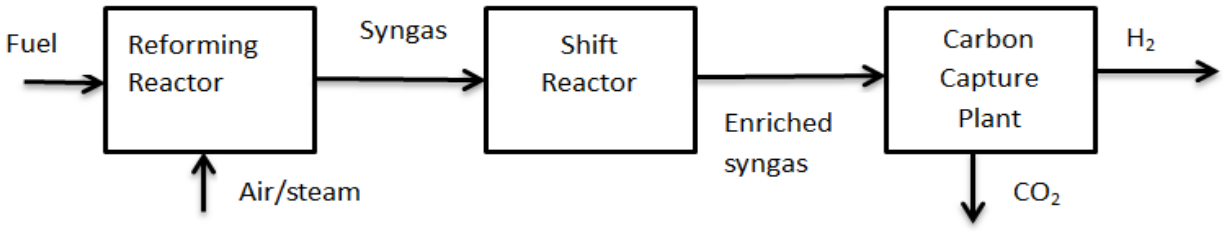


Figure 2.7: Schematic showing the main steps in pre-combustion capture (adapted from Pires *et al.* (2011)).

Oxy-fuel combustion capture

In oxy-fuel combustion, O_2 is separated from air using a cryogenic separation process and the fuel is combusted in the pure O_2 obtained (Pires *et al.*, 2011). Oxy-fuel combustion flue gas from this process has approximately 80 - 90% CO_2, 5% N_2 and 5% O_2 (by volume) compared to flue gas obtained from air combustion which contains approximately 79% N_2, 13 – 15% CO_2 and 5% O_2 (by volume) (Olajire, 2010; Uchida *et al.*, 2013). From this flue gas comparison, Yan *et al.* (2011) defines oxy-fuel combustion capture as a concentration of CO_2 and not a CO_2 selective method. Uchida *et al.* (2013) defines oxy-fuel combustion capture as a method used to obtain large concentrations of CO_2 by combusting fuel in highly pure O_2. Due to the combustion reaction taking place in an almost pure O_2 environment, the flame temperature is very high and has to be controlled to avoid material damage (Fujimori & Yamada, 2013). This control is done by recirculating flue gas to reduce the temperature in the combustion chamber (Fujimori & Yamada, 2013; Uchida *et al.*, 2013). Fujimori and Yamada (2013) and Uchida *et al.* (2013) mention several merits of oxy-fuel combustion capture, which include a ready for storage CO_2 stream, increased combustion efficiency, down-scaled downstream process units due to a decrease in the quantity of flue gas handled and a decrease in N_2 oxides. The two main combustion products are CO_2 and water vapor, which are separated by condensation (Intergovernmental Panel on Climate Change, 2005).

Chemical looping combustion capture

Chemical looping combustion capture refers to a process setup where O_2 is brought into contact with the fuel for combustion by use of solid carrier, usually a metal (Wall *et al.*, 2009). The solid metal used should have a variable oxidation state and this is the property exploited (Fan, 2010; Wall *et al.*, 2009). The metal is oxidized in an oxidation chamber, thereafter it is transported to the combustion chamber where the fuel is combusted. This results in the fuel combusting in highly concentrated O_2 , which produces a flue gas stream with a large volume fraction of CO_2 (Wall *et al.*, 2009). The O_2 carrier (metal) is reduced while the reaction is occurring and is transported back to the oxidation chamber (Fan, 2010). The cycle then repeats.

2.4.2 CO_2 emissions and CCS in South African coal-fired power plants

As mentioned in Chapter 1, South Africa is a significant CO_2 emitter on the African continent and the world at large, and this brings the need to reduce CO_2 emissions. Figure 2.8 shows the highest direct emitters of CO_2 in South Africa. Due to the highly intensive coal use in electricity production, Eskom, the country's electricity producer has the highest CO_2 emissions.

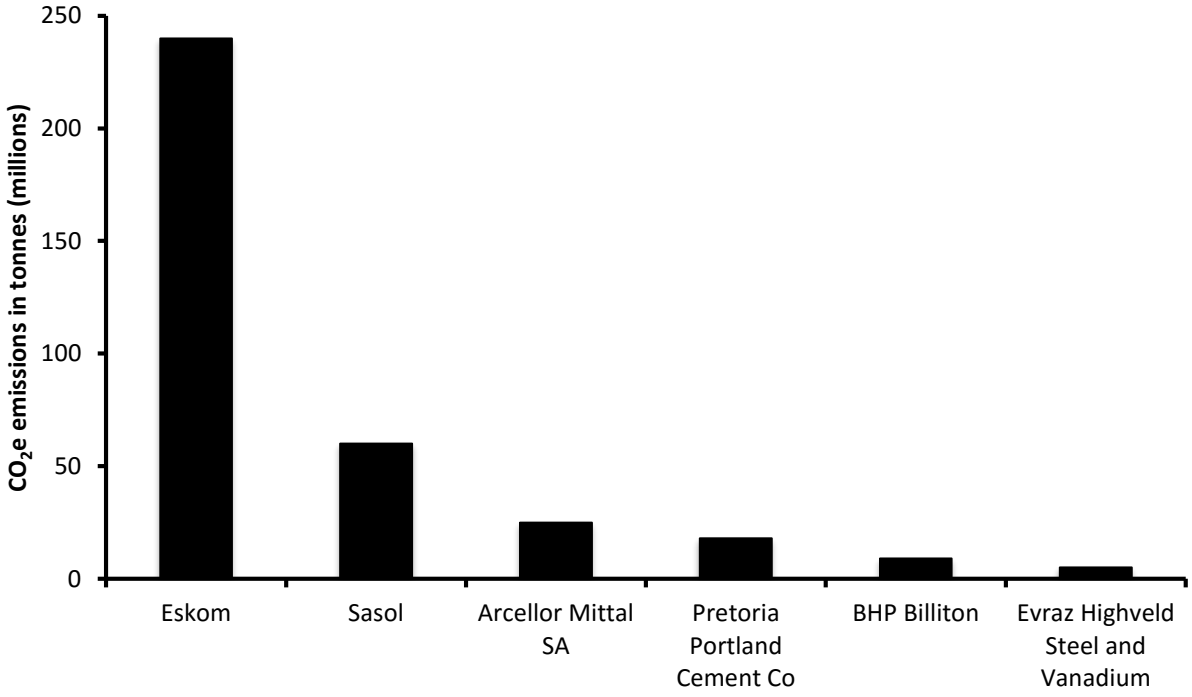


Figure 2.8: South Africa's highest CO_2 emitters (adapted from Urban Earth (2015)).

Total CO_2 emissions in South Africa amounted to over 400 million tonnes for the year 2011 and were expected to increase further (Urban Earth, 2012). Eskom alone contributes about 45 % of South Africa's CO_2 emissions. Eskom currently has a fleet 18 coal-fired power plants which all emit CO_2 to the atmosphere via flue gas (Eskom, 2015).

The South African government has been and is taking action to reduce CO_2 emissions through advocating for the use of renewable energy, energy efficiency improvement as well as application of CCS in South African coal-fired power plants. To achieve this, the government of South Africa through the department of energy set up SACCCS as mentioned in Chapter 1. SACCCS' primary function is to facilitate the deployment of CCS within South Africa. Currently, SACCCS is focusing mostly on the storage component of CCS, as mentioned in Chapter 1. For this reason, there is need to conduct research on the capture aspect of CCS as well. The aim of this work was to develop a material suitable for CO_2 capture in South African coal-fired power plants.

2.4.3 Techniques for CO_2 capture in existing coal-fired power plants

To define techniques to capture CO_2 in coal fired power plants, it is important to understand the structure of a coal-fired power plant. Figure 2.9 is a schematic of a typical coal fired power plant. The fuel, coal, is fed to a boiler where it is combusted. The combustion reaction produces heat and exhaust gases. The heat produced is used to heat up water which is converted into steam. The steam produced turns turbines which produce electricity, as shown in Figure 2.9. The exhaust gas from the combustion of coal is made up of N_2, water vapor, CO_2, O_2 and oxides of Sulphur.

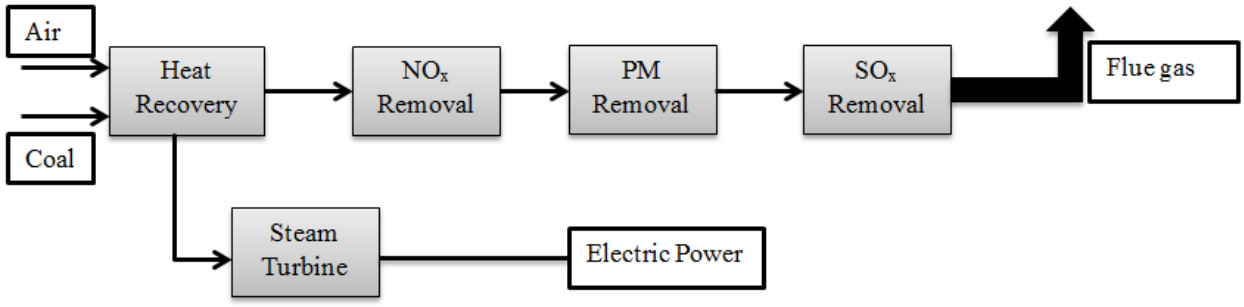


Figure 2.9: Flow diagram showing the structure of a coal fired power plant (Adopted from The USGS Water Science School, n.d.)

Based on the schematic shown in Figure 2.9, the most suitable approach to capture CO_2 in a coal fired power plant would be the post-combustion capture approach. This is so because the CO_2 is contained in the flue gas exiting the power plant. According to Li *et al.* (2015), post-combustion capture is appropriate for coal fired power plants due to the ease with which retrofitting can be carried out on existing power plants as compared to other approaches such as pre-combustion capture and oxy-fuel combustion capture. Post-combustion capture is therefore important in the South African context as South Africa has eighteen coal fired power plants, with two of the eighteen to fully come online soon, and comes thirteenth on the world CO_2 emissions list (International Energy Agency, 2004).

Several techniques can be used for CO_2 capture and these include cryogenic distillation techniques, membrane separation based techniques, absorption techniques, and adsorption techniques (Lee & Park, 2014; Pires *et al.*, 2011; Yang *et al.*, 2008). Each of the techniques are explored further below.

(i) Cryogenic distillation

In cryogenic distillation, the gases being separated are partially liquefied, followed by fractional distillation of the subsequent liquid (Gunardson, 1997). The basis of the distillation separation process is the difference in the boiling points of the components in the liquid (Gunardson, 1998). Pires *et al.* (2011) state that cryogenic temperatures are obtained by the use of closed cycle refrigeration cycles, that make use of compressors, Joule-Thompson valves, as well as multi-stage heat exchangers and expanders. Cryogenic distillation can be applied in CO_2 capture in all three CO_2 capture systems, that is post-combustion, pre-combustion and oxyfuel combustion capture (Pires *et al.*, 2011). Cryogenic distillation is advantageous when applied in CO_2 capture, because the CO_2 is captured in liquid phase, making downstream processes such as transport and storage easier and cheaper. Piet *et al.* (2006) also says that the recovery of CO_2 with cryogenic distillation is very high compared to other separation techniques. However, the major drawback of cryogenic distillation is the high energy requirement for refrigeration (Pires *et al.*, 2011).

(ii) Membrane separation

The membrane separation technique makes use of membranes. Pabby *et al.* (2009) defines membranes as barriers that allow passage and selective restriction of various substances through them. Membranes can be symmetric or asymmetric, homogenous or heterogenous, positive or

negative and neutral or bipolar (Pabby *et al.*, 2009). In membrane separation processes, the feed stream, known as the influent, separates into two streams, the permeate stream and the concentrate stream (Pabby *et al.*, 2009). According to Olajire, (2010), the use of membranes in CO_2 capture is quite a new technique, essentially still the research phase. It does, however, shows promise for application in post-combustion capture, pre-combustion capture and oxyfuel combustion capture. In CO_2 capture, membrane separation offers several advantages, including increased efficiencies in separation in comparison to equilibrium based processes, possible large packing density resulting in smaller installations in comparison to other techniques, and it is already in use in CO_2 separation from natural gas (Pires *et al.*, 2011). According to Pires *et al.*, (2011) the major drawback of membranes in CO_2 capture is that the flowrates encountered in power plants are significantly high. If membrane technology is to be applied, large areas would be required and this poses a large capital cost for this technique (Pires *et al.*, 2011).

(iii) Absorption

Pires *et al.* (2011) mentions that absorption can be a physical or chemical process where atoms, ions or molecules are dissolved in a bulk phase. Absorption is a common process used in CO_2 capture and it is widely used in gas cleaning processes in industry (Pires *et al.*, 2011). At a processing plant, absorption occurs in packed columns (Li *et al.*, 2015). Two packed columns may be used, an absorber and a stripper. The gas containing CO_2 is fed to the bottom of the absorber in which it is counter-currently contacted with the lean amine-solvent which absorbs CO_2. The CO_2 rich amine-solvent exits the absorber at the bottom, while the CO_2 clean gas exits at the top of the absorber. The CO_2 rich amine-solvent is fed to the stripper column, where the absorbed CO_2 is stripped off by adjusting operating conditions in the stripper column to recover the amine-solvent (Li *et al.*, 2015). CO_2 rich amine solvents mainly include mono-ethanol amines (MEA), diethyl amines (DEA) as well as triethyl amines (TEA) (Mortaheb *et al.*, 2012). The advantage of using absorption is that it is a very mature technology and it is understood very well (Pires *et al.*, 2011). The disadvantages are, however, quite a number and include high corrosion in equipment due to the solvents used (Pires *et al.*, 2011). Also, the regeneration of solvents used in absorption requires large amounts of energy, thus making the process expensive. Solvents applied also degrade in high oxygen systems (Pires *et al.*, 2011).

(iv) Adsorption

Adsorption is a selective process where molecules, ions or atoms of a substance in liquid or gaseous state adhere on a solid surface, which is the adsorbent (Bhatta *et al.*, 2015; Christophe *et al.*, 2015; Pires *et al.*, 2011). Crittenden and Thomas (1998) define adsorption as a process which results from interactive forces between the surface of porous solids (adsorbent) and component molecules (adsorbate) being extracted from the bulk phase (Figure 2.10). The substance that adheres to the solid surface (adsorbent) is the adsorbate (Mantell, 1951).

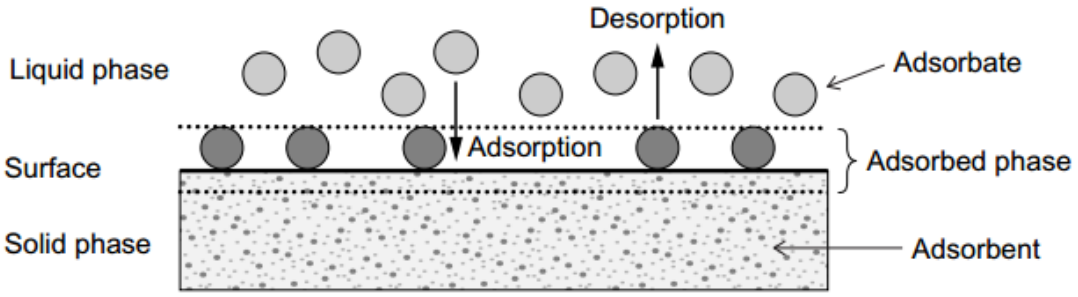


Figure 2.10: Simplified adsorption process diagram (Worch, 2012).

Adsorption's driving force is the decrease in surface tension due to the adsorbent-adsorbate interaction. Adsorption differs from absorption in that during adsorption, the concentration is at a surface, whereas in absorption it is in the bulk phase (Crittenden & Thomas, 1998; Wilcox, 2012). The process of adsorption occurs at the interface of the adsorbent and the adsorbate that is on the surface of the adsorbent where the two come in contact with each other (Mantell, 1951).

Mantell (1951) mentions that adsorption differs from absorption in that in most cases adsorption is without chemical reactions; that is the adsorbent and the adsorbate do not react with each other. In absorption, however, there are chemical reactions that occur (Mantell, 1951). With adsorption, the adsorbate does not enter or alter the force field that exists between the particles of the adsorbent (Mantell, 1951). According to Crittenden and Thomas (1998), adsorption gained fame as a separation technique during its early use in the First World War from 1914 to 1918, where charcoal was used as an adsorbent in gas masks. 90 % of chemicals are produced through heterogeneously catalyzed processes where the reactants adsorb onto a catalyst temporarily during a reaction and products form; thereafter the products desorb from the catalyst and the

process repeats (Masel, 1996). For this reason adsorption is an important technology in today's industries. Pires *et al.*, (2011) states that adsorption has high potential in CO_2 capture.

According to Mantell (1951), the adsorption of an adsorbate onto an adsorbent is dependent on the nature and character of the adsorbent and adsorbate. Adsorbents can be used once or they can be treated to eliminate the adsorbate and be re-used; this process can be done in-situ (Mantell, 1951). It is important to note that during adsorption processes, adsorbate molecules face resistance from mass transfer effects as they move from the bulk phase to the surface of the adsorbent as well as intra-particle diffusion (Crittenden & Thomas, 1998). Both these factors should be considered in adsorption equipment design to ensure that there is adequate contact time between the adsorbent and the adsorbate.

Mantell, (1951) and Crittenden and Thomas (1998) suggest that adsorption can be used in different applications, amongst them: separation of gases from gases, separation of vapors from gases, separation of solutes and colloids from solutions, ion separation from solutions and concentration of materials dissolved in solutions. Adsorption is an exothermic process resulting in the evolution of heat when it occurs (Crittenden & Thomas, 1998). Adsorption can either be physical, in which case it is termed physisorption or chemical, in which case it is termed chemisorption or a combination of both physical and chemical adsorption (Mantell, 1951; Wilcox, 2012). Physical adsorption occurs when weak Van der Waals' forces as well as electrostatic interactions which include polarization, dipole-dipole and quadruple interactions (Crittenden & Thomas, 1998; Ruthven, 1984; Wilcox, 2012). During physical adsorption, the adsorbate molecule having three degrees of translational freedom approaches the adsorbent surface where repulsive and attractive forces become balanced and adsorption occurs (Crittenden & Thomas, 1998). When this happens, the adsorbate molecule loses one degree of translational freedom resulting in a decrease in entropy as well as Gibbs free energy, resulting in adsorption being an exothermic process as shown in Equation 2.2 (Crittenden & Thomas, 1998; Keller & Staudt, 2005; Mantell, 1951).

$$\Delta G = \Delta H - T\Delta S \tag{2.2}$$

But ΔG *is negative and so is* ΔS *since* $G_{initial} - G_{ads} = < 0$ *and* $S_{initial} - S_{ads} = < 0$

Adsorption decreases with increase in temperature as it is an exothermic process (Mantell, 1951). Chemical adsorption occurs when there is transfer or sharing of electrons between the adsorbate and the adsorbent resulting in the formation of ionic or covalent bonds (Ruthven, 1984).When a combination of physisorption and chemisorption occurs, it is termed physico-chemisorption (Keller & Staudt, 2005). The heat of adsorption can be used as an indicator to determine whether physisorption occurs or chemisorption occurs (Mantell, 1951). Table 2.2 shows the major differences between physisorption and chemisorption (Keller & Staudt, 2005; Ruthven, 1984).

Table 2.2: Differences between physisorption and chemisorption (Wilcox, 2012).

Physisorption	**Chemisorption**
Lower adsorption enthalpy.	Higher adsorption enthalpy.
Mostly non-specific.	Highly specific.
Can be monolayer or multilayer.	Monolayer only.
No electron transfer. Weak Van der Waals' forces exist. Electron shells are maintained.	Electron transfer occurs resulting in bond formation.
Occurs at low temperatures.	Occurs over a broad temperature spectrum.
Mostly spontaneous and does not require activation.	Mostly requires activation and may be slow.
Usually reversible.	Mostly irreversible.

During adsorption, it is important to distinguish between physisorption and chemisorption; however, it is important to note that in most cases it is a challenge to perform the classification of the adsorption process. Distinction of physisorption and chemisorption is important for the purposes of equipment design, material behavior study and industrial applications. Keller and Staudt (2005), as well as Crittenden and Thomas (1998), state that reversible physisorption processes occur with the evolution of about 10 – 50 kJ/mole of enthalpy, and most chemisorption processes result in the evolution of 70 – 200 kJ/mole of enthalpy, both in the form of heat. In the enthalpy range 50 – 70 kJ/mole physico-chemisorption occurs. The adsorbate adsorbed per unit adsorbent depends on the temperature, pressure and the nature of the adsorbent (Mantell, 1951).

Further information on adsorption is discussed in following sections: a) adsorption isotherms; b) potential energy for adsorption; c) adsorption equilibria.

a) Adsorption isotherms

When a quantity (can be volume or mass) of gas *g* is adsorbed onto an adsorbent at a constant temperature and an equilibrium partial pressure, p the adsorption isotherm is defined by the function *g*(p). Adsorption isotherms are defined by the type of adsorption occurring and may be used to predict the behavior of adsorption systems (Crittenden & Thomas, 1998). Wilcox (2012) defines an adsorption isotherm as a representation of the equilibrium relationship between the adsorbate molecules in the fluid phase and adsorbed phase at any given temperature. There are several different forms that adsorption isotherms can take with five possible types (Figure 2.11) (Crittenden & Thomas, 1998; Keller & Staudt, 2005). Wilcox (2012) and Shi and Morreale (2015), however, mention that there are six types of adsorption isotherms (Figure 2.12). Figure 2.11 shows the five different types of adsorption isotherms according to the Brunauer, Emmett and Teller (BET) theory.

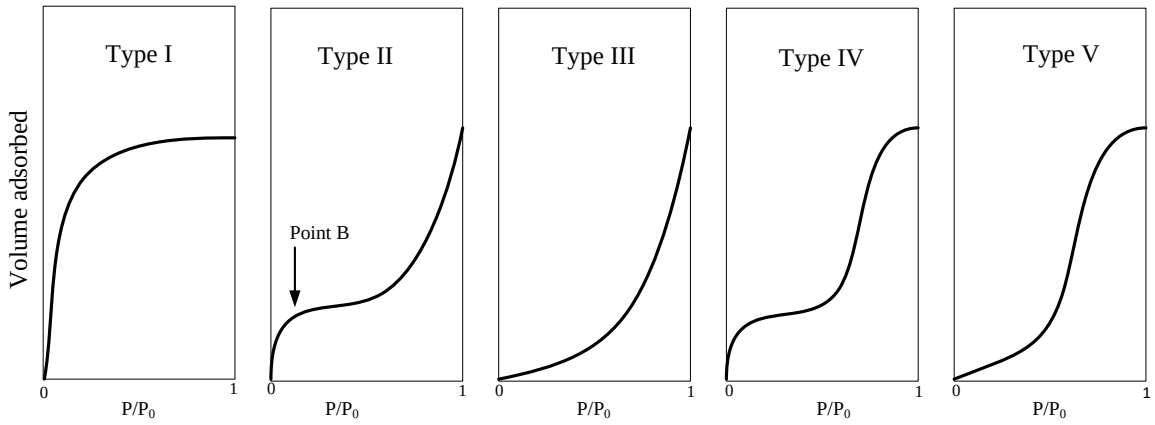


Figure 2.11: Possible adsorption isotherms according to the BET theory (Adapted from Crittenden & Thomas (1998)) (Type meanings are discussed in the text below).

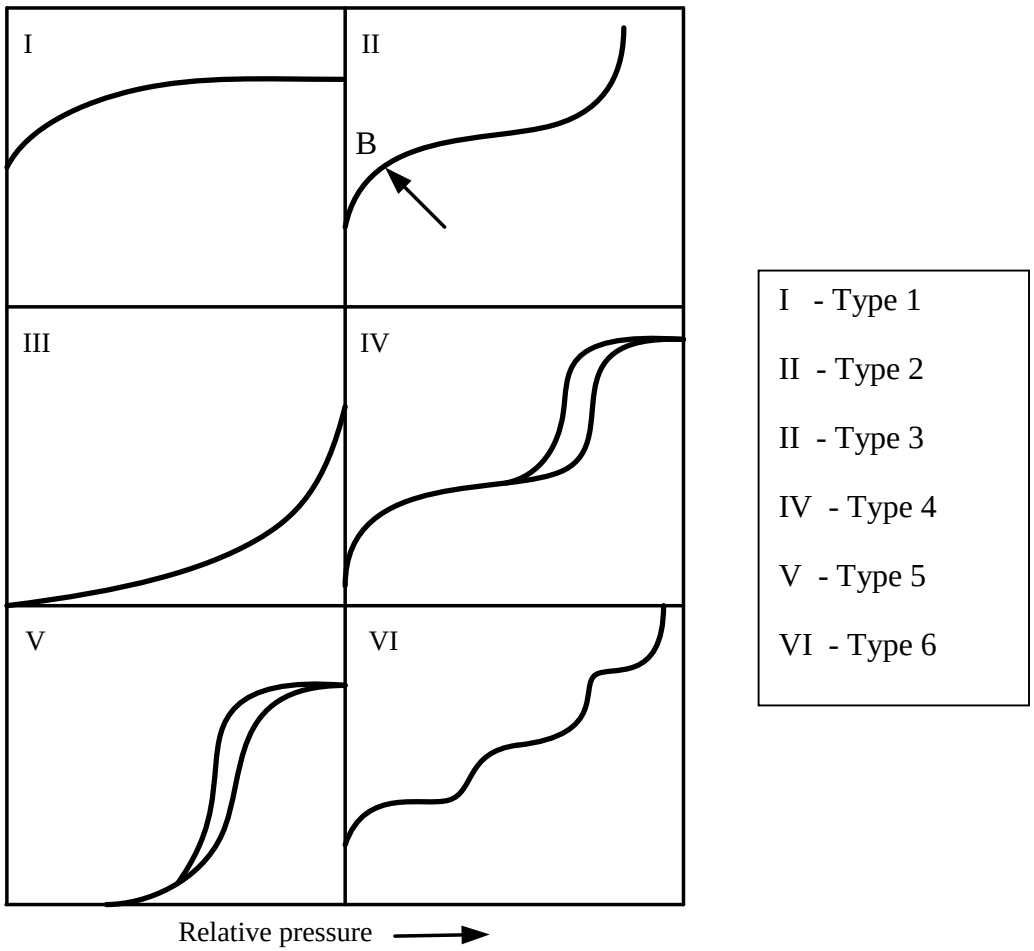


Figure 2.12: Possible adsorption isotherms according to the BET theory (Adapted from Shi & Morreale (2012) and Wilcox (2012)).

Monolayer adsorption is characteristic of Type I adsorption isotherms (Crittenden & Thomas, 1998; Shi & Morreale, 2015; Wilcox, 2012). A single layer of adsorbate molecules forms on the surface of the adsorbent. Monolayer adsorption is common on microporous adsorbents which have pore sizes which are comparable to the sizes of the adsorbate molecules but larger (Crittenden & Thomas, 1998; Wilcox, 2012). Microporous materials mostly display Type I isotherms during adsorption (Toth, 2005; Wilcox, 2012). When extensive multilayer adsorption occurs, in macroporous adsorbents, Type II adsorption isotherms are obtained. The point of inflection (point B) shown in Figure 2.11 and 2.12 is as a result of the completion of the monolayer adsorption and the initiation of multilayer adsorption (Crittenden & Thomas, 1998; Toth, 2005; Wilcox, 2012). According to Wilcox (2012), Type III isotherms are rare in adsorption processes and are described to be unfavorable and are as a result of interactions

between the adsorbent surface and the bulk fluid. When condensation of the adsorbate inside the pore occurs during adsorption, this results in Type IV adsorption isotherms (Crittenden & Thomas, 1998; Wilcox, 2012). Type IV adsorption isotherms are most common in mesoporous adsorption and they have a hysteresis loop which is present due to condensation inside the pore. Monolayer adsorption followed by multi-layer adsorption occurs and is depicted by the two plateaus on the Type IV adsorption isotherm graph (Crittenden & Thomas, 1998; Wilcox, 2012). In Type V adsorption isotherms, a combination of both condensation and hysteresis is displayed. Initially Type III adsorption isotherm phenomenon is displayed followed by Type IV adsorption isotherm phenomenon (Toth, 2005; Wilcox, 2012). According to Wilcox (2012), Type VI adsorption isotherms are obtained when a successive two-dimensional phase transition occurs for example from gas to liquid to solid during the adsorption process.

b) Potential energy for adsorption

Adsorption isotherms depict the quantity of adsorbate adsorbed onto the surface of the adsorbent as a function of its pressure at constant temperature (Rouquerol *et al.*, 2014). These isotherms are dependent on the interactions occurring between the adsorbent and the adsorbate molecules. These interactions can be modeled as the summation of attractive and repulsive interactions occurring between the adsorbate and the adsorbent giving a potential energy diagram shown in Figure 2.13. In Figure 2.13, the x-axis represents the distance of the adsorbate molecule from the surface of the adsorbent and the y-axis represents the potential energy.

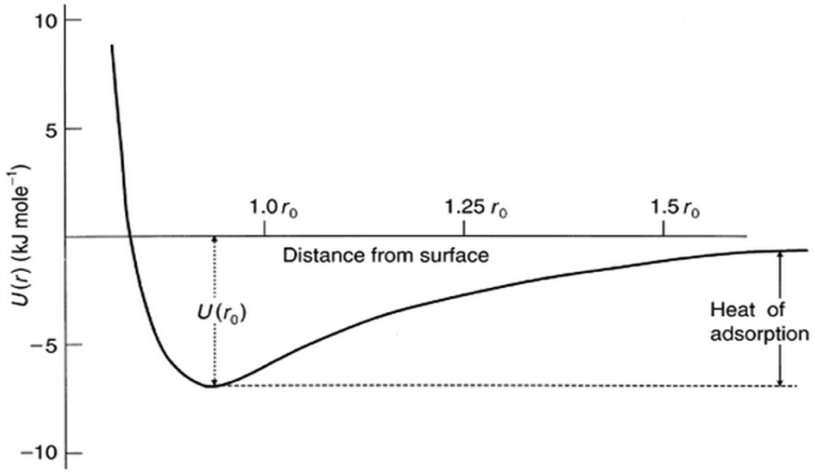


Figure 2.13: Adsorption potential energy diagram (Crittenden & Thomas, 1998)

As the distance between the adsorbate molecule and the adsorbent decreases, the potential energy for adsorption, U(r), increases and as it increases, U(r) decreases (Figure 2.13). Adsorption potential energy is thus defined as the work of compression of the gas to its saturation pressure (P_s) from a pressure p (P). Assuming a mole of gas occupies a volume v in a thermodynamic system, the potential energy for adsorption is given by (Yang, 2003):

$$\varepsilon = -\Delta G = \int_{P}^{P_s} V dP \tag{2.3}$$

Therefore,

$$\varepsilon = RT \ln \frac{P_s}{P} \tag{2.4}$$

But,

$$\varepsilon_{Total} = \varepsilon_{adsorabte-adsorbent} + \varepsilon_{adosorbate-adsorbate} \tag{2.5}$$

Where,

$$\varepsilon_{adsorbate-adsorbent} = \varepsilon_R + \varepsilon_I + \varepsilon_D + \varepsilon_{F\mu} + \varepsilon_{Fq} \tag{2.6}$$

In equation 2.6, the variables are defined as:

ε_R is the close range repulsion energy,

ε_I is the induction energy due to the interaction between the electric field and an induced dipole,

ε_D is the dispersion energy,

$\varepsilon_{F\mu}$ is the interaction energy between a permanent dipole (μ) and the electric field (F),

ε_{Fq} is the interaction between the quadruple moment (Q) and the field gradient (F).

c) Adsorption equilibria

Adsorption equilibria is represented by adsorption isotherms. Several theories of adsorption equilibria exist and these include the Langmuir theory, the Freundlich theory, the Temkin theory and the BET theory among others. Each theory makes assumptions based on whether monolayer

or multilayer adsorption is occurring. In this literature survey and research work, the Langmuir theory and the BET theory will be discussed as they are most relevant to the work carried out. According to Dabrowski (1999), the Langmuir and the BET theories introduce concepts of localized monolayer and multilayer adsorption occurring on an energetically homogenous surface.

The Langmuir theory

The Langmuir theory describes adsorption in which the adsorbate molecules form a monolayer at or just before a relative pressure of unity is reached (Mantell, 1951). The Langmuir theory is relevant for chemisorption description, but may be extended to many binary adsorbate systems which are not necessarily chemisorption (Dabrowski, 1999). The theory emanates from the basis of a dynamic equilibrium occurring between the adsorbed phase and the bulk fluid phase. The theory states that the rate at which adsorbate molecules strike the surface of the adsorbent is proportional to the product of the partial pressure, P, of the gas and the fraction of adsorbent surface remaining (1-θ) uncovered by the adsorbent, that is available adsorption sites. Langmuir further proposed that the rate of desorption from the surface is directly proportional to the fractional adsorbent surface coverage (θ) and that at equilibrium, the rate of adsorption is equal to the rate of desorption. This is shown in Equation 2.7.

$$k_a P(1-\theta) = k_d \theta \tag{2.1}$$

Where, k_a and k_d are the rate constants for adsorption and desorption respectively.

The more familiar form of the equation is shown as:

$$\theta = \frac{q}{q_m} = \frac{bP}{(1+bP)} \tag{2.2}$$

Where, $b = k_a/k_d$ and q_m is the quantity q of adsorbate adsorbed in a single monolayer.

Dabrowski (1999) states that the Langmuir theory may only be applied in adsorption processes where only monolayer adsorption is occurring. The Langmuir theory is important in that it may be applied in the determination of kinetics of monolayer adsorption processes (Dabrowski, 1999). Type I adsorption isotherms are characteristic of the Langmuir theory, and in other literature are described as Langmuir isotherms.

The BET Theory

The BET theory explains physical adsorption of gas molecules on solid adsorbent surfaces. This theory also finds relevant use in the determination of specific surface areas of different materials. Fundamentally, the BET theory is an extension of the Langmuir theory, that is from monolayer adsorption to multilayer adsorption. Assumptions made in the BET theory are that the adsorbate molecules adsorb onto the adsorbent surface in layers infinitely, each adsorption layer is independent of the other adsorption layer, that is there is no interaction between the layers, and lastly the Langmuir theory may be applied to each layer. Based on these assumptions, the BET equation is then expressed as:

$$\frac{1}{v\left[\left({}^{P_s}/_{P}\right)-1\right]} = \frac{c-1}{v_m c}\left(\frac{P}{P_s}\right) + \frac{1}{v_m c} \qquad (2.3)$$

In equation 2.9, the variables are defined as:

P_s is the saturation pressure of the adsorbate molecules at the adsorption temperature,

P is the equilibrium pressure of the adsorbate molecules at the adsorption temperature,

V is the adsorbed quantity of gas in volume units,

V_m is the monolayer adsorbed gas quantity,

C is the BET constant, which is expressed by:

$$c = exp\left(\frac{E_1 - E_L}{RT}\right)$$

Where E_1 is the heat of adsorption of the first layer and E_L is that for the second and higher layers which is equal to the heat of liquefaction, R is the gas constant and T is the temperature.

Large scale adsorption processes

Adsorption is an important industrial process and is applied in several different applications such as drying of air, sweetening of natural gas, as well as removal of solvents from air streams (Crittenden & Thomas, 1998). In large industries, adsorption is mostly applied in packed beds where the solid adsorbent material is packed in a column with the bulk fluid from which a

component is to be extracted is passed through the packed bed (Crittenden & Thomas, 1998; Yang, 2003; Wauquier, 1998). Packed beds are arranged adjacent to each other in an adsorber-stripper fashion to enable continuity of the adsorption process. As one bed adsorbs, another desorbs all in sequence such that the process is continuous.

2.4.4 CO_2 capture via adsorption

In CO_2 capture by adsorption, both adsorption and desorption should be studied as they are both important in the separation of CO_2 and in the regeneration of the spent adsorbent (Bandyopadhyay, 2014; Wilcox, 2012). Wilcox (2012) mentions that for adsorption to be thermodynamically favorable, it has to be exothermic. In the capture of CO_2, both chemisorption and physisorption may be applied, but for techno-economic feasibility, physisorption is the more favorable type of adsorption (Wilcox, 2012). Lee and Park (2014) mention that the capture of CO_2 by use of solid adsorbents is done based on gas-solid interactions between the adsorbent and the CO_2 gas molecules. In industry, packed columns are used for the separation of CO_2 from other components and adsorbents used include activated carbons and molecular sieves (Lee & Park, 2014; Wilcox, 2012). Wilcox (2014) gives a comprehensive flow diagram showing aspects that require costing in CO_2 capture (Figure 14).

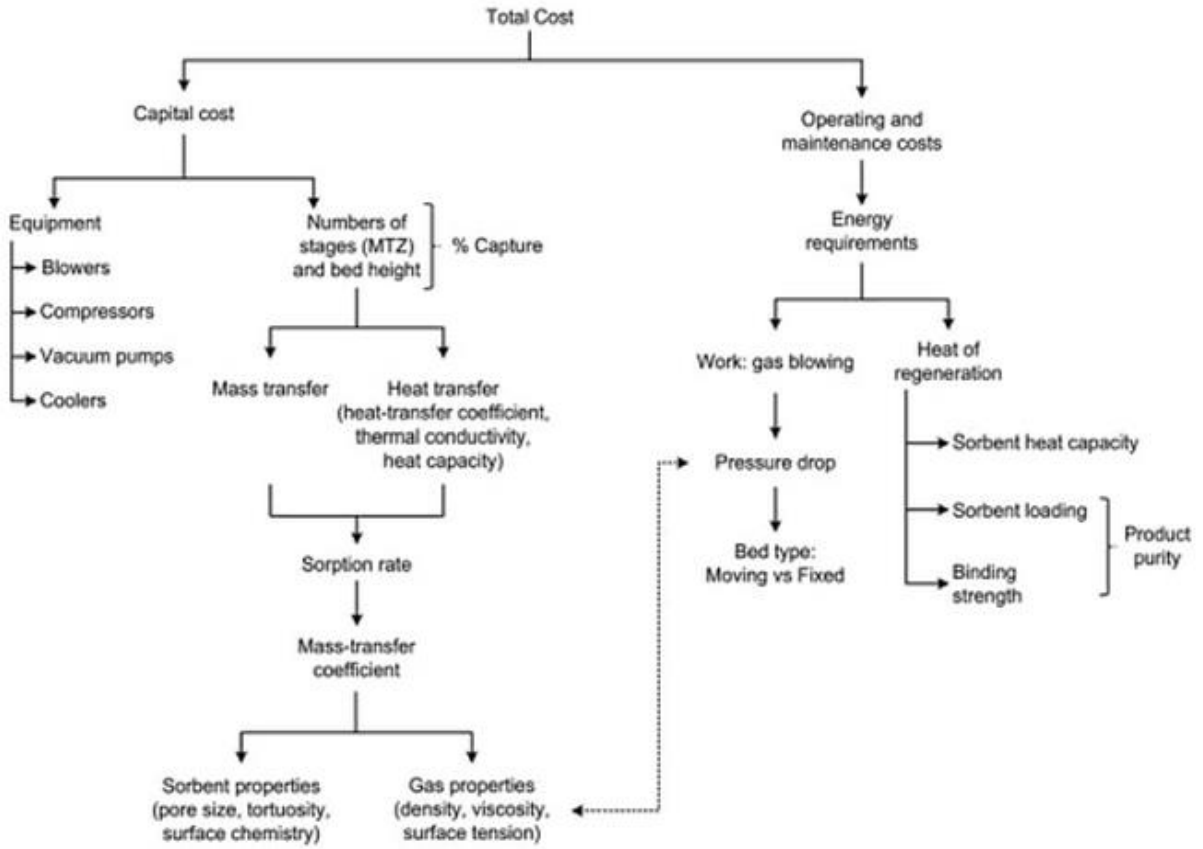


Figure 2.14: Typical cost analysis associated with CO_2 adsorption (Wilcox, 2012).

The schematic shown in Figure 2.14 does not exhaust all aspects that require costing or cost interlinkages associated with CO_2 adsorption capture. The schematic gives an overview of the cost analysis that may be associated to a CO_2 capture plant, but these are subject to change depending on the particular capture plant. Equipment such as blowers, compressors, vacuum pumps and coolers influence the capital cost of a CO_2 capture plant and they in turn are influenced by the kinetics of the adsorption process and the nature of adsorption occurring. The kinetics of the CO_2 adsorption process is influenced by the properties of the adsorbent. This shows how the various aspects of CO_2 adsorption capture are interlinked with each other in relation to cost. According to Wilcox (2012) it is important to understand the synthesis and properties of the adsorbent being applied for CO_2 capture as both capital and operating costs of a CO_2 capture facility depend almost entirely on it.

In CO_2 adsorption technology, the bulk-phase CO_2 concentration is displayed in the form of a mole percent or partial pressure. The CO_2 adsorbed on the surface of the adsorbent is expressed as the mass of CO_2 adsorbed per unit mass of adsorbent. The adsorption isotherms that govern CO_2 adsorption are dependent on the interactions between CO_2 and other components in the bulk phase, CO_2 and the adsorbent material, as well as other components in the bulk phase and the adsorbent material (Gao & Creamer, 2015; Wilcox, 2012). According to Wilcox (2012), adsorption mechanisms in CO_2 capture differ based on the pore size of the adsorbent material. An example would be in micropores, where the CO_2 adsorption is driven by interactions between CO_2 molecules and the adsorbent surface, with adsorbent-adsorbent surface interactions playing a role. Wilcox (2012) mentions that in mesopores, the phenomenon is different in that interactions within the bulk fluid molecules become significant and capillary condensation occurs in the pores of the adsorbent material. This is a result of the interactions between the bulk fluid and the surface of the adsorbent. Also in macropores, the phenomenon is different and the bulk fluid-adsorbent surface interactions play a smaller role with the density of the bulk fluid in the macropores being equal to the density of the bulk fluid at the operating temperature and pressure (Wilcox, 2012).

According to Lee and Park (2014), the most important variables in dry adsorption processes during CO_2 capture are the surface tension, pore size of the adsorbent and temperature as well as the partial pressure during the adsorption process. In post-combustion CO_2 capture via adsorption, it is essential to improve the selectivity of CO_2 as well as the capacity of the adsorbent materials. Lee and Park (2014) submitted that this can be done by introducing functional groups into the structures of the adsorbents. Functional groups also have an added advantage of improving stability of the adsorbate-adsorbent interactions. Functional groups to be introduced should have high affinities for CO_2 to enable CO_2 to be preferentially adsorbed over any other components that might be in the gas mixture (Lee & Park, 2014). In CO_2 capture via adsorption, functional groups that may be added to enhance the performance of adsorbents are amine groups. Several amine groups may be incorporated into the structures of adsorbents resulting in high polarization and high CO_2 capture as well as better kinetics during the process. Lee and Park (2014) mention that adsorbents doped with amine groups are advantageous in that there is potential elimination of corrosion problems and less regeneration energy costs. According to Lee and Park (2014), reactions between CO_2 and amine groups in anhydrous

conditions result in the formation of ammonium carbamates possibly in the reaction schemes shown in reactions 1 and 2 (Czaun *et al.*, 2013).

$$CO_2 + 2RNH_2 \leftrightarrow RNHCOO^- + RNH_3^+ \quad \text{(Reaction 1)}$$

$$CO_2 + 2R_2NH \leftrightarrow R_2NCOO^- + R_2NH_2^+ \quad \text{(Reaction 2)}$$

Lee and Park (2014) state that the reaction schemes depicted in reactions 1 and 2 are reversible and the efficiency of the resulting adsorption process may be improved by altering the structure of the adsorbent through use of different amines.

Several different adsorbent regeneration methods exist and may be used for CO_2 capture. Different adsorbent regeneration methods are distinguished by the method in which the adsorption-desorption cycle occurs. Desorption is a process where the adsorbent is recovered free of the adsorbate molecules, ready for the next adsorption cycle. The different adsorbent regeneration methods include pressure-swing adsorption (PSA), temperature-swing adsorption (TSA), electric-swing adsorption (ESA) and vacuum-swing adsorption (VSA) (Lee & Park, 2014; Yu *et al.*, 2012).

Pressure-swing adsorption (PSA)

Saleman *et al.* (2015) defines pressure-swing adsorption (PSA) as a technology employed to separate gas mixtures with the driving force being the differences in the adsorption capacities of the constituent gases. Pressure swing adsorption is dependent on the variation of pressure inside the adsorption bed. Increasing pressure results in the adsorbate molecules interacting more with the adsorbent surface (Bandyopadhyay, 2014; Crittenden & Thomas, 1998; Keller & Staudt, 2005; Yang *et al.*, 2008). This is because of a higher partial pressure of the adsorbate molecules, increasing their kinetic energy, and this favors the adsorption of the adsorbate molecules onto the adsorbent. The reverse process, which is the reduction of pressure in the bed, favors desorption of the adsorbate molecules from the surface of the adsorbent due to a reduction in the adsorbate partial pressure resulting in a decrease in the adsorbate molecules' kinetic energy. PSA is suitable for high adsorbate concentrations (Grande *et al.*, 2009; Yu *et al.*, 2012). Manipulation of pressure inside a packed adsorption bed can thus be used to control adsorption and desorption cycles (Crittenden & Thomas, 1998; Kidnay & Parrish, 2006; Yang, 2003). Other factors to be

considered include the physical properties of the adsorbent material and the nature of the adsorption process, whether chemisorption or physisorption or a combination of both is occurring. In industry, pressure-swing adsorption makes use of the two bed Skarstrom cycle where each bed acts as an adsorption bed or a desorption bed depending on the cycle (Crittenden & Thomas, 1998). Pressure-swing adsorption is most favored due to short cycle times and lower energy used compared to other types of adsorption. Most CO_2 capture applications make use of PSA (Intergovernmental Panel on Climate Change, 2005). Each of the adsorbent regeneration methods is discussed below.

Temperature-swing Adsorption (TSA)

Temperature-swing adsorption exploits the temperature of the adsorption bed. Most adsorption processes are exothermic and thus reducing the bed temperature favors the adsorption of the adsorbate molecules onto the adsorbent and this is achieved by passing a cold stream of gas through the bed (Bandyopadhyay, 2014; Towler & Sinnott, 2013). For desorption to occur, the temperature of the bed is increased by use of a hot gas stream resulting in the reverse process occurring. The gas used for desorption (stripping gas) is mostly steam, dry air or a slipstream of the purified product. TSA processes are mostly slow since they are dependent on the rates of heating and cooling of the adsorption beds (Intergovernmental Panel on Climate Change, 2005; Towler & Sinnott, 2013). Slow rates of heating and cooling impact on the cycle time of the adsorption-desorption process.

Electric-swing Adsorption (ESA)

Electric-swing adsorption (ESA) is defined by Bandyopadhyay (2014) and Grande *et al.* (2009), as an adsorption process which makes use of the Joule effect for desorption. The Joule effect is a phenomenon where temperature of a current-carrying conductor is increased as current flows through it. In ESA the adsorption bed acts as the conductor and current flows through it to increase the temperature. ESA seems to be similar to TSA but the two have differences which include faster rates of heating and for concentration of non-condensable gases, no diluent is required (Grande *et al.*, 2009; Lee *et al.*, 2015). According to Grande *et al.* (2009), ESA is mostly suitable for small adsorbate concentrations.

Vacuum-swing adsorption (VSA)

Vacuum-swing adsorption is a similar to a PSA, but different in that the adsorption process occurs at approximately ambient pressure and the desorption occurs under vacuum conditions (Roque-Malherbe, 2007).VSA of similar capacity to a PSA setup has two major advantages, which are a higher capacity and a smaller demand on energy use of up to 30 % (Crittenden & Thomas, 1998). Drawbacks of VSA include the use of moving parts in the use of pumps and / or compressors which are affected by wear and tear unlike ESA for example.

2.4.5 Types of adsorbents for CO_2 capture

An adsorbent is the solid material that is used to separate target adsorbate molecules from the bulk fluid during adsorption processes (Davidson, 2010). It is important that an adsorbent be effective in any commercial process where it is implemented, as the end goal of the process is significant separation of the target adsorbate molecules from the bulk fluid. For an adsorbent to perform its function, it is necessary that it has high internal volume to allow adsorbate molecules to access the adsorption sites (Crittenden & Thomas, 1998; Wilcox, 2012). It is also essential that an adsorbent possesses good mechanical properties, that is: strength and resistance to attrition, as well as good kinetic properties. Recyclability of the adsorbent material is also essential for techno-economic feasibility of adsorption processes. A good adsorbent should be able to maintain its adsorptive and mechanical properties. Processes and raw materials to produce the adsorbent should be inexpensive to enable adsorption as a technology to compete with already existing mature technologies such as absorption in areas like CO_2 capture. It is of importance to characterize an adsorbent in terms of its physical properties (pore size, pore volume and surface area), as these are the properties that influence the performance of the adsorbent (Yang, 2003). Pore sizes vary within an adsorbent; Table 2.3 shows three different types of pores based on their sizes.

Table 2.3: Different types of pores and their properties (Crittenden & Thomas, 1998).

Type of pore	**Diameter (nm)**	**Pore volume (cm^3/g)**	**Surface area (m^2/g)**
Micropores	< 2	0.15 – 0.5	100 – 1000
Mesopores (Transitional pores)	2 – 50	0.02 – 0.1	10 – 100
Macropores	> 50	0.2 – 0.5	0.5 - 2

In any adsorbent, the largest sized pores are of submicron size and they are a small fraction of the total volume. To determine the surface area of the adsorbent, N_2 adsorption experiments are conducted, and the results determined by use of the BET isotherm. Quantifying the amount of adsorbate, such as N_2 adsorbed over a pressure range up to the saturated vapor pressure, gives the pore volume of the adsorbent. The largest pore size of the adsorbent is determined based on the assumption that condensation occurs in small pores.

Several challenges are faced in the use of adsorption as a technology and these include low CO_2 adsorption capacities at low to moderate pressures, effect of moisture on the adsorbent material and selective adsorption of CO_2 in the presence of impurities (Lee & Park, 2014; Yang, 2003). Factors that are important in the design and production of adsorbents are low cost raw materials, low heat capacity, fast kinetics, high CO_2 adsorption capacity, high CO_2 selectivity as well as thermal, chemical and mechanical stabilities when in use (Crittenden & Thomas, 1998; Lee & Park, 2014).

There are several different types of adsorbents that are applied in CO_2 capture. Lee and Park (2014) as well as Yu *et al.* (2012) classify them as non-carbonaceous dry adsorbents and carbonaceous dry adsorbents. Different adsorbents have different properties which include pore structures, specific surface areas, and surface functional groups and are mostly adsorbate specific.

Non-carbonaceous adsorbents

Non-carbonaceous adsorbents are adsorbents that do not contain the element carbon in their structures. These include zeolites, silica materials, metal organic frameworks (MOFs), alkali-based materials, metal oxide carbonate materials.

Zeolites

Zeolites are defined as porous crystalline alumino-silicates which comprise of assemblies of SiO_4 and AlO_4 tetrahedral combined together (Crittenden & Thomas, 1998). According to Lee and Park (2014), zeolites are crystalline silicate framework materials. Zeolites can be synthesized or they can occur naturally. Different types of zeolites are synthesized by alteration of Si/Al ratio during the synthesis process (Crittenden & Thomas, 1998). Zeolites have a wide range of applications in industry, which include sweetening of sour gases and liquids, moisture removal from gas streams and recovery of CO_2 (Auerbach *et al.*, 2003); zeolites are currently being extensively studied for CO_2 capture. Within the structures of zeolites, pores exist with sizes ranging from 0.5-1.2nm (Auerbach *et al.*, 2003), forming cage-like structures which trap the adsorbate molecule, hence their application in CO_2 capture. Zeolites possess dipole and electrostatic interactions, as well as molecular sieving properties, making them suitable for CO_2 capture (Auerbach *et al.*, 2003). Zeolites also display high specific surface area which results in high CO_2 capacity (Lee & Park, 2014; Yu *et al.*, 2012). Further research concerning zeolites being applied in CO_2 capture, particularly zeolite 13X, has been done with the zeolite modified with Mono-Ethanol Amine (MEA). Here, the adsorption capacity of this zeolite was seen to increase even though the pore volume and specific surface area decreased. CO_2 capture by use of zeolites is applied via TSA and PSA (Yang, 2003), but drawbacks, which include high temperature and pressure of operation, are encountered when zeolites are used in CO_2 capture. Zeolite adsorbents function at pressures above 2bar and regeneration temperatures in excess of 300^oC. These operating conditions imply high adsorption operating costs and capital costs with regards to high-pressure withstanding equipment. CO_2/N_2 selectivity is also poor impeding the application of zeolites in post-combustion capture of CO_2, where the flue gas has a higher N_2 concentration than CO_2 (Breck, 1974; Xu & Hedin, 2014). Furthermore, Crittenden and Thomas *et al.* (1998), Lee and Park (2014) and Auerbach *et al.* (2003) state that CO_2 adsorption capacity drops drastically when moisture is introduced, because zeolites have a high affinity for moisture.

Silica Materials

Silica materials are also an upcoming type of adsorbent for use in CO_2 capture. Silica materials are materials based on silica (SiO_2) (Son *et al.*, 1998), and exhibit high surface areas, high pore volumes, good thermal, chemical and mechanical stability, as well as adjustable pore size. Most

applications of silica materials in CO_2 capture make use of surface modified silica materials. The surfaces of these silica materials are treated with amines to improve their affinity for CO_2. Examples of silica materials include the M41S group of silica, and silica gel, with the latter being the most common (Son *et al.*, 1998). According to Crittenden and Thomas (1998), silica gel is a partly dehydrated polymeric form of colloidal silicic acid with the formula $SiO_2.nH_2O$. Silica gel surfaces are mostly composed of Si-OH and Si-O-Si groups, making them highly suitable for application in water, alcohol, phenol and amine adsorption, by making use of hydrogen bonding (Crittenden & Thomas, 1998). Relative to zeolites, silica gel is easier to regenerate, with a regeneration temperature of 150^{o}C, whereas zeolites are regenerated at approximately 300^{o}C.

Metal Organic Frameworks (MOFs)

MOFs have become well known for their high surface areas, variable pore structures and modifiable surface properties. These properties may be adjusted by varying the metallic clusters or the surrounding ligands (Millward & Yaghi, 2005). MOFs are said to be highly crystalline materials comprising ordered, extended, one dimensional, two dimensional and three dimensional networks formed by metal ions or clusters connected to multifunctional organic ligands (Li *et al.*, 1999; MacGillivray & Lukehart, 2014; Millward & Yaghi, 2005). MOFs find application in methane (CH_4) and H_2 adsorption, where they display good selectivity and high adsorption capacity (Eddaoudi *et al.*, 2002; Li *et al.*, 1999). According to Lee & Park (2014), MOFs have molecules that are reticulate leaving voids at the centers, resulting in a large body volume. MOFs have recently been studied for CO_2 capture where they display remarkably high adsorption capacities in pure CO_2 gas streams (Rowsell & Yaghi, 2004). The drawbacks come with mixed gas streams, for example flue gas where the partial pressure of CO_2 is low, the adsorption capacity of MOFs decreases significantly (Lee & Park, 2014; Rowsell & Yaghi, 2004; Yu *et al.*, 2012). Increasing the partial pressure of CO_2 will ultimately increase the operating costs of the adsorption process. Research where MOFs have been treated with amines to enhance CO_2 capture is currently underway in an attempt to circumvent the low capacity challenge in low CO_2 partial pressures (Yu *et al.*, 2012). Furthermore, synthesis of MOFs is quite a complex process and the raw materials (metal complexes and organic ligands) required are expensive (Millward & Yaghi, 2005; Yu *et al.*, 2012). Literature also states that MOFs have a high affinity for moisture which weakens their mechanical strength and makes them less

durable (Eddaoudi *et al.*, 2002; Yu *et al.*, 2012). Given that the target application is in post-combustion capture, where CO_2 partial pressure is low and moisture may be present, more research to improve MOFs for post-combustion capture of CO_2 is necessary.

Alkali-based materials

Alkali-based materials are alkali-metal carbonates which are applied as dry adsorbents in CO_2 capture (Zhao *et al.*, 2013). Alkali-based materials are able to operate at moderate temperatures of below 200^{o}C (Yu *et al.*, 2012). When capturing CO_2, alkali-based materials undergo the reaction shown:

$$M_2CO_3(s) + H_2O(g) + CO_2(g) \leftrightarrow 2MHCO_3(s) \qquad \text{(Reaction 3)}$$

$$\Delta H = -ve\ (Reaction\ is\ exothermic)$$

Where M can be sodium (Na) or potassium (K).

In the reverse reaction which occurs after heating, the alkali based adsorbent is recovered, together with the CO_2 and H_2O in gaseous form. Passing this mixture through a condenser will ensure separation of the CO_2 from H_2O with a high purity CO_2 stream being produced. Adsorption of CO_2 using alkali-based materials occurs in the temperature range 60 - 110 ^{o}C, forming alkali-metal carbonates, and the reverse process occurs in the temperature range 100 – 200 ^{o}C, regenerating the alkali-metal carbonate (Wilcox, 2012). Alkali-metal carbonates are highly desirable for post-combustion CO_2 capture as they can withstand fairly high temperatures and do not require the flue gas to be cooled before entering the CO_2 capture plant. Furthermore, the alkali-metal carbonates are moisture tolerant. Challenges, however, arise with recyclability, particularly stability of the adsorbent material over time while in continuous use (Wilcox, 2012).

Metal Oxide Carbonate Materials

Metal oxide carbonate materials are based on the use of metal oxides such as calcium oxide (CaO) and magnesium oxide (MgO) as adsorbents. The CO_2 is captured in the form of an insoluble carbonate. Literature shows that MgO has been found to be a good adsorbent for CO_2 capture (Yu *et al.*, 2015). The advantages of using MgO as a CO_2 adsorbent include its low cost, abundance and low toxicity (Wilcox, 2012). Drawbacks include the fact that these metal oxides

have low CO_2 adsorption capacity. According to Bhatta *et al.* (2015), the adsorption by metal oxides is performed via:

$$MO\ (s) + CO_2(g) \leftrightarrow MCO_3\ (s) \quad \Delta H = -175\ kJ/mol \qquad \text{(Reaction 4)}$$

The reverse process which regenerates the adsorbent occurs via:

$$MCO_3(s) \leftrightarrow MO(s) + CO_2\ (g) \qquad \Delta H = +179.2\ kJ/mol \qquad \text{(Reaction 5)}$$

Assuming perfect conditions and no heat losses, it is possible to design an adsorption-desorption cycle such that a small quantity of heat is added to recover the solid adsorbent as the enthalpies of reaction are approximately equal.

Carbonaceous Adsorbents

Carbonaceous adsorbents are materials that are based on one material, carbon. These types of adsorbents have several advantages for adsorption which include electrical and heat conductivities (for ESA and TSA respectively), light weight, high specific surface areas and large pore volumes (Lee & Park, 2014; Yu *et al.*, 2012). Furthermore, carbonaceous adsorbents are not affected by moisture, they function at moderate temperatures and pressures, and hence consume less energy in adsorption relative to non-carbonaceous adsorbents; in addition, the cost of the base element, carbon, is moderate (Lee & Park, 2014; Yu *et al.*, 2012). All these properties make them lucrative for CO_2 capture. Several types of carbonaceous adsorbents exist and these include activated carbons (AC), ordered porous carbons (OPC), carbon molecular sieves (CMS), porous polymers, carbonized polymers, and resins as well as bone charcoals.

Activated Carbons (AC)

According to Li *et al.* (2008) and Lee and Park (2014), ACs are part of a group of carbons from carbon blacks to nuclear graphites. Crittenden and Thomas (1998) define ACs as elementary microcrystallites stacked in random orientation made by thermal decomposition of various carbonaceous materials which are then taken for activation. Activated carbons maybe prepared from several different materials that contain carbon, including coal, petroleum and wood. ACs have pore structures that can be manipulated during preparation processes (Li *et al.*, 2008; Yu *et al.*, 2012), and display good thermal stability with a moderate cost of production (Li *et al.*,

2008). To add to this, functional groups on the surfaces of ACs may be modified to enhance adsorption in CO_2 capture. Manipulating the pores entails altering pore size, to allow the ACs to act as molecular sieves. This can be very beneficial in CO_2 capture where the flue gas contains CO_2, O_2 and N_2 which are 3.6, 3.5 and 3.3 Â respectively. Use of ACs in CO_2 also has the added benefit of thermal stability. ACs are stable at temperatures in excess of 500^oC compared to several other adsorbents, and in addition they are cheap to produce (Lee & Park, 2014; Li *et al.*, 2008).

Ordered Porous Carbons (OPC)

OPCs have been mainly tested for gas storage and use in catalysis. OPCs display high specific surface areas, good chemical stabilities, large CO_2 adsorption capacities and may have their pore properties (volume and size) altered to enhance adsorption (Crittenden & Thomas, 1998). For this reason they are postulated to be good for CO_2 adsorption (Crittenden & Thomas, 1998).

Carbon Molecular Sieves (CMS), Carbonized polymers and resins

Wabhy *et al.* (2012) defines carbon molecular sieves as carbonaceous materials that have narrow pore size distributions, endowed with a selective adsorption capacity for particular components from a mixture. CMSs are able to separate molecules on the basis of size, shape, adsorption rate or a difference in adsorption equilibrium (Carruthers *et al.*, 2012; Wahby *et al.*, 2012). CMSs have a great potential in CO_2 capture. In the United States of America, CMSs produced from pyrolysis and activation of polyvinylidene have been commercialized and research is focusing on producing CMSs for CO_2 capture at a large scale (Carruthers *et al.*, 2012). Research with CMSs in CO_2 capture has shown that for a high adsorption capacity to be achieved, well developed micro porosity is necessary. CMSs have the added advantage of being able to perform adsorption at temperatures ranging from 0 to 50 ^oC, implying that energy costs with using this adsorbent are relatively low (Carruthers *et al.*, 2012; Wahby *et al.*, 2012).

Carbonized polymers and resins are produced from resins which include phenol, formaldehyde and styrene amongst others (Crittenden & Thomas, 1998). These materials are pyrolized with the products from the pyrolysis being carbonaceous adsorbents (Crittenden & Thomas, 1998). These adsorbents are still under research and there is interest in their application for CO_2 capture.

Porous polymers

Porous polymers are porous solid materials that are synthesized from organic building blocks (Xu & Hedin, 2014). According to Xu and Hedin (2014), there are no standardized names for them and they are similar in nature to conjugated porous polymers, porous aromatic frameworks and hyper-crosslinked polymers. Synthesis of porous polymers can be through simple and traditional reactions. Amongst adsorbents applied in CO_2 capture, use of porous polymers is advantageous in that they are organic in nature and because they are organic, they are biodegradable (Ngoy *et al.*, 2014; Xu & Hedin, 2014). Biodegradability is an important property in adsorbents as there is an environmental awareness drive to ensure that adsorbents used are environmentally friendly (Dai & Lu, 2014; Ngoy *et al.*, 2014). Given that porous adsorbents may also be synthesized from several different reactions, it is possible that the monomer units may be coupled and the polymer chain lengthened, allowing a larger surface area for CO_2 capture (Ngoy *et al.*, 2014). Furthermore, the surface of the polymer may be grafted with amines to enhance the CO_2 capture of the adsorbent (Xu & Hedin, 2014). Porous adsorbents, depending on the raw materials from which they are produced, could be less hydrophilic compared to other adsorbents. Porous adsorbents also possess good chemical and thermal stability (Xu & Hedin, 2014). Drawbacks of porous adsorbents are that their adsorption capacities are low compared to other adsorbents such as MOFs and zeolites (Ngoy *et al.*, 2014; Xu & Hedin, 2014).

Adsorbent surface treatment to enhance CO2 capture

Literature has shown that adsorbent surfaces may be treated with several chemicals to enhance their adsorption capability or affinity for CO_2 capture (Linneen *et al.*, 2014; Yu *et al.*, 2012). There is need to enhance CO_2 adsorption because currently, most adsorbents display low CO_2 adsorption capacities at low pressures and low selectivity when are introduced with the CO_2, as well as low tolerance to moisture (Lee & Park, 2014; Yang, 2003). In the enhancement of solid adsorbents, the adsorbent is treated with a chemical which results in the alteration of its properties such that CO_2 adsorption will improve in capacity, selectivity and moisture tolerance (Davidson, 2010). These properties are the chemical structure of the adsorbent surface, the pore size, pore volume and specific surface area of the adsorbent (Davidson, 2010). Research has shown that the most promising adsorbent modification can be done by use of the basic organic group, amines or by use of an inorganic metal oxide, for instance an alkali-metal or alkali earth

metal (Lee & Park, 2014; Yu *et al.*, 2012). CO_2 is known to be an acidic gas, hence the use of amines and inorganic metal oxides to enhance the adsorption of CO_2 (Aresta, 2010). When the metal oxide or amines interact with the CO_2, covalent bonds are formed resulting in the fixing of CO_2 onto the surface of the adsorbent. The reaction schemes shown earlier display the chemical reactions that occur. It has been found that the greater the amine or metal oxide loading, the greater the CO_2 capture (Lee & Park, 2014; Yu *et al.*, 2012). Amine or metal oxide loading, however, decreases the surface area and pore volume of the adsorbent (Lee & Park, 2014). For the purposes of this research, the literature survey will focus on amine-based adsorbents.

The type of interaction between solid adsorbents and amines used to enhance adsorption determines whether the adsorbent is amine-grafted or amine impregnated (Yu *et al.*, 2012). Amine-impregnation refers to penetration of polymeric fluids into an assembly of fibers (Linneen *et al.*, 2014; Yu *et al.*, 2012), whereas amine-grafting is the addition of polymer chains onto a surface (Linneen *et al.*, 2014; Yu *et al.*, 2012). Research has shown that the use of super critical fluids as a solvent to infuse amines into the supports improves the loading of amines onto the adsorbents (Lee & Park, 2014). Figure 2.15 shows some of the different types of amines used for impregnation and/or grafting to enhance CO_2 adsorption.

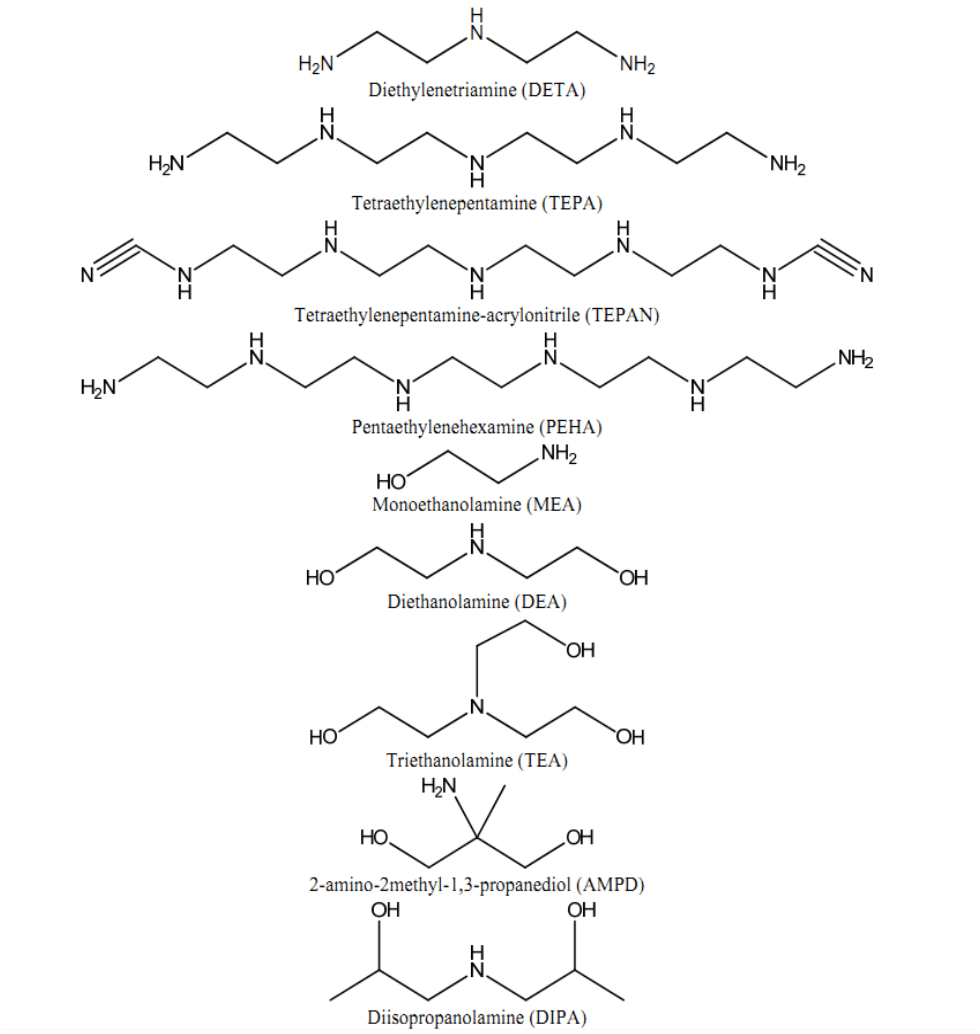


Figure 2.15: Examples of amines used in grafting or impregnation to enhance CO_2 capture (Yu *et al.*, 2012).

Amines grafted or impregnated in adsorbents are beneficial for CO_2 capture enhancement, but come with an environmental and health risk, already experienced in the CO_2 absorption industry (Olajire, 2010). It is thus essential that the synthesized adsorbent materials be environmentally friendly, that is biodegradable.

2.4.6 Amine grafted Polysuccinimide (PSI) for CO_2 capture via adsorption

Amine-grafted polymers have become very popular and are a promising type of adsorbent. The potential stems from the currently widely applied method (absorption) which makes use of amine solvents such as Polyethylenenimine (PEI) to capture CO_2 (Chungsying *et al.*, 2008). An amine-

grafted polymer consists of a backbone, which is the polymer, and an amine, which is attached to the polymer to act as the anchoring site onto which the CO_2 attaches. The CO_2 attaches to the anchoring site by formation of a weak intermediate carbamate (-COO-) as it reacts with the amine (Ngoy *et al.*, 2014). Amine groups are incorporated due to their high affinity for CO_2, and they also stabilize the CO_2 adsorption process as they form stable intermediates. An adsorbent should have a large surface area and a large enough pore size to enable the adsorbate (CO_2) to adsorb to it (Ruthven, 1984; Suzuki, 1990). These properties can be improved by use of a process known as freeze-drying. Freeze-drying is used extensively in the food and drug industry to improve properties such as pore volume, pore size and surface area. Freeze-drying is a process where mass and heat are both transferred simultaneously from a material, resulting in an improved physical and chemical composition as well as microstructure (Ishwarya *et al.*, 2015; Oikonomopoulou *et al.*, 2011). The material to be freeze-dried may contain water already or may be dissolved in water and is frozen by use of liquid N_2 (Ishwarya *et al.*, 2015; Oikonomopoulou *et al.*, 2011). Thereafter, the frozen water is sublimated and removed, leaving the material with an improved microstructure displaying higher porosity. A higher porosity implies that the pore size as well as the surface area of the material has increased (Ishwarya *et al.*, 2015; Oikonomopoulou *et al.*, 2011). Furthermore, freeze-drying is beneficial in that it can be applied to materials which are temperature sensitive because no heat is added; it prevents shrinkage of materials, and it reduces the possibility of material deterioration reactions due to almost complete dehydration of the material (Ishwarya *et al.*, 2015; Oikonomopoulou *et al.*, 2011). Freeze-dried materials have a spongy and highly porous structure which is desirable in adsorption processes (Ishwarya *et al.*, 2015).

Against this background, the current research investigated the synthesis and performance evaluation of a novel material for CO_2 capture. In particular, the effect of the presence of water-soluble amines in the amine-grafted poly-succinimide (PSI), herewith referred to as Polyaspartamide (PAA), adsorbent was investigated. Methyl Amine (MA) and Mono-Ethanol Amine (MEA) were employed as water-soluble amines and the effects of the change in their concentration on CO_2 adsorption capacity was investigated as well. The water-soluble amines were grafted to an Ethylenediamine (EDA) grafted PSI (PSI-EDA), with the EDA added to improve the chemical surface of the adsorbent for CO_2 capture to enhance the CO_2 adsorption capacity. The solubilizing group was added to enhance the water solubility of the adsorbent to

enable the adsorbent to dissolve in water, paving the way for freeze-drying to improve the geometric structure of the solid adsorbent. The dissolution of the adsorbent in water could enhance the CO_2 desorption process.

2.4.7 Adsorption mechanism during CO_2 capture

It is of paramount importance that solid adsorbents have high surface areas to achieve high capacity for adsorption. To achieve high surface areas, solid adsorbents should thus have fine pores in the microporous and/or mesoporous range. In the design of adsorbent processes, understanding the adsorbate transport mechanisms through the adsorbent is important. The movement of adsorbate molecules occurs via several different possible diffusion mechanisms, which depend on the pore size of the solid adsorbent material. Adsorption cycle times are significantly dependent on the transport mechanisms occurring, which are ultimately dependent on the pore size of the adsorbent material. Experiments conducted by Yu *et al.*, (2012) show the importance of understanding adsorption mechanisms. They determined that adsorption capacity increased with an increase in temperature. This was because of an increase in the temperature which introduced more kinetic energy for the adsorbate molecules and the diffusion improved, resulting in a higher adsorption capacity at a higher temperature. According to Wilcox (2012), when pore size becomes restrictive, as it is for some microporous adsorbents, the pore openings become smaller and the adsorption of the adsorbate molecules is limited by diffusion rather than by thermodynamics. The distinction between microporous, mesoporous and macroporous adsorption emanated from the different mass transfer (diffusion) processes occurring (Barnes & Gentle, 2011; Wilcox, 2012). In micropores, where the adsorbate molecule does not move away from the surface force field, the surface forces are very significant (Barnes & Gentle, 2011; Wilcox, 2012). In comparison, capillary forces are significant in mesopores with macropores contributing insignificantly to the adsorption capacity of the adsorbent material (Wilcox, 2012). Micropores are the smallest of classified pore sizes in adsorbents and can be impacted by steric hindrance where the molecule size becomes larger than the pore size of the material adsorbent material. Knudsen diffusion is significant in the mesoporous range because adsorbate-adsorbent interactions occur more often than adsorbate-adsorbate interactions in the bulk fluid phase (Wilcox, 2012). However, surface diffusion and capillary effects may influence transport of

adsorbate molecules. Primary diffusion mechanisms involved in mesopores and macropores are molecular diffusion, Knudsen diffusion and Poiseuille flow.

Several mass transfer processes occur for the selective transport of CO_2 from the gas phase to the active adsorption site on the adsorbent surface. Figure 2.16 shows the mass transfer processes that occur during CO_2 adsorption. When CO_2 adsorption occurs, bulk and film adsorption occur outside the solid adsorbent region in the bulk fluid phase and at the interface between the gas phase and the solid phase. Inter-particle mass transfer then occurs among the adsorbent particles and intra-particle mass transfer within the adsorbent particles. During these mass transfer processes, mass transfer resistance is experienced in the fluid film surrounding the adsorbent, in the macropores formed from inter-particle spacing of the bound micro-particles and in the micropores of the micro-particles.

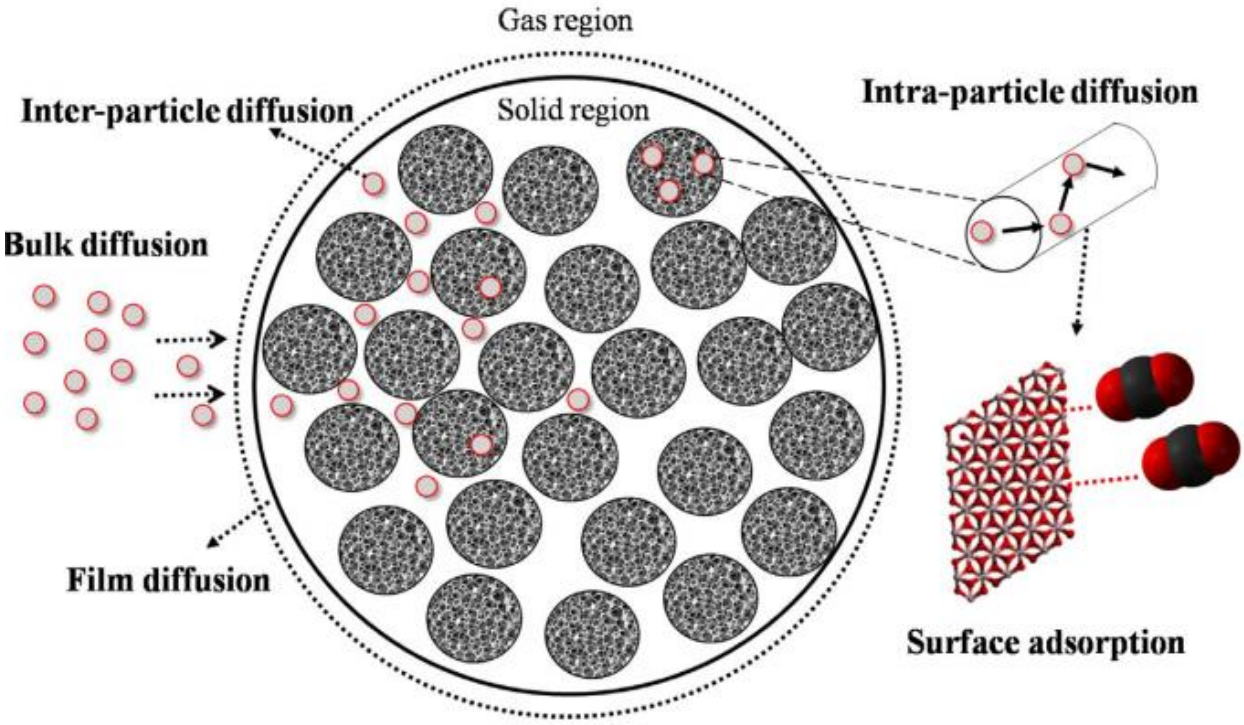


Figure 2.16: CO_2 adsorption mechanisms onto a solid adsorbent (Song *et al.*, 2015).

During mass transfer, water vapor in the atmosphere is present and the adsorbent surface is surrounded by a thin fluid film, and it is through this film that molecular diffusion occurs. The diffusion resistance, when external mass transfer occurs is, dependent on the thickness of the boundary layer of the thin fluid film, and this is dependent on the hydrodynamic conditions. The

external resistance may be correlated in terms of a mass transfer coefficient, k_f with the molar flux of CO_2 as:

$$J_{f,CO_2} = D_f \frac{(c_{i,CO_2} - c_{S,CO_2})}{\delta} = K_f\left(C_{i,CO_2} - C_{S,CO_2}\right) \quad (2.10)$$

In equation 2.10, the variables are defined as:

J_{f,CO_2} is the molar flux of CO_2 at the interface of the gas and the bulk fluid film,

D_f is the diffusivity of CO_2 in the film,

δ is the film thickness,

c_{i,CO_2} is the concentration of CO_2 at the gas-film interface,

c_{S,CO_2} is the concentration of CO_2 at the adsorbent surface,

k_f is the mass transfer coefficient of the film.

It should be noted that the concentration of CO_2 in the fluid film does not remain constant during the diffusion process.

2.4.8 Factors influencing post-combustion CO_2 capture via adsorption

CO_2 capture is influenced by several factors which include temperature, pressure, and purity of the feed gas, as well as the nature of the adsorbent. These factors will determine the magnitude of adsorption that occurs depending on how they are individually adjusted and how they interact with each other.

Temperature

Temperature of the incoming flue gas stream is an important factor in CO_2 adsorption processes. The effect of temperature depends on whether physisorption or chemisorption is occurring. As such, at equilibrium, if temperature is increased, adsorption decreases. The converse is true, if temperature is decreased, adsorption increases. This phenomenon is based on Le Chatelier's principle which when extrapolated to exothermic processes states that increasing temperature decreases the magnitude of the exothermic process (Brown *et al.*, 2012). If chemisorption is

occurring at equilibrium, the magnitude of adsorption initially increases to a maximum, thereafter it starts to decrease (Brown *et al.*, 2012; Faust & Aly, 1998). Brown *et al.* (2012) suggests that this is because for chemisorption to occur, the activation energy has to be achieved first, thereafter the reaction occurs and the subsequent decrease may be attributed to the adsorption process becoming exothermic after the reaction has been initiated.

Pressure

The pressure of the incoming flue gas stream is of importance in post-combustion CO_2 adsorption capture. The magnitude of the adsorption is proportional to the magnitude of the pressure. As pressure increases, adsorption also increases. The higher the pressure, the higher the partial pressures of the component to be adsorbed hence the increase in the adsorption of that component (Faust & Aly, 1998; Keller & Staudt, 2005). The converse is true, the lower the pressure, the lower the adsorption (Faust & Aly, 1998).

Composition of the flue gas

The composition of the flue gas also influences the adsorption process. According to Keller & Staudt (2005), the higher the critical temperature of the component in the mixture, the greater the amount of that component is adsorbed. This means that highly liquefiable components like water get adsorbed first and in higher quantities unlike components like N_2 which are not easily liquefiable.

Nature of the adsorbent

Adsorption occurs on the adsorbent surface and thus the nature of the adsorbent affects CO_2 adsorption greatly. The nature of the adsorbent encompasses all the properties of the adsorbent which are surface area, pore volume, pore size, physical form of the adsorbent (powder form or granule form) and the chemistry of the adsorbent surface (Crittenden & Thomas, 1998; Faust & Aly, 1998; Yang, 2003). The higher the surface area, pore size, forms of the adsorbent and pore volume of the adsorbent, the higher the adsorption. These properties enable the adsorbent to have a higher contact with the adsorbate molecules hence increasing the adsorption of CO_2 onto the adsorbent (Ngoy *et al.*, 2014). The chemistry of the adsorbent also affects the adsorption process with specific functional groups increasing the affinity of the adsorbent to adsorb particular molecules (Czaun *et al.*, 2013; Yang *et al.*, 2008). In the case of CO_2 adsorption, amine groups

may be grafted onto the adsorbent or impregnated into the adsorbent to enhance the selectivity of CO_2 being captured into the adsorbent (Linneen *et al.*, 2014).

2.4.9 Optimization studies in CO_2 capture

Several variables influence CO_2 capture via adsorption. Each of them when varied has its own individual influence on CO_2 adsorption and when they all interact with each other, it brings about some complexity in modeling the system. In engineering work, lab-scale runs are performed in the initial stages of process development to ensure that the processes are well designed and understood, thus it is necessary for optimization to be done on such an adsorption system. According to Mckeown *et al.* (1990), optimization is the solving of problems of the type: find the values of x, y and z such that some quantity F which depends on x, y and z is a maximum or a minimum. In post-combustion adsorption capture it is necessary to determine how the temperature, pressure and the composition of the flue gas all influence the adsorption of CO_2. In optimization, two approaches may be applied, the classical approach or the design of experiment approach (DoE) (Lazic, 2004; McKeown *et al.*, 1990). The classical approach is such that one factor is varied at a particular time and the remaining factors are kept constant. Thereafter, the optimum point of each factor is determined. The challenge with this method is that many experiments needs to be done in order to determine the optimum value of each factor, and furthermore, the method does not give the optimum values of all the factors interacting together. The DoE approach makes use of statistical methods and allows the investigator to design the experiment such that cause and effect relationships can be determined (Lazic, 2004). DoE method offers several advantages which include, reduction in the number of experiments to be conducted, simultaneous varying of factors involved and reliable solutions may be achieved from the results obtained (Lazic, 2004). Several DoE designs may be used depending on the nature of the factors being investigated, whether they are categorical, qualitative or quantitative (Lazic, 2004). Table 2.4 shows some of the possible designs.

Table 2.4: Some of the possible DoE designs applied in optimization studies (Lazic, 2004).

Experimental Design	**Factors**
Central composite orthogonal designs (CCD)	Quantitative
Central composite rotatable design (CCD)	Quantitative
Full Factorial design	Categorical/qualitative, quantitative and combined
Random balance design	Categorical/ qualitative and quantitative
Fractional replicate designs	Categorical/ qualitative and quantitative

Following the design of the experiment, the experiment is then performed and the results of the objective function are obtained at varying values of the factors considered. Regression models can then be proposed, variance calculated and cross validation performed to determine whether the proposed model can be applied. According to Demirel and Kayan (2012), there are four important stages when performing optimization studies, namely: 1) designing and performing statistically designed experiments; 2) proposing a mathematical model basis of the experimental data and focus on the data of analysis of variance; 3) the control of efficiency of the model directly and lastly; 4) estimating the response and to verify the model. The DoE results can then be plotted as response surfaces in Matlab to determine the optimum conditions.

2.5 Chapter Summary

Carbon dioxide capture by use of adsorbents is essential to reduce CO_2 emissions. Adsorption is a process where particular fluid molecules (adsorbate) are immobilized (adsorbed) onto the surface of a solid material (adsorbent). When adsorption occurs, it is necessary to recover the adsorbent, a process known as desorption. Adsorption-desorption cycles can be determined by manipulating the temperature, pressure, electric current and vacuum conditions of the adsorbent bed. Different types of adsorbents exist and may be used for adsorption capture of CO_2. These

adsorbents may be classified as carbonaceous or non-carbonaceous adsorbents. Carbonaceous adsorbents are adsorbents solely based on carbon as the material of synthesis while non-carbonaceous adsorbents are not entirely based on carbon. Examples of carbonaceous adsorbents are Activated Carbons, Ordered Porous Carbons, Carbon Molecular Sieves and Porous polymers. Examples of non-carbonaceous adsorbents include zeolites, silica materials, metal organic frameworks, alkali-based materials and metal oxide-carbonate materials. Different adsorbents may have their surfaces modified by doping or grafting with amines to enhance the capture of CO_2. The amines grafted onto the polymer act as CO_2 anchoring sites by forming carbamates with CO_2, thus it is adsorbed. When adsorption occurs, several mechanisms may occur. These are bulk diffusion, which is from the bulk phase to the film, film diffusion from the film to the solid surface or back to the bulk phase, inter-particle diffusion amongst the adsorbent particles and intra-particle adsorption within a single particle. Temperature, pressure, nature of the adsorbent (particle size, pore size, pore volume and surface area) and composition of the flue gas are the factors that influence adsorption of CO_2.

After adsorbent synthesis, characterization and performance evaluation, it is necessary that the adsorbent performs at the highest possible capacity. This is done by optimizing the operating variables which are the factors that affect adsorption. It is also essential to determine how the factors influence each other. This can be done by using the Central Composite Design (CCD) of experiment. This method of designing experiments determines the minimum the number of experiments to be conducted such that a regression model can be obtained; RSM is then employed to give a visual of how the factors interact with each other and the optimum operating ranges.

Chapter 3: Materials and Experimental Procedures

3.1 Introduction

In this work, amine grafted PSI (PAA) was synthesized with two different combinations of amines, MA-EDA and MEA-EDA grafted onto PSI. MA and MEA were incorporated as the water-soluble components to allow the resulting adsorbent ability to dissolve in water, a precursor to the freeze-drying process which was expected to enhance the physical properties (pore size, pore volume and surface area) of the adsorbent. The dissolution of the adsorbent in water could enhance the CO_2 desorption process in further development. The synthesized materials were evaluated for CO_2 adsorption.

3.2 Material and equipment used for the study

Phosphoric acid, D. L. Aspartic acid, Dicyclohexylcarbodiimide (DCC), Ethylenediamine (EDA), Sodium hydroxide and solvents such as N, N-Dimethylformamide (DMF > 99%), Acetone and Ethyl Ether, were obtained from Sigma-Aldrich, South Africa. The liquid N_2, gaseous N_2, CO_2 and air were of analytical grade obtained from Afrox, South Africa.

A rota-vapor R 114 was used during the synthesis of the PSI, the backbone polymer. All glassware and magnetic stirrers were obtained from the laboratory. A thermo-gravimetric analyzer (TGA), TA STD Q600, was used to determine the thermal stability of the synthesized adsorbent as well as for determination of the CO_2 adsorption capacity of the adsorbent.

The equipment used in this research was: a Rota-vapor R-114 and Pot heater and Rota-vapor R-210 were used to perform the polycondensation reaction to produce the polymer and for evaporation to eliminate solvent in the compound respectively. An oven LabCon: EGO4 (50 °C - 300 °C) was used for routinely post-drying samples. Simultaneous DSC-TGA Q Series thermo-gravimetric analyser (SDT Q600) was used for the thermal stability and the adsorption capacity determinations.

3.3 Experimental procedure

The experimental procedure was conducted in three main parts which were synthesis of the adsorbent, characterization of the adsorbent and performance evaluation of the adsorbent which included preliminary adsorption performance evaluation and the determination of the effects of

operating variables on the adsorption performance of the synthesized material. Figure 3.1 below shows the flow diagram summarizing the procedure followed in conducting the entire experiment. As shown in Figure 3.1, the initial stage was the synthesis of PAA (amine grafted PSI). The synthesized material was then characterized and preliminary studies testing the CO_2 adsorption performance were conducted by use of a TGA. The performance evaluation was then concluded by investigating the effect of operating variables on the CO_2 adsorption capacity of PAA. Upon evaluating the performance of the adsorbent, the performance was then compared to existing adsorbents to determine whether it was a good adsorbent or not.

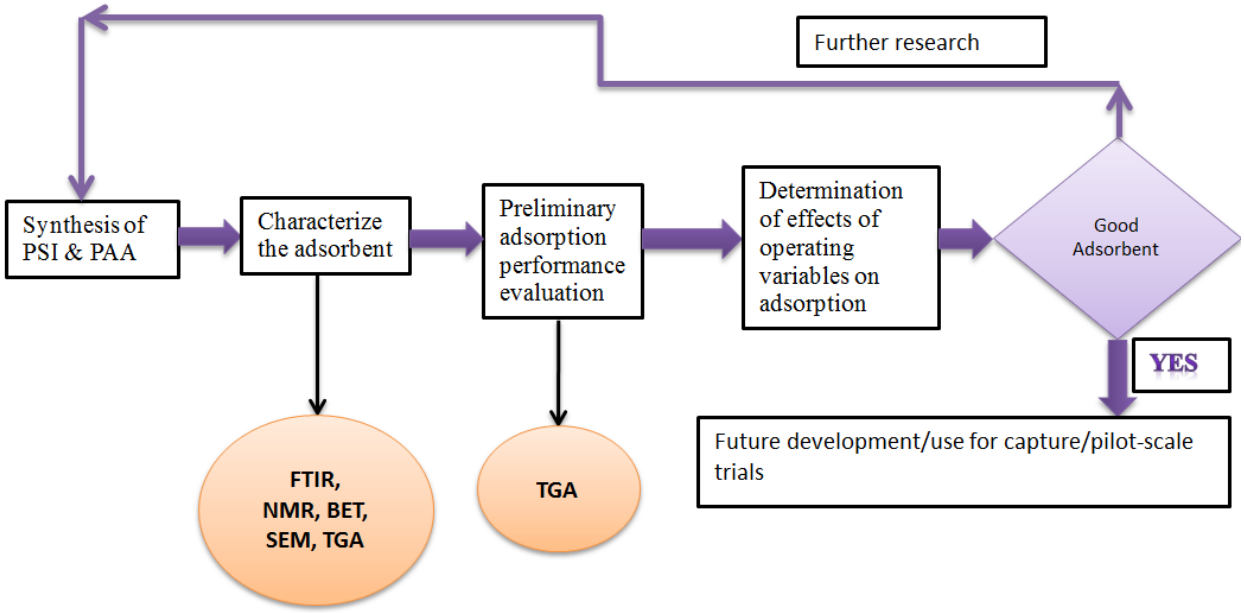


Figure 3.1: Flow diagram showing a summary of the procedure.

3.3.1 Synthesis of PSI and the water-soluble amine-grafted PSI

PSI was synthesized from a poly-condensation reaction of aspartic acid in a phosphoric acid medium (Kumar, 2012; Ngoy *et al.*, 2014). The procedure depicted in Figure 3.2 was followed during the synthesis of PSI. D.L. aspartic acid was homogenized with phosphoric acid in a mass ratio of 2:1 in a 2L volumetric flask. In each synthesized batch of PSI, 25 g of aspartic acid was used with 12.5 g of phosphoric acid due to available glassware capacity. The flask was then heated in an oil bath to 250 ^{o}C while rotating on a rota-vapor to ensure vacuum conditions as well as uniform heating of the reaction. A vacuum pump was used to create the necessary vacuum conditions. Liquid N_2 was used to protect the pump from damage by the chemicals that

were pulled out of the reactor during the vacuum process. The expansion was monitored and controlled by use of N_2 gas. At the end of the expansion, the reaction temperature was reduced to 190^{o}C and maintained at 190 ^{o}C for 2 hours. The product obtained was washed with distilled water and filtered off until the pH was between 6 and 7. The pH was monitored using pH paper. The washed product was dried in an oven at 45 ^{o}C for 72 hours. The dried product was weighed and dissolved in N, N Dimethylformamide (DMF) in preparation for the coupling and grafting process.

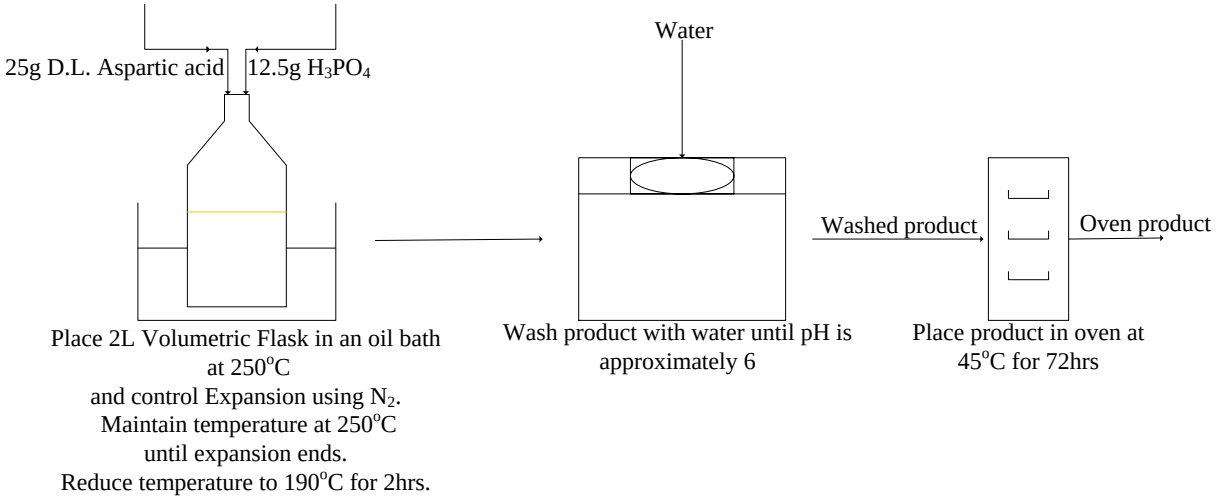


Figure 3.2: Schematic showing the experimental procedure for the synthesis of PSI.

The synthesis continued by dissolving 1g of oven product in 4.04 ml of DMF. The brownish mixture obtained was stirred for 12 hours in a flask. The flask was then cooled to approximately -2 ^{o}C, using an ice bath and stirred for 1 hour. Then DCC was added, as the coupling agent for the lengthening of the polymer chain in order to multiply the available sites for adsorption, at a ratio of 1 g of DCC to 8.57 g. The resulting mixture in the flask was stirred for 4 hours in an ice bath, thereafter it was left to warm to room temperature for 12 hours. After 12 hours, the mixture was centrifuged to obtain a clear liquid which was precipitated by addition to distilled water. The precipitation was achieved by stirring distilled water in a 4L beaker by use of a magnetic stirrer; thereafter the centrifuged solution was added after which precipitation occurred. Following the precipitation, the precipitate was filtered and dried at 45^{o}C in an oven for 48 hours to give a brittle solid, namely PSI. The synthesized PSI was subsequently grafted with two combinations of amines at a variable ratio in order to cover the backbone completely. Table 3.1 shows the amount of amine used, amine concentration, as well as amount of PSI used in the synthesis of the

water-soluble amine-grafted PSI (PAA). In Table 3.1, adsorbent samples 1-5 make use of MA-EDA amine combination and adsorbent sample 6-10 make use of MEA-EDA combination. Within each of the two combinations of amines, the amount of PSI was kept constant, while the amine combination concentration was varied.

Table 3.1: Materials used in the synthesis of the PAA.

Sample	**PSI amount (moles)**	**MA amount (moles)**	**MA fraction (%)**	**MEA amount (moles)**	**MEA fraction (%)**	**EDA amount (moles)**	**EDA fraction (%)**
1	0.0305	0.0305	100	-	-	0	0
2	0.0305	0.0244	80	-	-	0.0061	20
3	0.0305	0.0183	60	-	-	0.0122	40
4	0.0305	0.0122	40	-	-	0.0183	60
5	0.0305	0.0061	20	-	-	0.0244	80
6	0.0305	-	-	0.0305	100	0	0
7	0.0305	-	-	0.0244	80	0.0061	20
8	0.0305	-	-	0.0183	60	0.0122	40
9	0.0305	-	-	0.0122	40	0.0183	60
10	0.0305			0.0061	20	0.0244	80

The PSI was dissolved in DMF (to prepare it for grafting) (3 g was dissolved in 15 ml), and was added to methyl-amine also dissolved in DMF in the same ratio. The resulting solution was flushed with N_2 gas and stirred for 24 hours at room temperature. With stirring, this solution was then added drop-wise to EDA dissolved in DMF, in the same ratio as PSI, and cooled in an ice bath. The solution was flushed with N_2 gas and stirred for 20 hours in the ice bath, followed by 5 hours at room temperature. Concentration of the solution on the rota-evaporator at 60˚C followed, to half the volume. Precipitation of the concentrated solution with a mixture of diethyl ether and hexane in a ratio of 2 to 1 followed. The precipitate was then washed with hot toluene followed by hot acetone, and then the precipitate was dissolved in distilled water. The solution was freeze-dried to obtain the water-soluble PAA. The amount of MA and EDA was varied and this procedure was repeated with the MEA-EDA combination, making use of the amounts shown in Table 3.1.

3.3.2 Characterization of the synthesized PSI and amine-grafted PSI (PAA)

Nuclear Magnetic Resonance (NMR) analysis, Fourier Transform Infrared Spectroscopy (FTIR), Scanning Electron Microscopy (SEM), N_2 physisorption (by BET analysis) and Thermo-gravimetric Analyses (TGA) were performed to characterize the synthesized adsorbent and each of these techniques is discussed below.

Nuclear Magnetic Resonance (NMR)

NMR is an analytical technique that is used to determine the molecular structure and purity of a given material sample. The purity can then be used to determine what the sample contains. NMR is active in the magnetic field of ^{1}H (proton) or ^{13}C (carbon) where electromagnetic radiation can be absorbed at a frequency characteristic of the isotope (Balci, 2005). NMR works via a principle specific resonance of an intermolecular magnetic field around an atom in a molecule changing hence providing detail of the electronic structure of the molecule. For this work, ^{1}H NMR was performed at the in the School of Chemistry at the University of the Witwatersrand, Johannesburg. The equipment used was a Bruker AVANCE III 500 at 500.13 MHz. The spectra obtained were used to confirm the structure of PSI and PAA. The spectra were recorded in Dimethyl Sulfoxide (DMSO) solution.

Fourier Transform Infrared Spectroscopy (FTIR)

FTIR is used to determine inter-atomic bonds in molecules. FTIR is an analytical technique providing detail on solid, liquid or gas molecules through the infrared spectrum captured by absorption, emission, photoconductivity or raman scattering (Smith, 1996). Every atom in a molecule vibrates at a specific wave number making each atom identifiable. For this reason, FTIR analysis is based on the absorption of infrared radiation causing molecules to vibrate. This vibration then results in the bonds between atoms being strained and stretched, in particular bands with infrared radiation being emitted (Smith, 1996). In this research, FTIR analysis assisted in identifying primary amines ($-NH_2$), secondary amines (-NH), and the amide linkage (CONH). It was important to confirm the presence of amines as they are the CO_2 anchoring sites which enable the capturing of CO_2. The presence of the amide linkage was of importance to know whether the adsorbent synthesized was biodegradable or not. The FTIR analysis was conducted via solid state as the adsorbent was solid. The spectra obtained were then recorded.

Scanning Electron Microscopy (SEM)

Scanning electron microscopy was performed to obtain a visual image of the adsorbent before loading with amines and after loading with amines. A Sigma Zeiss SEM housed in the school of Chemical and Metallurgical Engineering at the University of the Witwatersrand, Johannesburg was used for SEM analysis.

BET analysis

The BET theory as discussed in Chapter 2 was used. N_2 physisorption was used to determine the pore size, pore volume and surface area of the synthesized adsorbent. BET was performed in the School of Chemistry at the University of the Witwatersrand, Johannesburg.

Thermo-gravimetric Analysis (TGA)

Thermo-gravimetric analysis is thermal analysis which provides information on how mass of sample varies with a change in temperature. TGA was performed to determine the thermal stability of the synthesized adsorbent. It is important when designing materials that the acceptable working temperature ranges are known. For this research, the thermal stability as well as part of the performance evaluation of the material synthesized was done using a TA SDT Q600 TGA. Thermal stability of the PAA was evaluated using 8 mg of the adsorbent in the TGA. Each sample was heated to 900 ^{o}C in air and the temperature was increased in a step-wise ramp fashion from 25 ^{o}C to 700 ^{o}C with a ramp of 5 ^{o}C / min.

Solubility

The solubility of the synthesized samples was also measured at room temperature and pressure (r.t.p.), 25 ^{o}C and 1 atm in Johannesburg, South Africa. About 0.5 g batches of PSI and each sample of amine-grafted PSI was dissolved in 10 ml of water at r.t.p. The undissolved material was filtered off using a filter pump and weighed to determine its mass. It was necessary to know the solubility of the synthesized material so as to know the effect of the water-soluble component (MA and MEA) incorporated. All solubility tests were conducted in the school of Chemical and Metallurgical Engineering at the University of the Witwatersrand, Johannesburg.

3.3.3 Evaluation of CO_2 adsorption performance of amine-grafted PSI (PAA)

Firstly, evaluation of the adsorption capacity of the synthesized PAA was carried out using the TGA. This was performed as a preliminary study on the performance of the novel material synthesized. About 8 mg of each sample was used and the sample was heated at a ramp rate of 5 ^{o}C/min to 110 ^{o}C, while N_2 gas was passed through the sample. The system was equilibrated at 110 ^{o}C for 30 min in the N_2 environment. This was to done to drive off impurities such as water vapor from the sample. Thereafter, the temperature was dropped to 40 ^{o}C and equilibrated at this value while simultaneously passing CO_2 gas (about 100% purity) through at a flowrate of 60 ml/min. Approximately 100 % CO_2 was used as part of the preliminary study of the synthesized material. This was carried out for 3 hours at atmospheric pressure and thereafter the process was stopped.

Secondly, the adsorption setup depicted in Figure 3.3 was used in the investigation of the effect of operating variables (temperature, pressure and gas flowrate) on the CO_2 adsorption capacity (response variable) of the best synthesized adsorbent amine-grafted PSI (PAA) sample.

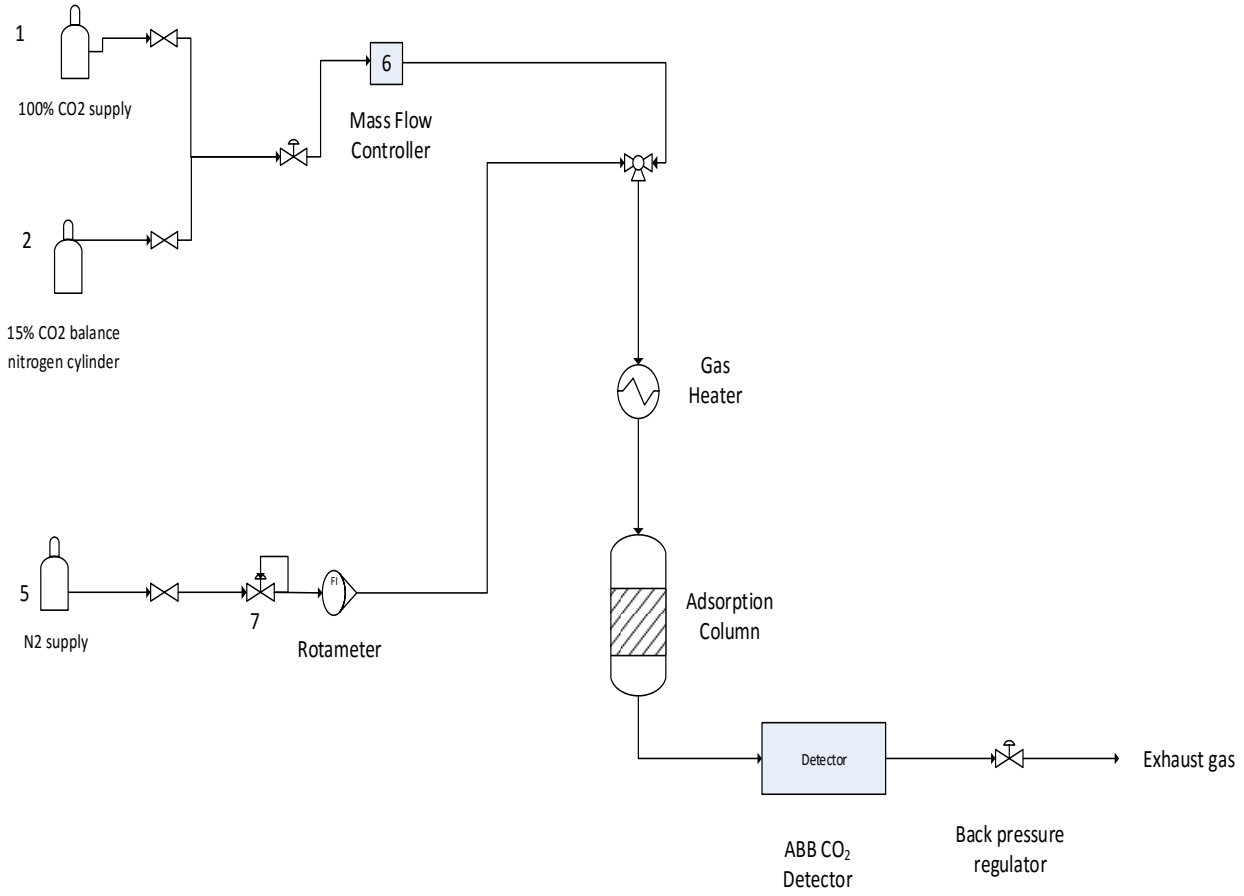


Figure 3.3: Process flow diagram of equipment used for optimization studies.

The CO_2 adsorption equipment which constituted a fixed bed adsorption column, gas supplies of 15 % as well as 100 % CO_2 and Nitrogen (N_2), mass flow controller and a gas analyzer. 15 % CO_2 was used in order to mimic the composition (CO_2 and N_2 only) of the flue gas from major South African coal-fired power plants to provide detailed information on the possible extrapolation of the data obtained to South African coal fried power plants. The experiment was conducted by varying the variables as shown in Tables 3.2 and 3.3 and exhausting all 20 experimental runs with the change in concentration recorded and the observed adsorption capacity calculated.

These variables were chosen as they significantly influence CO_2 adsorption capacity among other variables. Further, the equipment available for the investigation allowed for the variation of these chosen variables. A Central Composite Design (CCD) of experiment was employed to design the experimental runs conducted. The CCD of experiment is ideal for statistically designed experimentation where the objective is to determine the influence of specified variables on a response variable as well as to determine the optimum conditions. It is beneficial in that there is a significant reduction in the number of experiments to be carried out, unlike the classic method which requires that a single variable be varied at a time. In addition, with this method, it is possible to determine the effects of two factors simultaneously on the response variable which in this work was CO_2 adsorption capacity.

Table 3.2 shows the range and values of the variables used in the DoE. The design of experiment plan is shown in Table 3.3. Preliminary studies conducted in the TGA using the synthesized adsorbent gave the central point (temperature of 40 ^oC, Pressure of 1.1 bar and Gas flowrate of 60 ml/min) for the design of experiment shown in Table 3.3. Results from prior work using a similar adsorbent showed that at these conditions, the adsorption capacity was significant in comparison to other adsorbents found in literature (Ngoy *et al.*, 2014). The performance evaluation was conducted using CO_2 adsorption equipment housed in the school of Chemical and Metallurgical Engineering at the University of the Witwatersrand, Johannesburg manufactured by Chemvak and the gas analyzer used was loaned from ABB.

Table 3.2: Experimental range and levels

Variables	**Factor**	**Range and level**				
		-α	-1	0	+1	+α
Temperature (^oC)	X_1	5	25	40	55	70
Pressure (bar)	X_2	0.3	0.6	1.1	1.6	2.2
Gas flowrate (ml/min)	X_3	30	45	60	75	90

A second order polynomial was adopted to fit the experimental data. A form of the polynomial is shown in Equation 3.1.

$$Y_{estimate} = b_o + \sum_{i=1}^{n} b_i x_i + \sum_{i=1}^{n} b_{ii} x_i^2 + \sum_{i=1}^{n-1} \sum_{j=i+1}^{n} b_{ij} x_i x_j + e_i \quad (3.1)$$

Where Y is the predicted response, n is the number of factors, x_i and x_j are the coded variables, b_o is the offset term, b_i, b_{ii}, and b_{ij} are the first-order, quadratic and interaction effects, respectively. Also, j and i are the index numbers for the factors being investigated and e_i is the residual error.

The regression coefficients of the proposed models were determined in Matlab. The best model candidate that resembles the behavior of the material during CO_2 adsorption was selected by considering the mean error and variance of each candidate. A regression model was then proposed and Matlab was used to determine the equation coefficients and constants. The mean error and variance for each model was calculated and used to determine the best regression model of those proposed. An Analysis Of Variance (ANOVA) test was conducted using Microsoft Excel to determine the statistical significance of the model. Furthermore, response surfaces and their corresponding contours that explain the main effects of the factors and the effect of factor interaction on the CO_2 adsorption capacity were plotted using Matlab.

In this work, the focus was adsorption of CO_2. Desorption of CO_2 from the synthesized material is expected to be done by use of dissolving in water and performing freeze-drying to recover the adsorbent.

Table 3.3: Central composite design experimental plan.

Exp number	Experimental design			Experimental plan		
	Temp (^{0}C)	**Pressure (bar)**	**Gas flowrate (ml/min)**	**X_1**	**X_2**	**X_3**
1	-1	-1	-1	25	0.6	45
2	+1	-1	-1	55	0.6	45
3	-1	+1	-1	25	1.6	45
4	+1	+1	-1	55	1.6	45
5	-1	-1	+1	25	0.6	75
6	+1	-1	+1	55	0.6	75
7	-1	+1	+1	25	1.6	75
8	+1	+1	+1	55	1.6	75
9	-1.682	0	0	5	1.1	60
10	+1.682	0	0	70	1.1	60
11	0	-1.682	0	40	0.3	60
12	0	+1.682	0	40	2.2	60
13	0	0	-1.682	40	1.1	30
14	0	0	+1.682	40	1.1	90
15	0	0	0	40	1.1	60
16	0	0	0	40	1.1	60
17	0	0	0	40	1.1	60
18	0	0	0	40	1.1	60
19	0	0	0	40	1.1	60
20	0	0	0	40	1.1	60

Chapter 4: Synthesis and Characterization of amine-grafted PSI for CO_2 adsorption

4.1 Introduction

Materials can be categorized into different groups as a function of their type of intra-bonding and intermolecular bonding, crystal structure and overall macrostructures (Bandyopadhyay & Bose, 2013). Different categories of materials have similar properties within these categories. According to Bandyopadhyay and Bose (2013), materials may be categorized as metals, ceramics or polymers. Materials may also be categorized as natural or synthetic depending on whether they are synthesized or they occur naturally or dense or porous depending on their macrostructures (Bandyopadhyay & Bose, 2013). The purpose of synthesizing materials is to tailor them with specific properties for a specific functionality. According to Bandyopadhyay and Bose (2013) and Roque-Malherbe (2010), after the process of synthesizing the material, it is of paramount importance that the physical, chemical, biological and mechanical properties be determined, to be able to have knowledge of where and how to apply the material. Roque-Malherbe (2010) further states that it is challenging to accurately apply a material without fully understanding its properties which also include composition, structure and morphology. Characterization is a task of fundamental importance according to Roque-Malherbe (2010) and McGlinchey (2005). Roque-Malherbe (2010) has what is called the golden rule of characterization which is to apply several methods of characterization as a single method will not yield full understanding of the material synthesized. Several characterization techniques may be applied to further understand a synthesized material and these include x-ray diffraction (XRD), transmission electron microscopy (TEM), NMR, TGA, scanning electron microscopy (SEM), infrared spectroscopy (IR) and BET. It should be noted that this list of characterization techniques is not exhaustive.

Of interest in this research are synthetic polymers, particularly amine-grafted PSI, a polymer synthesized for the purposes of CO_2 adsorption. Characterization was performed to confirm whether what was set out to be synthesized was successfully synthesized and to determine the properties of the product and compare these to the performance of the material in the intended application.

The synthesis of the amine-grafted PSI was successful and performed in batches. Characterization was performed by the use of NMR analysis, FTIR, SEM, N_2 physisorption (by BET analysis) and TGA. (See Chapter 3 for detailed description).

4.2 Synthesis

The synthesis was performed in two parts. Initially, the backbone polymer PSI was synthesized, followed by the grafting of amines onto the polymer PSI. In the synthesis of PSI, the yield was calculated and found to be 73.7 % after 25 g of Aspartic acid underwent a polycondensation reaction in the presence of 12.5 g of Phosphoric acid; the calculation is shown in Appendix A. The loss of material (26.3 %) was attributed to the washing process that follows the polycondensation reaction as well as the drying in the oven. Ten samples of adsorbent material were synthesized, each of varying amine combination and concentration within each combination grafted onto the PSI. Five were grafted with a combination of MA and EDA and the remaining five were grafted with a combination of MEA and EDA. The combination in each of the MA-EDA and MEA-EDA grafted amines was varied and synthesized as described in Chapter 3 of this dissertation. The yield from each sample synthesized was calculated and is shown in Table 4.1. Three batches of each sample were synthesized and the standard deviation of the yield was calculated. The yield was calculated to determine the efficiency of the synthesis process.

Table 4.1: Adsorbent synthesis yields

Sample	Yield (%)	Standard deviation
1 (100 % MA)	62.3	0.326599
2 (80 % MA)	59.4	0.408248
3 (60 % MA)	61.5	0.244949
4 (40 % MA)	60.7	0.249444
5 (20 % MA)	59.8	0.249444
6 (100 % MEA)	60.2	0.249444
7 (80 % MEA)	58.8	0.771722
8 (60 % MEA)	60.9	0.498888
9(40 % MEA)	59.9	0.531246
10 (20 % MEA)	62.1	0.410961

The mass loss (approximately 40 %) can be attributed to the centrifuging process, where, after centrifuging, some material was lost, and from the oven drying, where some water vapor also resulted in mass loss.

4.3 Characterization

Characterization was performed to determine the quality of the material synthesized and to confirm whether the target material was actually synthesized.

4.3.1 NMR Analysis

^{1}H NMR analysis was performed on the backbone polymer PSI and the amine-grafted PSI samples to confirm the structure of PSI and amine-grafted PSI. The comparison of the two spectra obtained for PSI and amine-grafted PSI present a way of showing whether the amine-

grafting was successful and also whether the cleaning process after grafting was effective. The results presented here show the ^{1}H NMR performed on PSI and amine-grafted PSI (60 % MA and 40 % EDA grafted).

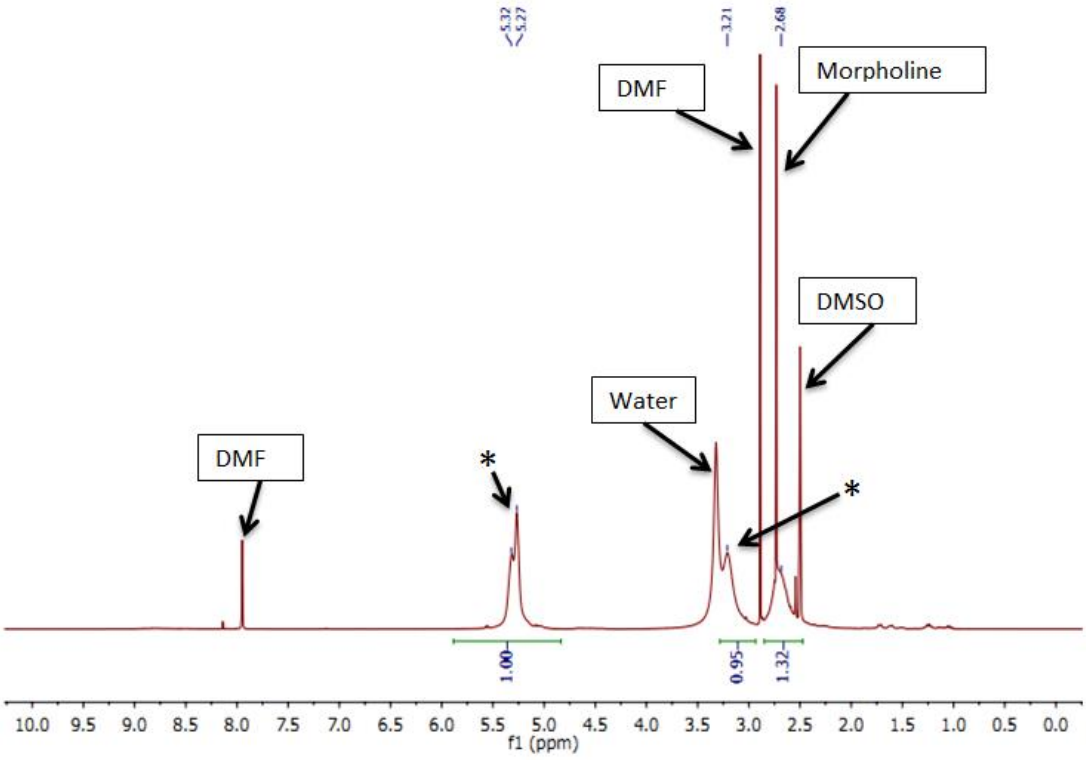


Figure 4.1: NMR analysis of PSI confirming the expected structure qualitatively.

Figure 4.1 shows the NMR spectra obtained. The peaks of importance are that of CH and CH_2 (starred in Figure 4.1), signaling the presence of two types of protons, the first in the shift range 3.5 – 2.9 ppm and the second in the range 5.8 – 4.8 ppm. This was expected as the structure of PSI in Appendix A shows the presence of two different protons. There were, however, impurities that were picked up during the NMR analysis as seen in Figure 4.1. These impurities included: dimethyl formamide (DMF), which was the solvent used during the synthesis of the PSI; water and morpholine which are common proton NMR impurities; and DMSO, the solvent used in the NMR analysis.

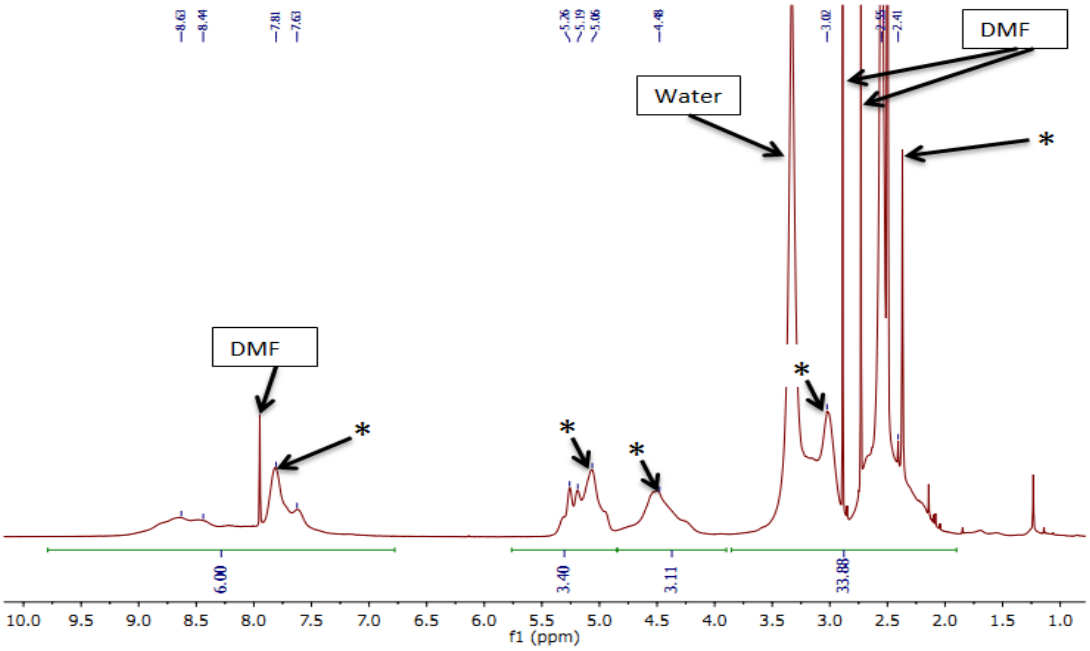


Figure 4.2: NMR analysis showing relevant peaks in the chemical structure of PSI-MA-EDA.

Figure 4.2 shows the proton NMR spectra obtained. The peaks of importance are those starred, confirming the presence of different proton types present in the amine-grafted PSI. Similar impurities to the PSI spectra were identified and are shown in Figure 4.2. The increase in the number of different protons shows that the grafting of amines onto PSI was successful. In PSI there were two different protons which agrees with the structure of PSI and for the amine-grafted amine, there were five protons.

4.3.2 BET Analysis

BET analysis was performed to determine the physical properties of the adsorbent material which are pore size, pore volume and BET surface area. Values of these properties assist in accounting for the adsorption performance of the material.

Table 4.2: BET analysis of the synthesized samples, Samples 1-10.

Sample	Pore size (nm)	Pore volume (cm^3/g)	Surface area (m^2/g)
PSI	35.43305	0.380804	42.9885
1 (100 % MA)	30.97479	0.018444	2.9446
2 (80 % MA)	26.78457	0.015319	2.6874
3 (60 % MA)	25.35419	0.011457	2.5847
4 (40 % MA)	23.54712	0.010149	2.1843
5 (20 % MA)	21.58498	0.010038	1.9546
6 (100 % MEA)	28.72746	0.015650	2.9667
7 (80 % MEA)	24.65874	0.014678	2.8247
8 (60 % MEA)	22.47981	0.012549	1.7436
9(40 % MEA)	22.68954	0.011247	1.5289
10 (20 % MEA)	20.45832	0.011134	1.4786

BET analysis was carried out on all the synthesized amine-grafted PSI (PAA) samples to determine their pore size, pore volume and BET surface area (Table 4.2). In literature, PAA is shown to have a pore size of 20.63 nm, a pore volume of 0.01 cm^3/g and a surface area of 1.93 m^2/g (Ngoy *et al.*, 2014). Sample 1 to sample 10 in Table 4.2 show similar values for the same properties with small variations. The PAA from the report of Ngoy *et al.* (2014) was obtained via a different drying method which did not involve freeze-drying. In this study, freeze-drying was used to prepare the adsorbent and the expectation was that the pore size, pore volume and surface area would significantly be improved. The pore size and the BET surface area of the synthesized PAA (samples 1 and 6) increased by approximately 50 %, while their pore volume remained unchanged in comparison to amine-grafted PSI (PAA) from (Ngoy *et al.*, 2014). Furthermore, comparing PSI, the backbone polymer, to the amine-grafted PSI, there is a decrease in pore size, pore volume and surface area. This was expected, because, as you graft more amines to the polymer, it loses its pore size, pore volume and surface area to the grafted amine.

4.3.3 SEM Analysis

SEM imaging was done to view the material structure, particularly to determine the differences between single amine-grafted PSI (for example 100 % MA grafted) or double amine-grafted PSI (for example 60 % MA and 40 % EDA grafted).

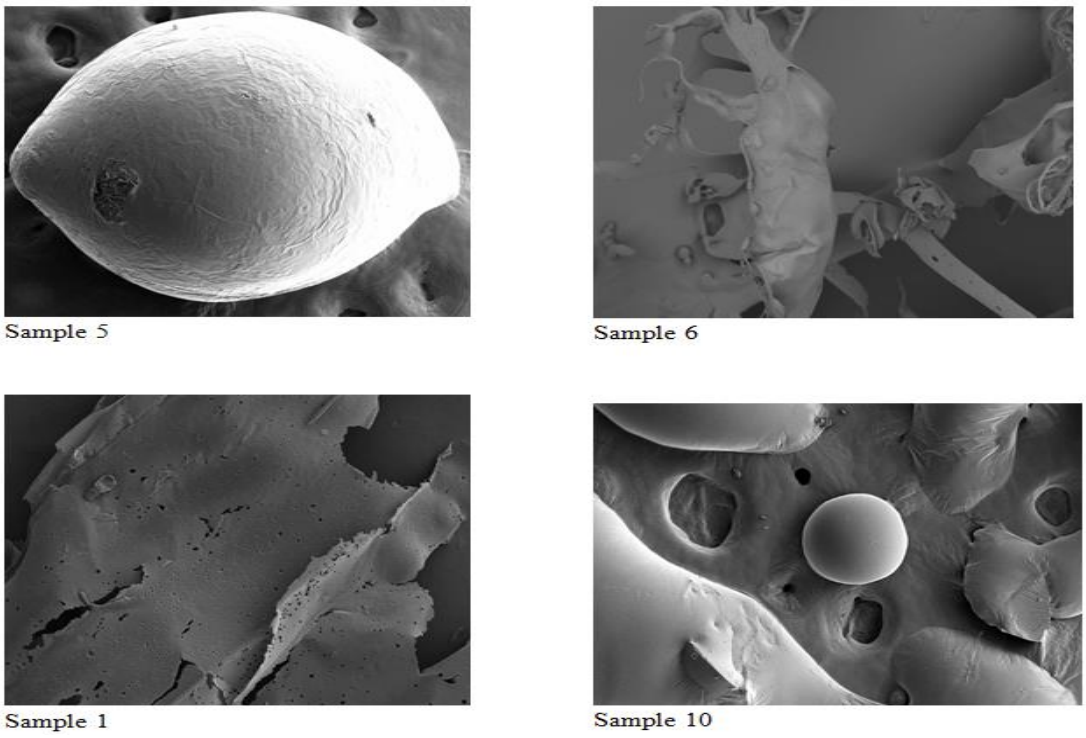


Figure 4.3: SEM imaging of PSI-MA, PSI-MEA, PSI-MA-EDA (20 % and 100 % respectively), and PSI-MEA-EDA (20 % and 100 % respectively) to a magnification of 2000 X.

SEM images of the synthesized amine-grafted PSI (PAA) samples are depicted in Figure 4.3. Amine-grafted PSI (PAA) samples with the highest MA and MEA concentrations and the lowest MA and MEA concentrations were selected for SEM analysis; samples 1 and 5 were thus selected for PSI-MA-EDA, and samples 6 and 10 were selected for PSI-MEA-EDA. The SEM images were taken at magnification of 2000 X. It was observed that as the concentrations of MA and MEA increased to 100 % onto the PSI, there was an increase in the 'thinness' of the adsorbent. This is observed by comparing the images for sample 5 and sample 1, as well as that of sample 6 and sample 10, which show how the structure of the amine-grafted PSI (PAA) changes as the amine concentration is varied. This 'thinness' also corresponds to an increase in surface area as the BET analysis shows in Table 4.2. Samples 1 and 6 have the highest surface

area. Samples with a combination of MA-EDA and MEA-EDA had granular structures and the SEM imaging shows the spheres in the sample representative of the granular structure.

4.3.4 FTIR Analysis

FTIR analysis was performed to determine the functional groups present in the backbone polymer, PSI and the adsorbent, amine-grafted PSI. The expectation was to see the amine functional group (-NH_2 and -NH) and the amide linkage (-CONH). The former functional group is as a result of the grafting process where PSI was grafted with amines and it is the CO_2 capture site that is anchoring site. The latter functional group is as a result of the polycondensation reaction of aspartic acid in the presence of phosphoric acid and is responsible for the biodegradability of the adsorbent to ensure that it is environmentally friendly if disposed of.

The FTIR analysis of the sample depicted in Figure 4.4 shows the presence of all the functional groups (C-N, C=O and C-H) in PSI, thereby confirming the successful synthesis of the PSI. The C=O and C-H functional groups occur within the wavenumber ranges of 1650-1740 cm^{-1} and 3100-3200 cm^{-1} respectively. The functional group C-N, which occurs within the wavenumber range of 1430-1530 cm^{-1}, was shown to be present in PSI, and confirms the presence of the amide group which acts as the cleavage bond for biodegradability (Ngoy *et al.*, 2014). The FTIR analysis performed on the synthesized PSI closely resembles what was obtained in literature (Ngoy *et al.*, 2014), again confirming the successful synthesis of the compound PSI.

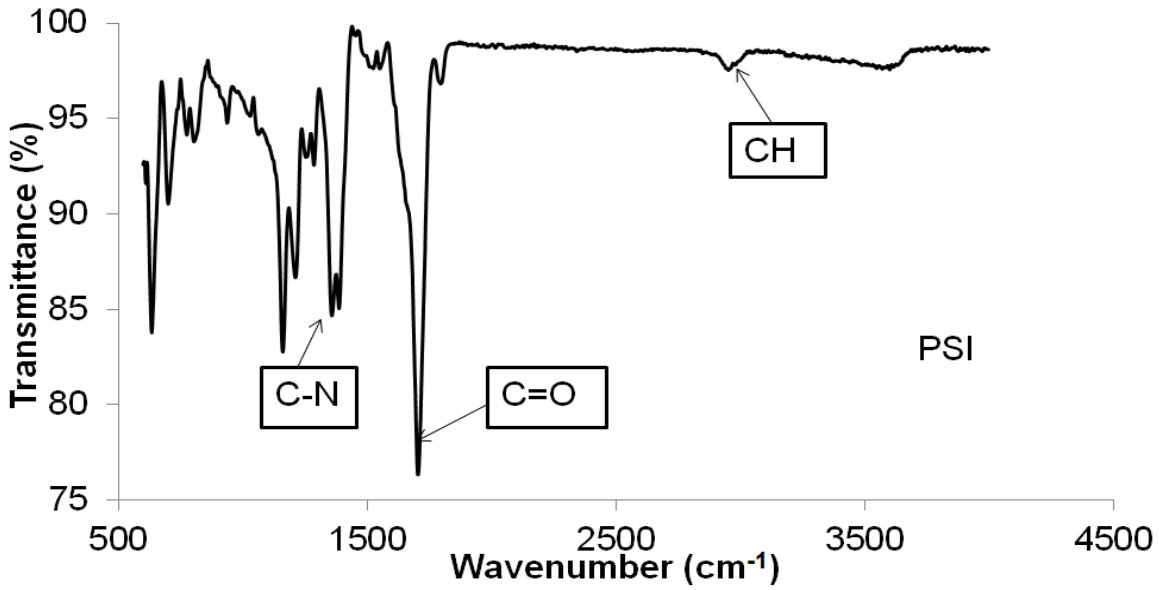


Figure 4.4: FTIR analysis showing relevant peaks in the chemical structure of PSI.

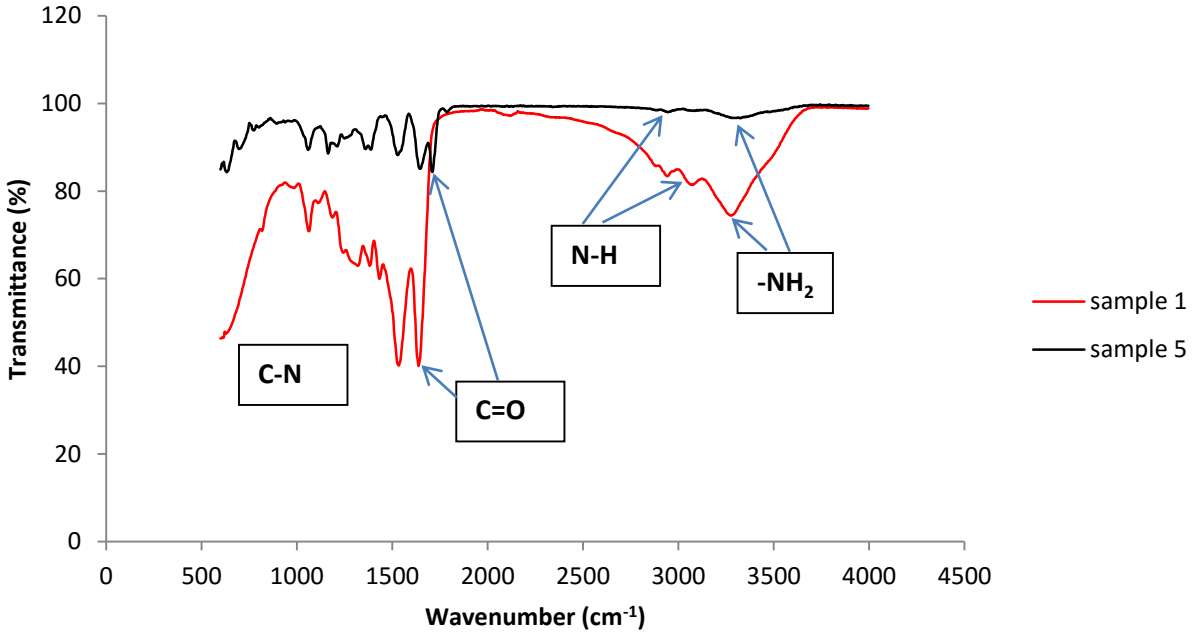


Figure 4.5: FTIR analysis showing relevant peaks in the chemical structure of PSI-MA-EDA.

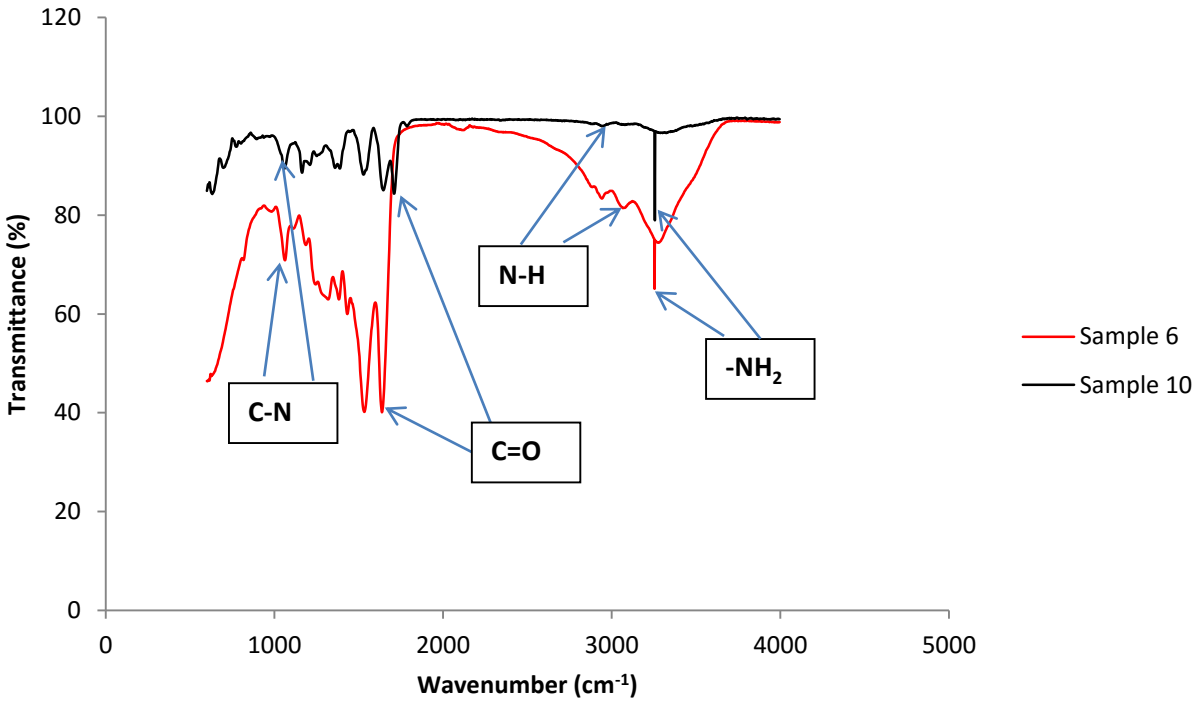


Figure 4.6: FTIR analysis showing relevant peaks in the chemical structure of PSI-MEA-EDA.

Amine-grafted PSI samples with the highest MA and MEA concentrations and the lowest MA and MEA concentrations were selected for FTIR analysis. This was done with the assumption that the other concentrations would fall within this range of analysis. Figure 4.5 shows the FTIR analysis of PSI-MA-EDA, 100 % MA (Sample 1) and 20 % MA (Sample 5). Figure 4.6 shows the FTIR analysis of PSI-MEA-EDA, 100 % MEA (Sample 6) and 20 % MEA (Sample 10). Both figures show that the amines were successfully grafted onto the PSI. The expected functional groups were obtained from the FTIR peaks, $-NH_2$ between 3300 cm^{-1} and 3500 cm^{-1}, N-H between 3100 cm^{-1} and 3200 cm^{-1}, C=O between 1650 cm^{-1} and 1740 cm^{-1} and C-N between 1430 cm^{-1} and 1530 cm^{-1}. The $–NH_2$ group shows the presence of a primary amine in the synthesized adsorbent, which in contact with CO_2 has a potential of forming carbamate, a reversible bond. The C=O, N-H and the C-N functional groups are part of the amide bond, which provides for biodegradability of the adsorbent by forming a bio-fission bond at which the molecule breaks. The presence of these functional groups confirms that the synthesized adsorbent is biodegradable (Ngoy *et al.*, 2014).

4.3.5 TGA Analysis

Thermal stability determination is important to determine the maximum temperature in which the synthesized material can operate in.

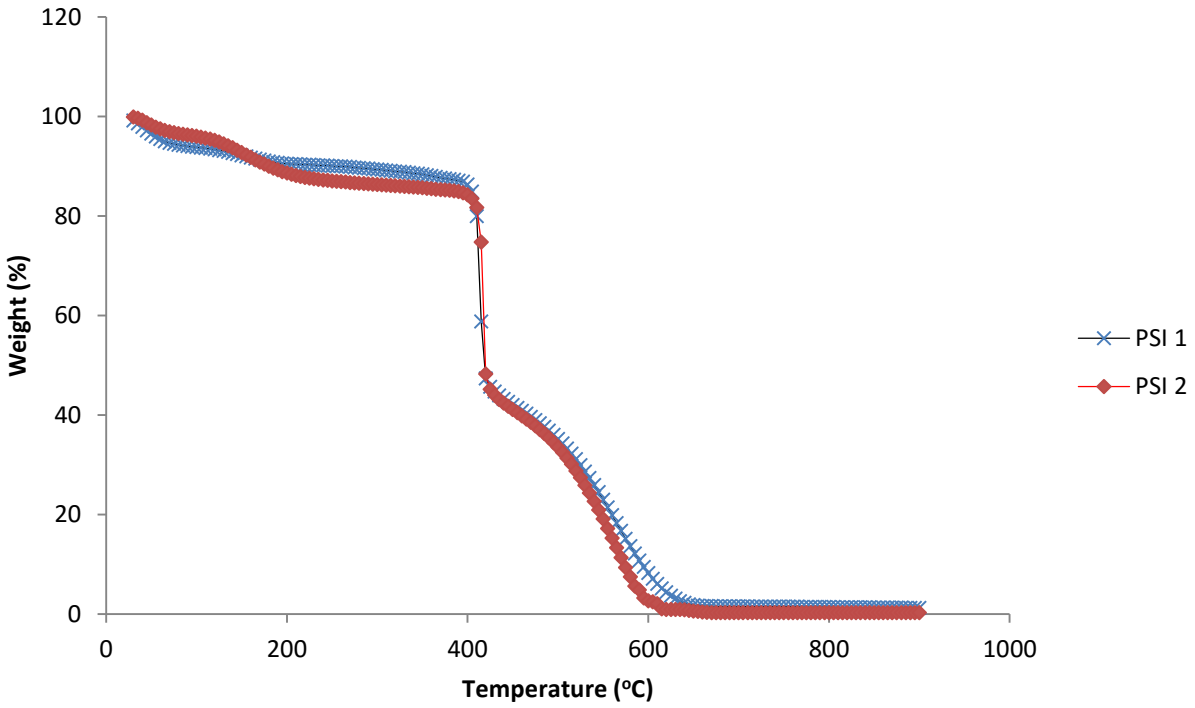


Figure 4.7: Thermal stability analysis of the synthesized PSI showing variation of weight with temperature, comparing PSI 1 adapted from the study by (Ngoy *et al.*, 2014), and PSI 2 – the sample from this study.

From the thermal stability analysis shown in Figure 4.7, PSI is safely stable up to a temperature of 400 °C, which is consistent with literature, hence again confirming the successful synthesis of PSI in this study (Ngoy *et al.*, 2014; Tudorachi & Chiriac, 2011).

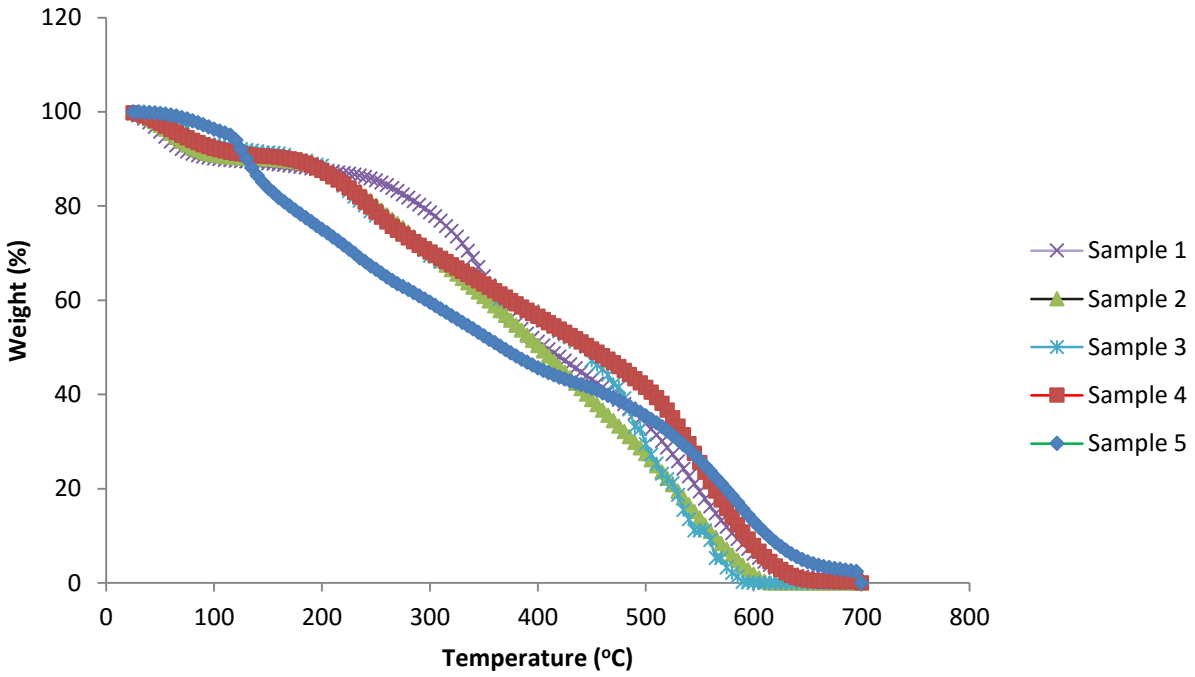


Figure 4.8: Thermal stability analysis of PSI-MA-EDA samples showing variation of weight loss with temperature.

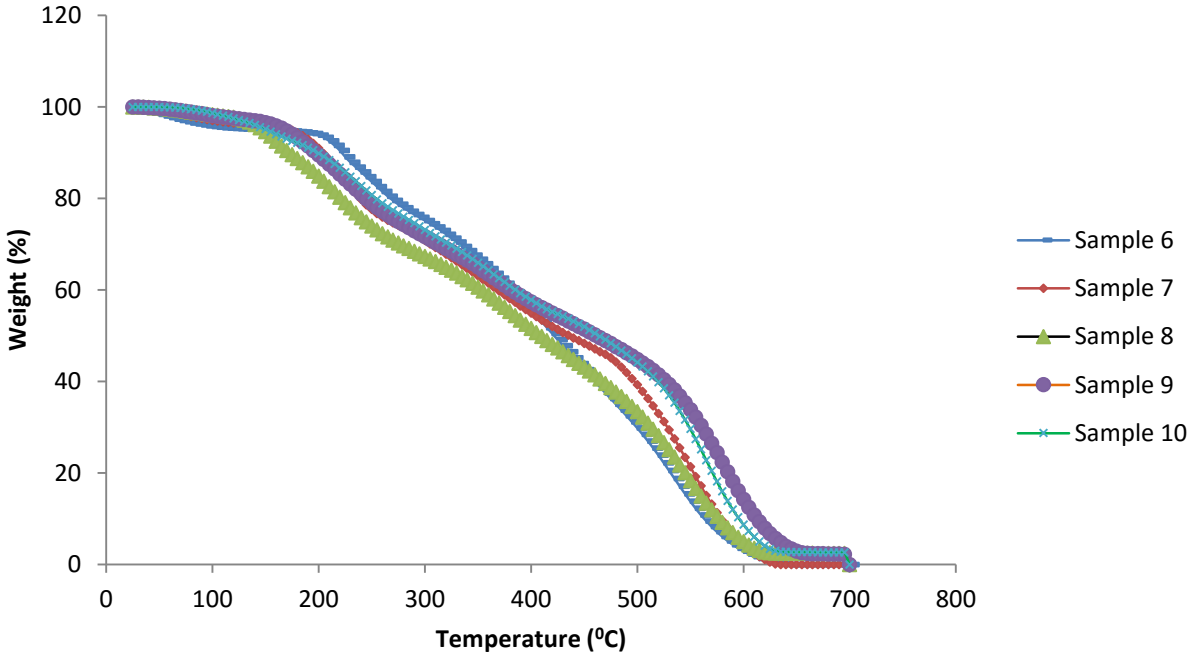


Figure 4.9: Thermal stability analysis of PSI-MEA-EDA samples showing variation of weight loss with temperature.

The amine-grafted PSI samples showed a thermal stability of up to 210 ^{o}C, a 48 % reduction in thermal stability when compared with that of the original PSI sample, which is at 400 ^{o}C (See Figures 4.7 through to 4.9); this can be attributed to the fact that during the grafting of the amines, the chemical ring in the structure of PSI is opened as the amines are grafted onto it. The thermal stability of the PAA obtained in this study is consistent to that in literature (Ngoy *et al.*, 2014).

4.3.6 Solubility determination

The solubility was determined by use of a classical method. The solubility of the synthesized samples was measured at room temperature and pressure (r.t.p.), 25 ^{o}C and 1 atm in Johannesburg, South Africa. 0.5 g batches of PSI and each sample of amine-grafted PSI was dissolved in 10 ml of water at r.t.p. The undissolved material was filtered off and weighed to determine its mass. Table 4.3 shows the solubility of each of the amine-grafted PSI samples and that of the PSI.

Table 4.3: Solubilities of PSI and amine-grafted PSI samples.

Sample	Solubility (g / L)
PSI	0
Sample 1 (100 % MA)	42.1
Sample 2 (80 % MA – 20 % EDA)	37.6
Sample 3 (60 % MA – 40 % EDA)	36.1
Sample 4 (40 % - 60 % EDA)	24.4
Sample 5 (20 % - 80 % EDA)	13.3
Sample 6 (100 % MEA)	39.5
Sample 7 (80 % MEA – 20 % EDA)	35.7
Sample 8 (60 % - 40 % EDA)	30.9
Sample 9 (40 % - 60 % EDA)	25.2
Sample 10 (20 % - 80 % EDA)	14.8

The solubility of amine grafted PSI increased with an increase in the water soluble components (MA and MEA). This is shown in Table 4.3 and Figure 4.10. It was expected that all the amine-

grafted PSI samples would be soluble in water to a greater extent, because the amines used in the grafting process, MA, MEA and EDA are all completely soluble in water. However, the displayed solubility was such that as the amount of MA and MEA grafted increased, the solubility of the resulting polymer increased as well. This could be attributed to the fact that the grafting of the MA-EDA and MEA- EDA amine combinations did not occur entirely as intended, due to cross-linking occurring as the grafting process was in progress. This would mean that the resulting adsorbent sample is not well-grafted, hence its solubility is lower.

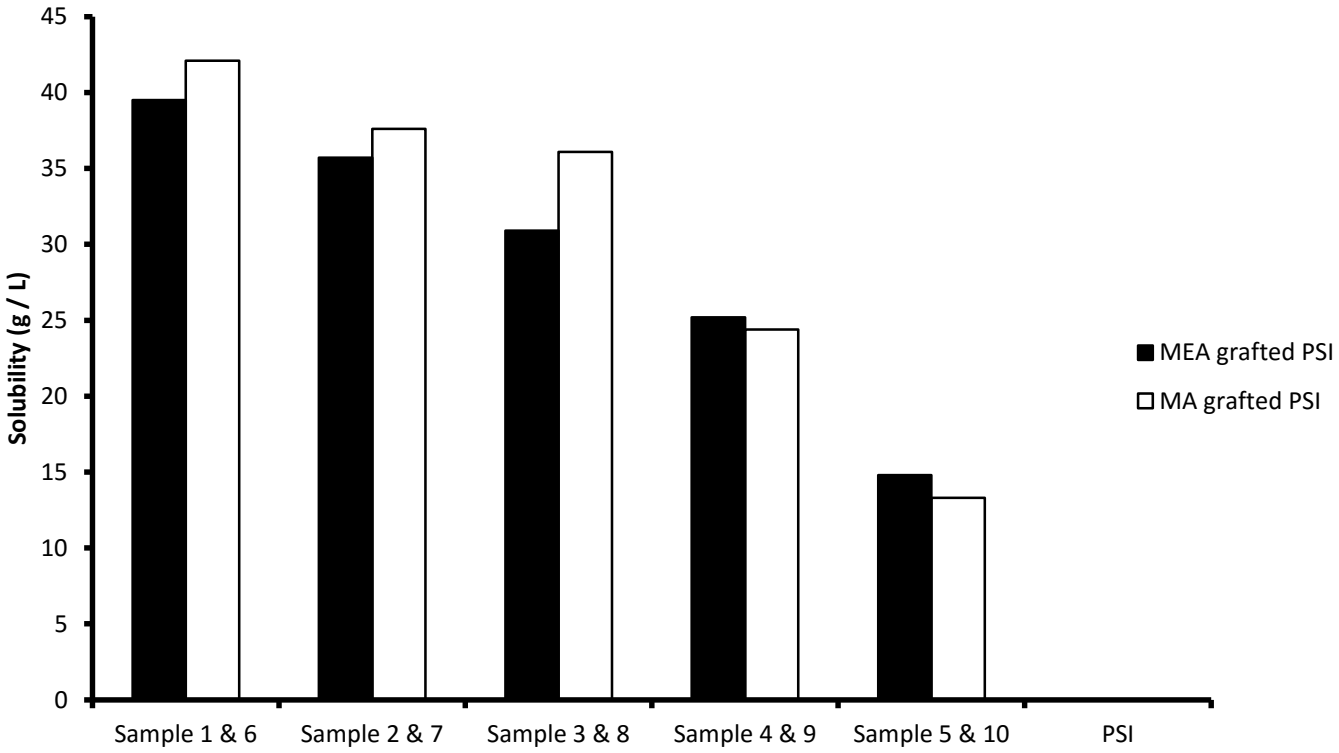


Figure 4.10: Comparison of solubilities of varying amine-grafted PSI samples.

Figure 4.10 shows the comparison of the two types of water-soluble amines used in the grafting process, samples 1 to 5 having been grafted with MA and samples 6 to 10 grafted with MEA. There is not much difference in the solubility of similar concentration but grafted with different water soluble amines (MA and MEA) samples. The general trend of decreasing water solubility as the water-soluble amine decreased was observed for both sets, samples 1 to 5 and samples 6 to 10.

4.4 Chapter Summary

Amine-grafted PSI with varying amine concentration and different amine combinations was synthesized. A total of ten amine-grafted PSI samples were produced. Five samples were grafted with varying concentrations of MA-EDA combinations and five samples were grafted with varying concentrations of MEA-EDA combinations. The water-soluble components incorporated were MA and MEA.

The synthesis of PSI, the backbone polymer, had a yield 73.7 %. A material loss of 26.3 % was determined. This is attributed to water loss during the polycondensation reaction as well as the washing and the oven drying processes that follow the polycondensation reaction. The average yield of the amine-grafting process was 60.6 %. The mass lost was attributed to the washing processes to clean the synthesized sample.

A water-soluble amine-grafted PSI adsorbent was synthesized. The NMR analysis confirmed the incorporation of MA and MEA amine groups in the PAA, thereby indicating the presence of the grafted amines on the backbone polymer. TGA analysis showed that the synthesized adsorbent is thermally stable up to 250 ^{o}C. SEM analysis showed images characterized with an increase in 'flakiness' and pores as the MA and MEA concentrations were increased displaying a change in the geometric structure of the adsorbent. The BET analysis showed that the surface area, pore volume and pore size did not improve significantly as compared to amine-grafted PSI from literature. FTIR analysis indicated the presence of the expected functional groups which are also relevant for CO_2 capture. Furthermore, from the FTIR results, it is evident that grafting occurred as there are new functional groups in the analysis results after grafting. TGA analysis gave the thermal stability of the materials synthesized which when compared to literature showed significant trend similarity. It was also necessary to determine the solubility of the amine-grafted PSI to evaluate the effect of the water-soluble component. The solubility was found to decrease as the quantity of water soluble component grafted decreased.

In conclusion, PSI, the backbone polymer was successfully synthesized. Grafting of amines was successfully performed with the characterization confirming what was synthesized. It is recommended, however, that the sample washing processes performed during the synthesis be repeated twice or thrice to ensure that there are no impurities detected during characterization. If

detected, this results in noise, for example this occurred during the NMR analysis. Furthermore, keeping the ice baths constantly cool by use of liquid N_2 is recommended. This ensures that no cross-linking occurs during the amine-grafting process. Lastly, it is recommended that quantitative analysis be performed to quantify the amount of amine incorporated into the adsorbent. The work done here focused on qualitative analysis.

Chapter 5: Effect of the presence of water-soluble amines on the CO_2 adsorption capacity of amine-grafted PSI (PAA)

5.1 Introduction

Amine-grafted polymers have become very popular and are a promising type of adsorbent. The potential stems from the currently widely applied method (absorption) which makes use of amine solvents such as Polyethylenenimine (PEI) to capture CO_2 (Chungsying *et al.*, 2008). An amine-grafted polymer consists of a backbone, which is the polymer, and an amine, which is attached to the polymer to act as the anchoring site onto which the CO_2 attaches. The CO_2 attaches to the anchoring site by formation of a weak intermediate carbamate (-COO-) as it reacts with the amine (Ngoy *et al.*, 2014). Amine groups are incorporated due to their high affinity for CO_2 and they also stabilize the CO_2 adsorption process as they form stable intermediates. Furthermore, the adsorption process is reversible; the adsorbent can be recovered by use of different types of desorption such as TSA, PSA, ESA or VSA as discussed in Chapter 2 (Chungsying *et al.*, 2008).

An adsorbent should have a large surface area and a large enough pore size to enable the adsorbate (CO_2) to adsorb to it (Ruthven, 1984; Suzuki, 1990). These properties can be improved by use of a process known as freeze-drying. Freeze-drying is used extensively in the food and drug industry to improve properties such as pore volume, pore size and surface area. Freeze-drying is a process where mass and heat are both transferred simultaneously from a material resulting in an improved physical and chemical composition as well as microstructure (Ishwarya *et al.*, 2015; Oikonomopoulou *et al.*, 2011). The material to be freeze-dried may contain water already or may be dissolved in water and is frozen by use of liquid N_2 (Ishwarya *et al.*, 2015; Oikonomopoulou *et al.*, 2011). Thereafter, the frozen water is sublimated and removed, leaving the material with an improved microstructure displaying higher porosity. A higher porosity implies that the pore size as well as the surface area of the material has increased (Ishwarya *et al.*, 2015; Oikonomopoulou *et al.*, 2011). Furthermore, freeze-drying is beneficial in that it can be applied to materials which are temperature sensitive because no heat is added, it prevents shrinkage of materials, and it reduces the possibility of material deterioration reactions due to almost complete dehydration of the material (Ishwarya *et al.*, 2015; Oikonomopoulou *et al.*,

2011). Freeze-dried materials have a spongy and highly porous structure which is desirable in adsorption processes (Ishwarya *et al.*, 2015).

Against this background, the current work investigated the synthesis and performance evaluation of a new material for CO_2 capture. In particular, the effect of the presence of water-soluble amines in the amine-grafted poly-succinimide (PSI), herewith referred to as Polyaspartamide (PAA) adsorbent, was investigated. MA and MEA were employed as water-soluble amines and the effects of the change in their concentration on CO_2 adsorption capacity was investigated as well. The water-soluble amines were grafted to an already EDA grafted PSI (PSI-EDA), with the EDA added to improve the chemical surface of the adsorbent for CO_2 capture to enhance the CO_2 adsorption capacity. The solubilizing group was added to enhance the water solubility of the adsorbent to enable the adsorbent to dissolve in water paving way for freeze-drying to improve the geometric structure of the solid adsorbent. The dissolution of the adsorbent in water could enhance the CO_2 desorption process.

This chapter reports the outcome of the evaluation of the CO_2 adsorption capacity of the synthesized materials.

5.2 Evaluation of CO_2 adsorption capacity of amine-grafted PSI

The adsorption capacity of the synthesized amine-grafted PSI was determined by use of the TA Q600 TGA. 100 % CO_2 was passed through the sample which was placed in the TGA. Pure CO_2 was used initially to evaluate the novel material. Gaseous impurities were added at a later stage. The operating conditions that were used in the TGA were: temperature of 40 ^oC, pressure of 1.1 bar and a flowrate of 60 ml/min. Three adsorption runs were performed per sample with the average CO_2 adsorption capacity calculated thereafter. Figures 5.1 and 5.2 are plots of average adsorption capacities of each sample (Samples 1 to 10 including PSI) over three adsorption runs at constant temperature and pressure as a function of time. Both figures show that the average adsorption capacity increased with an increase in MA and MEA (water-soluble components) amongst the amine-grafted PSI samples. Table 5.1 shows the adsorption capacities decrease with a decrease in the water-soluble component for both MA and MEA employed as water-soluble components. The expectation was that the adsorption capacity would increase with a decrease in the water-soluble component due to the presence of diamine grafted onto the PSI, both for the water-soluble component (MA or MEA) and the balance make-up amine, EDA. The non-

occurrence of this could be attributed to the fact that during the process of grafting two amines onto a solid polymer, the grafting may not be achieved completely, resulting in a lower number of CO_2 anchoring sites which are as result of the amines grafted onto the material. This could potentially be caused by crosslinking of amines; cross-linking occurs when polymers are chained together due to ionic or covalent bonds (Ngoy *et al.*, 2014). In this particular adsorbent synthesis it resulted in no amine-grafting occurring due to the loss of reaction sites between the polymer and the amines as a result of cross-linking between the amines. Therefore, after the washing process, the adsorbent left the flask without significant amine grafting onto it. Consequently, the number of CO_2 anchoring sites was reduced.

Table 5.1: Adsorption capacities of synthesized samples.

Sample	Adsorption capacity (g CO_2/kg Ads)
PSI	18.6
1 (100 % MA)	44.5
2 (80 % MA)	11.6
3 (60 % MA)	11.9
4 (40 % MA)	9.80
5 (20 % MA)	5.40
6 (100 % MEA)	43.6
7 (80 % MEA)	35.8
8 (60 % MEA)	16.4
9(40 % MEA)	9.59
10 (20 % MEA)	7.53

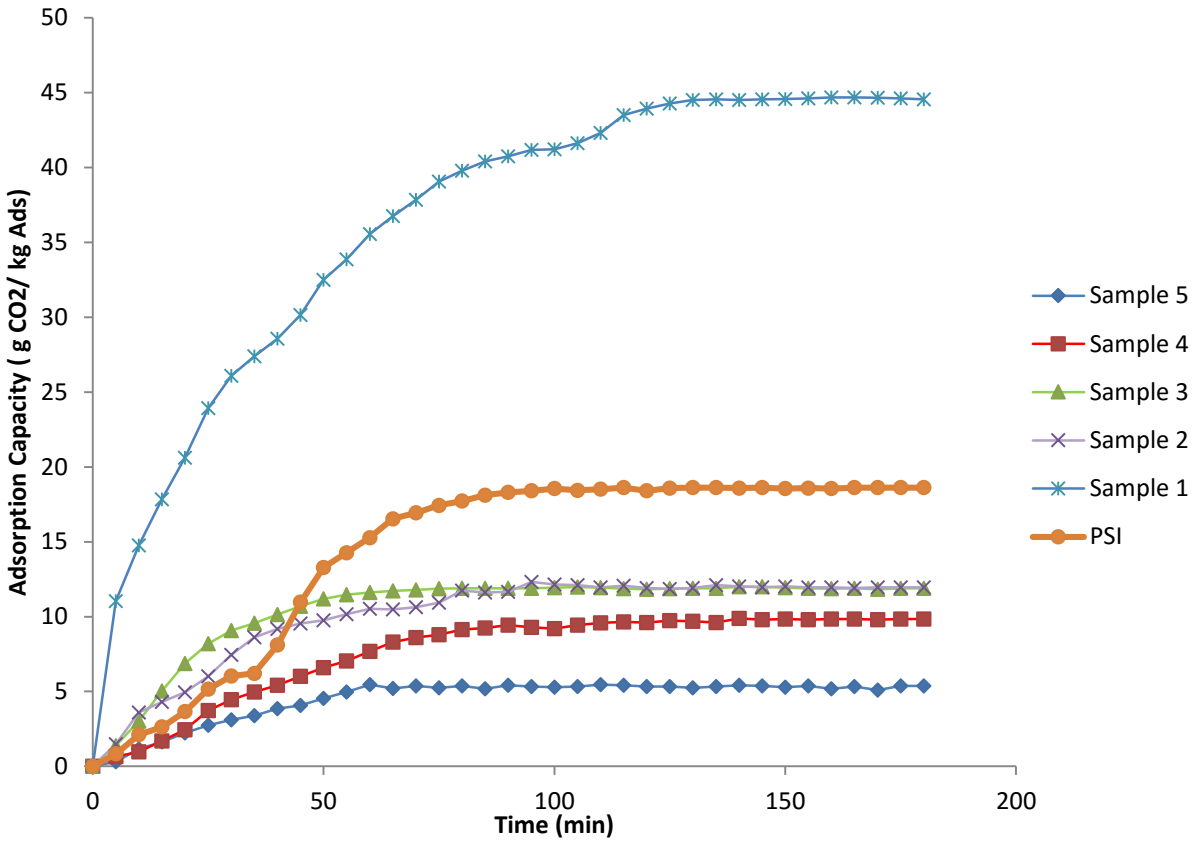


Figure 5.1: Average adsorption capacities of MA-EDA grafted PSI of varying concentrations of MA and EDA.

The adsorption performance of samples 1 to 5, all grafted with MA relative to the backbone polymer PSI was found to be such that PSI had a higher adsorption capacity than samples 2, 3, 4 and 5 (80 % MA - 20 % EDA, 60 % MA – 40 % EDA, 40 % MA – 60 % EDA and 20 % MA – 80 % EDA, respectively) as seen in Table 5.1 and Figure 5.1. The expectation was that the grafting of amines would enhance the affinity of CO_2 onto the solid adsorbent. However, this was not so, because of the differences in the physical properties of PSI and amine-grafted PSI. These properties are pore volume, pore size and surface area. PSI had a higher pore volume, pore size and surface area compared to samples 2, 3, 4 and 5 adsorbents, meaning that there was good contact between the adsorbent and the adsorbate (CO_2). Hence, PSI has a higher adsorption capacity than samples 2 to 5. Sample 1 (100 % MA grafted onto PSI), however, still has a lower pore size, pore volume and surface area than PSI, but displayed a higher adsorption capacity. This is because, even though the pore size of sample 1 is lower, it is comparable to that of PSI. This comparable pore size allows the adsorbate molecules to access the CO_2 anchoring sites

which are a result of the amine grafted onto the PSI. The comparable pore size means that the adsorbate molecules have approximately similar flux to the CO_2 anchoring sites in the PSI and the 100 % MA (water-soluble component) grafted PSI with amine grafted PSI having an amine which increases the affinity of CO_2 and CO_2 anchoring sites. For this reason it has a higher CO_2 adsorption capacity. Furthermore, during the synthesis of the amine-grafted PSI, excess EDA was made use of; this has the potential impact of reducing CO_2 adsorption capacity as the excess amine tends to occupy the pore lattice hence blocking CO_2 from accessing the anchoring sites (Linneen et al., 2014). This could also explain the observation that within the amine-grafted PSI samples, that is sample 1 to 5, CO_2 adsorption capacity decreased with an increase in EDA in the grafting process. A similar trend was observed for samples 6 to 10.

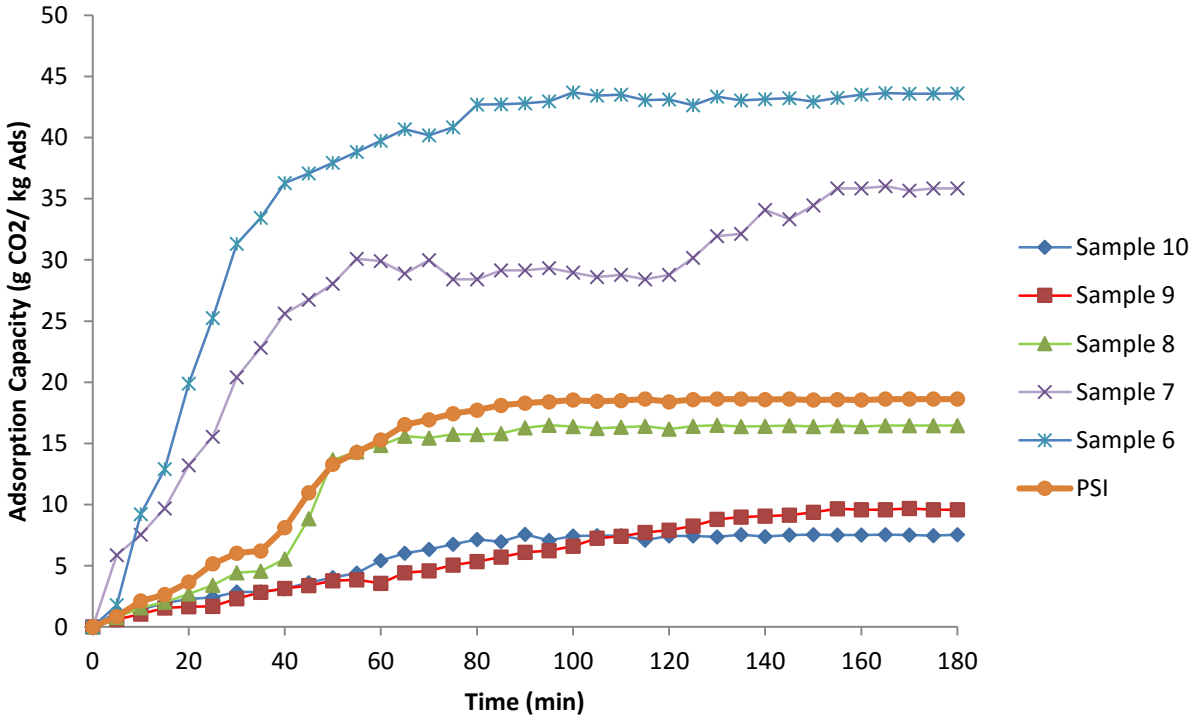


Figure 5.2: Average adsorption capacities of MEA-EDA grafted PSI of varying concentrations of MEA and EDA.

For samples 6 to 10 (100 % MEA, 80 % MEA- 20 % EDA, 60 % MEA – 40 % EDA, 40 % MEA – 60 % EDA, 20 % MEA – 80 % EDA), samples 8, 9 and 10 displayed adsorption capacities lower than that of PSI, as seen in Table 5.1 and Figure 5.2. This was expected as the physical properties of these samples (pore size, pore volume and surface area) were lower than

that of PSI even though they were grafted with amines. This confirms the significance of the physical properties of an adsorbent, pore size, pore volume and surface area in the adsorption process. The anomaly was observed for sample 7 (80 % MEA – 20 % EDA) which was expected to exhibit an adsorption capacity lower than that of PSI, but exhibited one higher than that PSI. This could be attributed to the presence of amines (MEA and EDA) coupled with an approximately comparable pore size of sample 7 (80 % MEA – 20 % EDA) to that of PSI. Sample 6 (100 % MEA grafted) displayed a higher adsorption capacity than PSI. This is attributed to the same reasons as for sample 1 (100 % MA grafted) displaying a higher CO_2 adsorption capacity than PSI. Raw results of adsorption tests conducted are shown in Appendix B.

5.3 Evaluation of the rate of adsorption with time

The rate of adsorption as a function of time in 5 minute intervals is shown in Figures 5.3 and 5.4. The rate of adsorption is initially high, but decreases with time. This is because, as the CO_2 initially gets into contact with the adsorbent material, the anchoring sites are free of CO_2, hence the flux is high. As the free CO_2 anchoring sites on the adsorbent material decrease, the rate of adsorption also decreases. The rate of adsorption as a function of time follows a similar trend to that of the adsorption capacity, with samples that displayed the highest adsorption capacity having the highest rate of adsorption and those that displayed the lowest rate of adsorption having the lowest rate of adsorption. This is because a higher adsorption capacity is as a result of more CO_2 anchoring sites. The number of CO_2 anchoring sites is in turn proportional to the rate of adsorption because they produce a higher CO_2 flux from the bulk phase onto the solid adsorbent.

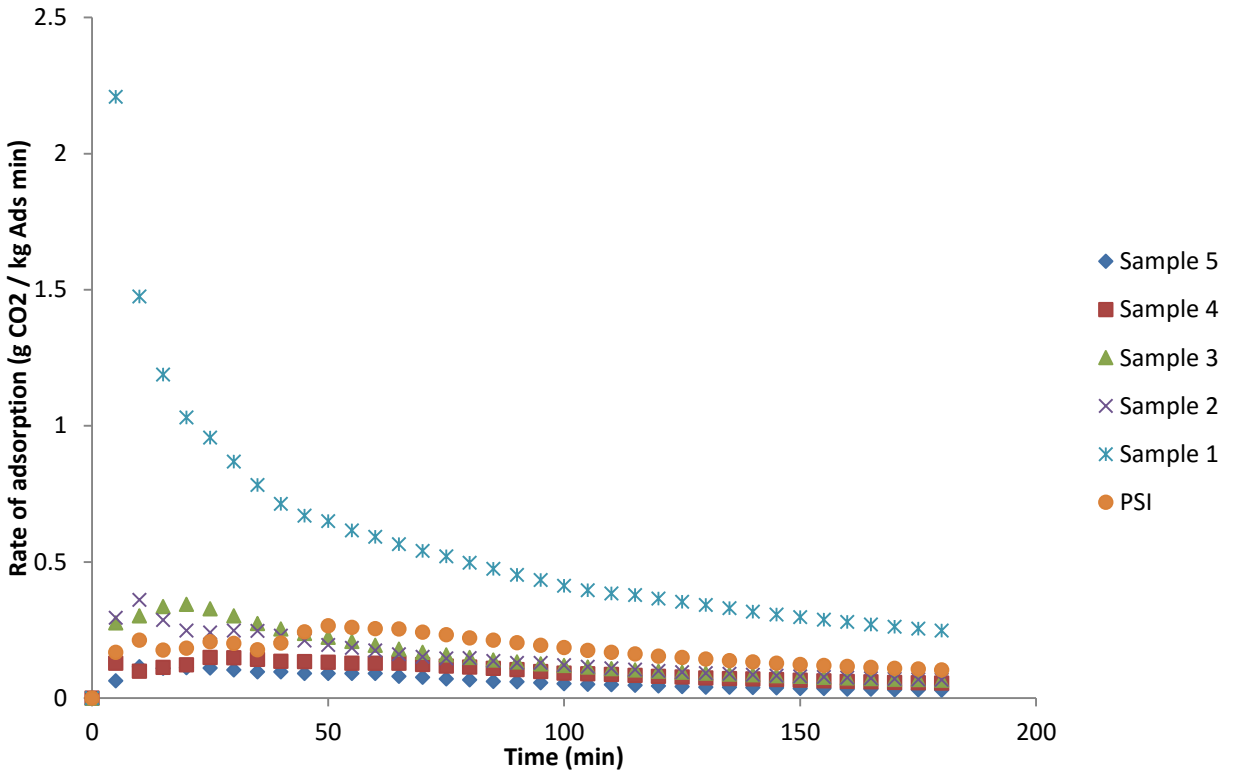


Figure 5.3: Rate of adsorption of PSI and amine-grafted PSI, samples 1 – 5 as a function of time.

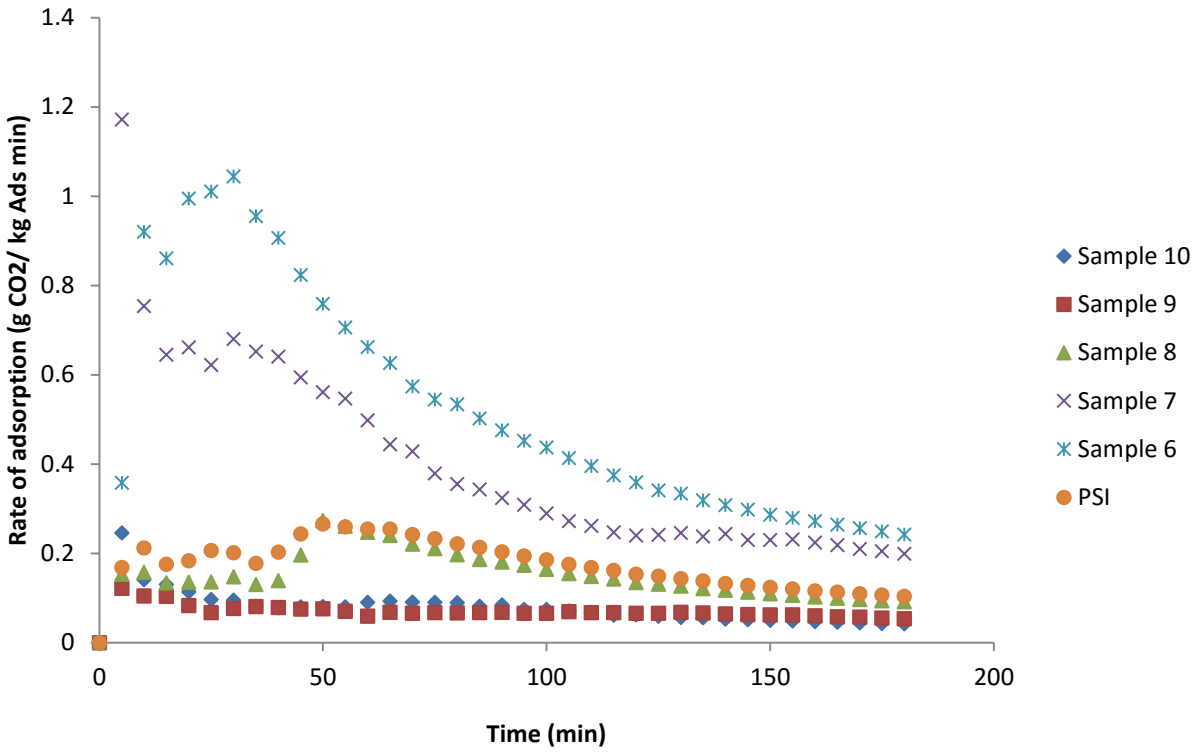


Figure 5.4: Rate of adsorption of PSI and amine-grafted PSI, samples 6 – 10 as a function of time.

In literature, several other adsorbents have been tested for CO_2 adsorption, such as zeolites, amine-rich nano-silicates, carbon-based adsorbents, metal organic frameworks, alkali-metal-based materials, as discussed in Chapter 2, Section 2.3.4. Zeolites currently display high CO_2 adsorption capacities of 98 g CO_2/ kg Ads (Lee & Park, 2014). Carbon-based adsorbents perform even better than zeolites, with a reported adsorption capacity of 374 g CO_2/ kg Ads. However, the adsorption process conditions utilized to obtain these capacities are high pressures, as high as 10 bar (Lee & Park, 2014). This implies that higher process costs will be incurred in terms of operation to create such pressure values and capital to construct equipment to handle such pressures. The amine-grafted PSI synthesized in this work captures CO_2 at approximately atmospheric conditions, with a highest achieved adsorption capacity of 44.5 g CO_2 / kg Ads making it an attractive option for further consideration as a suitable CO_2 adsorbent. The kinetics of the adsorption process presented in Figures 12 and 13 are quite slow. This has been attributed to the positioning of the sample inside the TGA where the adsorption experiments were conducted. The gas flows over the pan in which the adsorbent is contained, hence limiting contact between the adsorbent and the adsorbate. Contact between the adsorbate and the

adsorbent is poor and thus impacts on the kinetics and possibly the capacity. There is therefore Polyethyleneimine infused and functionalized Torlon-silica hollow fiber sorbents have also been investigated and they have been reported to display adsorption capacities of approximately 431.2 g / kg Ads depending on the whether the Torlon is functionalized or not (Li *et al.*, 2014). As the name, Polyethyleneimine infused and functionalized Torlon-silica hollow fiber sorbents, suggests they are a different type of amine functionalized adsorbent. Compared to amine-grafted PSI sorbents presented in this dissertation, functionalized Torlon-silica hollow fiber sorbents are better adsorbents in terms of capacity; however, the kinetics of the adsorption process are not reported hence they are of concern.

5.4 Chapter Summary

The synthesized amine-grafted PSI adsorbent was evaluated for CO_2 adsorption using pure component gas. An increase in adsorption capacity with an increase in MA and MEA concentrations in MA-PAA and MEA-PAA samples, respectively, was observed. At low amine concentrations (20 % amine and 80 % EDA grafted), MEA-PAA was observed to exhibit higher adsorption capacity compared to MA-PAA samples. At high amine (100% amine grafted) concentrations, MA-PAA samples displayed higher adsorption capacity. Three runs were performed on each sample and the results obtained were reproducible. The best adsorption capacity obtained was 44.2 g CO_2/kg Ads. However, the operating conditions during CO_2 adsorption should be optimized to enhance the CO_2 adsorption capacity. It is also important to understand the interaction of the operating variables on each other and this study should be investigated. The kinetics reported in the experiments conducted using the TGA are of concern and this has been attributed to the poor contact between the adsorbate and the adsorbent due to the configuration inside the TGA. A packed bed reactor should be developed where the adsorbate flows through the adsorbent to improve adsorption kinetics and possibly capacity. The study performed here paved way for further investigation into the influence of the operating variables during CO_2 capture as well as introduction of impurities in the gas stream.

Chapter 6: Influence of operating variables on the CO_2 adsorption capacity of amine-grafted PSI (PAA)

6.1 Introduction

In adsorption processes, understanding the influence of operating variables as well as how they interact with each other is of major importance to ensuring that the process is as efficient as possible. For adsorption to be effected economically in post-combustion capture there is need for high adsorption capacity material development, understanding the influence of operating variables on the adsorption capacity of designed adsorbents, as well as optimization of these operating variables during CO_2 capture to ensure the highest capacity possible. CO_2 capture via adsorption is influenced by several factors which include temperature, pressure, and purity of the feed gas as well as the nature of the adsorbent. These factors will determine the magnitude of adsorption that occurs depending on how they are individually adjusted and how they interact with each other. Temperature of the incoming flue gas stream is an important factor in CO_2 adsorption processes. The effect of temperature depends on whether physisorption or chemisorption is occurring. Physisorption is an exothermic process and thus results in the evolution of heat when it occurs (Bonjour *et al.*, 2002). As such, at equilibrium, if temperature is increased, adsorption decreases. The converse is true, if temperature is decreased, adsorption increases. This phenomenon is based on Le Chatelier's principle which when extrapolated to exothermic processes states that increasing temperature decreases the magnitude of the exothermic process (Brown *et al.*, 2012). If chemisorption is occurring at equilibrium, the magnitude of adsorption initially increases to a maximum, thereafter it starts to decrease (Brown *et al.*, 2012; Faust & Aly, 1998). Brown *et al.* (2012) suggests that this is because for chemisorption to occur, the activation energy has to be achieved first, thereafter the reaction occurs and the subsequent decrease may be attributed to the adsorption process becoming exothermic after the reaction has been initiated. The pressure of the incoming flue gas stream is of importance in post-combustion CO_2 adsorption capture. The magnitude of the adsorption is proportional to the magnitude of the pressure. As pressure increases, adsorption also increases. The higher the pressure, the higher the partial pressures of the component to be adsorbed hence the increase in the adsorption of that component (Faust & Aly, 1998; Keller & Staudt, 2005). The converse is true, the lower the pressure, the lower the adsorption (Faust & Aly, 1998). The

composition of the flue gas also influences the adsorption process. According to (Keller & Staudt, 2005) the higher the critical temperature of the component in the mixture, the greater the amount of that component is adsorbed. This means that highly liquefiable components get adsorbed first and in higher quantities unlike components which are not easily liquefiable. Adsorption occurs on the adsorbent surface and thus the nature of the adsorbent affects CO_2 adsorption greatly. The nature of the adsorbent encompasses all the properties of the adsorbent which are surface area, pore volume, pore size, physical form of the adsorbent (powder form or granule form) and the chemistry of the adsorbent surface (Crittenden & Thomas, 1998; Faust & Aly, 1998; Yang, 2003). The higher the surface area, pore size, forms of the adsorbent and pore volume of the adsorbent, the higher the adsorption. These properties enable the adsorbent to have a higher contact with the adsorbate molecules hence increasing the adsorption of CO_2 onto the adsorbent (Ngoy *et al.*, 2014). The chemistry of the adsorbent also affects the adsorption process with specific functional groups increasing the affinity of the adsorbent to adsorb particular molecules (Czaun *et al.*, 2013; Yang *et al.*, 2008). In the case of CO_2 adsorption, amine groups may be grafted onto the adsorbent or impregnated into the adsorbent to enhance the selectivity of CO_2 being captured into the adsorbent (Linneen *et al.*, 2014).

Against this background, this chapter evaluates the influence of operating variables, in particular temperature, pressure and gas flowrate, on the adsorption capacity of a new material, amine-grafted Polysuccinimide (PSI), for CO_2 capture. Furthermore, a regression model was proposed based on the results obtained. The material used as adsorbent was PSI was grafted with 100 % MA (sample 1) to enable CO_2 capture. The evaluation involved the use of RSM and finding an applicable approximating function for predicting and determining the further response, and studying the optimum adsorption capacity as well as the influence and interaction of the operating variables. The factors (variables) of temperature, pressure, and gas flow rate were investigated (Ma *et al.*, 2008). RSM is a mathematical and statistical technique for designing experiments, building models, evaluating the relative significance of several independent variables, and determining the optimum conditions for desirable responses (Draper & John, 1988; Draper, 1978; Gil *et al.*, 2013; Zhang & Zheng , 2009). The two most common designs extensively used in RSM are the CCD and the BBD. The CCD is ideal for sequential experimentation and allows a reasonable amount of information f or testing lack of fit while not involving an unusually large number of design points (Montgomery, 1996; Myers , 1971).

6.2 Model formulation and parameter estimation

In this work, RSM was used to identify the main and interactive effects of the operating variables investigated (temperature, pressure and gas flowrate). There are three important stages when performing optimization studies and these are to conduct statistically designed experiments from the experimental plan, to recommend a mathematical model that describes the behavior adequately based on the experimental data. Six regression models were proposed as candidates, based on the general form of the regression model presented in section 3.3 in Chapter 3. The regression model candidates are shown in Appendix E with the best one presented here in equation 6.1.

$$Y_{estimate} = b_o + \alpha_1 X_1 + \alpha_2 X_2 + \alpha_3 X_3 + \alpha_4 X_1^2 + \alpha_5 X_2^2 + \alpha_6 X_3^2 + \alpha_7 X_1 X_2 + \alpha_8 X_1 X_3 + \alpha_9 X_2 X_3 + \varepsilon \quad (6.1)$$

Where, $Y_{estimate}$ is the predicted response, X_1 represents temperature, X_2 represents pressure and X_3 represents gas flowrate. α_1, α_2 α_3, α_4, α_5, α_6, α_7, α_8 and α_9 are coefficients in each of equations 5 to 10 where they appear.

RSM was used to explain the relationship between factors and the response. Polynomial regression modeling was performed by making use of the responses obtained from the corresponding coded values of the three different process variables and the results were evaluated. The mean error and variance of the best model obtained are shown in Table 6.1, with those of the remaining model candidates shown in Appendix E.

Table 6.1: Variance and mean error values for the best model.

Model	Equation 6.1 (best model)
Mean variance	29.5849
Mean error	-2.6375×10^{-12}

Correlations between the predicted responses (calculated from the model), the parameter values estimated and the observed responses from the experiments carried out were plotted in Matlab

and are shown in Appendix E. The Matlab code used to determine the coefficients as well as the predicted adsorption capacity are shown in Appendix C. The coefficients for each model are given in Appendix E.

Of the proposed models, the model with the lowest variance was chosen to be the best model for the system amongst those proposed. The complete equation of the model is given as:

$$Y_{estimate} = 48.2277 - 0.5152X_1 + 22.7053X_2 - 0.0189X_3 - 0.0122X_1^2 - 15.7974X_2^2 - 0.0088X_3^2 + 0.1215X_1X_2 + 0.0248X_1X_3 + 0.2083X_2X_3 - 2.6375 \times 10^{-12} \quad (6.2)$$

6.3 Analysis of Variance (ANOVA) test

An ANOVA test was performed by use of the ANOVA tool in Ms Excel. The results are shown in Table 6.2. The observed adsorption capacity and the predicted adsorption capacity for all twenty runs were taken as the data to be analysed. Variance, degrees of freedom, sum of squares, mean squares, f-value, p-value and the f-critical value for this analysis are all reported in Table 6.2. The statistical significance of the second-order equation revealed that the regression is statistically significant ($P < 0.0001$).

Table 6.2: ANOVA of the regression model for CO_2 adsorption by Methyl-amine (MA) grafted PSI.

	Average Observed Adsorption	**Predicted Adsorption**	**Sum**	**Average**	**Variance**	
Run 1	40.73	52.44	93.18	46.59	68.59	
Run 2	43.41	43.41	86.82	43.41	0.00	
Run 3	47.17	52.81	99.97	49.99	15.92	
Run 4	52.40	47.42	99.82	49.91	12.37	
Run 5	48.72	42.71	91.42	45.71	18.05	
Run 6	56.75	56.02	112.77	56.39	0.27	
Run 7	50.48	49.32	99.80	49.90	0.68	
Run 8	68.21	66.28	134.49	67.25	1.87	
Run 9	44.18	40.40	84.58	42.29	7.13	
Run 10	48.45	52.95	101.40	50.70	10.15	
Run 11	43.50	40.40	83.90	41.95	4.80	
Run 12	45.58	46.69	92.28	46.14	0.62	
Run 13	40.83	47.52	88.35	44.17	22.43	
Run 14	43.86	56.64	100.50	50.25	81.70	
Run 15	63.62	59.97	123.58	61.79	6.66	
Run 16	63.62	59.97	123.58	61.79	6.66	
Run 17	63.62	59.97	123.58	61.79	6.66	
Run 18	63.62	59.97	123.58	61.79	6.66	
Run 19	63.62	61.10	124.72	62.36	3.16	
Run 20	63.62	59.97	123.58	61.79	6.66	
ANOVA Source of Variation	***SS***	***df***	***MS***	***F***	***P-value***	***F crit***
Runs	2553.865876	19	134.41399	9.086673	0.000006	2.1683

6.4 Effects of process variables on the adsorption capacity of MA grafted PSI

To understand the effect of each variable (temperature, pressure and gas flowrate), three dimensional (3D) plots were made for the estimated responses, which were the basis of the model polynomial function in equation 11 for analysis to investigate the interactive effect of the three factors on the adsorption capacity of MA grafted PSI.

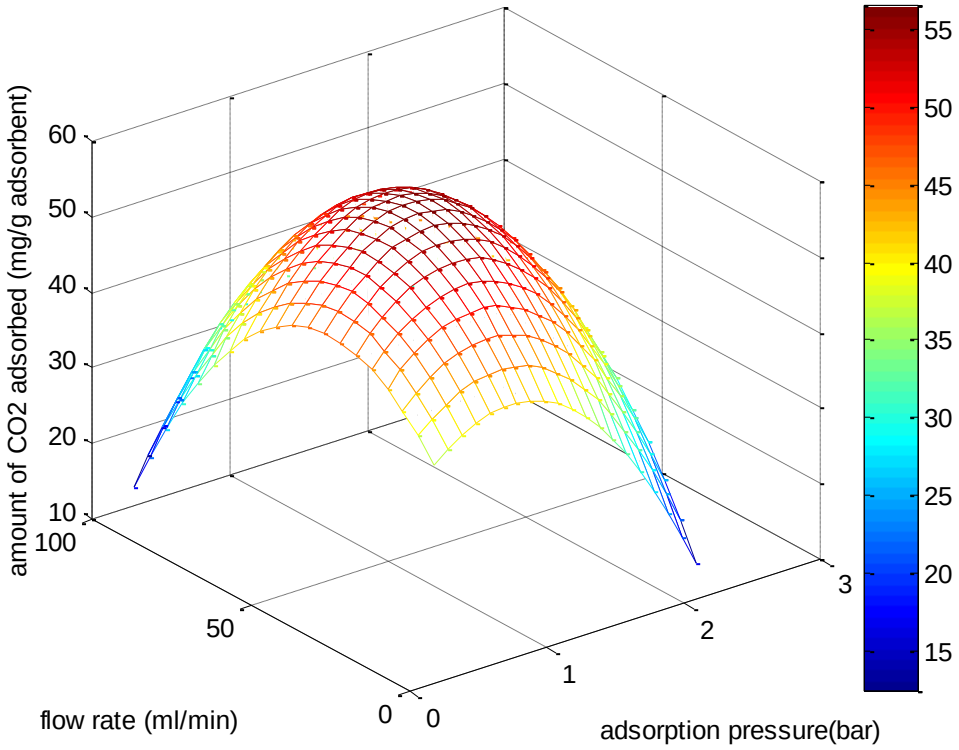


Figure 6.1: 3D surface response of adsorption capacity with respect to flow rate and adsorption pressure at 25^{o}C.

Figure 6.1 shows the effect of gas flow rate in ml/min and adsorption pressure in bars on the adsorption capacity of 100 % MA grafted PSI, sample 1. Figure 6.1 also shows the interaction of the adsorption pressure and the gas flow rate. The general observed trend is that as pressure increases in isolation, the adsorption capacity increases. This is because as pressure is increased, the partial pressure of the CO_2 molecules increases. As this occurs, more CO_2 molecules interact

with the adsorbent surface resulting in higher adsorption. A similar effect was observed from the gas flow rate, as the gas flow rate increased in isolation, the adsorption capacity increased. As the flow rate increases, more molecules are in contact with the adsorbent surface, thus the capacity increases. However, for each of the two factors, the adsorption capacity decreases with a decrease in one of the two factors regardless of the one increasing. This shows that for these two factors, the factor decreasing in value has more influence than the factor increasing, for both gas flow rate and adsorption pressure. At an operating of 2.2 bar and a flow rate of approximately 10 ml / min, the adsorption capacity is less than 15 mg CO_2 / g Ads. Similarly at a gas flow rate of 100 ml / min and pressure of 0.2 bar, again the adsorption capacity is less than 15 mg / g Ads. These results support the observation described.

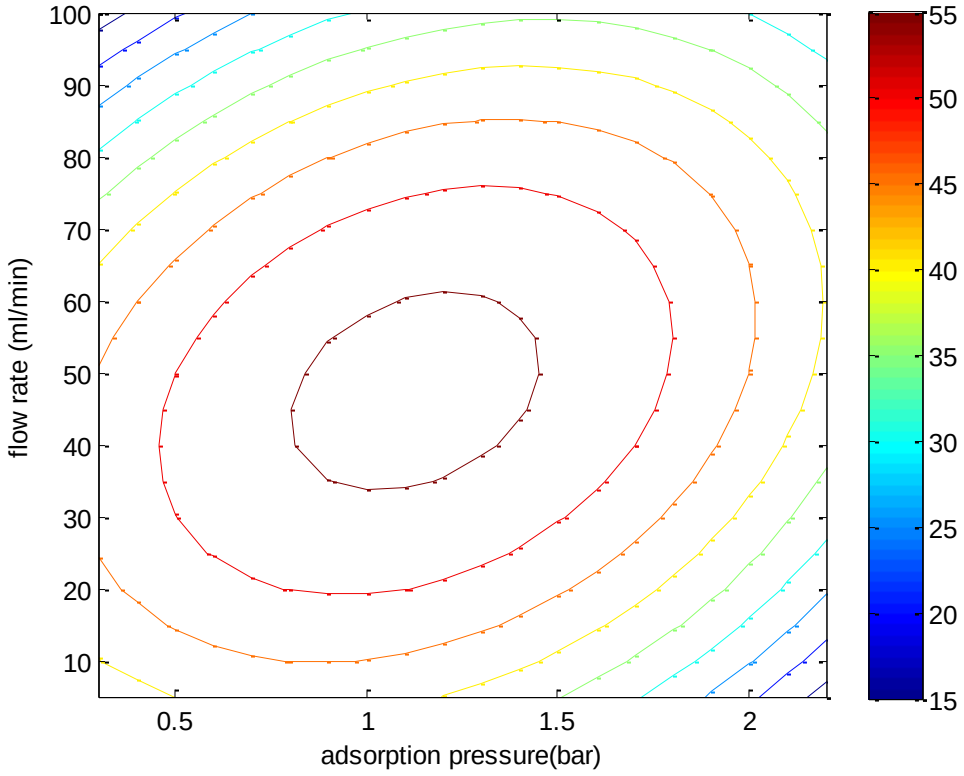


Figure 6.2: Contour diagram showing the interaction between the gas flowrate and the adsorption pressure.

Figure 6.2 shows the contours obtained from the 3D surface in Figure 6.1, with axes denoted by gas flowrate in ml / min and adsorption pressure in bar. The adsorption capacity is represented in the color spectrum which corresponds to the colors of the contours. Figure 6.2 confirms that

adsorption increases for both an increase in gas flowrate and adsorption pressure to maximum, thereafter it starts to decrease. The interaction of gas flowrate and adsorption pressure is such that the highest adsorption capacity is in the range 0.8 bar to 1.5 bar which coincides with the gas flowrate range from 35 ml / min to 60 ml / min. The contour diagram also confirms that of the two variables studied in Figure 6.2, the decreasing variable has more influence than the increasing variable.

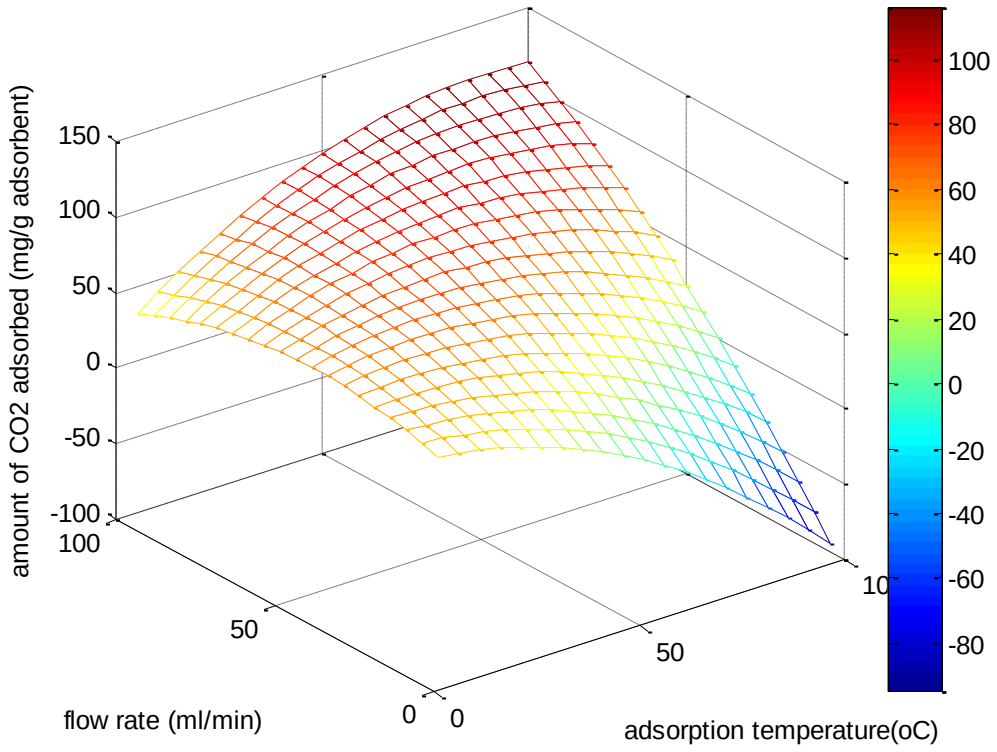


Figure 6.3: 3D surface response of adsorption capacity with respect to flow rate and adsorption temperature at 1.6 bar.

In Figure 6.3, the adsorption capacity of 100 % MA grafted PSI in mg / g CO_2 is shown as a function of the gas flowrate in ml / min and adsorption temperature in ^oC. Figure 6.3 also shows the interaction of the gas flow rate and the adsorption temperature. Figure 6.3 shows that as the adsorption operating temperature increases, the adsorption capacity increases to a maximum thereafter it decreases with further increase in temperature. A similar trend was observed for the gas flow rate as well. These observations can be attributed to adsorption being an exothermic process thus a continuous increase in temperature will ultimately result in a decrease in the

adsorption capacity. Also as the gas flow rate increases, the residence time of the gas inside the adsorption chamber is greatly reduced hence the limiting contact time between the gas and the adsorbent. For the interaction of the two factors, as temperature increases and gas flow rate decreases, adsorption capacity also decreases as seen in Figure 6.3. At a temperature of approximately 100 ^{o}C, and gas flow rate of approximately less than 15 ml / min, there is no adsorption occurring as the surface plotted goes below zero. However, as both temperature and gas flow rate increase, the adsorption capacity also increases.

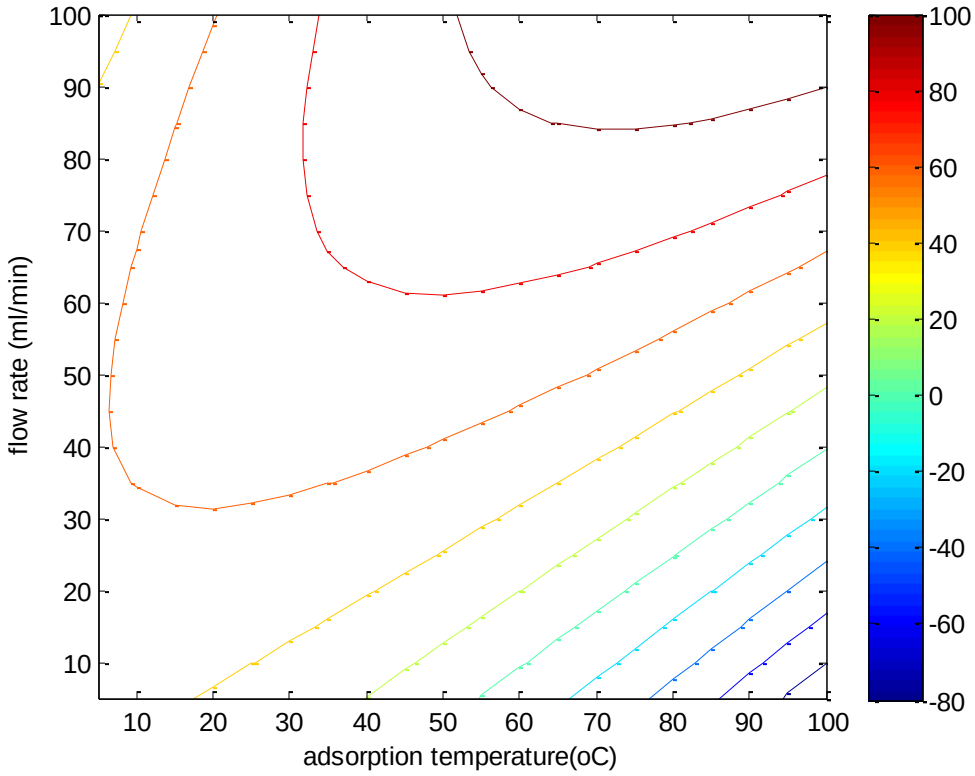


Figure 6.4: Contour diagram showing the interaction between the flowrate and the adsorption temperature.

Figure 6.4 is a contour diagram with gas flowrate and adsorption temperature on the axes. Figure 6.4 confirms that as the temperature increases, the adsorption capacity increases to a maximum, after which it starts to decrease. A similar trend was observed for the gas flowrate. The interaction of the gas flowrate and the temperature is such that the highest adsorption capacity is obtained at temperatures above 40 ^{o}C and gas flowrates in excess of 80 ml / min. The contour

diagram shows that low gas flowrates and high temperatures result in o adsorption occurring and that is above 40 ^{o}C and below 40 ml / min.

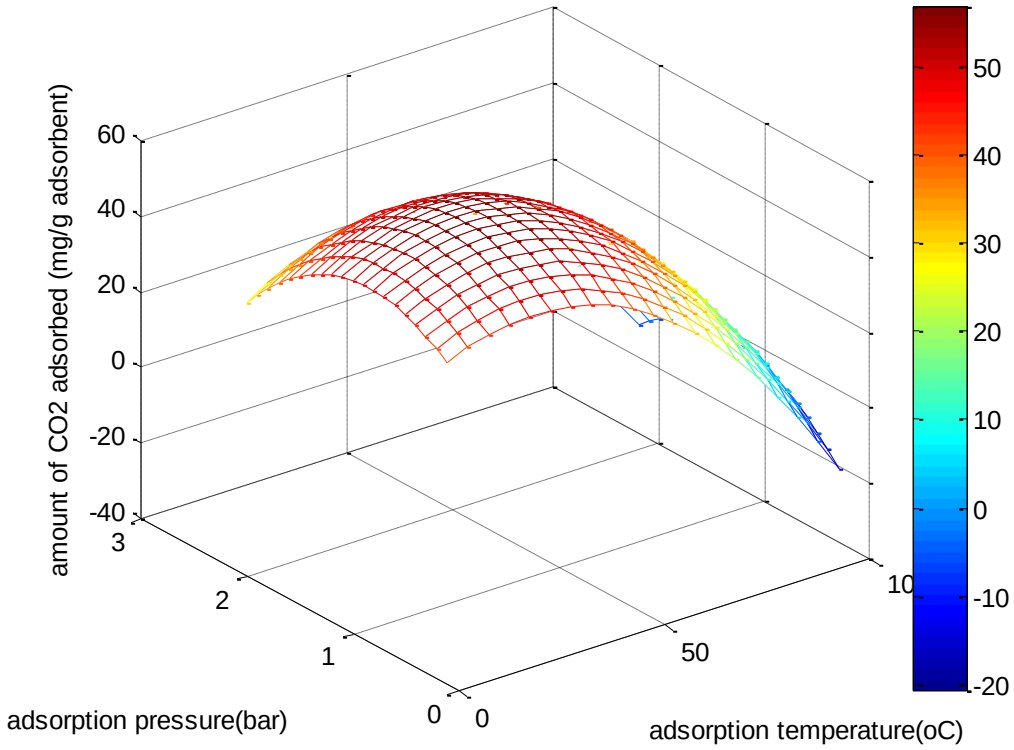


Figure 6.5: 3D surface response of adsorption capacity with respect to adsorption pressure and adsorption temperature at 45 ml/min of gas.

Figure 6.5 is a depiction of the effect of adsorption pressure in bar and adsorption temperature in ^{o}C on the adsorption capacity of 100 % MA grafted PSI, sample 1. Figure 6.5 also shows the interaction of the adsorption pressure and the adsorption temperature. The general observed trend is that as pressure increases in isolation, the adsorption capacity increases. This is because as pressure is increased, the partial pressure of the CO_2 molecules increases. As this occurs, more CO_2 molecules interact with the adsorbent surface resulting in higher adsorption. As adsorption operating temperature increases, the adsorption capacity increases to a maximum thereafter it decreases with further increase in temperature. However, for each of the two factors, the adsorption capacity decreases with a decrease in one of the two factors regardless of the one increasing. This shows that for these two factors, the factor decreasing in value has more influence than the factor increasing, for both adsorption pressure and adsorption temperature.

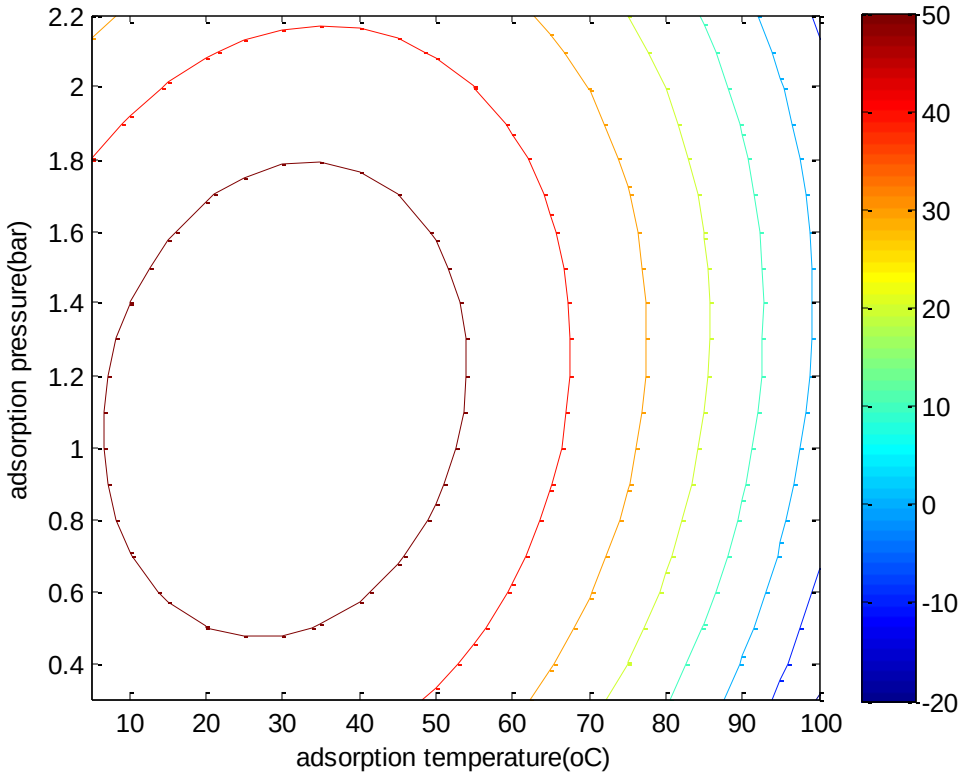


Figure 6.6: Contour diagram showing the interaction between the adsorption pressure and the adsorption temperature.

The contour diagram in Figure 6.6 displays the interaction between the process variables; adsorption pressure in bar and temperature in ^{o}C. According to Figure 6.6, the highest adsorption capacity is obtained in the pressure range 0.5 bar to 1.7 bar and also temperature range of 10 ^{o}C to 45 ^{o}C. It has also been confirmed that adsorption capacity increases with an increase in temperature and pressure to a maximum, thereafter it decreases. Figure 6.6 also shows that extremely high pressures and temperatures as well as low pressures and temperatures result in adsorption occurring.

6.5 Model cross validation

The validity of the RSM was confirmed by use of the model equation for predicting the optimum response values. Random process variables (temperature, pressure and gas flowrate) values were chosen from the range shown in Table 3.3 in Chapter 3 to validate the mathematical model obtained, shown in equation 6.2. Three sets of points were chosen with the results presented in

Table 16. Table 16 shows the observed responses, predicted responses and calculated error of validation experiments. To obtain the average observed adsorption, three experiments were conducted with the average adsorption evaluated from the three adsorption capacities obtained. The results in Table 6.3 show that the model gives fairly accurate results, with the highest percentage error calculated being 5 %.

Table 6.3: Cross validation results**.**

Random run	1	2	3	4
Temperature (ºC) (X_1)	30	45	60	80
Pressure (bar) (X_2)	0.8	1.3	2.0	2.5
Gas flowrate (ml/min) (X_3)	40	55	65	100
Average observed adsorption capacity (mg/g)	57.20	57.54	55.61	70.40
Predicted adsorption capacity from model (mg/g)	54.35	58.90	55.59	71.85
% Error	4.97	2.33	0.0410	2.06

Table 6.4: ANOVA analysis for the results obtained in Table 6.3.

Source of Variation	*SS*	*df*	*MS*	*F*	*P-value*	*F crit*
Rows	328.0301	3	109.3434	54.33616	0.004102	9.276628
Columns	0.00045	1	0.00045	0.000224	0.989008	10.12796
Error	6.03705	3	2.01235			
Total	334.0676	7				

Table 6.3 shows the ANOVA results obtained on the cross-validation results. The ANOVA analysis conducted is such that the P values are greater than 0.0001 which shows that there is need to perform further investigations into the regression analysis as well as propose higher order polynomials to model CO_2 adsorption using amine-grafted PSI (PAA).

6.6 Summary

An MA grafted PSI (PAA) adsorbent was applied for CO_2 capture. The objective of the work was to determine the influence of operating variables on the CO_2 adsorption capacity of MA

grafted PSI as well as to develop a model with temperature, pressure and gas flowrate as the independent variables and the CO_2 adsorption capacity as the response variable. The model, a quadratic polynomial was successfully developed. Analysis of variance (ANOVA) was performed on the model by use of the predicted and observed adsorption capacities and the model proved to be significant with a p-value less than 0.0001. Further, cross validation experiments were carried out, with four random experimental runs being carried out. In all the four runs conducted, the highest percentage error obtained was approximately 5%, which supports that the model is fairly accurate. Response surface methodology (RSM) was successfully used to evaluate the combined effect of temperature, pressure and gas flowrate on the CO_2 adsorption capacity of MA grafted PSI. It was observed in all cases that in isolation, as temperature, pressure and gas flowrate increase, the CO_2 adsorption capacity increases to a maximum, whence it will start to decrease. For the interaction of pressure and flowrate, the adsorption capacity increases to a maximum and then decreases with a decrease in one of the two factors regardless of the one increasing. For the interaction of gas flowrate and adsorption temperature, as the temperature increases and gas flowrate decreases, adsorption capacity also decreases. At a temperature of approximately 100 ^oC and gas flowrate of approximately less than 15 ml / min there is no adsorption occurring. Contours were also obtained from the RSM and these further confirmed the interaction between each of the factors. Operating variables were shown to have an effect on the adsorption capacity of MA grafted PSI.

Furthermore, these experiments were conducted using 15 % CO_2 with the balance being N_2, which in Chapter 3 was said to be done in order to mimic the flue gas concentration from South African coal-fired power plants. The important result obtained in this part of the work is that PAA (amine-grafted PSI) is usable in South African coal-fired power plant flue gas conditions and with further optimization studies, improved adsorption performance may be achieved.

Chapter 7: General conclusions and recommendations

7.1 Summary

Global warming is a challenge the world is facing currently. Increasing population and economic growth have resulted in a higher demand for energy. Most of this energy is supplied from fossil fuels which when combusted produce CO_2, a GHG which traps heat in the earth's atmosphere. This heating has several adverse impacts on societies and the environment which brings about the need to reduce CO_2 emissions, the cause. South Africa is not spared, a nation largely dependent on coal, a fossil fuel for energy. Several options exist to reduce CO_2 emissions and CCS with a potential of reducing global emissions by 20 % is an option worth considering. Power stations in South Africa make use of pulverized coal combustion boilers and thus a post-combustion capture approach best suits the scenario. The most widely applied capture method is absorption which has several shortcomings including high heats of regeneration and high corrosion rates. For this reason, this work aimed to develop an alternative CO_2 capture technology, adsorption through the production and performance evaluation of a novel adsorbent. In the commencement of this work, the following research objectives and expected outcomes were set out to be achieved:

Objectives of this research were as follows:

1. To synthesize Poly-DL-Succinimide (PSI) and amine-grafted PSI which is PAA, characterize the materials, and conduct CO_2 adsorption tests to compare their performance for CO_2 adsorption.
2. To synthesize amine-grafted PSI with varied water-soluble component, characterize and conduct CO_2 adsorption test to compare their performance and hence deduce the effect of the water-soluble component on their adsorption performance.
3. Conduct series of adsorption experiments to investigate the effect of operating variable (temperature, pressure and gas flowrate) using Design of Experiment (DoE). Using the results of the experiment to evaluate effect of the operating conditions using response surface methodology approach via a developed empirical model.

Expected outcomes:

4 A synthesized water soluble PAA (amine-grafted PSI) adsorbent with higher CO_2 adsorption capacity relative to the base material.

5 Information on the effect of operating variables in the CO_2 adsorption performance of PAA (amine-grafted PSI) and the optimum operating conditions possible for the material.

7.2 Results

Poly-DL-Succinimide (PSI) and amine-grafted PSI which is PAA were successfully synthesized. The PSI was synthesized from a poly condensation reaction of phosphoric acid and aspartic acid. The produced PSI was then grafted with amines, thereafter it was taken through the freeze-frying process. Synthesis and characterization results presented in Chapter 4, which also show comparison of previously synthesized PSI confirm this. Several characterization techniques were employed to confirm the synthesized products, being NMR, BET, TGA, SEM and FTIR analyses. The NMR results showed that the structure set out to be synthesized was synthesized, also showing the difference in the amine-grafted PSI and PSI, confirming the grafting of amines to the PSI. BET results showed the pore volume, pore size and surface area of the synthesized adsorbent samples. It was expected that the freeze-drying process mentioned earlier would improve the pore size, volume and surface area of the adsorbent in comparison to amine grafted PSI put through a different drying process from literature. This was shown as not to be the case as the BET values obtained for this work did not differ very much from those reported in literature, showing that freeze-drying did not have a significant impact. TGA analysis showed the maximum temperature at which amine-grafted PSI and PSI can work at which was found to be 210 ^oC and 400 ^oC respectively. This was also confirmed with values reported from literature. SEM imaging was used to show visually the effect of amine-grafting onto the PSI and there are distinct visible differences shown in Figure 4.3. FTIR analysis was used to show the functional groups present in the synthesized material, in particular, of interest in this work, CONH, $-NH_2$ and the –NH group. These were all shown to be present and from comparison with literature also confirm that the PSI and amine-grafted PSI were synthesized.

The PSI and amine grafted PSI were then employed for CO_2 capture by use of a Q600 TA TGA. These adsorption tests were performed at 100 % CO_2, 60 ml / min gas flowrate, temperature of 40 ^oC and pressure of 1.1 bar. From the findings of this work, amine-grafted PSI was shown to possess a higher adsorption capacity for CO_2 than PSI with no amines grafted. This was found to

be dependent on the quantity of amine grafted onto the PSI. PSI without grafting of amines displayed a CO_2 adsorption capacity of 18.6 g CO_2 / kg Ads, which was surpassed by the 100 % MA and MEA grafted PSI which displayed 44.5 g CO_2 / kg Ads and 43.6 g CO_2 / kg Ads respectively. However, as the quantity of water-soluble amine (MA and MEA) was varied, with the introduction of EDA, the displayed adsorption capacity was lower than that of PSI without grafting. The variation of amines grafted onto the PSI was found to affect the adsorption capacity of CO_2. CO_2 adsorption capacity increased with an increase in the water-soluble component (MA and MEA) grafted onto the PSI, with 100 % MA and 100 % MEA grafted onto the PSI giving the highest adsorption capacity.

Further in this work, an understanding of the influence of operating variables (temperature, pressure and gas flowrate) on the CO_2 adsorption capacity of 100 % MA grafted PSI (sample with highest CO_2 adsorption capacity from TGA results) was pursued. In all engineering work, it is of paramount importance that the influence of operating variables be determined as a precursor to process optimization. The investigation was performed by use of a packed bed adsorption column system. A Design of Experiment (DoE) method incorporating Central Composite Design (CCD), and response surface methodology (RSM) was used to design the experiment. A regression model of the CO_2 adsorption capacity as a function of temperature, pressure and gas flowrate was determined. The proposed model shown in equation 8 showed a fair fit to the adsorption data obtained experimentally. It was also observed that the adsorption capacity of 100 % MA grafted PSI got higher with use of the packed bed column system compared to that obtained by use of the TGA, 63.4 g CO_2 / kg Ads in the packed bed column compared to 44.5 g CO_2 / kg Ads obtained from the TGA. This showed that the flow regime in the TGA is a limiting factor in the adsorption process, unlike in the packed bed adsorption column where the gas flows through the sample. Response surfaces were then plotted showing the interaction between two of the factors at a time as presented in Chapter 6. The highest adsorption capacity was found to be in the region: 0.8 bar to 1.5 bar coinciding with 35 ml / min to 60 ml / min and 0.5 bar to 1.7 bar coinciding with 10 ^oC to 45 ^oC. The investigations conducted here made use of a dilute CO_2 stream, with 15 % CO_2 and the balance being N_2. This was done to mimic flue gas composition from South African coal fired power plants as explained in Chapter 3. The results obtained in this work are thus promising as the adsorbent performed comparatively better in the CO_2 adsorption equipment.

In conclusion, a synthesized water-soluble amine-grafted PSI which is PAA adsorbent was successfully synthesized and characterized. The synthesized adsorbent displayed a higher adsorption capacity than the base material, PSI depending on the quantity and type of amine grafted to the PSI. Furthermore, information concerning the influence of operating variables on the CO_2 adsorption capacity of amine-grafted PSI was obtained and reported.

7.3 Recommendations

It should be noted that this work serves as an initial study on using amine-grafted PSI, a novel adsorbent, for CO_2 capture and as such several research ideas may be generated with this work as a background study. It is recommended that further work be done on studying the kinetics and kinetic modeling of the material synthesized in this work. Kinetics are an important aspect of industrial processes and should be studied extensively, particularly where CO_2 capture is involved as determination process economic feasibility is important. The development of a more robust method of synthesis is also recommended, building up to further to bigger batch or continuous production of the adsorbent material. Adsorption is the first stage of the CO_2 capturing process, the second stage is desorption which recovers the captured CO_2 and more importantly the adsorbent material. It is recommended that studies on desorption with this material be performed, TSA or PSA or desorption by dissolving in water as the adsorbent is soluble in water. Further investigations of a combination of adsorption and absorption when moisture is introduced in the gas stream should be carried out. Moreover, this study serves as a precursor to studies with flue gas samples from actual power plants which should be conducted in future work. Finally, more optimization studies should be carried out to determine the exact conditions at which adsorption will be maximized. An economic evaluation would also be necessary alongside further performance tests to determine the feasibility of deploying the adsorbent at a fairly larger scale.

References

Administration, U.S.E.I., 2013. *International Energy Outlook 2013.* [Online] Available at: http://www.internationalenergyoutlook.com/FD/Energy/International/showDetail.asp&objID=5&ClassID=6 [Accessed 25 November 2015].

Aresta, M., 2010. *Carbon Dioxide as Chemical Feedstock*. Wiley-VCH Verlag GmbH and Co.

Auerbach, S.M., Carrado, K.A. and Dutta, P.K., 2003. *Handbook of Zeolite Science and Technology*. New York: Marcel Dekker Inc. 1283 pages.

Bandyopadhyay, A., 2014. *Carbon Capture and Storage: CO2 Management Technologies*. Oakville: Apple Academic Press Inc. 416 pages.

Bandyopadhyay, A. and Bose, S., 2013. *Chracterization of Biomaterials*. Oxford: Elsevier. 419 pages.

Barnes, G. and Gentle, I., 2011. *Interfacial Science: An Introduction*. New York: Oxford University Press. 321 pages.

Ben-Mansour, R. et al., 2016. Carbon capture by physical adsorption: Materials, experimental investigations and numerical modeling and simulations – A review. *Applied Energy*, (161), pp.225-55.

Benson, S.M., 2005. Carbon Dioxide Capture for Storage in Deep Geologic Formations. 2, p.1131.

Bhatta, L.K.G. et al., 2015. Progress in hydrotalcite like compounds and metal-based oxides for CO2 capture: a review. *Journal of Cleaner Production*, (103), pp.171-96.

Black, B.C. et al., 2013. *Climate Change: An Encyclopedia of Science and History*. Santa Barbara: ABC-CLIO.

Bonjour, J., CHalfen, J.B. and Meunier, F., 2002. Temperature swing adsorption process with indirect cooling and heating. *Industrial engineering and Chemistry Research*, (41), pp.5802-11.

Bouzalakos, S. and Mercedes Maroto-Valer, M., 2010. Overview of carbon dioxide capture and storage technology. *Developments and Innovation in Carbon Dioxide Capture and Storage Technology: Carbon Dioxide Storage and Utilisation*, pp.1-24.

Breck, D.W., 1974. *Zeolite Molecular Sieves: Structure, Chemistry and Use*. New York: John Wiley and Sons, Inc. 771 pages.

Brown, T.E. et al., 2012. *Chemistry: The Central Science*. 12th ed. Pearson Prentice Hall. 1200 pages.

Capture Ready, n.d. *Capture REady: CCS Information Team*. [Online] Available at: http://www.captureready.com/EN/Channels/OverViews/showDetail.asp?objID=2&ClassID=1 [Accessed 1 December 2015].

Carruthers, D.J., Petruska, M.A., Sturm, E.A. and Wilson, S.M., 2012. Molecular sieve carbons for CO2 capture. *Microporous and Mesoporous Materials*, (154), pp.62-67.

Casper, J.K., 2010. *Global Warming Greenhouse Gases Worldwide Impacts*. New York. 261 pages.

Chabangu, N. et al., 2014. The investigation of CO2 storage potential in the Zululand Basin in South Africa. *Energy Procedia*, (63), pp.2789-99.

Chabangu, N. et al., 2014. The investigation of CO2 storage potential in the Algoa basin in South Africa. *Energy Procedia*, (63), pp.2800-10.

Chandramowli, S.N. and Felder, F.A., 2014. Impact of climate change on electricity systems and markets- A review of models and forecasts. *Sustainable Energy Technologies and Assessments*, pp.62-74.

Chao, C., Su-Sung, K., Won-Seung, C. and Wha-Seung, A., 2015. Polyethylenimine-incorporated zeolite 13X with mesoporosity for post-combustion CO2 capture. *Applied Surface Science*, pp.167-71.

Christophe, J. et al., 2015. Multi-objective optimisation of a hybrid vacuum swing adsorption and low-temperature post-combustion CO2 capture. *Journal of Cleaner Production*, pp.1-11.

Chungsying, L. et al., 2008. Comparative study of CO2 Capture by carbon Nanotubes, Activated Carbons and Zeolites. *Energy and Fuels*, (22), pp.3050-56.

Crittenden, B. and Thomas, J.W., 1998. *Adsorption Technology and Design*. Oxford: Butterworth-Heinemann. 259 pages.

Czaun, M. et al., 2013. Organoamines-grafted on nano-sized silica for carbon dioxide capture. *Journal of CO2 Utilization*, (1), pp.1-7.

Czaun, M. et al., 2013. Organoamines-grafted on nano-sized silica for carbon dioxide capture. *Journal of Carbon dioxide Utilisation*, pp.1-7.

Dabrowski, A., 1999. *Adsorption and its Applications in Industry and Environmntal Protection: Applications in Industry*. Amsterdam: Elsevier Science.

Dabrowski, J.M. et al., 2008. Anthropogenic mercury emissions in South Africa: Coal combustion in power plants. *Atmospheric Environment*, (42), pp.6620-26.

Dai, S. and Lu, A.-H., 2014. *Porous Materials for Carbon Dioxide Capture*. London: Springer-Verlag Berlin Heidelberg. 245 pages.

Dasgupta , S. et al., 2015. Adsorption properties and performance of CPO-27-Ni/alginate spheres during multicycle pressure-vacuum-swing adsorption (PVSA) CO2 capture in the presence of moisture. *Chemical Engineering Science*, (137), pp.525-31.

Davidson, R.M., 2010. Adavanced adsorption processes and technology for carbon dioxide (CO2) capture in power plants. *Developments and Innovation in Carbon Dioxide (CO2) Capture and Storage Technology* , pp.183-202.

Demirel, M. and Kayan, B., 2012. Application of response surface methodology and central composite design for the optimization of textile dye degradation by wet air oxidation. *International Journal of Industrial Chemistry (IJIC)*.

Draper, N.R., 1978. *Empirical model-building and response surfaces*. New York: Wiley. 669 pages.

Draper, N. and John, J., 1988. Response surface design for quantitative and qualitative variables. *Technometrics*, (30), pp.423-28.

Eddaoudi, M. et al., 2002. Systematic design of size and functionality in isoreticular MOFs and their application in methane storage. *Science*, (18), pp.469-72.

Fan, L.-S., 2010. *Chemical Looping Systems for Fossil Energy Conversions*. John Wiley and Sons. 420 pages.

Faust, S.D. and Aly, O.M., 1998. *Chemistry of Water Treatment*. Florida, USA: CRC Press LLC. 600 pages.

Forbes, S.M. et al., 2008. World Resources Instutute (WRI). CCS Guidelines: Guidelines for Carbon Dioxide Capture, Transport and Storage.

Fujimori, T. and Yamada, T., 2013. Realization of oxyfuel combustion for near zero emission power generation. *Proceedings of the Combustion Institute*, pp.2111-30.

Gao, B. and Creamer, A.E., 2015. *Carbon Dioxide Capture: An Effective Way to Combat Global Warming*. London: Springer International Publishoing.

Garcia, S. et al., 2011. Breakthrough adsorption study of a commercial activated carbon for pre-combustion CO2 capture. *Chemical Engineering Journal*, pp.549-56.

Garret, C.W., 1992. On global climate change, carbon dioxide and fossil fuel combustion. *Progress in Energy and Combustion Science*.

Gholinezad, J., Chapoy, A. and Tohidi, B., 2011. Separation and capture of carbon dioxide from CO2/H2 syngas mixture using semi-clathrate hydrates. *Chemical Engineering Research and Design*, pp.1747-51.

Gil, M.V. et al., 2013. Response surface methodology as an efficient tool for optimizing carbon adsorbents for CO2 capture. *Fuel Processing Technology*, 106, pp.55-61.

Global CCS Institue, 2015. [Online] [Accessed 1 December 2015].

Global CCS Institute, n.d. [Online] Available at: https://www.globalccsinstitute.com/projects/large-scale-ccs-projects [Accessed 1 December 2015].

Gluyas, J. and Mathias, S., eds., 2013. *Geological storage of carbon dioxide (CO2): Geoscience, technologies, environmental aspects and legal frameworks*. Woodhead Publishing.

Goto, K., Yogo, K. and Higashii, T., 2013. A review of efficiency penalty in a coal-fired power plant with post-combustion CO2 capture. *Applied Energy*, pp.710-20.

Grande, C.A., Ribeiro, R.P.L., Oliveira, E.L.G. and Rodrigues, A.E., 2009. Electric swing adsorption as emerging CO2 capture technique. *Energy Procedia*, (1), pp.1219-25.

Hammond, G. and Spargo, J., 2014. The prospects for coal-fired power plants with carbon captureand storage: A UK perspective. *Energy Conversion and Management*, pp.476-89.

Holloway, S. et al., 2006. *IPCC Guidelines for National Greenhouse Gas Inventories*. Cambridge University Press. 354 pages.

Höök, M. and Tang, X., 2013. Depletion of fossil fuels and anthropogenic climate change- A review. *Energy Policy*, pp.797-809.

Hu, H.-W. et al., 2016. Effects of climate warming and elevated CO2 on autotrophic nitrification and nitrifiers in dryland ecosystems. *Soil Biology & Biochemistry*, (92), pp.1-15.

Intergovernmental Panel on Climate Change, 2005. *Carbon Dioxide Capture And Storage*. New York: Cambridge University Press.

International Energy Agency, 2004. *CO2 Emissions from fuel combustion: 1971 - 2002*. Paris.

International Energy Agency, 2012. *IEA Statistics: Carbon dioxide emissions from fuel combustion, Highlights*. International Energy Agency. 136 pages.

International Energy Agency, 2013. *IEA Statistics: Carbon dioxide emissions from fuel combustion, Highlights*. International Energy Agency.

Ishwarya, P.S., Anandharamakrishnan, C. and Stapley, A.G.F., 2015. Spray-freeze drying: A novel process fro the drying of foods and bioproducts. *Trends in Food Science and Technology*, (41), pp.161-81.

Jiang, G. et al., 2015. A new mesoporous amine-TiO2 based pre-combustion CO2 capture technology. *Applied Energy*, pp.214-23.

Jian-Rong, L. et al., 2011. Carbon dioxide capture-related gas adsorption and separation in metal-organic frameworks. *Coordination Chemistry Reviews*, pp.1791-823.

Keller, J. and Staudt, R., 2005. *Gas Adsorption Equilibria*. Boston: Springer Science.

Kidnay, A.J. and Parrish, W.R., 2006. *Fundamentals of Natural Gas Processing*.

Kohli , S. et al., 2004. Enhancement of Biogas production from solid substances using different techniques- A review. *Bioresource Technology*, (95), pp.1-10.

Koskimäki, P.-L., 2012. Africa could take a leap to energy efficiency: What lessons could Sub-Saharan countries learn from European energy efficiency policy implementation? *Energy for Sustainable Development*, (76), pp.189-96.

Kumar, A., 2012. Polyaspartic Acid- A Versatile Green Chemical. *Chemical Science Review and Letters*.

Lazic, Z.R., 2004. *Design of Experiments in Chemical Engineering*. Wiley-VCH.

Lee, T.S., Cho, J.H. and Chi, S.H., 2015. Carbon dioxide removal using carbon monolith as electric swing adsorption to improve indoor air quality. *Building and Environment*, (92), pp.209-21.

Lee, S.-Y. and Park, s.-J., 2014. A review on solid sorbents for carbon dioxide capture. *Journal of Industrial and Engineering Chemistry*.

Letcher, M., 2008. *Future Energy: Improved, Sustainable and Clean Options for our Planet*. Amsterdam: Elsevier.

Letcher, T.M., 2014. *Future Energy: Imporved, Sustainable and Clean Options for our Planet*.

Liebscher, A. and Munch, U., 2015. *Geological Storage of CO2 - Long term Security Aspects*. Springer International Publishing AG Switzerland.

Li, H., Eddaoudi, M., O'Keeffe, M. and Yaghi, O.M., 1999. Design and synthesis of an exceptionally stable and highly porous metal-organic framework. *Nature*, (402), pp.276-79.

Li, F.S. et al., 2014. Poly(ethyleneimine) infused and functionalized Torlon®-silica hollow fiber sorbents for post-combustion CO2 capture. *Polymer*, 55(6), pp.1341-46.

Linneen, N.N., Pfeffer, R. and Lin, Y.S., 2014. CO2 adsorption performance for amine grafted particulate silica aerogels. *Chemical Engineering Journal*, (254), pp.190-97.

Li, F., Zhang, J., Oko, E. and Wang, M., 2015. Modelling of post-combistion CO2 capture process using neural networks. *Fuel*, (151), pp.156-63.

Li, W., Zhang, L.B., Peng, J.H. and Zhu, X.Y., 2008. Preparation of high surfacearea activated carbons from tobacco stems with K2CO3 activation using microwave radiation. *Science Direct. Industrial Crops and Products*, 27, pp.341-47.

Mabon, L., Shackley, S. and Bower-Bir, N., 2014. Perceptions of sub-seabed carbon dioxide storage in Scotland and implications for policy: A qualitative study. *Marine Policy*, pp.9-15.

MacGillivray, R. and Lukehart, C.M., 2014. *Metal-Organic Framework Materials*. West Sussex, United Kingdom: John Wiley and Sons.

Ma, R., Marzouki, N. and Korbahti, B.K., 2008. Photolytic decolorization of Rose Bengal by UV/H(2)O(2) and data optimization using response surface method. *J Hazard Mater*, 159, pp.602-09.

Manancourt, A. and Gale, J., 2005. A review of capacity estimates for the geological storage of carbon dioxide. *Greenhouse Gas Control Technologies*.

Mantell, C.L., 1951. *Adsorption*. 2nd ed. New York: McGraw-Hill.

Maroto-Valer, M.M., ed., 2010. *Developments and Innovation in Carbon Dioxide (CO2) Capture and Storage technology*. Oxford: Woodhead Publishing Limited.

Masel, R.I., 1996. *Principles of Adsorption and Reaction on Solid Surfaces*. Danvers: John Wiley and Sons.

McGlinchey, D., 2005. *Characterisation of Bulk Solids*. Oxford: Blackwell Publishing Ltd.

McKeown, J.J., Meegan, D. and Sprevak, D., 1990. *An Introduction to Unconstrained Optimisation*. British Library Cataloguing in Publication.

Millward, A.R. and Yaghi, O.M., 2005. Metal-Organic Frameworks with Exceptionally High Capacity for Storage of Carbon Dioxide at Room Temperature. *J. AM. CHEM. SOC.*, 127.

Mohammed , Y.S., Mustafa, M.W. and Bashir, N., 2013. Status of renewable energy consumption and developmental challenges in Sub-Sahara Africa. *Renewable and Sustainable Energy Review*, pp.453-63.

Montgomery, D.C., 1996. *Design and analysis of experiments*. 4th ed. New York: Wiley.

Mortaheb, H.R., Nozaeim, A.A., Mafi, M. and Mokhtarani, B., 2012. Absorption of carbon dioxide in emulsions of aqueous monoethanolamine/diethanolamine solutions in kerosene/n-heptane. *Chemical Engineering Science*, 82, pp.44-51.

Myers , R.H., 1971. *Response Surface Methodology*. Boston: Allyn and Bacon.

Ngoy, J.M., Wagner, N., Riboldi, L. and Bolland, O., 2014. A CO2 capture technology using multi-walled carbon nanotubes with polyaspartamide surfactant. *Energy Procedia*, 63, pp.2230-48.

Nordic Council of Ministers, 2007. *Carbon Capture and Storage In a Nordic Perspective*.

Oikonomopoulou, V.P., Krokida, M.K. and Karathanos, V.T., 2011. The influence of freeze-drying conditions on microstructural changes of food products. *Procedia Food Science*, 1, pp.647-54.

Olajire, A.A., 2010. CO2 capture and separation technologies for end-of-pipe applications- A review. *Energy*, pp.2610-28.

Pegels, A., 2010. Renewable energy in South Africa: Potentials, barriers and options for support. *Energy Policy*, pp.4945-54.

Pires, J.C.M., Martins, F.G., Alvim-Ferraz, M.C.M. and Simôes, M., 2011. Recent developments on carbon capture and storage: An overview. *Chemical Engineering Research and Design*, pp.1446-60.

Pires, J.C.M., Martins, G., Alvin-Ferraz, M.C.M. and Simoes, M., 2011. Recent developments on carbon capture and storage: An overview. *Chemical Engineering research and Design*, pp.1446-60.

Pollet, B.G., Staffell, I. and Adamson, K.-A., 2015. Current energy landscape in the Republic of South Africa. *International journal of hydrogen energy*, pp.1-17.

Roque-Malherbe, R.M.A., 2007. *Adsorption and Diffusion in Nanoporous Materials*. Taylor and Francis Group.

Roque-Malherbe, R.M.A., 2010. *The Physical Chemistry of Materials: Energy and Environmental Applications*. Florida: CRC Press.

Rouquerol, J. et al., 2014. *Adsorption by Powders and Porous Solids: Principles, Methodology and Applications*. 2nd ed. San Diego: Academic Press.

Rowsell, J.L.C. and Yaghi, O.M., 2004. Metal-organic frameworks: a new class of porous materials. *Microporous Mesoporous Mater*, 73, pp.3-14.

Ruthven, D.M., 1984. *Principles of Adsorption and Adsorption Processes*. John Wiley and Sons.

Ruthven, D.M., 1984. *Principles of Adsorption Processes*. John Wiley and Sons Inc.

Saleman, T.L. et al., 2015. Capture of low grade methane from nitrogen gas using dual-reflux. *Chemical Engineering* , 281, pp.739-48.

Seymore, R., Inglesi-Lotz, R. and Blignaut, J., 2014. A greenhouse gas emissions inventory for South Africa: A comparative analysis. *Renewable and Sustainable Energy Reviews* , pp.371-79.

Seymore, R., Inglesi-Lotz, R. and Blignaut, J., 2014. A greenhouse gas emissions inventory for South Africa: A comparative analysis. *Renewable and Sustainable Energy Reviews*, pp.371-79.

Shi, F. and Morreale, B., 2015. *Novel Materials for Carbon Dioxide Mitigation Technology*. Oxiford: Elesevier.

Snyman, C.P. and Botha, W.J., 1993. Coal in South Africa. *African Earth Sciences*, pp.171-80.

Son, H.-K., Cho, K.W. and Lee, K.-H., 1998. Adsorption of Carbon dioxide. *Journal of Non-Crystalline Solids* , 242, pp.69-80.

Song, G. et al., 2015. An investigation of CO_2 adsorption kinetics on porous magnesium oxide. *Chemical Engineering Journal*, (283), pp.175-83.

Spigarelli, B.P. and Kawatra, K.S., 2013. Opportunities and challenges in carbon dioxide capture. *Journal of CO2 Utilization*, pp.69-87.

Sreenivasulu, B., Gayatri, D.V., Sreedhar, I. and Raghavan, K.V., 2015. A journey into the process and engineering aspects of carbon capture technologies. *Renewable and Sustainable Energy Reviews*, pp.1324-50.

Sreenivasulu, B., Gayatri, D.V., Sreedhar, I. and Raghavan, K.V., 2015. A journey into the process and engineering aspects of carbon capture technologies. *Renewable and Sustainable Energy Reviews*, 41, pp.1324-50.

Surridge, A.D. and Cloete, M., 2009. Carbon Capture and Storage in South Africa. *Energy Procedia*, pp.2741-44.

Susarla, N. et al., 2015. Energy and cost estimates for capturing CO2 from a dry flue gas using pressure/vacuum swing adsorption. *Chemical Engineering Research and Design*, 102, pp.354-67.

Susarla, et al., 2015. Energy and cost estimates for capturing CO2 from a dry flue gas using pressure/vacuum swing adsorption. *Chemical Engineering Research and Design*, 102, pp.354-67.

Suzuki, M., 1990. *Adsorption Engineering*. Tokyo: Kodansha Ltd.

Svendsen, H.F., Hessen, E.T. and Mejdell, T., 2011. Carbon dioxide capture by absorption, challenges and possibilities. *Chemical Engineering Journal*, pp.718-24.

Tao, F. et al., 2014. Respones of wheat growth and yield to climate cjange in different climate zones of China, 1981-2009. *Agricultural and Forest Meteorology*, pp.91-104.

Toth, J., 2005. *Adsorption: Theory, Modeling and Analysis*. New York: Marcel Dekker Inc.

Towler, G. and Sinnott, R., 2013. *Chemical Engineering Design: Principles, Practice and Economics of Plant and Process Design*. Oxford: Butterworth-Heinemann.

Tudorachi, N. and Chiriac, A.P., 2011. TGA/FTIR/MS study on thermal decomposition of poly(succinimide) and sodium poly(aspartate). *Polymer Testing*, pp.397-407.

Uchida, T. et al., 2013. Oxyfuel combustion as CO2 capture technology advancing for practical use- Callide Oxyfuel Project. *Energy Procedia 37*, pp.1471-79.

Understanding the Long-Term fate of geologically, 2015. [Online] Available at: http://www.ultimateco2.eu/page/maps-databases-ccs-activity-around-world [Accessed 1 December 2015].

Wahby, A., Silvestre-Albero, J., Sepúlveda-Escribano, A. and Rodríguez-Reinoso, F., 2012. CO2 adsorption on carbon molecular sieves. *Microporous and Mesoporous Materials*, 164, pp.280-87.

Wall , T. et al., 2009. An overview on oxyfuel coal combustion- State of the art research and technoogy development. *Chemical Engineering Research and Design*, pp.1003-16.

Wang, M. et al., 2011. Post-combustion CO2 capture with chemical absorption: A state-of-the-art review. *Chemical Engineering Research and Design*.

Wauquier, J.P., 1998. *Petroleum Refining: Separation Processes*. Paris.

Wilcox, J., 2012. *Carbon Capture*. London: Springer Science.

Worch, E., 2012. *Adsorption Technology in Water Treatment*. Berlin: Walter de Gruyter GmbH and Co.

Wu, X. et al., 2016. Impact of climate change on human infectious diseases: Empirical evidence and human adaptation. *Environment International*, 86, pp.14-23.

Wu, X., Yu, Y., Qin, Z. and Zhang , Z., 2014. The Advances of Post-Combustion CO2 Capture with Chemical Solvents: Review and Guidelines. *Energy Procedia*, pp.1339-46.

Xu, C. and Hedin, N., 2014. Microporous adsorbents for CO2 capture – a case for microporous polymers? *Materials Today*, 17.

Yang, R.T., 2003. *Adsorbents: Fundamentals and Applications*. New Jersey: John Wiley and Sons, Inc.

Yang, R.T., 2003. *Adsorbents: Fundamentals and Applications*. New Jersey: John Wiley and Sons. Inc.

Yang, H. et al., 2008. Progress in carbon dioxide separation and capture: A review. *Journal of Environmental Sciences*, pp.14-27.

Yang, H. et al., 2008. Progress in carbon dioxide separation and capture: A review. *Environmental Sciences*, pp.14-27.

Yu, C.-H., Huang, C.-H. and Tan, C.-S., 2012. A Review of CO2 Capture by Absorption and Adsorption. *Aerosol and Air Quality Research*, 12, pp.745-69.

Yu, C.-T., Lin, H.-M. and Cheng, H.-W., 2015. Synthesis of mercury sorbent including metal oxides with layered carbonates material. *Chemical Engineering Journal*, 277, pp.79-85.

Zhang , Z. and Zheng , H., 2009. Optimization for decolorization of azo dye acid green 20 by ultrasound and H2O 2 using response surface methodology. *J Hazard Mater*, 172, pp.1388-93.

Zhao, C. et al., 2013. Capturing CO2 in flue gas from fossil fuel-fired power plants using dry regenerable alkali metal-based sorbent. *Progress in Energy and Combustion Science*, 39, pp.515-34.

Appendices

Appendix A: Synthesis and characterization information

In Appendix A, additional information on the synthesis and characterization results is presented here.

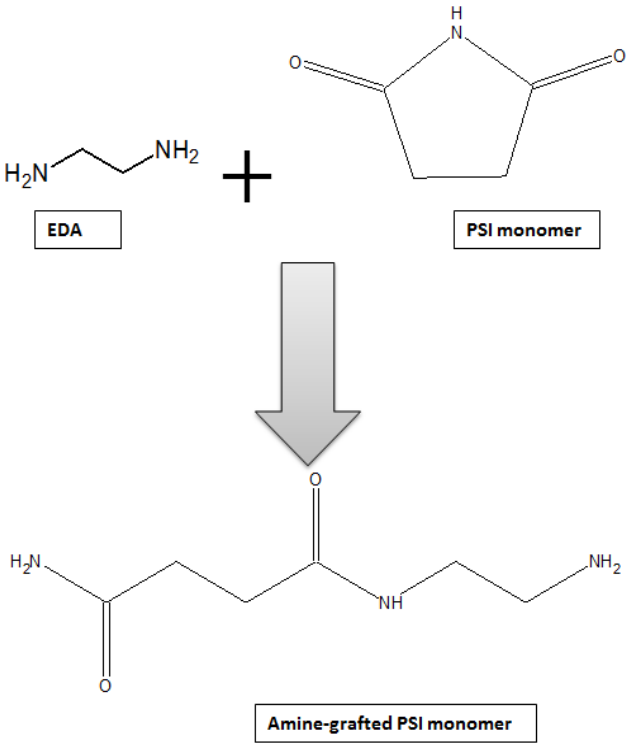
A1 Percentage Yield Calculation:

$$\% \, Yield = \frac{total \; product \; mass}{total \; reactant \; mass} \times 100 \; \%$$

$$\% \, Yield = \frac{27.638}{25 + 12.5} \times 100 \; \%$$

$$\% \, Yield = 73.7 \; \%$$

A2 Reaction scheme showing PSI monomer being grafted with amines:



Appendix B: TGA adsorption results

For the purposes of this dissertation, the TGA raw graphs for the 100 % Methyl-amine (MA) grafted poly-succinimide (PSI) are shown. The remaining results have been extracted from the TGA and tabulated in Ms Excel. A total of 10 samples were synthesized, five were grafted with a combination of MA and EDA and the remaining five were grafted with a combination of MonoEthanol Amine (MEA) and EDA. Three adsorption runs were conducted for each sample and the average adsorption capacity was calculated.

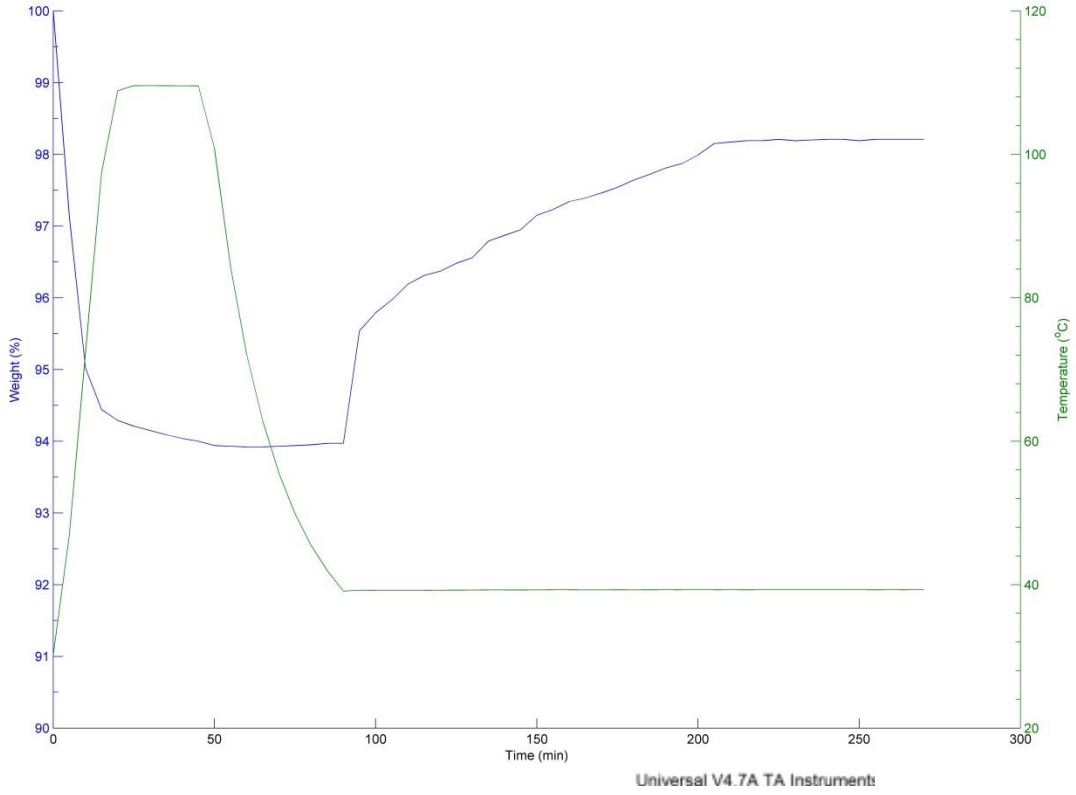


Figure B1: TGA results for the first adsorption run on 100 % MA grafted polysuccinimide.

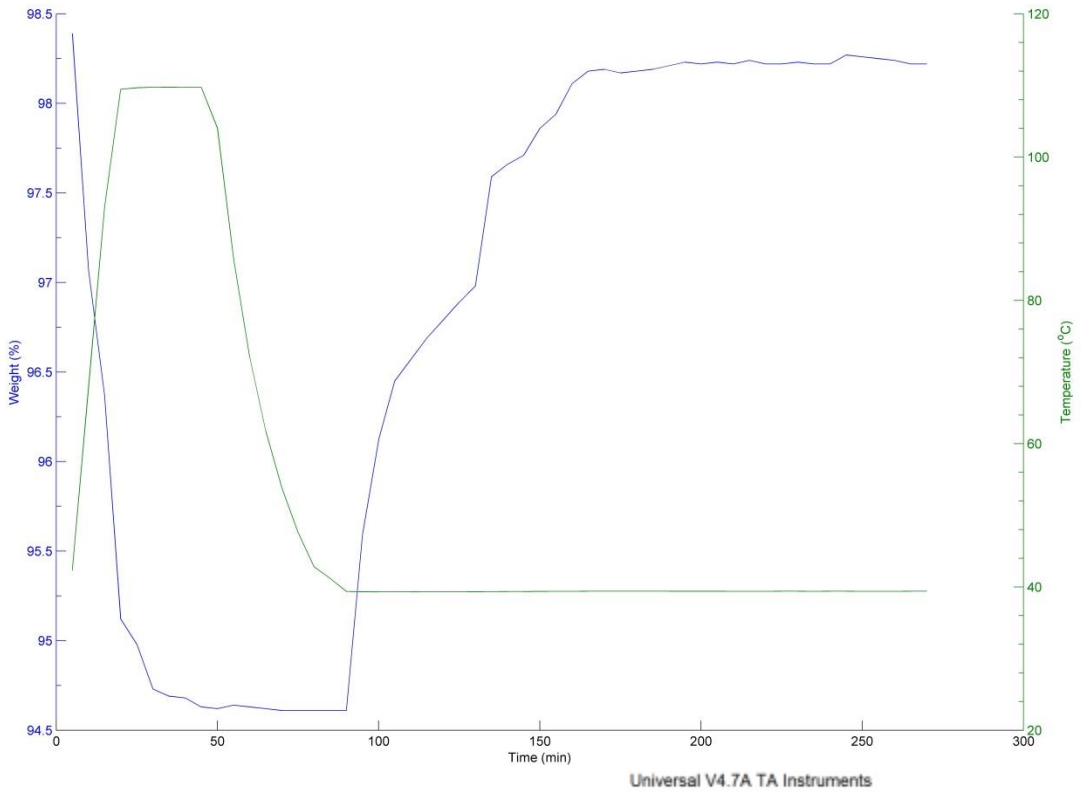


Figure B2: TGA results for the second adsorption run on 100 % MA grafted polysuccinimide.

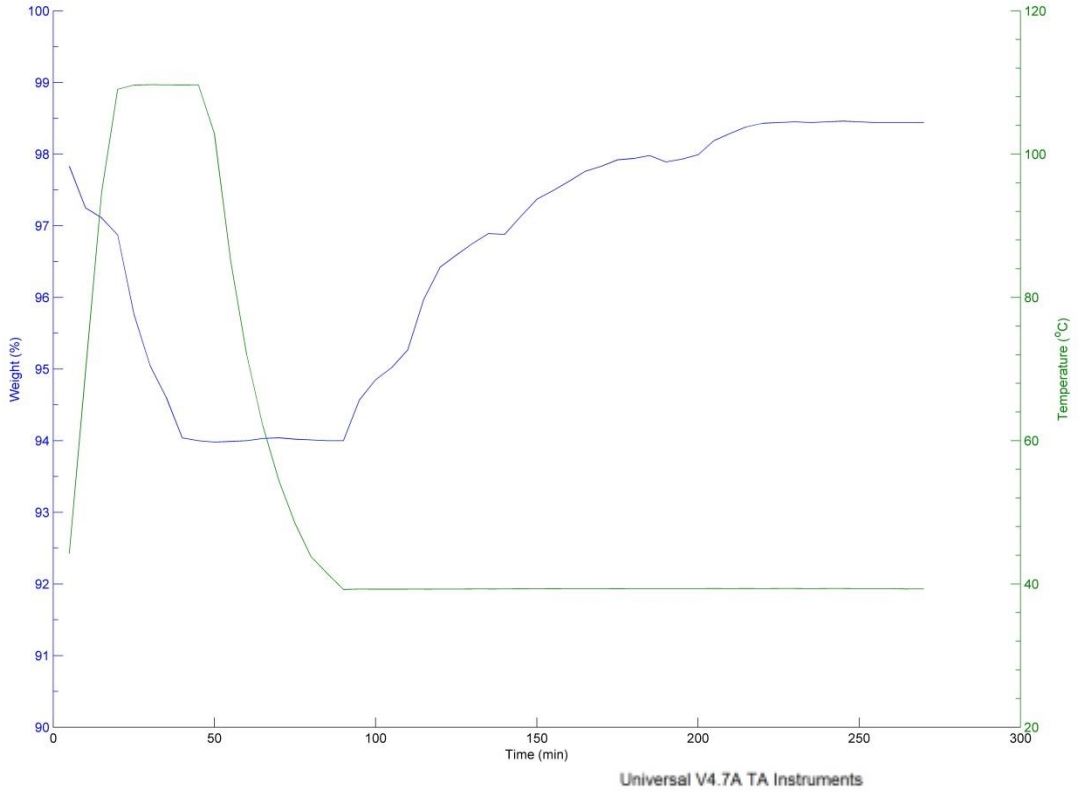


Figure B3: TGA results for the third adsorption run on 100 % MA grafted polysuccinimide.

Table B1: TGA results for the first adsorption run on 100 % MA grafted polysuccinimide.

Adsorption Time (min)	Experimental Time (min)	Weight (%)	Temperature (^{0}C)	Cumulative Adsorption Capacity (g CO_2/ kg Ads)
0	90	93.97	39.1	0
5	95	95.54	39.23	16.70745983
10	100	95.79	39.22	19.32416487
15	105	95.97	39.22	21.20327543
20	110	96.19	39.22	23.49565846
25	115	96.31	39.22	24.74318939
30	120	96.37	39.23	25.36617766
35	125	96.48	39.24	26.50761171
40	130	96.56	39.25	27.33679911
45	135	96.79	39.26	29.7187378
50	140	96.87	39.26	30.54526947
55	145	96.95	39.27	31.37111854
60	150	97.15	39.28	33.43403758
65	155	97.23	39.29	34.25750644
70	160	97.34	39.29	35.3888445
75	165	97.39	39.28	35.90250795
80	170	97.46	39.28	36.62126758
85	175	97.54	39.29	37.44211716
90	180	97.64	39.28	38.46733758
95	185	97.72	39.29	39.28667392
100	190	97.81	39.3	40.20767269
105	195	97.87	39.29	40.8211069
110	200	97.99	39.29	42.04722317
115	205	98.15	39.29	43.68004285
120	210	98.17	39.3	43.88381259
125	215	98.19	39.29	44.08754082
130	220	98.19	39.3	44.08754082
135	225	98.21	39.3	44.29122755
140	230	98.19	39.3	44.0875823
145	235	98.2	39.3	44.18942566
150	240	98.21	39.3	44.29125865
155	245	98.21	39.3	44.29125865
160	250	98.19	39.3	44.0876134
165	255	98.21	39.29	44.29130013
170	260	98.21	39.3	44.29130013
175	265	98.21	39.29	44.29130013

180	270	98.21	39.29	44.29130013

Table B2: TGA results for the second adsorption run on 100 % MA grafted polysuccinimide.

Adsorption Time (min)	**Experimental Time (min)**	**Weight (%)**	**Temperature (^{0}C)**	**Cumulative Adsorption Capacity (g CO_2/ kg Ads)**
0	90	94.61	39.36	0
5	95	95.59	39.33	10.35831307
10	100	96.12	39.31	15.9028261
15	105	96.45	39.31	21.44733912
20	110	96.57	39.31	24.88054761
25	115	96.69	39.32	26.12471558
30	120	96.79	39.32	27.36733751
35	125	96.89	39.32	28.40157062
40	130	96.98	39.33	29.43473521
45	135	97.59	39.34	30.36362364
50	140	97.66	39.35	36.65358033
55	145	97.71	39.35	37.37086694
60	150	97.86	39.37	37.88284728
65	155	97.94	39.38	39.41800233
70	160	98.11	39.38	40.23549671
75	165	98.18	39.39	41.97125329
80	170	98.19	39.39	42.68473816
85	175	98.17	39.39	42.78659189
90	180	98.18	39.39	42.58290516
95	185	98.19	39.39	42.68476928
100	190	98.21	39.39	42.78662302
105	195	98.23	39.4	42.99030975
110	200	98.22	39.39	43.193955
115	205	98.23	39.4	43.0921531
120	210	98.22	39.38	43.19396536
125	215	98.24	39.38	43.09216347
130	220	98.22	39.38	43.29578798
135	225	98.22	39.39	43.09220492
140	230	98.23	39.39	43.09220492
145	235	98.22	39.38	43.19401718
150	240	98.22	39.39	43.09221529
155	245	98.27	39.39	43.09221529

160	250	98.26	39.38	43.60127658
165	255	98.25	39.38	43.49951612
170	260	98.24	39.38	43.39774531
175	265	98.22	39.39	43.29596414
180	270	98.22	39.39	43.09238108

Table B3: TGA results for the third adsorption run on 100 % MA grafted polysuccinimide.

Adsorption Time (min)	**Experimental Time (min)**	**Weight (%)**	**Temperature (^{0}C)**	**Cumulative Adsorption Capacity (g CO_2/ kg Ads)**
0	90	94	39.22	0
5	95	94.57	39.28	6.063829787
10	100	94.85	39.27	9.024599587
15	105	95.02	39.26	10.81690322
20	110	95.27	39.27	13.44792827
25	115	95.98	39.27	20.90043168
30	120	96.42	39.28	25.48472008
35	125	96.59	39.28	27.24783976
40	130	96.75	39.29	28.90432594
45	135	96.89	39.29	30.35135436
50	140	96.88	39.3	30.24814454
55	145	97.13	39.31	32.82865651
60	150	97.37	39.32	35.29957178
65	155	97.49	39.33	36.53198423
70	160	97.62	39.34	37.86545433
75	165	97.76	39.34	39.29958668
80	170	97.83	39.34	40.01562596
85	175	97.92	39.33	40.93558916
90	180	97.94	39.34	41.13983752
95	185	97.98	39.34	41.54825084
100	190	97.89	39.34	40.62969603
105	195	97.93	39.34	41.03831795
110	200	97.99	39.34	41.65100048
115	205	98.19	39.35	43.69202508
120	210	98.29	39.34	44.71045873
125	215	98.38	39.35	45.62611647
130	220	98.43	39.34	46.13434985
135	225	98.44	39.35	46.2359449
140	230	98.45	39.35	46.33752962

145	235	98.44	39.34	46.23595521
150	240	98.45	39.35	46.33753994
155	245	98.46	39.35	46.43911434
160	250	98.45	39.34	46.33755025
165	255	98.44	39.34	46.23597585
170	260	98.44	39.34	46.23597585
175	265	98.44	39.29	46.23597585
180	270	98.44	39.29	46.23597585

Table B4: TGA results for the first adsorption run on 80 % MA grafted polysuccinimide.

Adsorption Time (min)	**Experimental Time (min)**	**Weight (%)**	**Temperature (^{0}C)**	**Cumulative Adsorption Capacity (g CO_2/ kg Ads)**
0	95	89.32	38.95	0
5	100	89.4	39	1.794526694
10	105	89.42	39.02	2.690182762
15	110	89.44	39.02	2.913896408
20	115	89.57	39.02	3.137560018
25	120	89.69	39.02	4.59104839
30	125	89.85	39.01	5.930782676
35	130	89.84	39.03	7.714705076
40	135	89.83	39.04	7.60340847
45	140	89.79	39.04	7.492099476
50	145	89.83	39.04	7.046813937
55	150	89.86	39.05	7.492297844
60	155	89.83	39.05	7.826261998
65	160	89.87	39.05	7.492409339
70	165	89.95	39.06	7.937694878
75	170	90.15	39.07	8.827869575
80	175	90.12	39.07	11.05132705
85	180	90.13	39.08	10.71854835
90	185	90.24	39.08	10.82951151
95	190	90.21	39.08	12.04997085
100	195	90.2	39.09	11.71752404
105	200	90.2	39.1	11.60667158
110	205	90.22	39.1	11.60667158
115	210	90.2	39.1	11.82840107

120	215	90.2	39.11	11.60672074
125	220	90.2	39.11	11.60672074
130	225	90.23	39.11	11.60672074
135	230	90.2	39.12	11.93931497
140	235	90.21	39.12	11.60683132
145	240	90.22	39.13	11.71769606
150	245	90.2	39.12	11.82854852
155	250	90.21	39.13	11.60686818
160	255	90.2	39.13	11.71773293
165	260	90.2	39.14	11.60688047
170	265	90.2	39.13	11.60688047
175	270	90.2	39.14	11.60688047
180	275	90.2	39.14	11.60688047

Table B5: TGA results for the second adsorption run on 80 % MA grafted polysuccinimide.

Adsorption Time (min)	**Experimental Time (min)**	**Weight (%)**	**Temperature (^{0}C)**	**Cumulative Adsorption Capacity (g CO_2/ kg Ads)**
0	95	91.24	39.3	0
5	100	91.35	39.29	1.205611574
10	105	91.64	39.28	4.380214748
15	110	91.69	39.29	4.925828018
20	115	91.75	39.28	5.580206903
25	120	91.84	39.3	6.561133334
30	125	91.93	39.29	7.54109849
35	130	91.96	39.3	7.867433746
40	135	92.07	39.3	9.063605994
45	140	92.12	39.31	9.606671054
50	145	92.21	39.32	10.58365759
55	150	92.25	39.33	11.01745002
60	155	92.31	39.34	11.66785653
65	160	92.32	39.36	11.77618715
70	165	92.31	39.36	11.66786826
75	170	92.3	39.37	11.55953764
80	175	92.31	39.36	11.66788
85	180	92.32	39.36	11.77621062
90	185	92.33	39.36	11.88452951
95	190	92.39	39.36	12.53437247
100	195	92.36	39.36	12.209662

105	200	92.35	39.36	12.10139002
110	205	92.32	39.37	11.77653891
115	210	92.33	39.36	11.8848578
120	215	92.32	39.37	11.77655064
125	220	92.31	39.36	11.66823175
130	225	92.32	39.36	11.77656238
135	230	92.33	39.36	11.88488127
140	235	92.32	39.37	11.77657411
145	240	92.31	39.37	11.66825522
150	245	92.32	39.36	11.77658585
155	250	92.32	39.36	11.77658585
160	255	92.32	39.36	11.77658585
165	260	92.33	39.37	11.88490474
170	265	92.33	39.35	11.88490474
175	270	92.32	39.35	11.77659758
180	275	92.32	39.35	11.77659758

Table B6: TGA results for the third adsorption run on 80 % MA grafted polysuccinimide.

Adsorption Time (min)	**Experimental Time (min)**	**Weight (%)**	**Temperature (^{0}C)**	**Cumulative Adsorption Capacity (g CO_2/ kg Ads)**
0	95	90.8	39.34	0
5	100	90.93	39.32	1.431718062
10	105	91.14	39.32	3.741186884
15	110	91.26	39.33	5.057842578
20	115	91.36	39.32	6.153612905
25	120	91.43	39.34	6.919812555
30	125	91.61	39.34	8.888531793
35	130	91.74	39.35	10.30759085
40	135	91.79	39.36	10.85260938
45	140	91.85	39.36	11.50627536
50	145	91.86	39.38	11.61514852
55	150	91.89	39.39	11.94173245
60	155	91.9	39.41	12.05055822
65	160	91.91	39.41	12.15937215
70	165	91.92	39.41	12.26817424
75	170	91.93	39.41	12.37696449

80	175	91.94	39.41	12.48574291
85	180	91.93	39.41	12.37697632
90	185	91.92	39.4	12.2681979
95	190	91.93	39.41	12.37698816
100	195	91.94	39.42	12.48576657
105	200	91.95	39.41	12.59453316
110	205	91.94	39.42	12.4857784
115	210	91.94	39.41	12.4857784
120	215	91.93	39.4	12.37701182
125	220	91.92	39.41	12.2682334
130	225	91.93	39.4	12.37702365
135	230	91.94	39.41	12.48580207
140	235	91.96	39.41	12.70333524
145	240	91.94	39.4	12.48584938
150	245	91.94	39.41	12.48584938
155	250	91.94	39.4	12.48584938
160	255	91.93	39.39	12.37708279
165	260	91.92	39.39	12.26830437
170	265	91.93	39.39	12.37709463
175	270	91.94	39.39	12.48587304
180	275	91.94	39.39	12.48587304

Table B7: TGA results for the first adsorption run on 60 % MA grafted polysuccinimide.

Adsorption Time (min)	**Experimental Time (min)**	**Weight (%)**	**Temperature (^{0}C)**	**Cumulative Adsorption Capacity (g CO_2/ kg Ads)**
0	85	93.97	38.91	0
5	90	94.05	39.23	0.851335533
10	95	94.13	39.26	1.70194691
15	100	94.37	39.24	4.251612266
20	105	94.41	39.24	4.675475782
25	110	94.56	39.25	6.264290526
30	115	94.63	39.24	7.004561254
35	120	94.72	39.25	7.955633852
40	125	94.79	39.26	8.694654123
45	130	94.91	39.26	9.960610447
50	135	94.98	39.26	10.69815128

55	140	95.03	39.25	11.22457789
60	145	95.03	39.27	11.22457789
65	150	95.03	39.27	11.22457789
70	155	95.03	39.28	11.22457789
75	160	95.03	39.28	11.22457789
80	165	95.03	39.29	11.22457789
85	170	95.03	39.28	11.22457789
90	175	95.03	39.28	11.22457789
95	180	95.03	39.28	11.22457789
100	185	95.04	39.28	11.32980782
105	190	95.05	39.28	11.43502667
110	195	95.04	39.28	11.32981889
115	200	95.03	39.27	11.22460003
120	205	95.03	39.27	11.22460003
125	210	95.03	39.26	11.22460003
130	215	95.03	39.25	11.22460003
135	220	95.03	39.27	11.22460003
140	225	95.05	39.26	11.43505989
145	230	95.04	39.26	11.3298521
150	235	95.03	39.26	11.22463325
155	240	95.03	39.25	11.22463325
160	245	95.03	39.25	11.22463325
165	250	95.03	39.25	11.22463325
170	255	95.02	39.24	11.11940332
175	260	95.03	39.25	11.22464432
180	265	95.03	39.25	11.22464432

Table B8: TGA results for the second adsorption run on 60 % MA grafted polysuccinimide.

Adsorption Time (min)	**Experimental Time (min)**	**Weight (%)**	**Temperature (^{0}C)**	**Cumulative Adsorption Capacity (g CO_2/ kg Ads)**
0	85	94.21	39.33	0
5	90	94.46	39.37	2.65364611
10	95	94.71	39.36	5.300269019
15	100	94.87	39.37	6.989636562
20	105	95.17	39.34	10.15185855
25	110	95.24	39.35	10.88738445
30	115	95.31	39.36	11.62236975
35	120	95.33	39.38	11.83221132

40	125	95.34	39.38	11.93711009
45	130	95.35	39.37	12.04199786
50	135	95.36	39.38	12.14687463
55	140	95.36	39.37	12.14687463
60	145	95.36	39.37	12.14687463
65	150	95.36	39.39	12.14687463
70	155	95.36	39.37	12.14687463
75	160	95.37	39.37	12.25174041
80	165	95.37	39.38	12.25174041
85	170	95.37	39.38	12.25174041
90	175	95.37	39.39	12.25174041
95	180	95.37	39.39	12.25174041
100	185	95.37	39.39	12.25174041
105	190	95.37	39.39	12.25174041
110	195	95.37	39.39	12.25174041
115	200	95.37	39.4	12.25174041
120	205	95.37	39.39	12.25174041
125	210	95.37	39.4	12.25174041
130	215	95.37	39.39	12.25174041
135	220	95.37	39.4	12.25174041
140	225	95.37	39.4	12.25174041
145	230	95.37	39.4	12.25174041
150	235	95.37	39.4	12.25174041
155	240	95.37	39.41	12.25174041
160	245	95.37	39.4	12.25174041
165	250	95.37	39.41	12.25174041
170	255	95.37	39.4	12.25174041
175	260	95.37	39.41	12.25174041
180	265	95.37	39.4	12.25174041

Table B9: TGA results for the third adsorption run on 60 % MA grafted polysuccinimide.

Adsorption Time (min)	**Experimental Time (min)**	**Weight (%)**	**Temperature (^{0}C)**	**Cumulative Adsorption Capacity (g CO_2/ kg Ads)**
0	85	92.78	39.88	0
5	90	92.84	39.88	0.646691097
10	95	92.97	39.88	2.046949606

15	100	93.14	39.88	3.87549645
20	105	93.32	39.86	5.808071068
25	110	93.47	39.88	7.41544355
30	115	93.58	39.83	8.592291737
35	120	93.61	39.84	8.912873058
40	125	93.69	39.88	9.767482608
45	130	93.72	39.88	10.08768754
50	135	93.78	39.88	10.7278924
55	140	93.81	39.51	11.04779004
60	145	93.85	39.22	11.47418381
65	150	93.88	39.19	11.79384284
70	155	93.9	39.18	12.00688076
75	160	93.91	39.19	12.11337704
80	165	93.92	39.17	12.21986197
85	170	93.92	39.17	12.21986197
90	175	93.92	39.17	12.21986197
95	180	93.92	39.18	12.21986197
100	185	93.92	39.47	12.21986197
105	190	93.92	39.47	12.21986197
110	195	93.92	39.47	12.21986197
115	200	93.91	39.48	12.11338837
120	205	93.9	39.47	12.00690344
125	210	93.91	39.46	12.11339971
130	215	93.92	39.47	12.21988465
135	220	93.92	39.47	12.21988465
140	225	93.93	39.48	12.32635824
145	230	93.94	39.47	12.4328205
150	235	93.93	39.47	12.32636957
155	240	93.92	39.47	12.21990731
160	245	93.91	39.47	12.11343372
165	250	93.92	39.49	12.21991865
170	255	93.91	39.48	12.11344506
175	260	93.92	39.48	12.21992999
180	265	93.92	39.48	12.21992999

Table B10: TGA results for the first adsorption run on 40 % MA grafted polysuccinimide.

Adsorption Time (min)	Experimental Time (min)	Weight (%)	Temperature (^{0}C)	Cumulative Adsorption Capacity (g CO_2/ kg Ads)
0	85	88.54	39.57	0
5	90	88.55	39.27	0.112943302
10	95	88.55	39.33	0.112943302
15	100	88.57	39.31	0.338804398
20	105	88.63	39.31	1.016234679
25	110	88.79	39.31	2.821492492
30	115	88.83	39.32	3.271993675
35	120	88.87	39.31	3.722291998
40	125	88.93	39.32	4.397435466
45	130	89.01	39.33	5.297019408
50	135	89.07	39.33	5.971100972
55	140	89.11	39.35	6.420185961
60	145	89.13	39.35	6.644627662
65	150	89.19	39.36	7.317801678
70	155	89.27	39.37	8.214763221
75	160	89.31	39.36	8.662842083
80	165	89.35	39.36	9.11072026
85	170	89.36	39.36	9.222639678
90	175	89.39	39.35	9.558360358
95	180	89.35	39.35	9.110883012
100	185	89.35	39.35	9.110883012
105	190	89.4	39.35	9.670480102
110	195	89.43	39.35	10.00605057
115	200	89.46	39.35	10.34150847
120	205	89.45	39.35	10.22972667
125	210	89.45	39.35	10.22972667
130	215	89.44	39.34	10.11793237
135	220	89.46	39.35	10.34154597
140	225	89.47	39.35	10.45332777
145	230	89.45	39.35	10.22978915
150	235	89.47	39.35	10.45337775
155	240	89.47	39.34	10.45337775
160	245	89.47	39.34	10.45337775

165	250	89.47	39.34	10.45337775
170	255	89.47	39.34	10.45337775
175	260	89.47	39.34	10.45337775
180	265	89.47	39.34	10.45337775

Table B11: TGA results for the second adsorption run on 40 % MA grafted polysuccinimide.

Adsorption Time (min)	**Experimental Time (min)**	**Weight (%)**	**Temperature (^{0}C)**	**Cumulative Adsorption Capacity (g CO_2/ kg Ads)**
0	85	88.11	40.56	0
5	90	88.21	39.25	1.134944955
10	95	88.25	39.25	1.588408281
15	100	88.31	39.24	2.268294967
20	105	88.39	39.24	3.174194638
25	110	88.46	39.24	3.966139429
30	115	88.52	39.25	4.644412094
35	120	88.59	39.25	5.435193838
40	125	88.65	39.26	6.112471184
45	130	88.73	39.27	7.014896451
50	135	88.78	39.29	7.578403721
55	140	88.82	39.29	8.028955647
60	145	88.84	39.31	8.254130157
65	150	88.86	39.32	8.479253975
70	155	88.84	39.33	8.254180826
75	160	88.85	39.33	8.366742735
80	165	88.86	39.34	8.479291976
85	170	88.87	39.34	8.59182855
90	175	88.88	39.34	8.704352461
95	180	88.89	39.34	8.816863713
100	185	88.88	39.35	8.704365119
105	190	88.89	39.35	8.81687637
110	195	88.9	39.36	8.929374964
115	200	88.89	39.36	8.816889024
120	205	88.89	39.36	8.816889024
125	210	88.93	39.37	9.2668834
130	215	88.92	39.37	9.154435407
135	220	88.91	39.37	9.041974768
140	225	88.94	39.36	9.379394631

145	230	88.93	39.38	9.266959281
150	235	88.93	39.37	9.266959281
155	240	88.93	39.37	9.266959281
160	245	88.93	39.38	9.266959281
165	250	88.93	39.37	9.266959281
170	255	88.93	39.37	9.266959281
175	260	88.93	39.37	9.266959281
180	265	88.93	39.38	9.266959281

Table B12: TGA results for the third adsorption run on 40 % MA grafted polysuccinimide.

Adsorption Time (min)	**Experimental Time (min)**	**Weight (%)**	**Temperature (^{0}C)**	**Cumulative Adsorption Capacity (g CO_2/ kg Ads)**
0	85	88.4	39.57	0
5	90	88.46	39.27	0.678733032
10	95	88.51	39.33	1.243960253
15	100	88.62	39.31	2.486757677
20	105	88.68	39.31	3.163805747
25	110	88.79	39.31	4.404220723
30	115	88.88	39.32	5.417848383
35	120	88.91	39.31	5.755382137
40	125	88.91	39.32	5.755382137
45	130	88.91	39.33	5.755382137
50	135	88.95	39.33	6.205275287
55	140	88.99	39.35	6.654966125
60	145	89.12	39.35	8.115804421
65	150	89.21	39.36	9.125678748
70	155	89.23	39.37	9.349868861
75	160	89.23	39.36	9.349868861
80	165	89.27	39.36	9.798148588
85	170	89.28	39.36	9.910168303
90	175	89.29	39.35	10.02217547
95	180	89.28	39.35	9.910180847
100	185	89.27	39.35	9.798173679
105	190	89.27	39.35	9.798173679
110	195	89.27	39.35	9.798173679
115	200	89.27	39.35	9.798173679
120	205	89.27	39.35	9.798173679

125	210	89.26	39.35	9.686153963
130	215	89.27	39.34	9.798186229
135	220	89.24	39.35	9.462127082
140	225	89.27	39.35	9.798299202
145	230	89.28	39.35	9.910318918
150	235	89.27	39.35	9.798311749
155	240	89.26	39.34	9.686292034
160	245	89.27	39.34	9.798324299
165	250	89.27	39.34	9.798324299
170	255	89.26	39.34	9.686304584
175	260	89.27	39.34	9.798336849
180	265	89.27	39.34	9.798336849

Table B13: TGA results for the first adsorption run on 20 % MA grafted polysuccinimide.

Adsorption Time (min)	**Experimental Time (min)**	**Weight (%)**	**Temperature (^{0}C)**	**Cumulative Adsorption Capacity (g CO_2/ kg Ads)**
0	85	83.9	38.91	0
5	90	83.94	39.34	0.476758045
10	95	83.99	39.36	1.072421615
15	100	84.01	39.34	1.310545201
20	105	84.07	39.34	2.024745891
25	110	84.13	39.34	2.738436863
30	115	84.19	39.35	3.451618843
35	120	84.19	39.35	3.451618843
40	125	84.25	39.36	4.164292557
45	130	84.27	39.35	4.401681281
50	135	84.31	39.37	4.876346049
55	140	84.37	39.37	5.588005402
60	145	84.45	39.38	6.53620974
65	150	84.37	39.39	5.588903642
70	155	84.37	39.39	5.588903642
75	160	84.37	39.39	5.588903642
80	165	84.39	39.39	5.825954726
85	170	84.34	39.39	5.233467465
90	175	84.37	39.39	5.589170571
95	180	84.37	39.39	5.589170571
100	185	84.37	39.4	5.589170571

105	190	84.37	39.4	5.589170571
110	195	84.38	39.39	5.707696113
115	200	84.37	39.39	5.589184618
120	205	84.37	39.38	5.589184618
125	210	84.37	39.38	5.589184618
130	215	84.36	39.39	5.470659075
135	220	84.37	39.39	5.589198668
140	225	84.37	39.38	5.589198668
145	230	84.37	39.38	5.589198668
150	235	84.37	39.37	5.589198668
155	240	84.37	39.38	5.589198668
160	245	84.33	39.38	5.115096499
165	250	84.37	39.38	5.589423547
170	255	84.32	39.38	4.996795836
175	260	84.37	39.38	5.589774963
180	265	84.37	39.38	5.589774963

Table B14: TGA results for the second adsorption run on 20 % MA grafted polysuccinimide.

Adsorption Time (min)	**Experimental Time (min)**	**Weight (%)**	**Temperature (^{0}C)**	**Cumulative Adsorption Capacity (g CO_2/ kg Ads)**
0	85	83.96	38.91	0
5	90	83.98	39.34	0.238208671
10	95	84.11	39.36	1.786196287
15	100	84.14	39.34	2.142872069
20	105	84.18	39.34	2.618270215
25	110	84.2	39.34	2.85585634
30	115	84.19	39.35	2.737091494
35	120	84.22	39.35	3.093428351
40	125	84.26	39.36	3.56837492
45	130	84.26	39.35	3.56837492
50	135	84.28	39.37	3.80573547
55	140	84.32	39.37	4.280343918
60	145	84.33	39.39	4.398939744
65	150	84.34	39.39	4.517521506
70	155	84.37	39.4	4.873224612
75	160	84.35	39.39	4.636173528

80	165	84.36	39.4	4.754727173
85	170	84.35	39.39	4.636187581
90	175	84.37	39.39	4.873294872
95	180	84.37	39.39	4.873294872
100	185	84.37	39.41	4.873294872
105	190	84.37	39.4	4.873294872
110	195	84.38	39.39	4.991820414
115	200	84.39	39.39	5.11033191
120	205	84.37	39.38	4.873337005
125	210	84.37	39.38	4.873337005
130	215	84.36	39.39	4.754811463
135	220	84.37	39.39	4.873351055
140	225	84.38	39.38	4.991876598
145	230	84.39	39.38	5.110388093
150	235	84.38	39.37	4.991890641
155	240	84.39	39.38	5.110402137
160	245	84.37	39.38	4.873407232
165	250	84.37	39.38	4.873407232
170	255	84.36	39.38	4.75488169
175	260	84.38	39.38	4.991960874
180	265	84.38	39.38	4.991960874

Table B15: TGA results for the third adsorption run on 20 % MA grafted polysuccinimide.

Adsorption Time (min)	**Experimental Time (min)**	**Weight (%)**	**Temperature (^{0}C)**	**Cumulative Adsorption Capacity (g CO_2/ kg Ads)**
0	85	82.94	41.94	0
5	90	82.96	39.1	0.241138172
10	95	82.99	39.23	0.60275823
15	100	83.06	39.22	1.446233348
20	105	83.11	39.22	2.048207824
25	110	83.16	39.22	2.649820145
30	115	83.2	39.22	3.130820626
35	120	83.24	39.23	3.611589857
40	125	83.26	39.24	3.851858958
45	130	83.29	39.25	4.212176037
50	135	83.35	39.26	4.932550632
55	140	83.36	39.26	5.052526637

60	145	83.39	39.27	5.412411473
65	150	83.4	39.28	5.532329929
70	155	83.41	39.29	5.652234006
75	160	83.4	39.29	5.532344304
80	165	83.4	39.28	5.532344304
85	170	83.41	39.28	5.652248381
90	175	83.42	39.29	5.772138082
95	180	83.4	39.28	5.532387423
100	185	83.39	39.29	5.412483346
105	190	83.4	39.3	5.532401802
110	195	83.41	39.29	5.652305879
115	200	83.4	39.29	5.532416177
120	205	83.4	39.29	5.532416177
125	210	83.4	39.3	5.532416177
130	215	83.4	39.29	5.532416177
135	220	83.4	39.3	5.532416177
140	225	83.41	39.3	5.652320254
145	230	83.39	39.3	5.412540851
150	235	83.38	39.3	5.292622395
155	240	83.39	39.3	5.412555233
160	245	83.4	39.3	5.532473688
165	250	83.4	39.3	5.532473688
170	255	83.4	39.29	5.532473688
175	260	83.4	39.3	5.532473688
180	265	83.4	39.29	5.532473688

Table B16: TGA results for the first adsorption run on 100 % MEA grafted polysuccinimide.

Adsorption Time (min)	**Experimental Time (min)**	**Weight (%)**	**Temperature (^{0}C)**	**Cumulative Adsorption Capacity (g CO_2/ kg Ads)**
0	125	91.14	39.28	0
5	130	91.6	39.29	5.047180162
10	135	92.4	39.3	13.78080462
15	140	92.95	39.31	19.73318557
20	145	93.65	39.32	27.26411618
25	150	93.97	39.33	30.68109429
30	155	94.25	39.35	33.66076865

35	160	94.37	39.35	34.9339782
40	165	94.49	39.37	36.20556875
45	170	94.61	39.38	37.47554441
50	175	94.67	39.37	38.10972684
55	180	94.75	39.37	38.95476751
60	185	94.83	39.37	39.79909468
65	190	94.88	39.38	40.32635399
70	195	94.89	39.37	40.43175028
75	200	94.95	39.38	41.06406138
80	205	94.97	39.38	41.27469855
85	210	94.97	39.38	41.27469855
90	215	94.95	39.38	41.06410574
95	220	94.98	39.38	41.3800615
100	225	94.99	39.38	41.48534683
105	230	94.98	39.38	41.38007259
110	235	94.97	39.38	41.27478726
115	240	94.96	39.38	41.16949085
120	245	94.9	39.38	40.53764587
125	250	94.89	39.38	40.43227179
130	255	94.98	39.38	41.38073843
135	260	94.99	39.38	41.48602376
140	265	94.98	39.38	41.38074952
145	270	94.98	39.38	41.38074952
150	275	94.98	39.38	41.38074952
155	280	94.97	39.38	41.27546419
160	285	94.98	39.38	41.3807606
165	290	94.99	39.38	41.48604593
170	295	94.98	39.38	41.38077169
175	300	94.98	39.38	41.38077169
180	305	94.98	39.38	41.38077169

Table B17: TGA results for the second adsorption run on 100 % MEA grafted polysuccinimide.

Adsorption Time (min)	**Experimental Time (min)**	**Weight (%)**	**Temperature (^{0}C)**	**Cumulative Adsorption Capacity (g CO_2/ kg Ads)**
0	125	88.98	40.71	0
5	130	88.99	39.87	0.112384806

10	135	89.69	39.43	7.978437171
15	140	89.97	39.22	11.10030137
20	145	90.49	39.21	16.88000572
25	150	90.98	39.2	22.2949687
30	155	91.96	39.21	33.06656685
35	160	91.99	39.2	33.39279564
40	165	92.25	39.2	36.21918982
45	170	92.34	39.19	37.19479957
50	175	92.45	39.19	38.3860493
55	180	92.52	39.19	39.14321534
60	185	92.58	39.19	39.79172377
65	190	92.65	39.19	40.5478266
70	195	92.45	39.2	38.38916497
75	200	92.51	39.19	39.03816443
80	205	92.98	39.18	44.11869626
85	210	92.96	39.19	43.90359624
90	215	92.99	39.19	44.22631569
95	220	93	39.18	44.33385414
100	225	93.2	39.19	46.48439177
105	230	93.12	39.18	45.62602267
110	235	93.15	39.19	45.94818762
115	240	93.05	39.18	44.87465031
120	245	93.1	39.18	45.41199583
125	250	93	39.19	44.33788197
130	255	93.11	39.19	45.52067767
135	260	93	39.19	44.33927932
140	265	93.05	39.19	44.87691373
145	270	93.07	39.19	45.09185194
150	275	93	39.19	44.33972988
155	280	93.09	39.2	45.30747181
160	285	93.13	39.19	45.73716351
165	290	93.18	39.18	46.27404744
170	295	93.17	39.19	46.16672827
175	300	93.16	39.18	46.05939758
180	305	93.18	39.19	46.274082

Table B18: TGA results for the third adsorption run on 100 % MEA grafted polysuccinimide.

Adsorption Time (min)	Experimental Time (min)	Weight (%)	Temperature (^{0}C)	Cumulative Adsorption Capacity (g CO_2/ kg Ads)
0	125	92.25	39.41	0
5	130	92.27	39.23	0.216802168
10	135	92.79	39.23	5.852436719
15	140	92.98	39.22	7.900071162
20	145	93.69	39.22	15.53612193
25	150	94.37	39.21	22.79410037
30	155	94.79	39.23	27.24466728
35	160	95.24	39.22	31.9920035
40	165	95.66	39.2	36.4019153
45	170	95.67	39.23	36.5064522
50	175	95.75	39.23	37.34266
55	180	95.85	39.23	38.38704642
60	185	95.97	39.23	39.63900261
65	190	96.12	39.23	41.20199104
70	195	96.17	39.23	41.72217414
75	200	96.24	39.23	42.45005186
80	205	96.26	39.23	42.65786566
85	210	96.29	39.23	42.96952159
90	215	96.3	39.24	43.07337453
95	220	96.31	39.24	43.17721669
100	225	96.3	39.24	43.07338532
105	230	96.32	39.24	43.28106964
110	235	96.32	39.25	43.28106964
115	240	96.31	39.25	43.17724904
120	245	96.33	39.24	43.38491179
125	250	96.31	39.24	43.17729215
130	255	96.31	39.26	43.17729215
135	260	96.32	39.26	43.28112353
140	265	96.31	39.26	43.17730293
145	270	96.31	39.26	43.17730293
150	275	96.3	39.26	43.07347156
155	280	96.31	39.26	43.17731372
160	285	96.33	39.26	43.38497647
165	290	96.31	39.26	43.17735683
170	295	96.31	39.26	43.17735683

175	300	96.32	39.26	43.28118821
180	305	96.31	39.26	43.17736761

Table B19: TGA results for the first adsorption run on 80 % MEA grafted polysuccinimide.

Adsorption Time (min)	**Experimental Time (min)**	**Weight (%)**	**Temperature (^{0}C)**	**Cumulative Adsorption Capacity (g CO_2/ kg Ads)**
0	125	94.41	39.34	0
5	130	94.44	39.34	15.88814744
10	135	94.44	39.36	15.88814744
15	140	94.45	39.36	21.18251424
20	145	94.45	39.37	21.18251424
25	150	94.46	39.38	26.47632048
30	155	94.46	39.39	26.47632048
35	160	94.46	39.39	26.47632048
40	165	94.46	39.4	26.47632048
45	170	94.46	39.4	26.47632048
50	175	94.46	39.4	26.47632048
55	180	94.46	39.4	26.47632048
60	185	94.46	39.4	26.47632048
65	190	94.45	39.41	21.18307466
70	195	94.45	39.42	21.18307466
75	200	94.44	39.42	15.88926842
80	205	94.44	39.42	15.88926842
85	210	94.44	39.42	15.88926842
90	215	94.44	39.42	15.88926842
95	220	94.44	39.43	15.88926842
100	225	94.44	39.43	15.88926842
105	230	94.44	39.44	15.88926842
110	235	94.44	39.44	15.88926842
115	240	94.44	39.44	15.88926842
120	245	94.44	39.44	15.88926842
125	250	94.45	39.44	21.18363521
130	255	94.46	39.44	26.47744146
135	260	94.46	39.43	26.47744146
140	265	94.47	39.43	31.77068728
145	270	94.47	39.42	31.77068728

150	275	94.47	39.42	31.77068728
155	280	94.48	39.41	37.06337278
160	285	94.48	39.41	37.06337278
165	290	94.48	39.40	37.06337278
170	295	94.48	39.40	37.06337278
175	300	94.48	39.39	37.06337278
180	305	94.48	39.39	37.06337278

Table B20: TGA results for the second adsorption run on 80 % MEA grafted polysuccinimide.

Adsorption Time (min)	**Experimental Time (min)**	**Weight (%)**	**Temperature (^{0}C)**	**Cumulative Adsorption Capacity (g CO_2/ kg Ads)**
0	125	89.18	39.38	0
5	130	89.19	39.38	0.560663826
10	135	89.25	39.39	3.924269611
15	140	89.25	39.38	3.924269611
20	145	89.41	39.39	12.88785505
25	150	89.43	39.39	14.00629817
30	155	89.52	39.4	19.03816667
35	160	89.56	39.4	21.2723043
40	165	89.63	39.4	25.18029894
45	170	89.65	39.4	26.29599681
50	175	89.69	39.41	28.52689474
55	180	89.77	39.42	32.98670074
60	185	89.75	39.42	31.87274285
65	190	89.76	39.42	32.42984591
70	195	89.79	39.43	34.10096891
75	200	89.78	39.43	33.54411402
80	205	89.77	39.44	32.98719712
85	210	89.79	39.44	34.10115501
90	215	89.78	39.44	33.54430012
95	220	89.78	39.45	33.54430012
100	225	89.78	39.44	33.54430012
105	230	89.75	39.45	31.8735494
110	235	89.78	39.46	33.54485859
115	240	89.76	39.45	32.43102478
120	245	89.78	39.46	33.54510677
125	250	89.77	39.46	32.98818986

130	255	89.78	39.45	33.54516881
135	260	89.78	39.46	33.54516881
140	265	89.78	39.46	33.54516881
145	270	89.74	39.47	31.31750118
150	275	89.79	39.46	34.1033269
155	280	89.78	39.45	33.54647201
160	285	89.78	39.44	33.54647201
165	290	89.79	39.45	34.10338892
170	295	89.77	39.46	32.98967915
175	300	89.78	39.46	33.5466581
180	305	89.78	39.46	33.5466581

Table B21: TGA results for the third adsorption run on 80 % MEA grafted polysuccinimide.

Adsorption Time (min)	**Experimental Time (min)**	**Weight (%)**	**Temperature (^{0}C)**	**Cumulative Adsorption Capacity (g CO_2/ kg Ads)**
0	125	89.59	41.12	0
5	130	89.62	40.56	1.122334456
10	135	89.65	39.88	2.805458334
15	140	89.66	39.51	3.927163325
20	145	89.69	39.22	5.609343431
25	150	89.72	39.19	6.169881547
30	155	89.74	39.18	15.69796136
35	160	89.75	39.19	20.73264473
40	165	89.77	39.17	25.20341706
45	170	89.78	39.17	27.43680623
50	175	89.79	39.17	29.11110023
55	180	89.77	39.18	30.78483377
60	185	89.78	39.17	31.34255826
65	190	89.76	39.17	33.0155451
70	195	89.76	39.17	34.68797235
75	200	89.76	39.18	35.80255104
80	205	89.75	39.17	36.35971618
85	210	89.74	39.16	37.47392231
90	215	89.75	39.17	38.03090125
95	220	89.76	39.17	38.58781816
100	225	89.76	39.18	37.4741084

105	230	89.77	39.17	38.03108734
110	235	89.76	39.17	36.91725353
115	240	89.76	39.17	36.91725353
120	245	89.76	39.17	36.91725353
125	250	89.76	39.19	36.36021253
130	255	89.76	39.18	35.80310946
135	260	89.76	39.18	36.36027461
140	265	89.76	39.18	36.91737767
145	270	89.76	39.17	36.91737767
150	275	89.76	39.18	37.47441867
155	280	89.77	39.18	36.91743972
160	285	89.78	39.19	36.91743972
165	290	89.77	39.2	36.91743972
170	295	89.76	39.19	36.91743972
175	300	89.76	39.18	36.91743972
180	305	89.76	39.18	36.91743972

Table B22: TGA results for the first adsorption run on 60 % MEA grafted polysuccinimide.

Adsorption Time (min)	**Experimental Time (min)**	**Weight (%)**	**Temperature (^{0}C)**	**Cumulative Adsorption Capacity (g CO_2/ kg Ads)**
0	125	91.9	39.4	0
5	130	91.95	39.41	0.544069641
10	135	91.95	39.42	0.544069641
15	140	91.97	39.43	0.761579157
20	145	91.98	39.45	0.870310265
25	150	92.01	39.47	1.196468125
30	155	92.15	39.48	2.718041867
35	160	92.19	39.49	3.152116745
40	165	92.25	39.49	3.802946553
45	170	93	39.48	11.93302785
50	175	93.2	39.48	14.08356549
55	180	93.24	39.48	14.51275004
60	185	93.27	39.49	14.83450036
65	190	93.3	39.48	15.15614719
70	195	93.31	39.49	15.26332833
75	200	93.31	39.48	15.26332833

80	205	93.29	39.49	15.04898903
85	210	93.27	39.48	14.83460378
90	215	93.33	39.48	15.47789744
95	220	93.37	39.48	15.90648418
100	225	93.36	39.49	15.7993834
105	230	93.35	39.48	15.69227114
110	235	93.35	39.48	15.69227114
115	240	93.36	39.49	15.79939487
120	245	93.37	39.48	15.90650712
125	250	93.36	39.49	15.79940634
130	255	93.37	39.49	15.90651859
135	260	93.35	39.49	15.69231703
140	265	93.36	39.49	15.79944076
145	270	93.37	39.49	15.90655301
150	275	93.37	39.49	15.90655301
155	280	93.37	39.49	15.90655301
160	285	93.37	39.49	15.90655301
165	290	93.37	39.49	15.90655301
170	295	93.37	39.49	15.90655301
175	300	93.37	39.49	15.90655301
180	305	93.37	39.49	15.90655301

Table B23: TGA results for the second adsorption run on 60 % MEA grafted polysuccinimide.

Adsorption Time (min)	**Experimental Time (min)**	**Weight (%)**	**Temperature (^{0}C)**	**Cumulative Adsorption Capacity (g CO_2/ kg Ads)**
0	125	90.84	39.44	0
5	130	90.82	39.45	0.220167327
10	135	90.89	39.44	0.550588013
15	140	90.92	39.44	0.880657328
20	145	90.98	39.44	1.540578137
25	150	91.07	39.44	2.529806539
30	155	91.13	39.44	3.188640403
35	160	91.21	39.44	4.066507187
40	165	91.27	39.45	4.724329794
45	170	91.35	39.44	5.600850009
50	175	92.13	39.45	14.13943786

55	180	92.2	39.45	14.8992338
60	185	92.26	39.45	15.54999302
65	190	92.35	39.46	16.52549703
70	195	92.34	39.46	16.41721332
75	200	92.38	39.46	16.85039504
80	205	92.36	39.46	16.63389797
85	210	92.34	39.46	16.41735401
90	215	92.37	39.47	16.7422403
95	220	92.37	39.46	16.7422403
100	225	92.36	39.46	16.63398004
105	230	92.35	39.47	16.52570806
110	235	92.37	39.48	16.74227547
115	240	92.36	39.46	16.63401521
120	245	92.34	39.47	16.41747125
125	250	92.37	39.46	16.74235754
130	255	92.37	39.45	16.74235754
135	260	92.36	39.46	16.63409728
140	265	92.37	39.47	16.74236926
145	270	92.36	39.48	16.63410901
150	275	92.36	39.49	16.63410901
155	280	92.36	39.48	16.63410901
160	285	92.36	39.47	16.63410901
165	290	92.36	39.46	16.63410901
170	295	92.36	39.47	16.63410901
175	300	92.36	39.46	16.63410901
180	305	92.36	39.47	16.63410901

Table B24: TGA results for the third adsorption run on 60 % MEA grafted polysuccinimide.

Adsorption Time (min)	**Experimental Time (min)**	**Weight (%)**	**Temperature (^{0}C)**	**Cumulative Adsorption Capacity (g CO_2/ kg Ads)**
0	125	91.77	39.38	0
5	130	92.12	39.38	1.979109401
10	135	92.19	39.39	3.62510962
15	140	92.24	39.39	4.391980786
20	145	92.33	39.39	5.705609686
25	150	92.29	39.39	6.470887919
30	155	92.34	39.39	7.344822811

35	160	92.37	39.4	6.471651014
40	165	92.43	39.4	8.110278937
45	170	92.47	39.4	8.982784117
50	175	92.49	39.4	12.79666665
55	180	92.48	39.41	13.55654507
60	185	92.46	39.41	14.09890324
65	190	92.47	39.41	15.07461877
70	195	92.49	39.41	14.64139013
75	200	92.43	39.41	15.18316064
80	205	92.48	39.41	15.50804693
85	210	92.49	39.41	16.15760847
90	215	92.49	39.42	16.5903684
95	220	92.48	39.41	16.80665476
100	225	92.49	39.42	16.69853497
105	230	92.47	39.43	16.48227199
110	235	92.49	39.42	16.59042687
115	240	92.47	39.42	16.80671323
120	245	92.49	39.43	16.15799445
125	250	92.49	39.43	16.69894436
130	255	92.49	39.42	16.80707585
135	260	92.49	39.43	16.80707585
140	265	92.49	39.42	16.69895605
145	270	92.49	39.43	16.80708754
150	275	92.49	39.43	16.59084794
155	280	92.49	39.44	16.80713431
160	285	92.49	39.45	16.59089471
165	290	92.49	39.46	16.80718108
170	295	92.49	39.44	16.80718108
175	300	92.49	39.43	16.80718108
180	305	92.49	39.43	16.80718108

Table B25: TGA results for the first adsorption run on 40 % MEA grafted polysuccinimide.

Adsorption Time (min)	**Experimental Time (min)**	**Weight (%)**	**Temperature (^{0}C)**	**Cumulative Adsorption Capacity (g CO_2/ kg Ads)**
0	100	98.98	39.64	0
5	105	99.07	39.46	0.909274601

10	110	99.08	39.45	1.010213331
15	115	99.09	39.44	1.111141874
20	120	99.1	39.44	1.212060231
25	125	99.13	39.45	1.514784751
30	130	99.14	39.44	1.615662387
35	135	99.18	39.44	2.019132228
40	140	99.19	39.44	2.119959007
45	145	99.21	39.44	2.321592236
50	150	99.25	39.44	2.724777399
55	155	99.26	39.44	2.825533067
60	160	99.3	39.45	3.228515134
65	165	99.33	39.44	3.530629937
70	170	99.35	39.45	3.731978976
75	175	99.39	39.45	4.134595987
80	180	99.41	39.45	4.335823474
85	185	99.42	39.46	4.436416976
90	190	99.46	39.46	4.83875051
95	195	99.48	39.46	5.039836374
100	200	99.51	39.46	5.341404528
105	205	99.6	39.46	6.245836244
110	210	99.61	39.47	6.34623785
115	215	99.64	39.46	6.647412431
120	220	99.65	39.46	6.747773732
125	225	99.67	39.47	6.94847619
130	230	99.68	39.48	7.048807283
135	235	99.74	39.46	7.650733447
140	240	99.74	39.47	7.650733447
145	245	99.73	39.47	7.550472769
150	250	99.8	39.47	8.252367886
155	255	99.89	39.47	9.154171493
160	260	99.9	39.48	9.254281614
165	265	99.9	39.49	9.254281614
170	270	99.9	39.47	9.254281614
175	275	99.9	39.47	9.254281614
180	280	99.9	39.47	9.254281614

Table B26: TGA results for the second adsorption run on 40 % MEA grafted polysuccinimide.

Adsorption Time (min)	Experimental Time (min)	Weight (%)	Temperature (^{0}C)	Cumulative Adsorption Capacity (g CO_2/ kg Ads)
0	100	98.07	39.27	0
5	105	98.12	39.27	0.50983991
10	110	98.17	39.27	1.019420016
15	115	98.25	39.29	1.834332922
20	120	98.23	39.29	1.630770581
25	125	98.17	39.29	1.01995922
30	130	98.27	39.3	2.038600353
35	135	98.35	39.31	2.852684
40	140	98.4	39.32	3.361072409
45	145	98.43	39.33	3.665950458
50	150	98.47	39.34	4.072330626
55	155	98.45	39.34	3.869223081
60	160	98.3	39.33	2.345607032
65	165	98.52	39.34	4.583653828
70	170	98.55	39.33	4.888160527
75	175	98.59	39.33	5.294045864
80	180	98.63	39.34	5.699766526
85	185	98.72	39.35	6.612267793
90	190	98.77	39.34	7.118750775
95	195	98.76	39.34	7.017505458
100	200	98.81	39.34	7.523783303
105	205	98.86	39.34	8.029804961
110	210	98.88	39.33	8.232111252
115	215	98.9	39.34	8.434376625
120	220	98.94	39.33	8.838825563
125	225	98.99	39.34	9.344182345
130	230	99.1	39.33	10.4554057
135	235	99.07	39.35	10.15268118
140	240	99.07	39.33	10.15268118
145	245	99.09	39.33	10.35455864
150	250	99.08	39.33	10.25364028
155	255	99.07	39.34	10.15271174
160	260	99.06	39.35	10.05177301
165	265	99.07	39.33	10.15272193
170	270	99.09	39.33	10.35459939
175	275	99.07	39.34	10.15276268

180	280	99.07	39.33	10.15276268

Table B27: TGA results for the third adsorption run on 40 % MEA grafted polysuccinimide.

Adsorption Time (min)	**Experimental Time (min)**	**Weight (%)**	**Temperature (^{0}C)**	**Cumulative Adsorption Capacity (g CO_2/ kg Ads)**
0	100	98.78	39.26	0
5	105	98.82	39.27	0.404940271
10	110	98.89	39.27	1.113298903
15	115	98.95	39.28	1.720033659
20	120	98.99	39.29	2.124278227
25	125	99.03	39.29	2.528359447
30	130	99.1	39.3	3.235215955
35	135	99.14	39.31	3.63884865
40	140	99.17	39.33	3.94145103
45	145	99.19	39.34	4.143124923
50	150	99.23	39.35	4.546391382
55	155	99.26	39.35	4.848719307
60	160	99.29	39.35	5.150955857
65	165	99.29	39.36	5.150955857
70	170	99.29	39.37	5.150955857
75	175	99.35	39.36	5.755246319
80	180	99.37	39.36	5.956554825
85	185	99.38	39.37	6.057188819
90	190	99.41	39.37	6.359060423
95	195	99.44	39.37	6.660840928
100	200	99.47	39.38	6.962530389
105	205	99.52	39.37	7.465194509
110	210	99.54	39.37	7.666159139
115	215	99.58	39.37	8.068007642
120	220	99.59	39.38	8.168429413
125	225	99.62	39.38	8.469664477
130	230	99.66	39.37	8.871190275
135	235	99.69	39.38	9.172213755
140	240	99.71	39.38	9.372835683
145	245	99.72	39.38	9.473126527
150	250	99.73	39.37	9.573407313
155	255	99.74	39.38	9.673678044

160	260	99.72	39.39	9.473156688
165	265	99.71	39.4	9.372875902
170	270	99.72	39.38	9.473166745
175	275	99.71	39.38	9.372885959
180	280	99.71	39.38	9.372885959

Table B28: TGA results for the first adsorption run on 20 % MEA grafted polysuccinimide.

Adsorption Time (min)	**Experimental Time (min)**	**Weight (%)**	**Temperature (^{0}C)**	**Cumulative Adsorption Capacity (g CO_2/ kg Ads)**
0	125	92.08	39.36	0
5	130	92.14	39.38	0.651607298
10	135	92.18	39.38	1.085729286
15	140	92.2	39.4	1.30269609
20	145	92.21	39.41	1.41115596
25	150	92.26	39.43	1.953396498
30	155	92.35	39.43	2.928900509
35	160	92.4	39.45	3.470319025
40	165	92.41	39.45	3.578544133
45	170	92.49	39.44	4.444251308
50	175	92.52	39.44	4.768610698
55	180	92.56	39.44	5.200949652
60	185	92.61	39.44	5.741139799
65	190	92.66	39.44	6.281038298
70	195	92.71	39.46	6.820645464
75	200	92.73	39.45	7.036371923
80	205	92.74	39.44	7.144211888
85	210	92.77	39.44	7.4676969
90	215	92.77	39.44	7.4676969
95	220	92.77	39.44	7.4676969
100	225	92.77	39.43	7.4676969
105	230	92.77	39.44	7.4676969
110	235	92.77	39.44	7.4676969
115	240	92.77	39.44	7.4676969
120	245	92.75	39.45	7.252109965
125	250	92.77	39.44	7.467743388
130	255	92.77	39.44	7.467743388
135	260	92.77	39.44	7.467743388
140	265	92.77	39.44	7.467743388

145	270	92.76	39.44	7.35994992
150	275	92.77	39.44	7.467755008
155	280	92.77	39.44	7.467755008
160	285	92.77	39.44	7.467755008
165	290	92.77	39.44	7.467755008
170	295	92.76	39.44	7.359961541
175	300	92.76	39.44	7.359961541
180	305	92.77	39.44	7.467766629

Table B29: TGA results for the second adsorption run on 20 % MEA grafted polysuccinimide.

Adsorption Time (min)	**Experimental Time (min)**	**Weight (%)**	**Temperature (^{0}C)**	**Cumulative Adsorption Capacity (g CO_2/ kg Ads)**
0	125	92.17	39.46	0
5	130	92.34	39.43	1.844417923
10	135	92.35	39.43	1.952713353
15	140	92.37	39.43	2.16928076
20	145	92.4	39.44	2.494061533
25	150	92.38	39.43	2.277611316
30	155	92.42	39.43	2.710605471
35	160	92.39	39.44	2.386000407
40	165	92.44	39.45	2.927184518
45	170	92.47	39.43	3.251719351
50	175	92.5	39.43	3.576148896
55	180	92.54	39.43	4.008581329
60	185	92.61	39.43	4.765010981
65	190	92.69	39.43	5.628848579
70	195	92.74	39.43	6.168281096
75	200	92.75	39.43	6.276109433
80	205	92.79	39.45	6.70737628
85	210	92.78	39.43	6.599606046
90	215	92.84	39.46	7.246297143
95	220	92.82	39.43	7.030872757
100	225	92.81	39.44	6.923137355
105	230	92.85	39.43	7.354125395
110	235	92.84	39.44	7.246424803
115	240	92.83	39.43	7.13871261
120	245	92.84	39.45	7.246436406
125	250	92.81	39.46	6.923299827

130	255	92.81	39.43	6.923299827
135	260	92.85	39.43	7.354287867
140	265	92.81	39.43	6.923485498
145	270	92.83	39.43	7.138979518
150	275	92.84	39.43	7.246703314
155	280	92.83	39.43	7.138991121
160	285	92.84	39.43	7.246714917
165	290	92.84	39.43	7.246714917
170	295	92.84	39.43	7.246714917
175	300	92.83	39.43	7.139002724
180	305	92.84	39.43	7.24672652

Table B30: TGA results for the first adsorption run on 20 % MEA grafted polysuccinimide.

Adsorption Time (min)	**Experimental Time (min)**	**Weight (%)**	**Temperature (^{0}C)**	**Cumulative Adsorption Capacity (g CO_2/ kg Ads)**
0	125	92.15	39.36	0
5	130	92.26	39.38	1.193705914
10	135	92.26	39.38	1.193705914
15	140	92.37	39.4	2.385988594
20	145	92.42	39.41	2.927289882
25	150	92.43	39.44	3.03549157
30	155	92.42	39.43	2.927301588
35	160	92.4	39.45	2.710898212
40	165	92.41	39.47	2.819123321
45	170	92.44	39.48	3.143763511
50	175	92.5	39.46	3.792833178
55	180	92.52	39.44	4.009049394
60	185	92.68	39.44	5.738405209
65	190	92.72	39.44	6.169997786
70	195	92.71	39.46	6.062146189
75	200	92.79	39.45	6.925052025
80	205	92.85	39.44	7.571673428
85	210	92.78	39.44	6.817769282
90	215	92.89	39.44	8.003369626
95	220	92.77	39.44	6.711519051
100	225	92.88	39.43	7.897247195
105	230	92.85	39.44	7.574249779

110	235	92.86	39.44	7.681950372
115	240	92.77	39.44	6.712749424
120	245	92.87	39.45	7.790684101
125	250	92.88	39.44	7.8983615
130	255	92.86	39.44	7.683029889
135	260	92.87	39.44	7.790718883
140	265	92.87	39.44	7.790718883
145	270	92.89	39.44	8.00607368
150	275	92.88	39.44	7.898419466
155	280	92.88	39.45	7.898419466
160	285	92.87	39.44	7.79075366
165	290	92.88	39.43	7.898431059
170	295	92.88	39.42	7.898431059
175	300	92.88	39.44	7.898431059
180	305	92.88	39.41	7.898431059

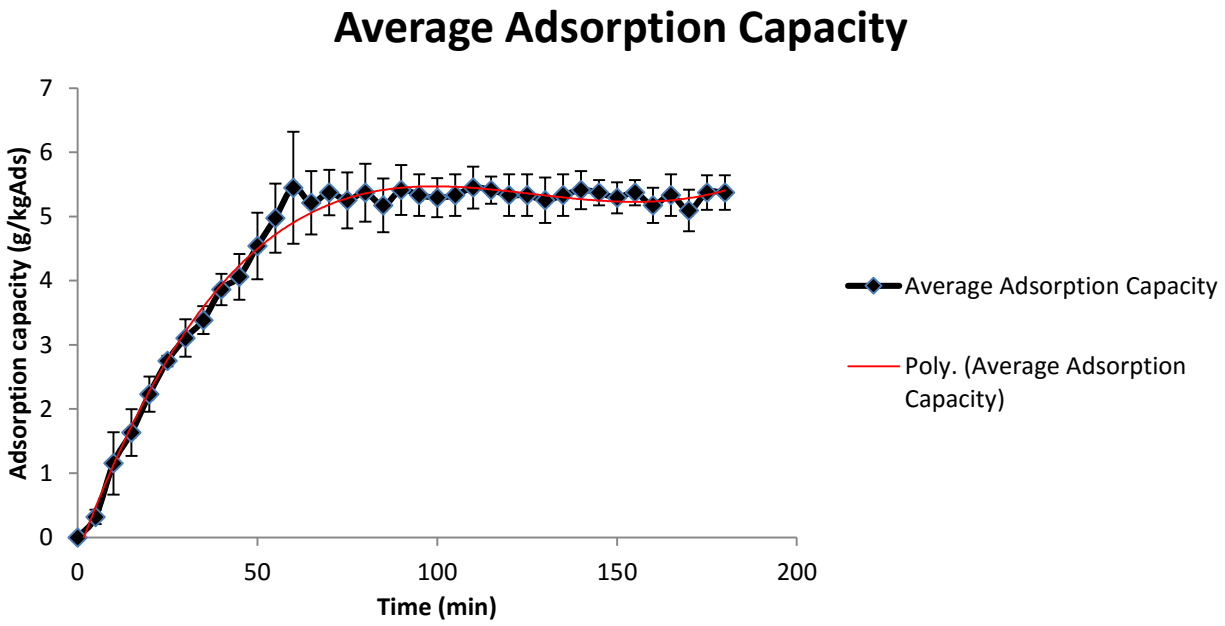


Figure B4: Average adsorption capacity of 20 % MA- 80 % EDA in 100 % CO_2 using the Q600 TA TGA.

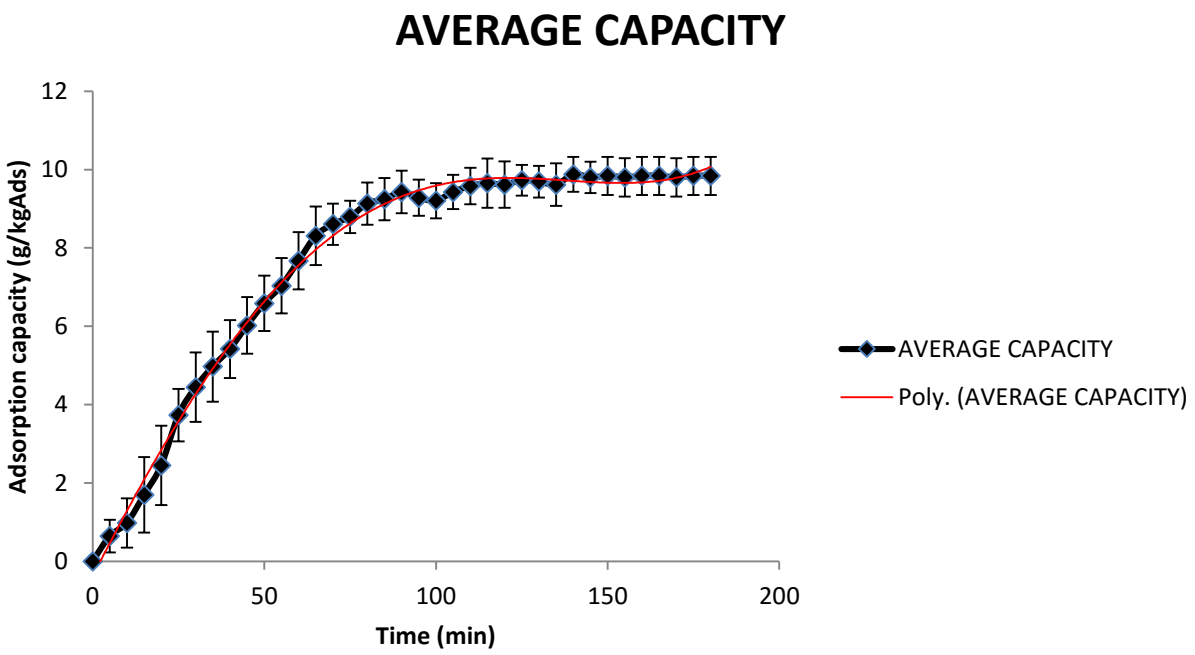


Figure B5: Average adsorption capacity of 40 % MA- 60 % EDA in 100 % CO_2 using the Q600 TA TGA.

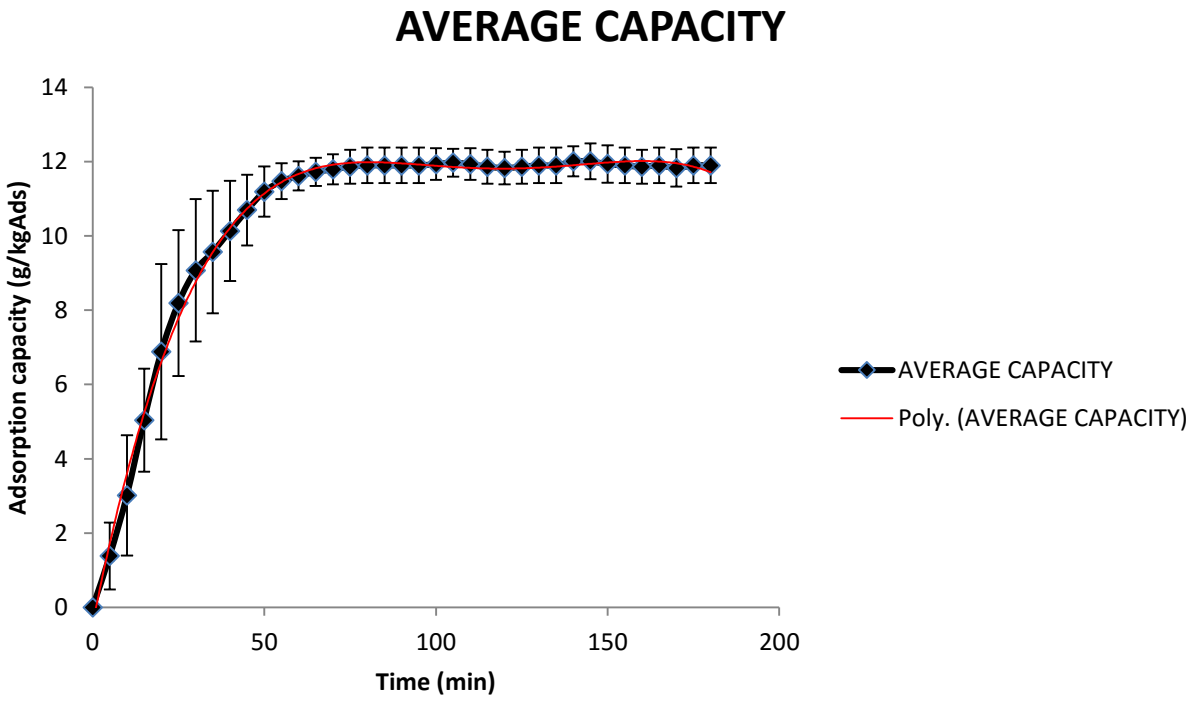


Figure B6: Average adsorption capacity of 60 % MA- 40 % EDA in 100 % CO_2 using the Q600 TA TGA.

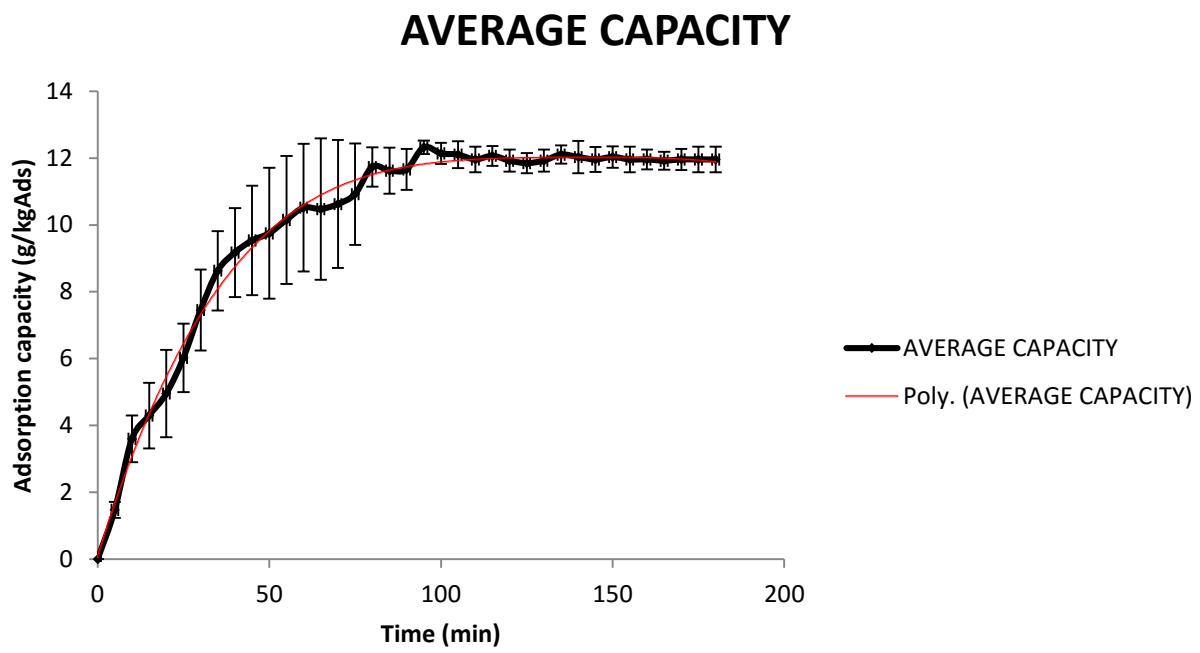


Figure B7: Average adsorption capacity of 80 % MA- 20 % EDA in 100 % CO_2 using the Q600 TA TGA.

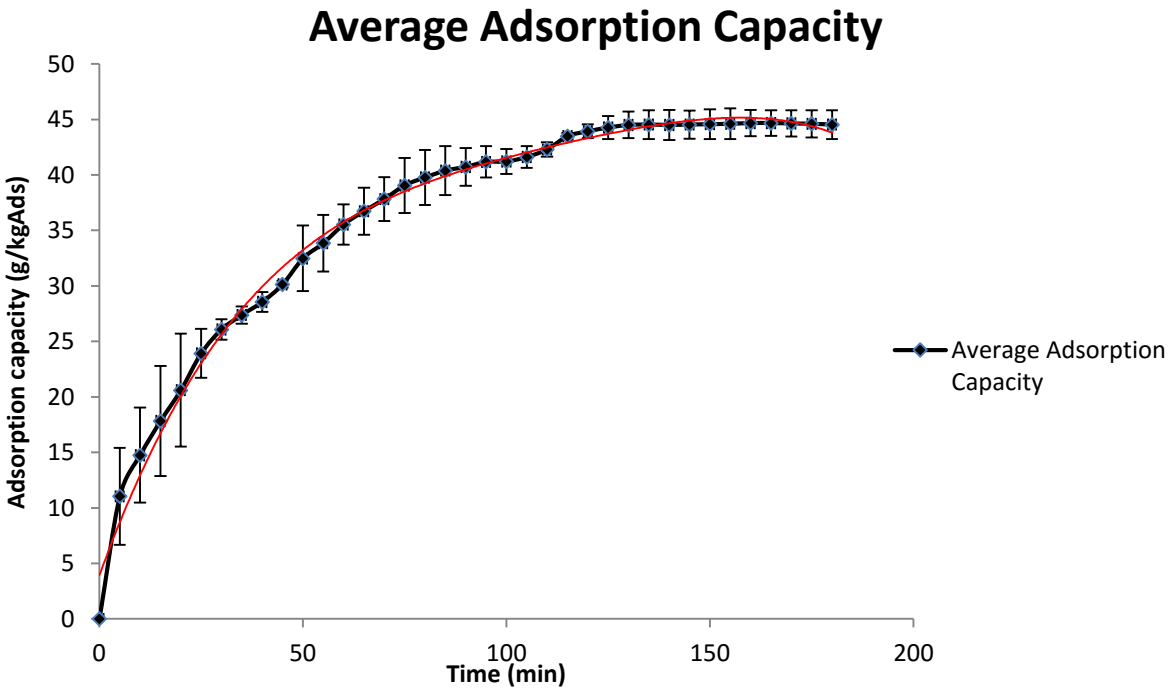


Figure B8: Average adsorption capacity of 100 % MA in 100 % CO_2 using the Q600 TA TGA.

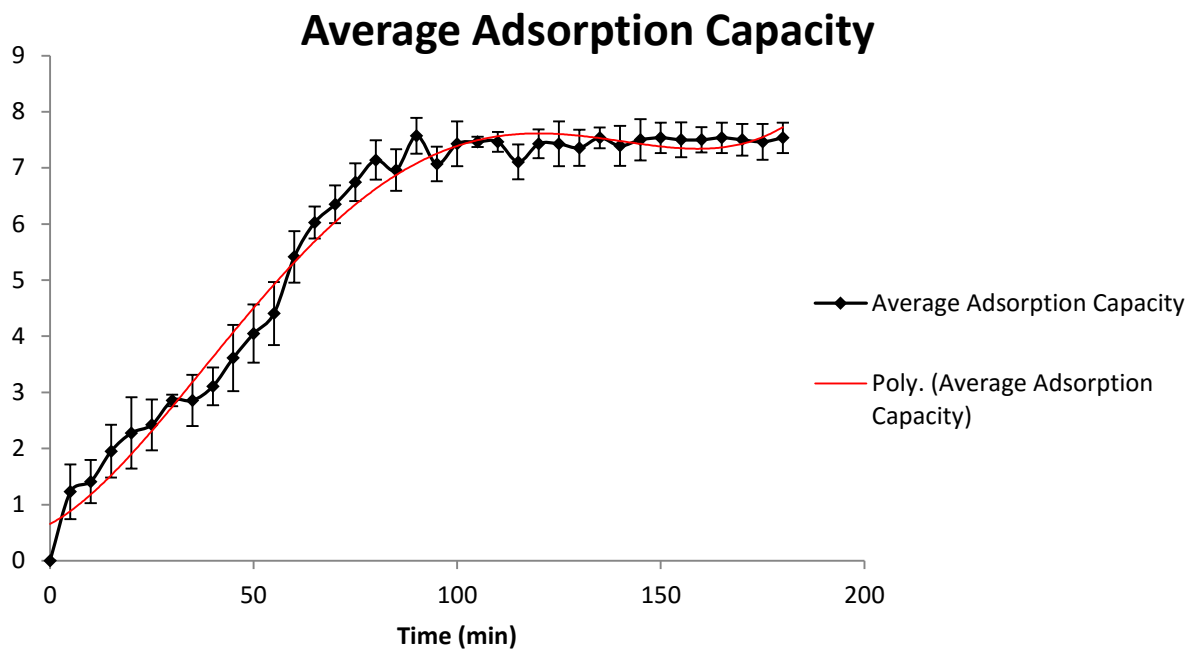


Figure B9: Average adsorption capacity of 20 % MEA- 80 % EDA in 100 % CO_2 using the Q600 TA TGA.

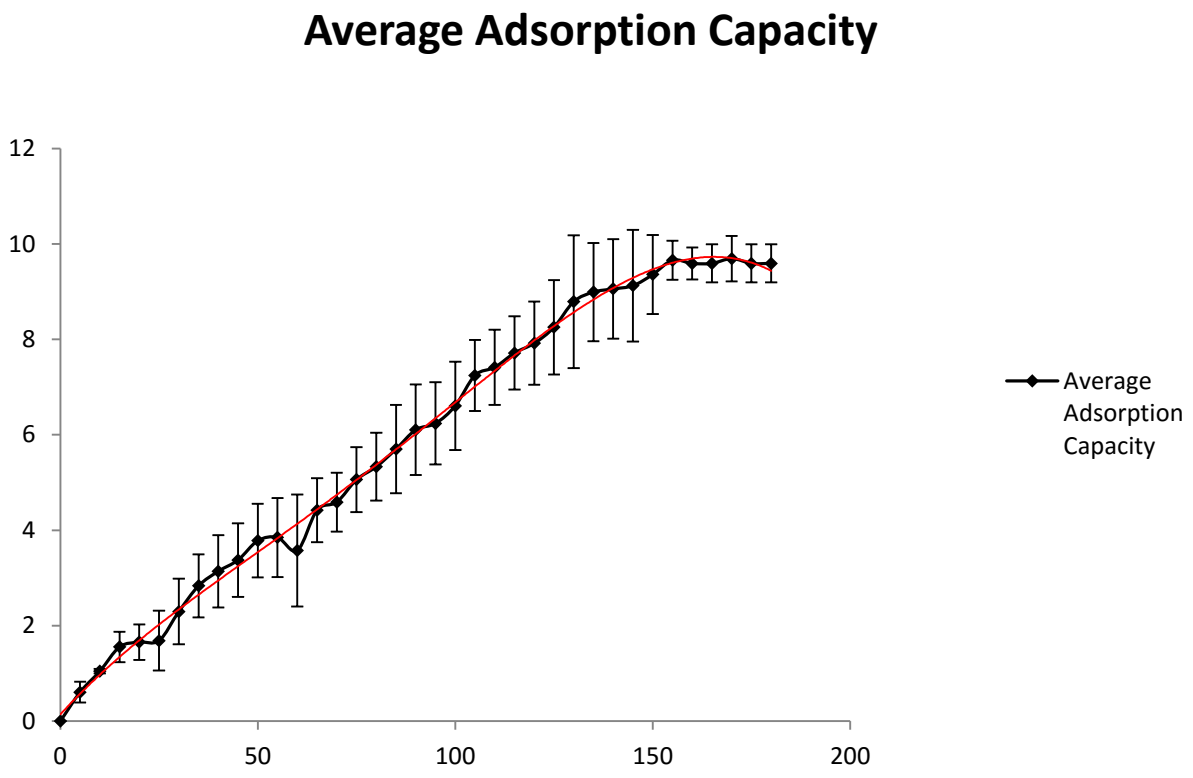


Figure B10: Average adsorption capacity of 40 % MEA- 60 % EDA in 100 % CO_2 using the Q600 TA TGA.

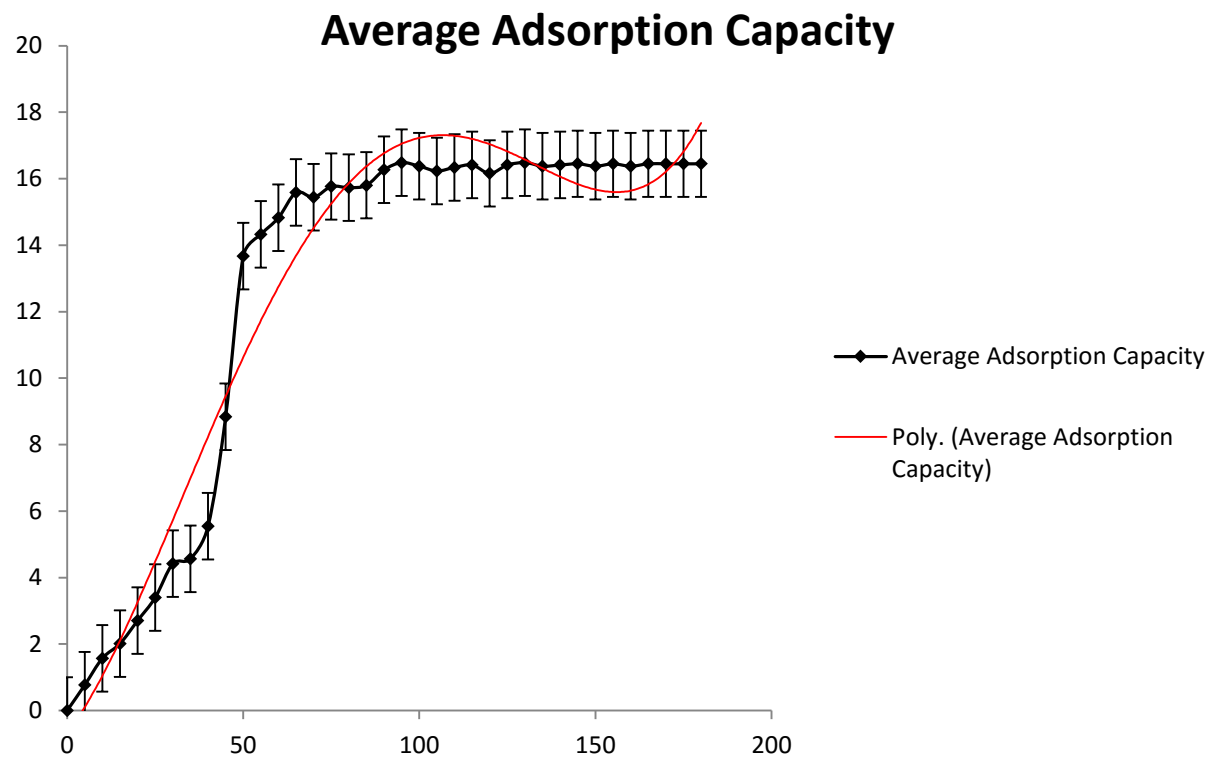


Figure B11: Average adsorption capacity of 60 % MA- 40 % EDA in 100 % CO_2 using the Q600 TA TGA.

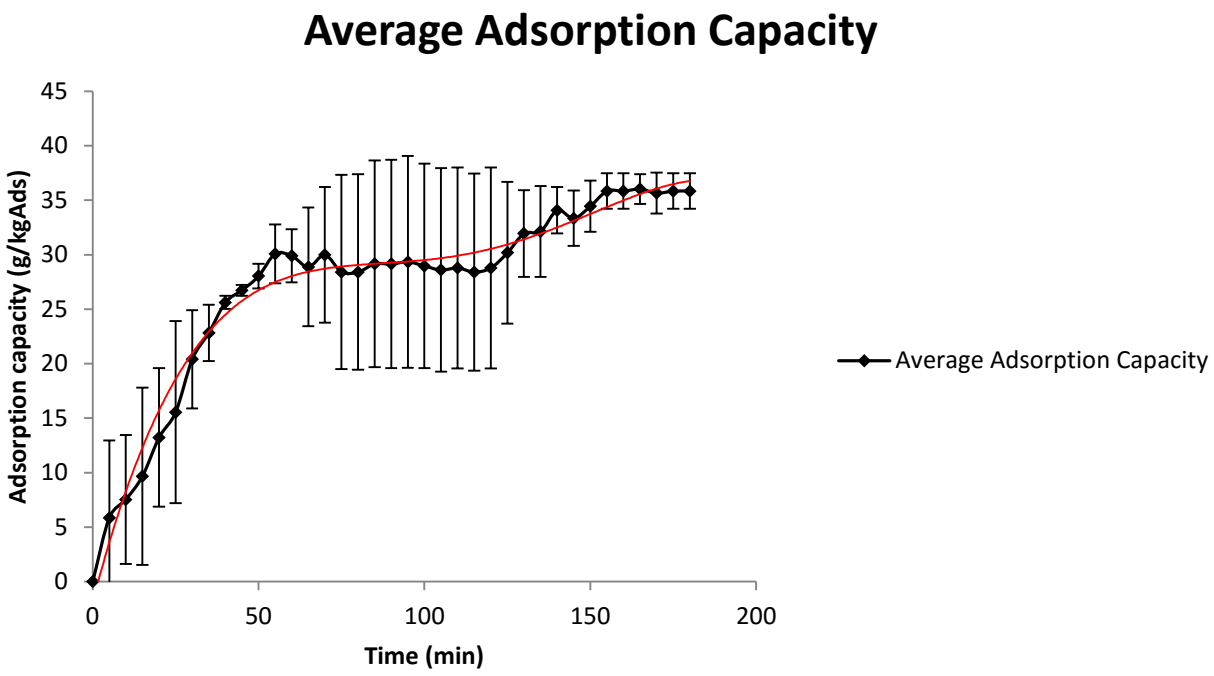


Figure B12: Average adsorption capacity of 80 % MEA- 20 % EDA in 100 % CO_2 using the Q600 TA TGA.

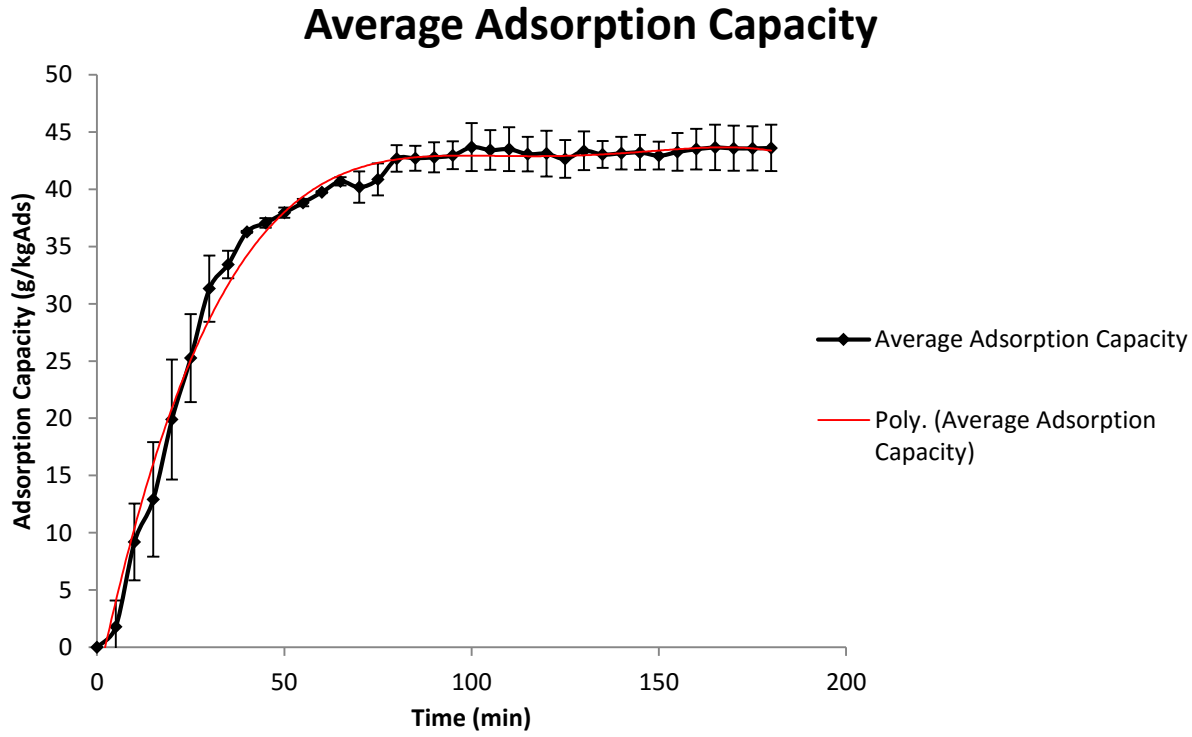
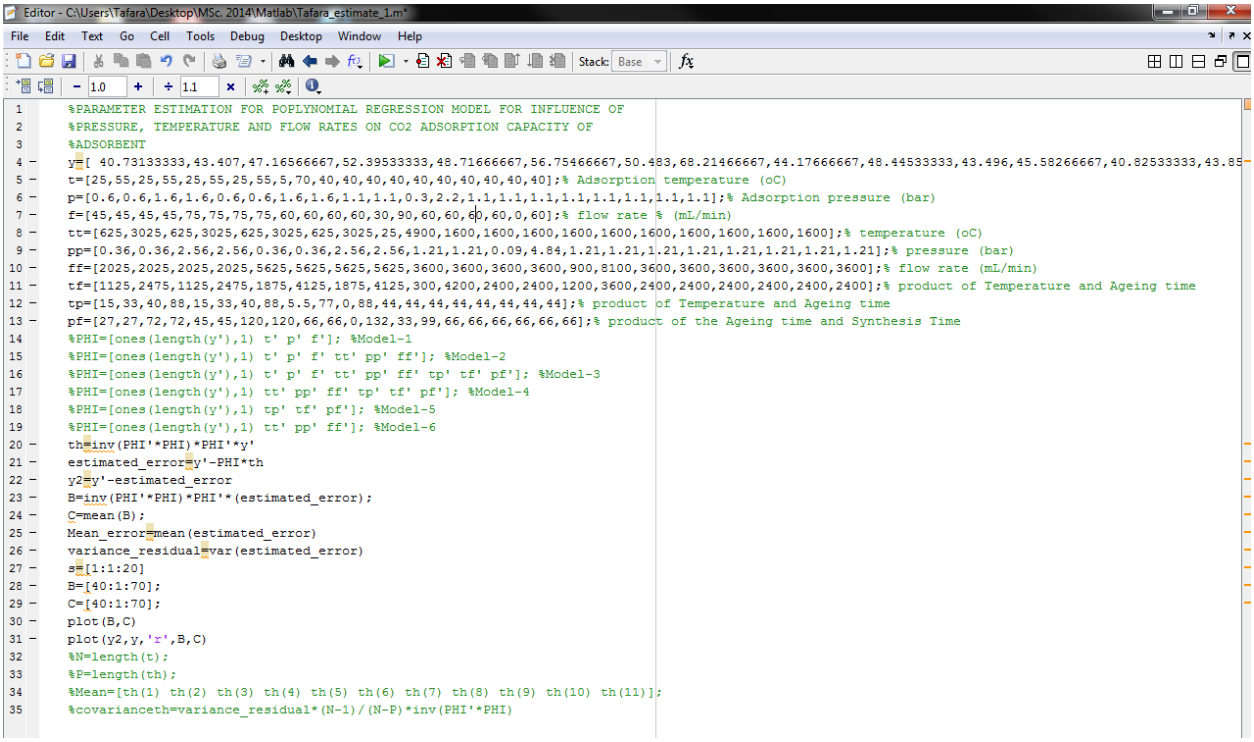


Figure B13: Average adsorption capacity of 100 % MEA- 0 % EDA in 100 % CO_2 using the Q600 TA TGA.

Appendix C: Matlab code used in optimization studies

The following Matlab code was used in determining the parameters of the candidate model equations for the performance evaluation of the synthesized adsorbent.



```
%PARAMETER ESTIMATION FOR POPLYNOMIAL REGRESSION MODEL FOR INFLUENCE OF
%PRESSURE, TEMPERATURE AND FLOW RATES ON CO2 ADSORPTION CAPACITY OF
%ADSORBENT
y=[ 40.73133333,43.407,47.16566667,52.39533333,48.71666667,56.75466667,50.483,68.21466667,44.17666667,48.44533333,43.496,45.58266667,40.82533333,43.85
t=[25,55,25,55,25,55,25,55,5,70,40,40,40,40,40,40,40,40,40,40];% Adsorption temperature (oC)
p=[0.6,0.6,1.6,1.6,0.6,0.6,1.6,1.6,1.1,1.1,0.3,2.2,1.1,1.1,1.1,1.1,1.1,1.1,1.1,1.1];% Adsorption pressure (bar)
f=[45,45,45,45,75,75,75,75,60,60,60,60,30,90,60,60,60,0,60];% flow rate % (mL/min)
tt=[625,3025,625,3025,625,3025,625,3025,25,4900,1600,1600,1600,1600,1600,1600,1600,1600,1600,1600];% temperature (oC)
pp=[0.36,0.36,2.56,2.56,0.36,0.36,2.56,2.56,1.21,1.21,0.09,4.84,1.21,1.21,1.21,1.21,1.21,1.21,1.21,1.21];% pressure (bar)
ff=[2025,2025,2025,2025,5625,5625,5625,5625,3600,3600,3600,3600,900,8100,3600,3600,3600,3600,3600,3600];% flow rate (mL/min)
tf=[1125,2475,1125,2475,1875,4125,1875,4125,300,4200,2400,2400,1200,3600,2400,2400,2400,2400,2400,2400];% product of Temperature and Ageing time
tp=[15,33,40,88,15,33,40,88,5.5,77,0,88,44,44,44,44,44,44,44,44];% product of Temperature and Ageing time
pf=[27,27,72,72,45,45,120,120,66,66,0,132,33,99,66,66,66,66,66,66];% product of the Ageing time and Synthesis Time
%PHI=[ones(length(y'),1) t' p' f']; %Model-1
%PHI=[ones(length(y'),1) t' p' f' tt' pp' ff']; %Model-2
%PHI=[ones(length(y'),1) t' p' f' tt' pp' ff' tp' tf' pf']; %Model-3
%PHI=[ones(length(y'),1) tt' pp' ff' tp' tf' pf']; %Model-4
%PHI=[ones(length(y'),1) tp' tf' pf']; %Model-5
%PHI=[ones(length(y'),1) tt' pp' ff']; %Model-6
th=inv(PHI'*PHI)*PHI'*y'
estimated_error=y'-PHI*th
y2=y'-estimated_error
B=inv(PHI'*PHI)*PHI'*(estimated_error);
C=mean(B);
Mean_error=mean(estimated_error)
variance_residual=var(estimated_error)
s=[1:1:20]
B=[40:1:70];
C=[40:1:70];
plot(B,C)
plot(y2,y,'r',B,C)
%N=length(t);
%P=length(th);
%Mean=[th(1) th(2) th(3) th(4) th(5) th(6) th(7) th(8) th(9) th(10) th(11)];
%covarianceth=variance_residual*(N-1)/(N-P)*inv(PHI'*PHI)
```

Appendix D: Experimental equipment

Figure D1 is a picture showing the CO_2 adsorption equipment as well as the ABB gas analyzer used to evaluate the performance of amine-grafted PSI (PAA).

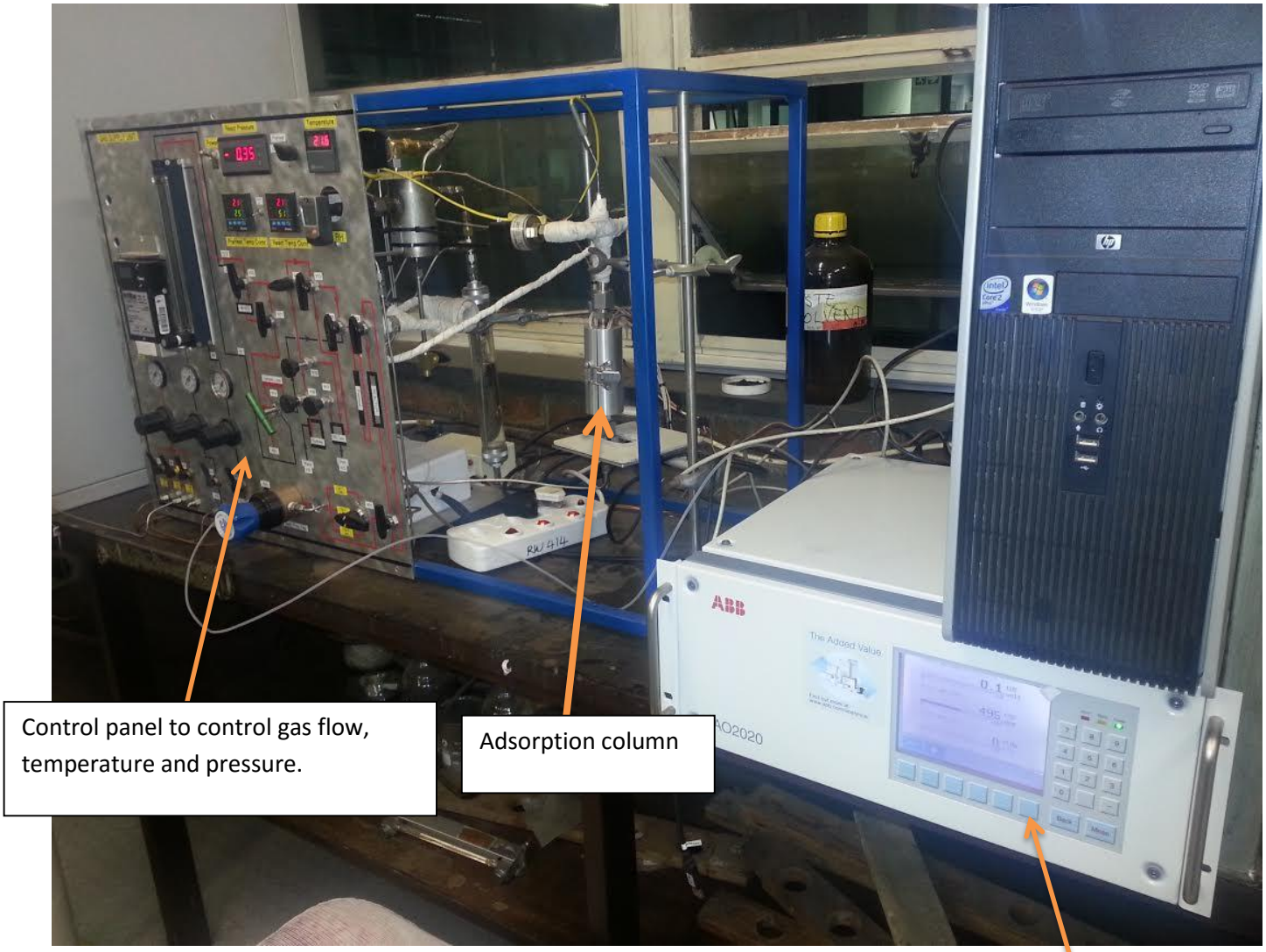


Figure D1: CO_2 adsorption equipment used for optimization studies.

Appendix E: Further information on model formulation and parameter estimation

Six candidate models were proposed as shown in equations E1 to E6.

$$Y_{estimate} = b_o + \alpha_1 X_1 + \alpha_2 X_2 + \alpha_3 X_3 + \varepsilon \quad \text{(Equation E1)}$$

$$Y_{estimate} = b_o + \alpha_1 X_1 + \alpha_2 X_2 + \alpha_3 X_3 + \alpha_4 X_1^2 + \alpha_5 X_2^2 + \alpha_6 X_3^2 + \varepsilon \quad \text{(Equation E2)}$$

$$Y_{estimate} = b_o + \alpha_1 X_1 + \alpha_2 X_2 + \alpha_3 X_3 + \alpha_4 X_1^2 + \alpha_5 X_2^2 + \alpha_6 X_3^2 + \alpha_7 X_1 X_2 + \alpha_8 X_1 X_3 + \alpha_9 X_2 X_3 + \varepsilon \quad \text{(Equation E3)}$$

$$Y_{estimate} = b_o + \alpha_1 X_1^2 + \alpha_2 X_2^2 + \alpha_3 X_3^2 + \alpha_4 X_1 X_2 + \alpha_5 X_1 X_3 + \alpha_6 X_2 X_3 + \varepsilon \quad \text{(Equation E4)}$$

$$Y_{estimate} = b_o + \alpha_1 X_1 X_2 + \alpha_2 X_1 X_3 + \alpha_3 X_2 X_3 + \varepsilon \quad \text{(Equation E5)}$$

$$Y_{estimate} = b_O + \alpha_1 X_1^2 + \alpha_2 X_2^2 + \alpha_3 X_3^2 + \varepsilon \quad \text{(Equation E6)}$$

The mean error and variance of each candidate model were obtained from Matlab using the code shown in Appendix C and are reported in Table E1.

Table E1: Variance and mean error values for the proposed models.

Model	Mean Error (ε)	Variance
1 (Equation E1)	-5.2935×10^{-14}	80.6306
2 (Equation E2)	1.6069×10^{-12}	50.9875
3 (Equation E3)	-2.6375×10^{-12}	29.5849
4 (Equation E4)	-1.2996×10^{-12}	32.6859
5 (Equation E5)	3.4817×10^{-14}	71.9470
6 (Equation E6)	4.9738×10^{-14}	82.3916

The coefficients of each candidate model were also calculated using Matlab making use of the code shown in Appendix C. The results are given in Table E2.

Table E2: Coefficient values for models 1 to 6 shown in Equations 5 to 10.

	Model 1	**Model 2**	**Model 3**	**Model 4**	**Model 5**	**Model 6**
$\mathbf{b_o}$	41.5524	6.9016	48.2277	50.8627	44.9338	41.4769
$\boldsymbol{\alpha_1}$	0.1723	0.9328	-0.5152	-0.0141	0.0015	0.0104
$\boldsymbol{\alpha_2}$	3.5912	41.3444	22.7053	-12.3007	0.5531	0.0030
$\boldsymbol{\alpha_3}$	0.0069	-0.0341	-0.0189	-0.0088	0.0012	0.0561
$\boldsymbol{\alpha_4}$	-	-0.0099	-0.0122	0.1364	-	-
$\boldsymbol{\alpha_5}$	-	-15.80	-15.7974	0.0186	-	-
$\boldsymbol{\alpha_6}$	-	0.0013	-0.0088	0.4162	-	-
$\boldsymbol{\alpha_7}$	-	-	0.1215	-	-	-
$\boldsymbol{\alpha_8}$	-	-	0.0248	-	-	-
$\boldsymbol{\alpha_9}$	-	-	0.2083	-	-	-

Further, correlation graphs were plotted to show how the estimated CO_2 adsorption capacity compared to the experimentally obtained CO_2 adsorption capacity for each model. The results are shown and discussed below.

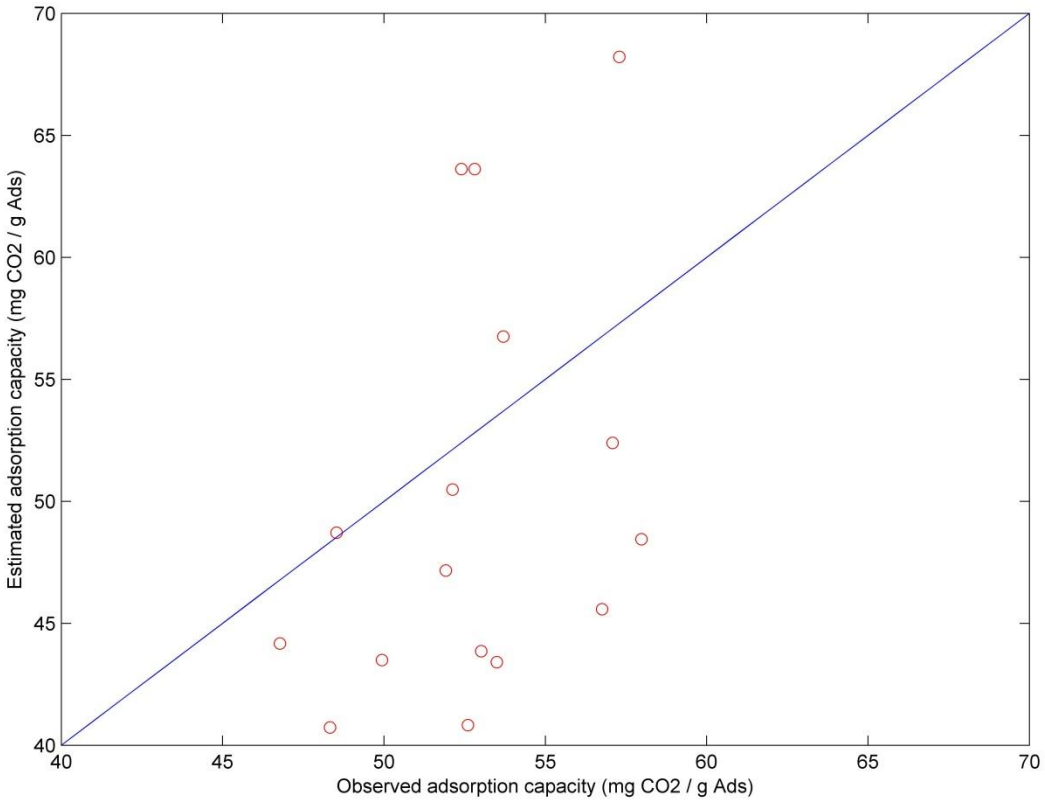


Figure E1: Correlation between observed and estimated adsorption capacity by use of model 1.

Model 1 shown in equation E1 is a linear model in all the factors investigated in this study. These factors are temperature, pressure and gas flow rate. Figure E1 is a correlation between the observed adsorption capacity and the estimated adsorption capacity from regression model 1, and shows that the regression model does not accurately describe the system. The correlation graph shown in Figure E1 also corresponds with the variance and mean error values of 80.6306 and -5.2935×10^{-14}, respectively, as shown in Table E1. The variance is significant, hence the points are scattered on either side of the straight line. This can be explained by the fact that regression model 1 only focuses on the linearity of the factors involved. A more complex regression model is necessary to model the system.

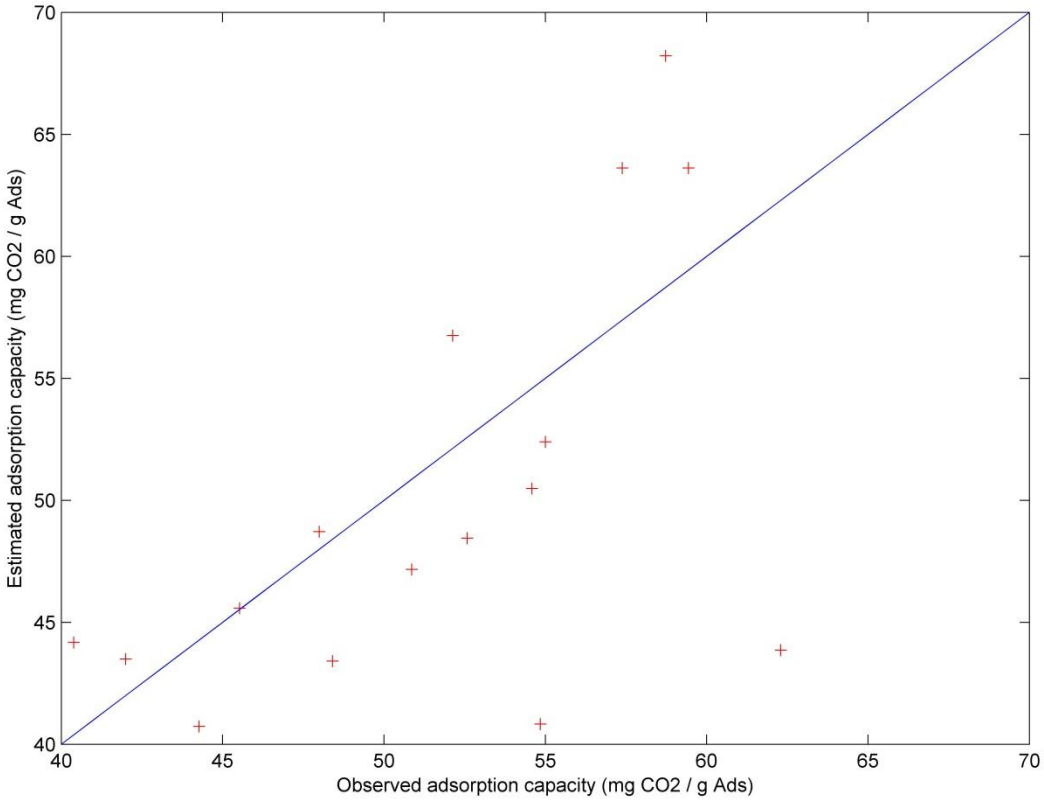


Figure E2: Correlation between observed and estimated adsorption capacity by use of model 2.

Model 2 shown in equation E2 is a regression model in all the factors investigated in this study. These factors are temperature, pressure and gas flow rate. The model has two components, a linear part and a quadratic part both in terms of the factors being investigated. Figure E2 is a correlation between the observed adsorption capacity and the estimated adsorption capacity from regression model 2. Figure E2 also shows that the regression model does not quite fit the system. The correlation graph shown in Figure E2 also corresponds with the variance and average error values of 50.9875 and 1.6069 X 10^{-12}, respectively as shown in Table E1. The variance is significant but less significant than that of model 1, hence the points are scattered on either side of the straight line. Model 2 is a better fit than model 1 due to the inclusion of the quadratic part in equation E2.

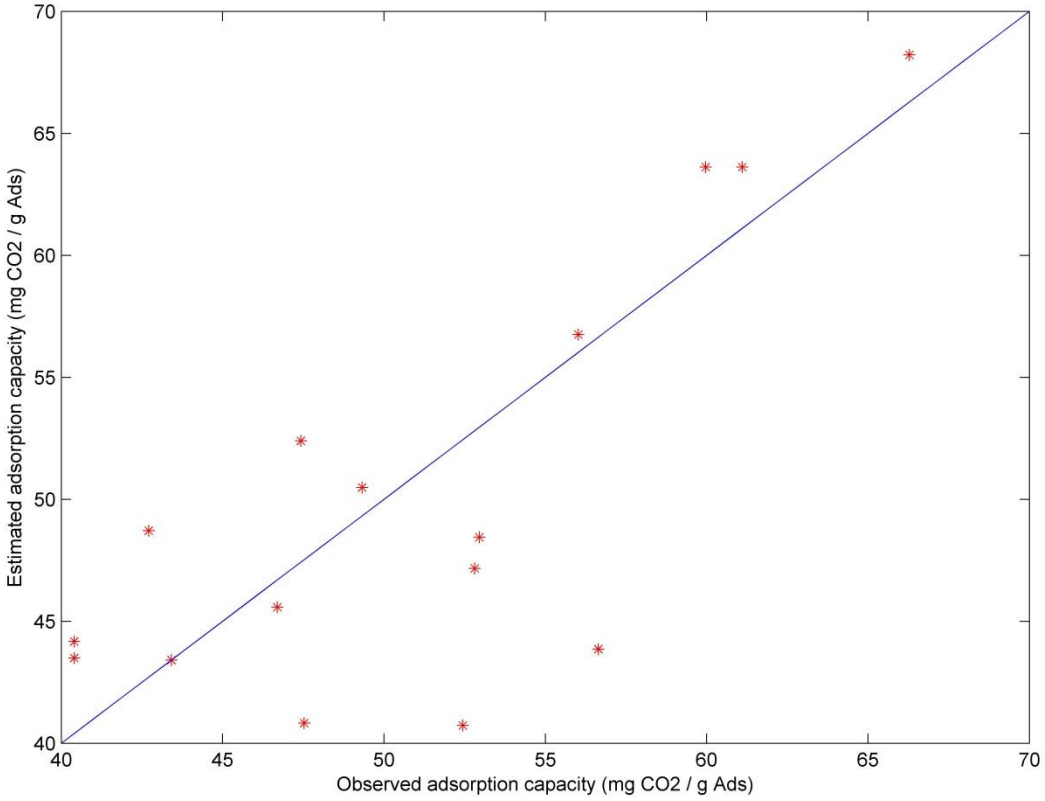


Figure E3: Correlation between observed and estimated adsorption capacity by use of model 3.

Model 3 shown in equation E3 is a regression model in all the factors investigated in this study. These factors are temperature, pressure and gas flow rate. The model has three components, a linear part, a quadratic part and a second quadratic part in terms of the factors and interactions of the factors being investigated. Figure E3 is a correlation between the observed adsorption capacity and the estimated adsorption capacity from regression model 3. Figure E3 also shows that the regression model is not a perfect fit to the system. The variance and average error values of 29.5849 and -2.6375×10^{-12}, respectively were obtained and are shown in Table E1. The variance obtained for model 3 is less significant than that of model 1 and of model 2, hence the points are scattered on either side of the straight line. Model 3 is a better fit than model 1 and model 2 based on the lower variance.

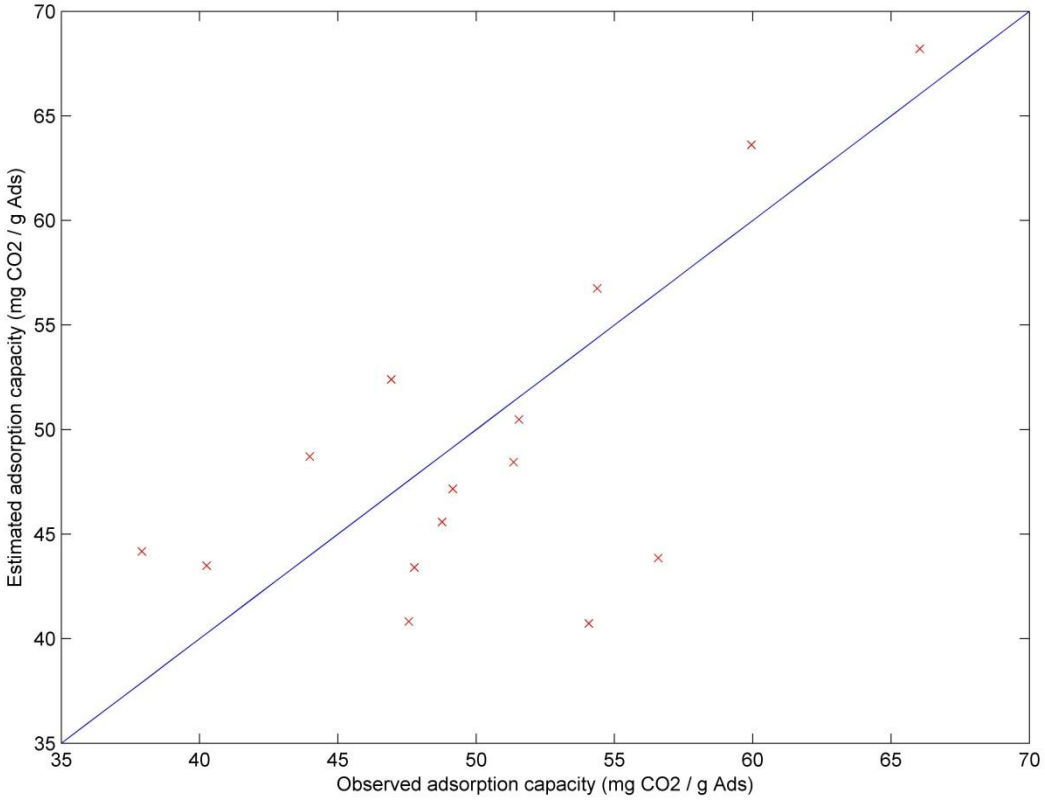


Figure E4: Correlation between observed and estimated adsorption capacity by use of model 4.

Model 4 shown in equation E4 is a regression model in all the factors investigated in this study. These factors are temperature, pressure and gas flow rate. The model has two components, two quadratic parts both in terms of the factors being investigated and interactions of the factors. Figure E4 is a correlation between the observed adsorption capacity and the estimated adsorption capacity from regression model 4. Figure E4 also shows that the regression model does not quite fit the system. A variance and average error of 32.6859 and -1.2996 X 10^{-12}, respectively were obtained, as shown in Table E1. The variance is significant but less significant than that of model 1 and of model 2, hence the points are scattered on either side of the straight line. The variance and average error of model 4 are, however, comparable to those of model 3. Model 4 is a better fit than model 1 and 2.

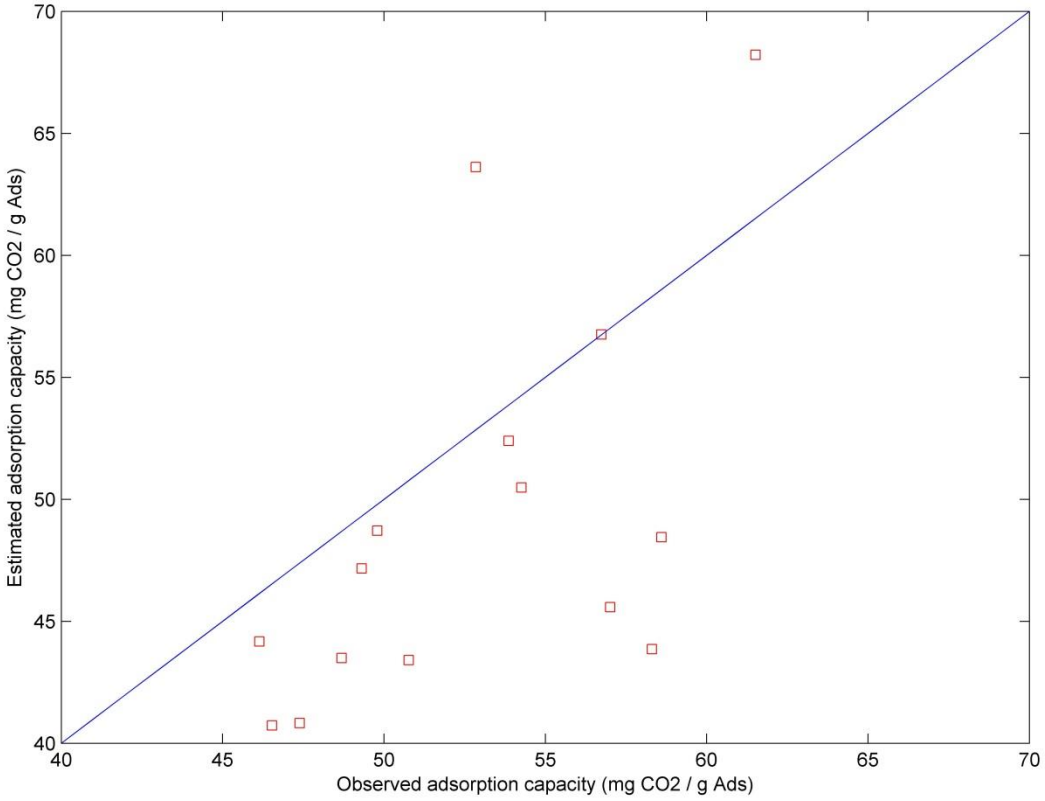


Figure E5: Correlation between observed and estimated adsorption capacity by use of model 5.

Model 5 shown in equation E5 is a regression model in all the factors investigated in this study. These factors are temperature, pressure and gas flow rate. The model only focuses on the interaction of the factors being investigated. Figure E5 is a correlation between the observed adsorption capacity and the estimated adsorption capacity from regression model 5. Figure E5 also shows that the regression model does exactly fit the system. Variance and average error values of 71.9470 and 3.4817×10^{-14}, respectively, were obtained and shown in Table E1. The variance is significant and hence the points are scattered on either side of the straight line. It can be observed that non-inclusion of the linear section and the quadratic section of the regression model has resulted in the variance and error increasing compared to that of model 4.

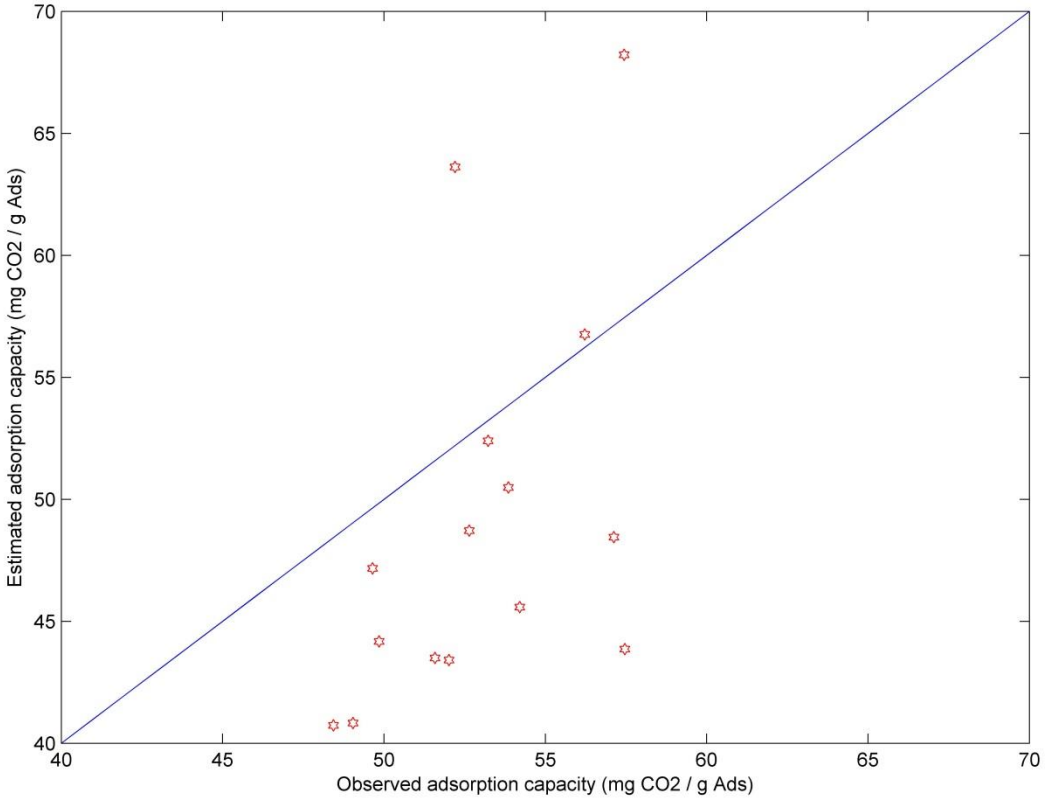
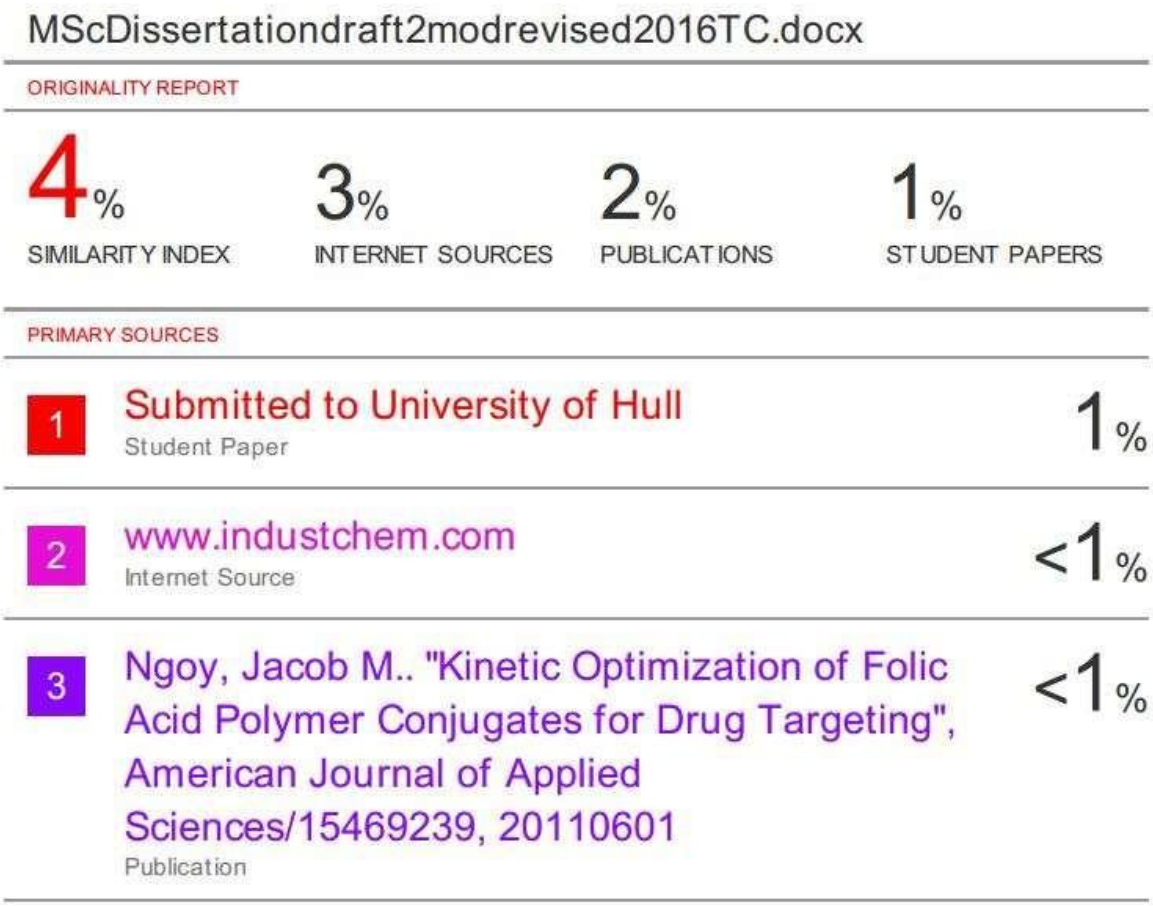


Figure E6: Correlation between observed and estimated adsorption capacity by use of model 6.

Model 6 shown in equation E6 is a regression model in all the factors investigated in this study. These factors are temperature, pressure and gas flow rate. The model is a quadratic in terms of the individual factors being investigated. Figure E6 is a correlation between the observed adsorption capacity and the estimated adsorption capacity from regression model 6. Figure E6 also shows that the regression model does not quite fit the system, with more points below the regression line. Variance and average error values of 82.3916 and 4.9738 X 10^{-14} respectively were obtained and are shown in Table E1. Similar trends to model 5 were observed.

Appendix F: Plagiarism report



MScDissertationdraft2modrevised2016TC.docx

ORIGINALITY REPORT

4%	3%	2%	1%
SIMILARITY INDEX	INTERNET SOURCES	PUBLICATIONS	STUDENT PAPERS

PRIMARY SOURCES

1	Submitted to University of Hull Student Paper	1%
2	www.industchem.com Internet Source	<1%
3	Ngoy, Jacob M.. "Kinetic Optimization of Folic Acid Polymer Conjugates for Drug Targeting", American Journal of Applied Sciences/15469239, 20110601 Publication	<1%

Appendix G: Publications

The publications are attached on the next page.